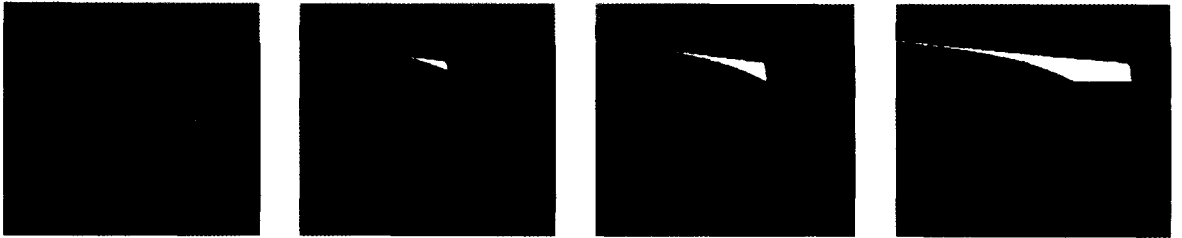


# Sand-mud segregation in estuaries and tidal basins



Mathijs van Ledden



## STELLINGEN

behorende bij het proefschrift

**Zand-slibsegregatie in estuaria en getijdebekkens**

van

Mathijs van Ledden

Delft, 16 september 2003

1. Het bepalen van de volledige korrelgrootteverdeling van bodemonsters in estuaria en getijdebekkens voor de karakterisering van de sedimentsamenstelling is inefficiënt. Volstaan kan worden met het slibpercentage, de lutum/silt verhouding en de gemiddelde of mediane zandkorrelgrootte (Dit proefschrift).
2. Het lutumpercentage bepaalt de overgang van niet-cohesief naar cohesief erosiegedrag van zand-slibbodems en niet het slibpercentage, zoals gesuggereerd door Mitchener & Torfs (1996) (Dit proefschrift).  
  
Mitchener, H. & Torfs, H., 1996. *Erosion of mud/sand mixtures*. Coastal Engineering (29), 1-25.
3. De vuistregel "Hoe langzamer het stroomt, hoe meer slib" is een halve waarheid (Dit proefschrift).
4. Scherpe overgangen tussen zandige en (potentieel) slibrijke gebieden treden alleen op in getijsystemen met een relatief laag slibaanbod (Dit proefschrift).
5. De uitdrukking 'complex model' is een contradictio in terminis en moet daarom vermeden worden.

6. Een zingevingskader is een belangrijke voorwaarde voor een zinvolle discussie over normen en waarden in de maatschappij.

7. Rekken en strekken voor en na het sporten is medisch gezien pure tijdverspilling.

Herbert, D. & Gabriel, M., 2003. *Effects of stretching before and after exercising on muscle soreness and risk of injury*. British Medical Journal, 325-468.

8. De discussie in Nederland over het dichtslibben van de autosnelwegen is volledig verzand omdat mensen doormodderen met de auto en niet bereid zijn een ander vervoermiddel te overwegen.

9. Mensen die zeggen kort van stof te zijn, zijn vaak langdradig.

10. Nuchterheid verkleint de kans op dronkenschap.

*Deze stellingen worden verdedigbaar geacht en zijn als zodanig goedgekeurd door de promotor prof.dr.ir. H.J. de Vriend.*

# PROPOSITIONS

pertaining to the thesis

## **Sand-mud segregation in estuaries and tidal basins**

by

Mathijs van Ledden

Delft, 16 September 2003

1. The determination of the full grain size distribution of sediment samples in estuaries and tidal basins is inefficient. The mud content, the lutum/silt ratio and the mean or median sand grain size provide sufficient information (This thesis).
2. It is the clay content that governs the transition from non-cohesive to cohesive erosion behaviour of sand-mud beds, not the mud content, as suggested by Mitchener & Torfs (1996) (This thesis).

Mitchener, H. & Torfs, H., 1996. *Erosion of mud/sand mixtures*. Coastal Engineering (29), 1-25.

3. The rule-of-thumb "The calmer the water, the higher the mud content" is a half-truth (This thesis).
4. Sharp transitions between sandy areas and areas (potentially) rich in mud only occur in tidal systems with a relatively low mud availability (This thesis).
5. The expression 'complex model' is a contradiction in terms and should therefore be avoided.

6. A framework of meaning is an important condition for a meaningful discussion about norms and values in society.
7. From a medical point of view stretching before and after exercising is an absolute waste of time.

Herbert, D. & Gabriel, M., 2003. *Effects of stretching before and after exercising on muscle soreness and risk of injury*. British Medical Journal, 325-468.

8. The discussion in the Netherlands about the motorways being congested has got bogged down completely because people muddle on with the automobile and are not willing to consider another means of transport.

9. People who say they will be brief are often long-winded.  
[verbatim translation]

10. Soberness reduces the risk of drunkenness.  
[verbatim translation]

*These propositions are considered defensible and as such have been approved by the supervisor prof.dr.ir. H.J. de Vriend.*

9-1-1977  
1-1-1977  
1-1-1977

6095  
TR 4095

Sand-mud segregation  
in estuaries and tidal basins

Zand-slibsegregatie  
in estuaria en getijdebekkens

12  
13  
14  
15  
16



# Sand-mud segregation in estuaries and tidal basins

PROEFSCHRIFT



ter verkrijging van de graad van doctor  
aan de Technische Universiteit Delft,  
op gezag van de Rector Magnificus prof.dr.ir. J.T. Fokkema,  
voorzitter van het College voor Promoties,  
in het openbaar te verdedigen op dinsdag 16 september 2003 om 13.00 uur

door

Mathijs VAN LEDDEN  
civiel ingenieur  
geboren te Culemborg

Dit manuscript is goedgekeurd door de promotor:

Prof.dr.ir. H.J. de Vriend

Toegevoegd promotor:

Dr.ir. J.C. Winterwerp

Samenstelling promotiecommissie:

|                             |                                                              |
|-----------------------------|--------------------------------------------------------------|
| Rector Magnificus           | voorzitter                                                   |
| Prof.dr.ir. H.J. de Vriend  | Technische Universiteit Delft, promotor                      |
| Dr.ir. J.C. Winterwerp      | Technische Universiteit Delft, toegevoegd promotor           |
| Prof.dr. K.R. Dyer          | University of Plymouth, United Kingdom                       |
| Prof.dr. A.J. Mehta         | University of Florida, United States                         |
| Prof.dr.ir. M.J.F. Stive    | Technische Universiteit Delft                                |
| Dr. E.J. Houwing            | Rijksinstituut voor Zoetwaterbeheer en Afvalwaterbehandeling |
| Dr.ir. Z.B. Wang            | Technische Universiteit Delft                                |
| Prof.dr.ir. H.H.G. Savenije | Technische Universiteit Delft, reservelid                    |

This research has been supported by the Technology Foundation STW, applied science division of NWO and the technology programme of the Ministry of Economic Affairs under contract number DCT.4895. The project was also embedded in the Delft Cluster project DC 03.01.02 "Eco-morphology in estuaries and coasts".

Cover design: Arjan Schoonhoven

The four snapshots on the front cover show the bed level and bed composition development in an idealised reservoir with sand and mud. The segregation of sand (yellow) and mud (brown) is clearly visible (see also Section 5.3).

Copyright © 2003 by M. van Ledden

Printed by PrintPartners Ipskamp BV, the Netherlands

ISBN 90-9016786-2

This thesis is also published in the series of 'Communications on Hydraulic and Geotechnical Engineering', Faculty of Civil Engineering and Geosciences, Delft University of Technology, Report No. 03-2, ISSN 0169-6548.

## Abstract

Large-scale sand-mud segregation, i.e. mud content ( $\% \leq 0.063$  mm) variations in the horizontal direction at a spatial scale of kilometers, is found in estuaries and tidal basins all over the world. Understanding and predicting the distribution of sand and mud in these systems is important because of management issues such as the maintenance of navigation channels, the sediment bed quality and the distribution of flora and fauna. Although various mechanisms behind large-scale sand and mud behaviour have been investigated separately, a comprehensive large-scale model in which these mechanisms are brought together to explain and predict this phenomenon does not presently exist.

The research reported in this thesis aims at contributing to the understanding and modelling of large-scale sand-mud segregation in estuaries and tidal basins. Specific objectives are:

- to characterise the phenomenon of large-scale sand-mud segregation and to identify the underlying processes and mechanisms;
- to propose a model in which (part of) these processes and mechanisms are reproduced and which can be used for describing morphological behaviour including the effect of sand-mud segregation;
- to predict the trends of morphological evolution of systems including the effect of sand-mud segregation and to verify these trends with field data;

An analysis of bed composition data in Dutch tidal systems has revealed two important characteristics with respect to the phenomenon of sand-mud segregation. Firstly, the sediment composition is characterised by a nearly uniform sand fraction ( $\%0.063 - 2$  mm) and a mud fraction ( $\% \leq 0.063$  mm) with a constant ratio between the silt ( $\%0.004 - 0.063$  mm) and the clay ( $\% < 0.004$  mm) content. The constant clay/silt ratio in the tidal basins of the Dutch Wadden Sea, the Ems-Dollard estuary and the Western Scheldt varies within a narrow range between 0.16 and 0.25 ( $R^2 > 0.72$ ). Secondly, sand-mud patterns are observed at a wide range of (horizontal) spatial scales. These characteristics are not unique, but appear to occur in tidal systems all over the world.

A literature survey has demonstrated that the processes directly affecting the sediment composition are erosion, deposition, and mixing in the sediment bed itself. Furthermore, the large-scale distribution of sand and mud is generally explained by bed shear stress variations, but other mechanisms such as tidal asymmetry and gravitational circulation have been put forward, as

well. Finally, the currently used (semi-)empirical models for predicting the mud content at the bed surface can discriminate between areas with less than 10% mud content and areas in which the mud content cannot be predicted and varies between 0 and 100%.

A key element in a process-based sand-mud model is an erosion formulation for sand-mud mixtures. Recently, several erosion experiments have demonstrated that the erosion behaviour of these mixtures can change dramatically when a small amount of mud is added to a sand bed or vice versa. Therefore, a classification has been proposed for the behaviour of sand-mud mixtures based on appropriate parameters for the cohesion and the network structure of these mixtures. In particular, the transition between non-cohesive and cohesive behaviour at a clay content of 5 - 10% has been validated by a re-analysis of several laboratory and field experiments. The use of a 'critical mud content' for this transition is not generic, but practical because of the aforementioned constant clay/silt ratio in the mud fraction. Based on experimental data, erosion formulations for non-cohesive and cohesive sand-mud mixtures have been developed. A comparison with a limited number of laboratory and field experiments has shown that the erosion formulations can be used as a first step in a sand-mud model.

A three-dimensional process-based morphodynamic sand-mud model has been proposed. The model extends currently used morphodynamic models in a number of ways. Firstly, the erosion characteristics of sand and mud depend on the mud content at the bed surface. Secondly, the temporal and spatial variations in mud content are taken into account. The bed composition varies due to erosion and deposition of sand and mud at the bed surface and mixing in the sediment bed itself. Consolidation and flocculation processes have not yet been included explicitly in the model set-up. A numerical prototype of the process-based sand-mud model has been developed by extending the three-dimensional software package Delft3D from WL|Delft Hydraulics.

Large-scale sand-mud patterns in estuaries and tidal basins have been investigated by analysing three idealised situations with the process-based sand-mud model: a local situation, a reservoir and a short tidal basin. In the local situation, a certain point in a tidal system is considered by omitting all non-local terms in the model equations except for the mud concentration equation. A parameterised horizontal transport term has been included in this equation to avoid trivial solutions. The set-up of the reservoir consists of a one-dimensional bed level profile with increasing water depth in the downstream direction, a constant river discharge at the upstream boundary and no tidal influence. This situation is qualitatively comparable with the southern area of the Rhine-Meuse estuary (the Netherlands) in which sand and mud has been deposited after the construction of the Haringvliet Sluices in 1970. The tidal basins in the Dutch and German Wadden Sea are taken as a reference for investigating the behaviour of a tidal basin. A one-dimensional rectangular short tidal basin without tidal flats has been investigated with an  $M_2$ -tide at the sea boundary and a constant water depth.

The analysis of the local situation has provided an expression for the equilibrium mud content

at the bed surface under tidal conditions. It depends on the bed shear stress amplitude ( $\hat{\tau}_b$ ), the critical shear stress for erosion ( $\tau_e$ ) and deposition ( $\tau_d$ ), the settling velocity ( $w_m$ ), the mud concentration ( $c_m$ ) and the erosion rate ( $M$ ). In the expression of the equilibrium mud content an important dimensionless parameter is found by  $w_m c_m / M$ , which indicates the ratio between the mud deposition and mud erosion capacity. The equilibrium mud content turns out to be the upper envelope of the observed mud content in a large number of points at the Molenplaat, an intertidal flat in the Western Scheldt estuary (the Netherlands). The sharp transition between areas with low mud content and areas with (potential) high mud content appears to be a result of the relatively small deposition capacity in this area (i.e.  $w_m c_m / M \ll 1$ ). When the bed shear stress amplitude is lower than the critical erosion shear stress, net mud deposition occurs and the bed is (potentially) muddy. For higher bed shear stress, net mud deposition is almost completely absent and the bed is sandy.

The initial morphological behaviour of the reservoir and the tidal basin has shown separate deposition waves of sand and mud. This separation can be related directly to differences in sediment properties (i.e. the critical shear stress for erosion and deposition), whereas the relatively small deposition capacity is important in the tidal basin, too (i.e.  $w_m c_m / M \ll 1$ ). In the reservoir and the tidal basin, a clear distinction can be made between areas in which the low mud content at the bed surface is explained by the relatively high bed shear stress ('flow-limited') and by the low supply of sediment ('supply-limited'). The analytical solution of the mud deposition wave in the reservoir has demonstrated that the shape of the mud deposition wave is determined by two length scales: a settling length scale and a flow length scale. The occurrence and shape of the deposition patterns of sand and mud in the reservoir have been validated qualitatively by the sediment balances in the Rhine-Meuse estuary (the Netherlands) after the construction of the Haringvliet Sluices (1970).

When compared to the situation with sand only, the long-term morphological development of the reservoir and the tidal basin with sand and mud gives rise to two opposing observations. On the one hand, the morphological adaptation time scale decreases, due to the extra availability of sediment and the high mud deposition near the head of the basin. On the other hand, the bed level profile in the equilibrium situation is quite similar to the equilibrium bed level profiles for sand only. The accompanying bed composition pattern in the equilibrium state of the reservoir and the tidal basin are as follows. In the reservoir, the bed composition near the bed surface is completely sandy, but mud layers covered with sand are still present further below the bed surface. The bed composition pattern at the bed surface in the tidal basin is almost entirely sandy with a small muddy area only near the head of the basin. Qualitatively, the bed level and bed composition profile in the equilibrium state of the basin agree well with the observations in the Dutch and German Wadden Sea.

Finally, the Friesche Zeegat (the Netherlands) has been taken as a real-world case to hindcast the morphological response of the system quantitatively for the period 1970 - 1994 after the

closure of the Lauwerszee (1969). The agreement between hydrodynamic field data and model results in the 1990's appears to be reasonably good. Starting with a geometry in 1970, the computed net deposition in the deep channels and at the intertidal area of the basin and the net erosion in between agree qualitatively with the observations. Unfortunately, the observed net erosion in the ebb-tidal delta just after the closure and the observed decreasing import rate in the basin are not predicted correctly. These discrepancies are presumably the result of neglecting wave-driven currents in the model set-up and a poor quantitative prediction of the changes in the hypsometry of the basin. The computed distribution of sand and mud in the Friesche Zeegat appears to be realistic. The ebb-tidal delta is dominated by sand, due to the relatively high bed shear stress. In the basin, sand deposition is mainly found at the entrance of the main channel, whereas mud deposition occurs in the deeper parts of the main channel, in the shallow areas near the borders and in particular in the channel near the dike of the Lauwerszee.

In conclusion, the present research has resulted in an increased understanding of and greater modelling capabilities for large-scale sand-mud segregation in estuaries and tidal basins. An innovative three-dimensional process-based model for sand and mud has been developed and good qualitative agreement has generally been obtained between model results and field data. In principle, the sand-mud model is applicable to other water systems (e.g. rivers, coastal seas). The model can be used to estimate the effects of human interventions and/or natural changes on the large-scale bed level and the bed composition development in time and space. An important restriction of its applicability is that the bed has to consist of a nearly uniform sand fraction and a mud fraction with a constant clay/silt ratio. Furthermore, the application of the model requires bed level and bed composition data to verify the model results. Recommendations for future work include a new set of erosion experiments with sand-mud mixtures to improve the erosion formulations, an extension of the analysis of idealised situations by investigating other boundary conditions, geometries and processes, and the application of the model to new realistic cases with abundant bed level and bed composition data.

Mathijs van Ledden  
September 2003

## Samenvatting

Grootschalige zand-slibsegregatie, dat is de horizontale variatie in het slibpercentage ( $\% \leq 0.063$  mm) op een ruimtelijke schaal van kilometers, wordt waargenomen in estuaria en getijdebekkens over de gehele wereld. Het begrijpen en voorspellen van de verdeling van zand en slib in deze systemen is belangrijk vanwege beheersvraagstukken zoals het onderhoud van vaargeulen, de waterbodemkwaliteit en de verspreiding van flora en fauna. Hoewel verschillende mechanismen achter het grootschalige gedrag van zand en slib afzonderlijk zijn onderzocht, bestaat op dit moment geen uitgebreid grootschalig model waarin deze mechanismen zijn samengebracht om dit fenomeen te verklaren en voorspellen.

Het beschreven onderzoek in dit proefschrift wil een bijdrage leveren aan het begrijpen en voorspellen van grootschalige zand-slibsegregatie in estuaria en getijdebekkens. Specifieke doelen zijn:

- Het karakteriseren van het fenomeen grootschalige zand-slibsegregatie en het identificeren van de onderliggende processen en mechanismen;
- Het opstellen van een model waarin (een gedeelte van) deze processen en mechanismen worden gereproduceerd en dat kan worden gebruikt om het morfologische gedrag te beschrijven inclusief het effect van zand-slibsegregatie;
- Het voorspellen van de trends in de morfologische ontwikkeling van systemen inclusief het effect van zand-slibsegregatie en het verifiëren van deze trends met veldgegevens;

Een analyse van bodemsamenstellingsgegevens in Nederlandse getijsystemen heeft twee belangrijke karakteristieken opgeleverd met betrekking tot het fenomeen van zand-slibsegregatie. Ten eerste wordt de sedimentsamenstelling gekarakteriseerd door een vrijwel uniforme zandfractie ( $\%0.063 - 2$  mm) en een slibfractie ( $\% \leq 0.063$  mm) met een constante verhouding tussen het silt- ( $\%0.004 - 0.063$  mm) en het lutumgehalte ( $\% < 0.004$  mm). De constante lutum/silt verhouding in de getijdebekkens van de Nederlandse Waddenzee, het Eems-Dollard estuarium en de Westerschelde varieert in een smalle band tussen 0.16 en 0.25 ( $R^2 > 0.72$ ). Daarnaast worden zand-slibpatronen waargenomen op een groot scala van (horizontale) ruimteschalen. Deze karakteristieken zijn niet uniek, maar komen voor in getijdesystemen over de gehele wereld.

Een literatuuronderzoek heeft laten zien dat de processen, die direct de sedimentsamenstelling beïnvloeden, erosie, depositie en menging van het sediment in de bodem zijn. Verder wordt

de grootschalige verdeling van zand en slib in het algemeen verklaard door bodemschuifspanningsvariaties, maar andere mechanismen zoals getijasymmetrie en estuarine circulatie zijn ook naar voren gebracht. Tenslotte kunnen de huidige (semi-)empirische modellen voor het voorspellen van het slibpercentage aan het bodemoppervlak onderscheid maken tussen gebieden met een slibpercentage kleiner dan 10% en gebieden waarin het slibpercentage niet kan worden voorspeld en varieert tussen 0 en 100%.

Een sleutelement in een proces-gebaseerd zand-slibmodel is een erosieformulering voor zand-slibmengsels. Recentelijk hebben verschillende experimenten laten zien dat het erosiegedrag van zand-slibmengsels dramatisch kan veranderen wanneer een kleine hoeveelheid slib wordt toegevoegd aan zandbodem of omgekeerd. Daarom is een classificatie voorgesteld voor het gedrag van zand-slibmengsels dat gebaseerd is op geschikte parameters voor cohesie en de netwerkstructuur van deze mengsels. Met name de overgang van niet-cohesief naar cohesief gedrag bij een lutumpercentage van 5 - 10% is gevalideerd door een heranalyse van laboratorium- en veld-experimenten. Het gebruik van een zgn. 'kritisch slibpercentage' voor deze overgang is niet generiek, maar wel praktisch vanwege de eerder genoemde constante lutum/silt verhouding in de slibfractie. Gebaseerd op experimentele gegevens zijn erosieformuleringen ontwikkeld voor niet-cohesieve en cohesieve zand-slibmengsels. Een vergelijking met een beperkt aantal laboratorium- en veld-experimenten laat zien dat deze formuleringen kunnen worden gebruikt als een eerste stap in een zand-slibmodel.

Een drie-dimensionaal proces-gebaseerd morfologisch zand-slib model is voorgesteld. Het model breidt de huidige morfologische modellen uit op verschillende manieren. Ten eerste zijn de erosiekenmerken van zand en slib afhankelijk van het slibpercentage aan het bodemoppervlak. Ten tweede worden de tijdsafhankelijke en ruimtelijke variaties in het slibpercentage in rekening gebracht. De bodemsamenstelling varieert ten gevolge van erosie en depositie van zand en slib aan het bodemoppervlak en menging van sediment in de bodem. Consolidatie en flocculatie zijn op dit moment nog niet expliciet meegenomen in het model. A numeriek prototype van het proces-gebaseerde zand-slibmodel is ontwikkeld door het uitbreiden van het drie-dimensionale software pakket Delft3D van WL|Delft Hydraulics.

Grootschalige zand-slibpatronen in estuaria en getijdebekken zijn onderzocht door het analyseren van drie geïdealiseerde situaties met het proces-gebaseerde zand-slibmodel: een lokale situatie, een reservoir en een kort getijdebekken. In de lokale situatie wordt een zeker punt in een getijdesysteem beschouwd door het verwijderen van alle niet-lokale termen in de modelvergelijkingen met uitzondering van de slibconcentratie vergelijking. Een geparameteriseerde horizontale transport term is in deze vergelijking meegenomen om triviale oplossingen te vermijden. De opzet van het reservoir bestaat uit een één-dimensionaal bodemliggingsprofiel met een toenemende waterdiepte in de benedenstroomse richting, een constante rivierafvoer aan de bovenstroomse zijde en geen invloed van getij. Deze situatie is kwalitatief vergelijkbaar met de Zuidrand van het Noordelijk Deltabekken waarin zand en slib zijn gesedimenteerd na de



aanleg van de Haringvlietsluizen in 1970. De getijdebekken in de Nederlandse en Duitse Waddenzee zijn als referentie genomen om het gedrag van een getijdebekken te onderzoeken. Een één-dimensionaal rechthoekig kort getijdebekken zonder intergetijdegebied is onderzocht met een tweemaal daags getij aan de zeerand en een constante waterdiepte.

De analyse van de lokale situatie heeft een uitdrukking opgeleverd voor het evenwichtsslibpercentage aan het bodemoppervlak onder getijcondities. Het hangt af van de bodemschuifspanningsamplitude ( $\hat{\tau}_b$ ), de kritische schuifspanning voor erosie ( $\tau_e$ ) en depositie ( $\tau_d$ ), de valsnelheid ( $w_m$ ), de slibconcentratie ( $c_m$ ) en de erosiesnelheid ( $M$ ). In de uitdrukking van het evenwichtsslibpercentage wordt een belangrijke dimensieloze parameter gevormd door  $w_m c_m / M$  die de verhouding aangeeft tussen de slibdepositie en sliberosie capaciteit. Het evenwichtsslibpercentage blijkt de omhullende te zijn van het waargenomen slibpercentage in een groot aantal punten op de Molenplaat, een intergetijdegebied in de Westerschelde. De scherpe overgang tussen gebieden met een laag slibpercentage en gebieden met een (potentieel) hoog slibpercentage blijkt het resultaat te zijn van de relatief kleine slibdepositie capaciteit (i.e.  $w_m c_m / M \ll 1$ ). Wanneer de maximale bodemschuifspanning gedurende het getij kleiner is dan de kritische erosieschuifspanning treedt netto slibsedimentatie op en is de bodem potentieel slibrijk. Bij een hogere schuifspanning is netto slibsedimentatie verwaarloosbaar en is de bodem zanderig.

Het aanvankelijke morfologische gedrag van het reservoir en het getijdebekken laat gescheiden sedimentatiegolven zien van zand en slib. Deze scheiding kan direct worden gerelateerd aan verschillen in sedimenteigenschappen (bijv. kritische schuifspanning voor erosie en sedimentatie), terwijl de relatief kleine slibdepositie capaciteit ook van belang is in het getijdebekken (i.e.  $w_m c_m / M \ll 1$ ). In het reservoir en het getijdebekken kan een duidelijk onderscheid gemaakt worden tussen gebieden waarin het lage slibpercentage aan het bodemoppervlak wordt verklaard door de relatief hoge bodemschuifspanning ('stromings-gelimiteerd') en door het lage slibaanbod ('aanbod-gelimiteerd'). De analytische oplossing van de slibsedimentatiegolf laat zien dat de vorm van de slibsedimentatiegolf wordt bepaald door twee lengteschalen: een uitzakkingslengteschaal en een stromingslengteschaal. Het optreden en de vorm van de sedimentatiepatronen van zand en slib in het reservoir zijn kwalitatief gevalideerd met de sedimentbalansen in het Noordelijk Deltabekken na de aanleg van de Haringvlietsluizen (1970).

De lange-termijn morfologische ontwikkeling van het reservoir en het getijdebekken met zand en slib heeft twee tegengestelde effecten laten zien in vergelijking met alleen zand. Enerzijds neemt de morfologische tijdschaal af door de grotere beschikbaarheid van sediment en de sterke slibsedimentatie nabij de landwaartse zijde van het bekken. Anderzijds is het bodemprofiel in de evenwichtssituatie sterk vergelijkbaar met de evenwichtsbodemprofielen voor alleen zand. Het bijbehorende bodemsamenstellingspatroon in de evenwichtstoestand van het reservoir en het getijdebekken zijn als volgt. In het reservoir is de bodemsamenstelling nabij het bodemoppervlak volledig zandig, terwijl met zand bedekte sliblagen aanwezig zijn dieper onder het bodemoppervlak. De bodemsamenstelling aan het bodemoppervlak in het getijdebekken is vrij-

wel geheel zandig met alleen een klein slibrijk gebied aan de landwaartse kant van het bekken. Kwalitatief komen het bodemliggings- en de bodemsamenstellingsprofiel goed overeen met de observaties in de Nederlandse en Duitse Waddenzee.

Tenslotte is het Friesche Zeegat genomen als een realistisch geval om de morfologische ontwikkeling kwantitatief te simuleren in de periode 1970 - 1994 na de sluiting van de Lauwerszee (1969). De overeenkomst met de hydrodynamische veldgegevens en modelresultaten in de jaren negentig is redelijk goed. Startend met een geometrie van 1970 komt de berekende netto depositie in de diepe geulen en op het intergetijdegebied van het bekken, en de netto erosie daartussenin kwalitatief goed overeen met de observaties. Helaas wordt de waargenomen netto erosie van de buitendelta direct na de sluiting en de waargenomen afname van de import in het bekken niet correct voorspeld. Deze discrepanties zijn waarschijnlijk het gevolg van het verwaarlozen van golf-gedreven stroming in de modelopzet en een slechte kwantitatieve voorspelling van de veranderingen in de hypsometry van het bekken. De berekende verdeling van zand en slib in het Friesche Zeegat blijkt realistisch te zijn. De buitendelta wordt gedomineerd door zand vanwege de relatief hoge bodemschuifspanning. In het bekken wordt zandsedimentatie voornamelijk gevonden bij het begin van de hoofdgeul, terwijl slibdepositie voorkomt in de diepere gedeelten van de hoofdgeul, in de ondiepe gebieden nabij de randen en in het bijzonder in de geul bij de dijk van de Lauwerszee.

Concluderend heeft dit onderzoek geresulteerd in beter begrip en grotere modelleringsmogelijkheden van grootschalige zand-slibsegregatie in estuaria en getijdebekken. Een innovatief driedimensionaal proces-gebaseerd model is ontwikkeld voor zand en slib en een goede kwalitatieve overeenkomst is in het algemeen verkregen tussen modelresultaten en veldgegevens. In principe is het zand-slib model toepasbaar voor andere watersystemen (bijv. rivieren, kustzeeën). Het model kan worden toegepast om effecten in te schatten van menselijke ingrepen en/of natuurlijke veranderingen op de grootschalige bodemliggings- en bodemsamenstellingsontwikkeling in de tijd en in de ruimte. Een belangrijke beperking van de toepasbaarheid is dat de bodem moet bestaan uit een vrijwel uniforme zandfractie en een slibfractie met een constante lutum/silt verhouding. Verder vereist de toepassing van het model bodemliggings- en bodemsamenstellingsgegevens om de modelresultaten te verifiëren. Aanbevelingen voor verder onderzoek zijn een nieuwe serie erosie experimenten met zand-slibmengsels om de erosieformuleringen te verbeteren, uitbreiding van de analyse van geïdealiseerde situaties door het onderzoeken van andere randvoorwaarden, geometrieën en processen, en de toepassing van het model op nieuwe realistische gevallen met een ruim voldoende bodemliggings- en bodemsamenstellingsgegevens.

Mathijs van Ledden  
September 2003

# Contents

|                                                                      |           |
|----------------------------------------------------------------------|-----------|
| <b>Abstract</b>                                                      | v         |
| <b>Samenvatting</b>                                                  | ix        |
| <b>1 Introduction</b>                                                | <b>1</b>  |
| 1.1 <i>Sand-mud segregation</i>                                      | 1         |
| 1.2 <i>The need for modelling sand-mud segregation</i>               | 1         |
| 1.3 <i>Problem definition</i>                                        | 5         |
| 1.4 <i>Objectives</i>                                                | 8         |
| 1.5 <i>Approach</i>                                                  | 8         |
| <b>2 Conceptual framework for sand-mud segregation</b>               | <b>11</b> |
| 2.1 <i>Introduction</i>                                              | 11        |
| 2.2 <i>Large-scale bed composition measurements in Dutch systems</i> | 12        |
| 2.2.1 <i>Object and methods</i>                                      | 12        |
| 2.2.2 <i>Data inventory</i>                                          | 14        |
| 2.2.3 <i>Segregation parameters</i>                                  | 17        |
| 2.2.4 <i>Sand-mud patterns in the Wadden Sea</i>                     | 19        |
| 2.2.5 <i>Sand-mud patterns in the Scheldt estuary</i>                | 20        |
| 2.2.6 <i>Sand-mud patterns in the Haringvliet - Hollandsch Diep</i>  | 24        |
| 2.3 <i>Processes and mechanisms behind sand-mud segregation</i>      | 24        |
| 2.3.1 <i>Scale concept</i>                                           | 24        |
| 2.3.2 <i>Hydrodynamic processes</i>                                  | 26        |
| 2.3.3 <i>Vertical sediment transport processes</i>                   | 26        |
| 2.3.4 <i>Mechanisms</i>                                              | 31        |
| 2.4 <i>Predictive models</i>                                         | 35        |
| 2.4.1 <i>Empirical and hybrid models</i>                             | 35        |
| 2.4.2 <i>Process-based models</i>                                    | 36        |
| 2.4.3 <i>Bed composition variations in process-based models</i>      | 38        |
| 2.5 <i>Conclusions</i>                                               | 41        |

|          |                                                      |           |
|----------|------------------------------------------------------|-----------|
| <b>3</b> | <b>Erosion of sand-mud mixtures</b>                  | <b>45</b> |
| 3.1      | <i>Introduction</i> . . . . .                        | 45        |
| 3.2      | <i>Classification</i> . . . . .                      | 46        |
| 3.2.1    | Limitations . . . . .                                | 46        |
| 3.2.2    | Classification parameters . . . . .                  | 47        |
| 3.2.3    | Classification diagram . . . . .                     | 49        |
| 3.2.4    | Experimental validation . . . . .                    | 51        |
| 3.2.5    | Relevance of bed types in natural systems . . . . .  | 55        |
| 3.3      | <i>Mathematical formulations</i> . . . . .           | 57        |
| 3.3.1    | Sand and mud only . . . . .                          | 57        |
| 3.3.2    | Non-cohesive sand-mud mixtures . . . . .             | 58        |
| 3.3.3    | Cohesive sand-mud mixtures . . . . .                 | 62        |
| 3.3.4    | Experimental validation . . . . .                    | 67        |
| 3.4      | <i>Conclusions</i> . . . . .                         | 68        |
| <b>4</b> | <b>Set-up of a process-based sand-mud model</b>      | <b>71</b> |
| 4.1      | <i>Introduction</i> . . . . .                        | 71        |
| 4.2      | <i>Flow module</i> . . . . .                         | 72        |
| 4.2.1    | Equations . . . . .                                  | 72        |
| 4.2.2    | Parameters . . . . .                                 | 73        |
| 4.3      | <i>Sediment transport module</i> . . . . .           | 74        |
| 4.3.1    | Equations . . . . .                                  | 74        |
| 4.3.2    | Boundary conditions . . . . .                        | 75        |
| 4.3.3    | Parameters . . . . .                                 | 77        |
| 4.4      | <i>Bed module</i> . . . . .                          | 78        |
| 4.4.1    | Equations . . . . .                                  | 78        |
| 4.4.2    | Boundary conditions . . . . .                        | 80        |
| 4.4.3    | Parameters . . . . .                                 | 81        |
| 4.5      | <i>Numerical implementation</i> . . . . .            | 83        |
| 4.5.1    | Overview of extensions . . . . .                     | 83        |
| 4.5.2    | Discretization of bed composition equation . . . . . | 84        |
| 4.5.3    | Stability and accuracy restrictions . . . . .        | 86        |
| 4.6      | <i>Summary</i> . . . . .                             | 88        |
| <b>5</b> | <b>Behaviour analysis of idealised situations</b>    | <b>91</b> |
| 5.1      | <i>Introduction</i> . . . . .                        | 91        |
| 5.2      | <i>Local situation</i> . . . . .                     | 92        |
| 5.2.1    | Model set-up . . . . .                               | 92        |
| 5.2.2    | Overview of situations . . . . .                     | 94        |
| 5.2.3    | Situation I: Deposition . . . . .                    | 95        |

|          |                                                                          |            |
|----------|--------------------------------------------------------------------------|------------|
| 5.2.4    | Situation 2: Deposition and non-cohesive erosion . . . . .               | 98         |
| 5.2.5    | Situation 3: Deposition, non-cohesive and cohesive erosion . . . . .     | 101        |
| 5.2.6    | Field measurements . . . . .                                             | 102        |
| 5.3      | <i>Reservoir</i> . . . . .                                               | 105        |
| 5.3.1    | Model set-up . . . . .                                                   | 105        |
| 5.3.2    | Results . . . . .                                                        | 109        |
| 5.3.3    | Analysis . . . . .                                                       | 111        |
| 5.3.4    | Field measurements . . . . .                                             | 114        |
| 5.4      | <i>Tidal basin</i> . . . . .                                             | 117        |
| 5.4.1    | Model set-up . . . . .                                                   | 117        |
| 5.4.2    | Results . . . . .                                                        | 120        |
| 5.4.3    | Analysis . . . . .                                                       | 121        |
| 5.4.4    | Previous investigations on short tidal basins . . . . .                  | 127        |
| 5.4.5    | Field measurements . . . . .                                             | 129        |
| 5.5      | <i>Conclusions</i> . . . . .                                             | 130        |
| <b>6</b> | <b>Application to Friesche Zeegat</b>                                    | <b>133</b> |
| 6.1      | <i>Introduction</i> . . . . .                                            | 133        |
| 6.2      | <i>Morphological development</i> . . . . .                               | 134        |
| 6.2.1    | Area description . . . . .                                               | 134        |
| 6.2.2    | Data availability . . . . .                                              | 135        |
| 6.2.3    | Morphological response . . . . .                                         | 136        |
| 6.3      | <i>Model set-up</i> . . . . .                                            | 140        |
| 6.3.1    | Computational grid and bathymetry . . . . .                              | 140        |
| 6.3.2    | Open sea boundary conditions . . . . .                                   | 141        |
| 6.3.3    | Initial conditions . . . . .                                             | 143        |
| 6.3.4    | Parameter settings . . . . .                                             | 143        |
| 6.4      | <i>Calibration and verification of the hydrodynamic module</i> . . . . . | 144        |
| 6.4.1    | Flow . . . . .                                                           | 144        |
| 6.4.2    | Short waves . . . . .                                                    | 149        |
| 6.5      | <i>Results morphological computations</i> . . . . .                      | 150        |
| 6.5.1    | General . . . . .                                                        | 150        |
| 6.5.2    | Ebb-tidal delta . . . . .                                                | 151        |
| 6.5.3    | Tidal basin . . . . .                                                    | 153        |
| 6.5.4    | Sensitivity analysis . . . . .                                           | 158        |
| 6.6      | <i>Discussion of the morphological computations</i> . . . . .            | 162        |
| 6.6.1    | Ebb-tidal delta . . . . .                                                | 162        |
| 6.6.2    | Tidal basin . . . . .                                                    | 164        |
| 6.6.3    | Perspectives of model applicability . . . . .                            | 169        |

---

|          |                                                   |            |
|----------|---------------------------------------------------|------------|
| 6.7      | <i>Conclusions</i> . . . . .                      | 170        |
| <b>7</b> | <b>Conclusions and recommendations</b>            | <b>173</b> |
| 7.1      | <i>Conclusions</i> . . . . .                      | 174        |
| 7.2      | <i>Recommendations</i> . . . . .                  | 177        |
|          | <b>References</b>                                 | <b>179</b> |
| <b>A</b> | <b>Erosion formulations for sand-mud mixtures</b> | <b>189</b> |
| <b>B</b> | <b>Stability</b>                                  | <b>193</b> |
| <b>C</b> | <b>Mud deposition and erosion coefficient</b>     | <b>195</b> |
| <b>D</b> | <b>Mud wave characteristics</b>                   | <b>199</b> |
| D.1      | <i>Onset</i> . . . . .                            | 199        |
| D.2      | <i>Mud concentration</i> . . . . .                | 200        |
| D.3      | <i>Maximum mud deposition</i> . . . . .           | 201        |
|          | <b>List of Figures</b>                            | <b>205</b> |
|          | <b>List of Tables</b>                             | <b>211</b> |
|          | <b>List of Symbols</b>                            | <b>213</b> |

# Chapter 1

## Introduction

### 1.1 Sand-mud segregation

Estuaries and tidal basins interrupt a large part of the world coastline (Figure 1.1). For instance, Emery (1967) estimates that these systems occupy 80 - 90% of the Atlantic and Gulf coasts and 10 - 20% of the Pacific Coasts around the United States. Their appearances vary strongly throughout the world and are dependent on the local climatological, geographical, geological and hydrodynamic conditions (Perillo, 1995).

Bed sediments in estuaries and tidal basins often consist of sand as well as mud. The term mud is widely used and refers to the combination of silt and clay fractions. The river discharge and tidal motion in these systems cause displacements of the bed sediments. The magnitude and the direction of these displacements generally depend on the sediment properties, particularly the grain size distribution and its cohesiveness. Sand and mud can be deposited as mixtures, in alternating layers or in different areas of the system. As a result, the mud content in these systems is not uniform, but shows strong variations in both horizontal and vertical directions. This phenomenon is called sand-mud segregation.

Venema et al. (1999) present an example of horizontal sand-mud segregation based on detailed bed composition measurements in the Hollandsch Diep (Figure 1.2) (see also Venema et al., 1998; Van Wijngaarden et al., 2002a, 2002b). This area is part of the Rhine-Meuse estuary in the southwest of the Netherlands (Figure 1.2a) and consists of a deep channel with shallow borders and several flats (Figure 1.2b). Mud content variations can be observed in the cross-direction between borders and the channel, but the mud content also varies in the longitudinal direction (Figure 1.2c). The mud content in the central part of the Hollandsch Diep is much higher than in the west and near the river branches Nieuwe Merwede and Amer in the east.

### 1.2 The need for modelling sand-mud segregation

Estuaries and tidal basins are attractive areas for both nature and mankind. The intertidal flats form important feeding, resting and breeding zones for large populations of birds and the deeper

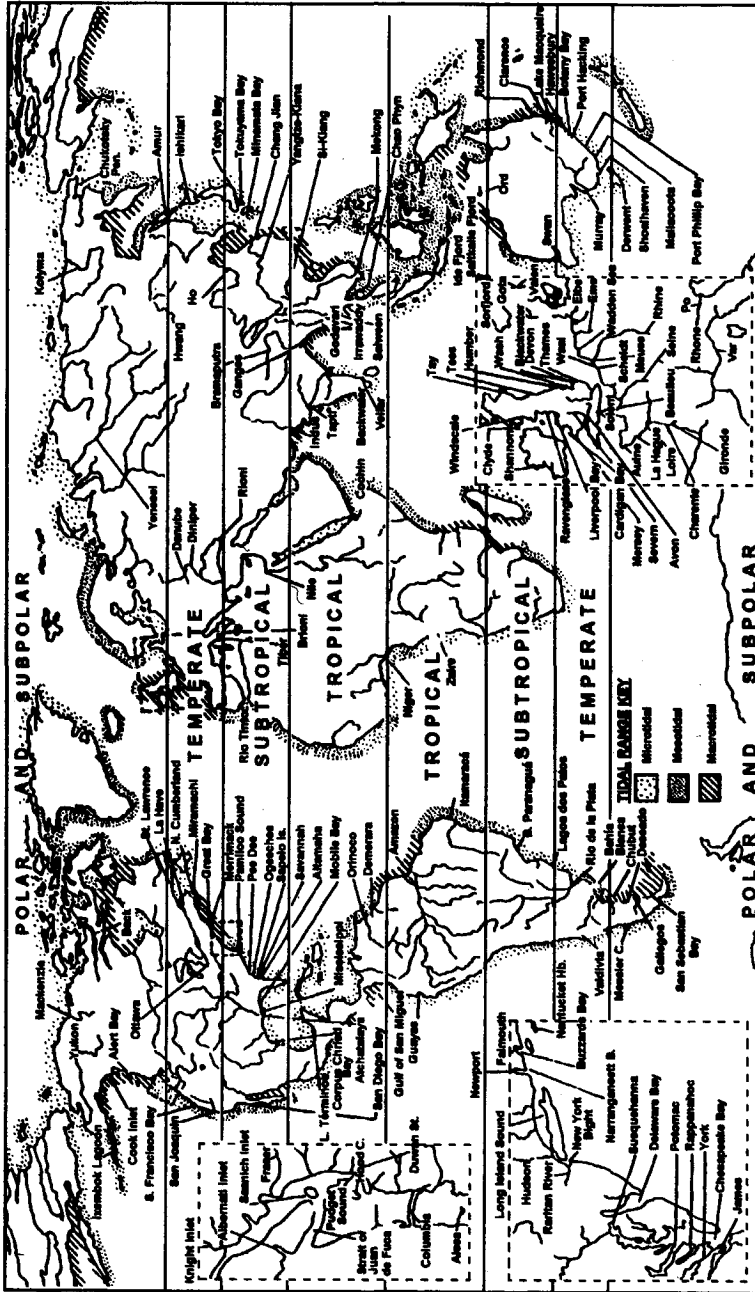
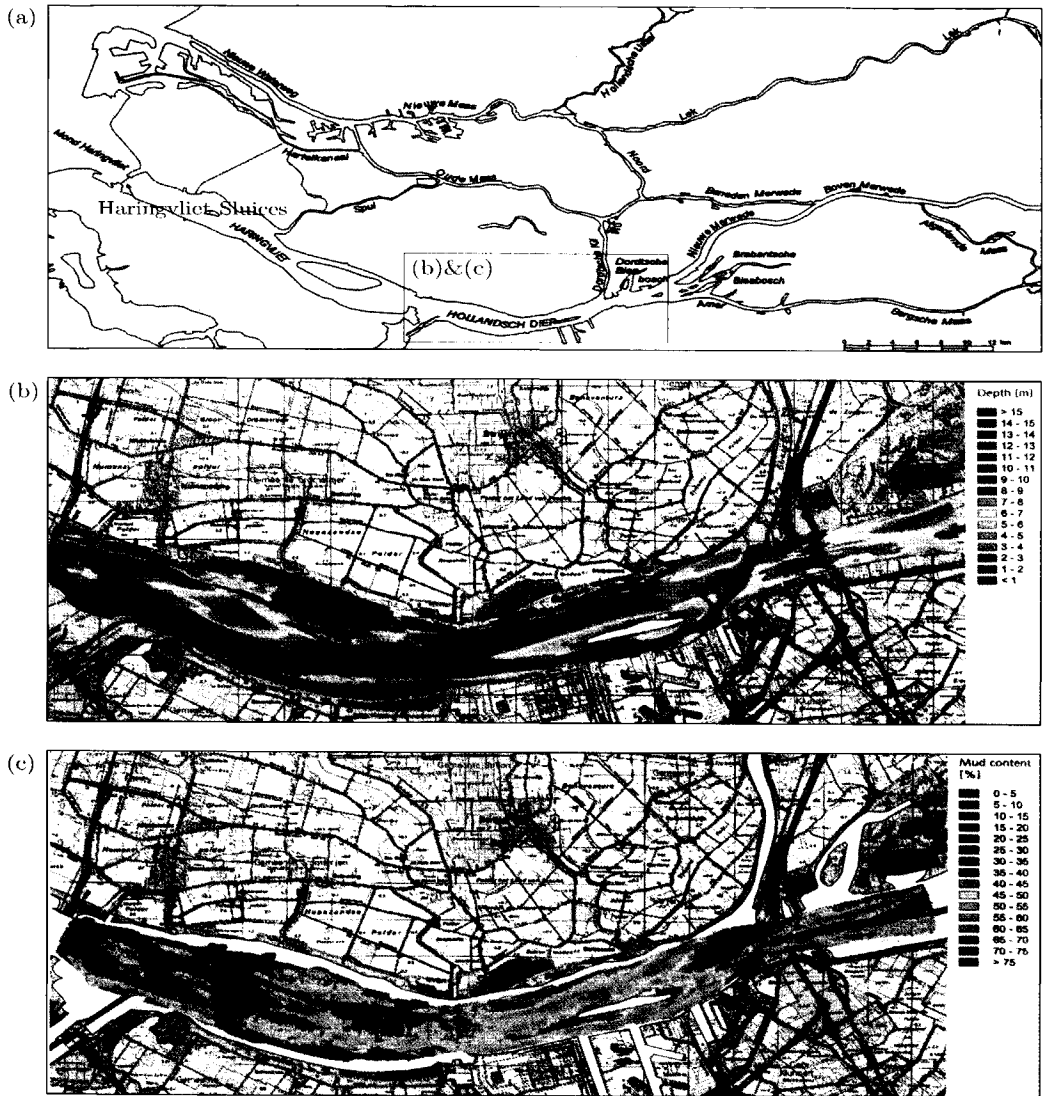


Figure 1.1: Distribution of major estuaries and tidal basins in the world (Perillo, 1995).





**Figure 1.2:** Horizontal sand-mud segregation in the Hollandsch Diep, the Netherlands: a) Location, b) water depth and c) mud content ( $\% \leq 0.063$  mm) in the upper 30 cm of the bed (Venema et al., 1999).

channels often serve as major shipping routes. Additionally, the surroundings of these systems are often occupied with large cities, harbours, industrial areas and recreational facilities. The attractiveness of these zones is largely explained by the relatively mild natural conditions, the abundant availability of food for species and the special geographical position between the river and the sea.

Sustainable management and development of these valuable systems require profound knowledge and reliable predictive modelling tools for estimating the effects of human interventions or natural changes on the system behaviour. Well-known examples of these alterations are channel deepening, land reclamations, harbour extensions or sea level rise. An important aspect of the system behaviour concerns the horizontal and vertical distributions of sand and mud (i.e. sand-mud segregation) in these systems. Physical understanding and predictive capability concerning this phenomenon is of particular interest for various management issues. These are discussed below:

- Large mud content variations at the bed surface indicate that both sand and mud contribute significantly to bed level changes in estuaries and tidal basins. In general, these changes affect the navigation depth and high water levels. Predicting the distribution of sand and mud is therefore important for the safety of the surrounding areas and the maintenance of navigation channels.
- Furthermore, it has long been known that the pollutants tend to adhere to mud because of its cohesive properties (see e.g. Förstner & Wittmann, 1979; De Groot et al., 1982). In general, a linear correlation is obtained between the concentration of heavy metals and the mud content (De Groot et al., 1982). This parameter is therefore an important indicator of the (potential) degree of pollution in the sediment bed.
- Finally, the mud content in the sediment bed is also a crucial habitat parameter, which controls the distribution of flora and fauna in these systems (see e.g. Reid & Wood, 1976; Kennish, 1986). For example, Dyer et al. (2000) show that the sediment type and the grain size are the best physical descriptors of floral and faunal assemblages in the upper zone of the intertidal mud flats.

The need for understanding and modelling sand-mud segregation can be further illustrated when the aforementioned Rhine-Meuse estuary is considered (see Section 1.1). The Haringvliet Sluices, indicated in Figure 1.2a, were constructed in 1970 to protect the hinterland from storm surges and to control the navigation depth and salt intrusion in the Rotterdam harbour under low river discharge conditions. As a result, an enormous amount of sand and mud has been deposited in the various branches of the system. The present management strategy is that these sluices are only open during ebb tide. In future, the sluices will also be partially open during flood in order to re-introduce tidal motion into the system. An intriguing question is what the bed level and bed composition development will be after changing the management. An important prerequisite for a reliable answer to this question is a modelling tool in which the effect of sand-mud segregation is included.

### 1.3 Problem definition

Bed sediments in estuaries and tidal basins generally consist of sand, silt and clay and sometimes gravel. These sediment fractions are classified according to their individual particle size into gravel (2 - 64 mm), sand (0.063 - 2 mm), silt (0.004 - 0.063) and clay (< 0.004 mm). The silt and clay fractions are often combined and called mud ( $\leq 0.063$  mm). Other widely used bed composition parameters are the mean grain size of the sand and gravel fraction. We will limit ourselves to systems with predominantly sand, silt and clay.

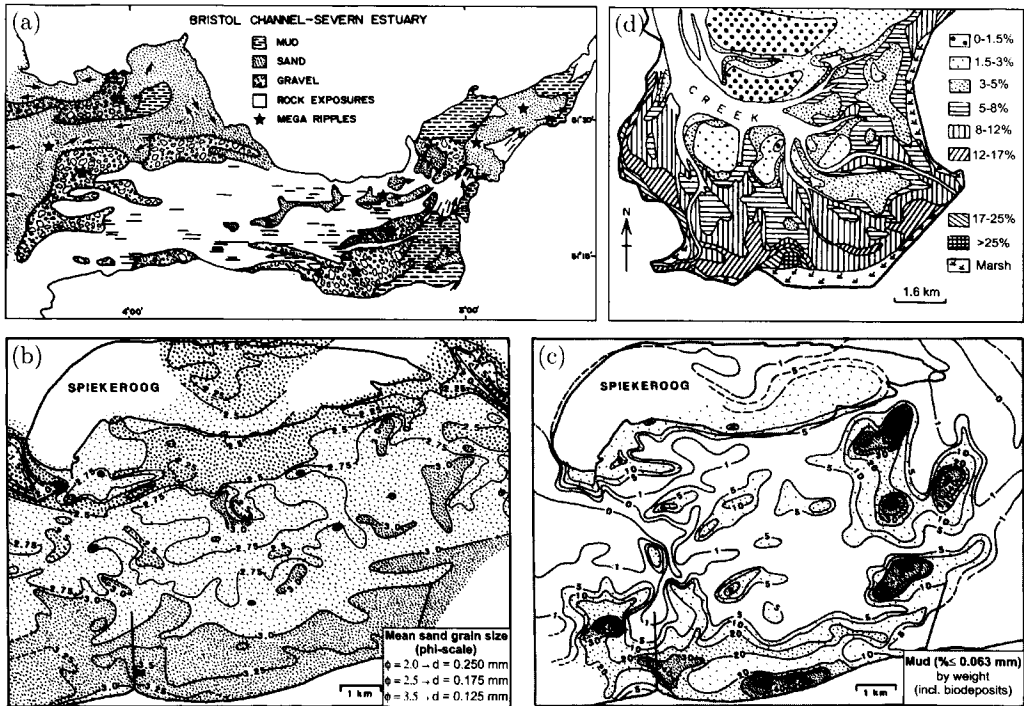


**Figure 1.3:** Examples of horizontal bed composition variations: a) Distribution of sediments in the Bristol Channel and Severn estuary (Wells, 1995), b) Mean sand grain size and c) Mud content distribution in the tidal basin south of Spiekeroog Island, German Wadden Sea (Flemming and Ziegler, 1995), d) Percentages of fine-grained matter ( $\% < 0.002$  mm) in the Lauwerszee, Dutch Wadden Sea (Van Straaten and Kuenen, 1957).

Various authors have discussed horizontal bed composition variations in estuaries and tidal basins all over the world. Three examples are shown in Figure 1.3. Wells (1995) shows global distributions of gravel, sand and mud in the Severn estuary and the adjacent Bristol channel (England) (Figure 1.3a). At a somewhat smaller scale, Flemming and Ziegler (1995) present the mean sand grain size (Figure 1.3b) and the mud content distribution (Figure 1.3c) at the bed surface south of Spiekeroog Island in the German Wadden Sea. Van Straaten and Kuenen

(1957) give a very detailed example of the clay content variations in the Lauwerszee, a former part of the Friesche Zeegat in the Dutch Wadden Sea (Figure 1.3d).

These examples show two important aspects for the definition of the phenomenon that is the subject of this thesis (Figure 1.3). Firstly, the example of the tidal basin near Spiekeroog Island indicates horizontal segregation of different sand grain sizes (Figure 1.3b), but also segregation of sand and mud fractions (Figure 1.3c). Clearly, these segregation phenomena cannot be treated separately, but we will focus on horizontal distributions of sand and mud in these systems. Secondly, the examples also indicate that bed composition variations can be observed at different spatial scales, varying from global variations along the main axis of an estuary over hundreds of kilometers (Figure 1.3a) to very detailed variations on a tidal flat within several hundreds of meters (Figure 1.3d). Such a hierarchy of different spatial scales (and temporal scales) is a well-known characteristic in these systems (see e.g. De Vriend, 1991a; De Boer, 1992; Jeuken, 2000). For defining our scale of interest, a useful classification of different scale levels is given in Figure 1.4. Herein, we focus on the large-scale distributions of sand and mud. The scale of interest varies from several kilometers (decade) to tens of kilometers (centuries).

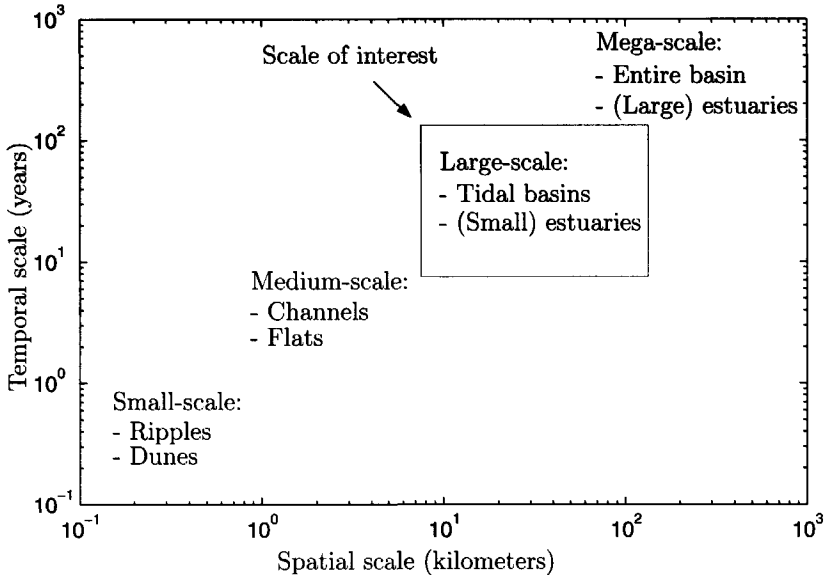


**Figure 1.4:** Spatial and temporal scales in estuaries.

At present, the mechanisms which lead to large-scale sand-mud segregation are insufficiently understood. The rule-of-thumb:

**“The calmer the water, the finer the bed sediment”**

is generally used for explaining the variation in mud content. From a physical point of view, this

explanation is not satisfactory, because fine sediments can be transported over large distances before settling. Other segregation mechanisms which are often mentioned, are differences in settling and pick-up (De Glopper, 1967), tidal asymmetry for coarse particles (Aubrey, 1986) and fine particles (Groen, 1967; Dronkers, 1986a), gravitational circulation (Dyer, 1994), local wind waves and biological activity on tidal flats (Ten Brinke, 1993; Oost, 1995).

The lack of understanding is reflected in the currently used large-scale models for estuaries and tidal basins. These models are commonly classified into empirical models, hybrid models, process-based and idealised models (De Vriend, 1991b). At present, only a few empirical models (WL|Delft Hydraulics, 1998) and one hybrid model (Wang, 1997) are available for predicting mud content variations. The empirical modelling approaches are to a large extent based on the aforementioned rule-of-thumb. A parameter is computed based on local hydrodynamic conditions and correlated with the local bed composition. The hybrid approach includes information about the basic processes influencing sediment transport, too. An example of the predictive performance of the hybrid model LHEC (acronym for Local Hypothetical Equilibrium Concentration) is shown in Figure 1.5 (Wang, 1997). Although LHEC can discriminate between areas with low mud content ( $< 10\%$ ) and other areas, a quantitative relationship cannot be defined. The scatter is large especially for low values of LHEC, which corresponds with low bed shear stress (see also Kuijper, 2001). So far, explanations for this typical pattern have not been given.

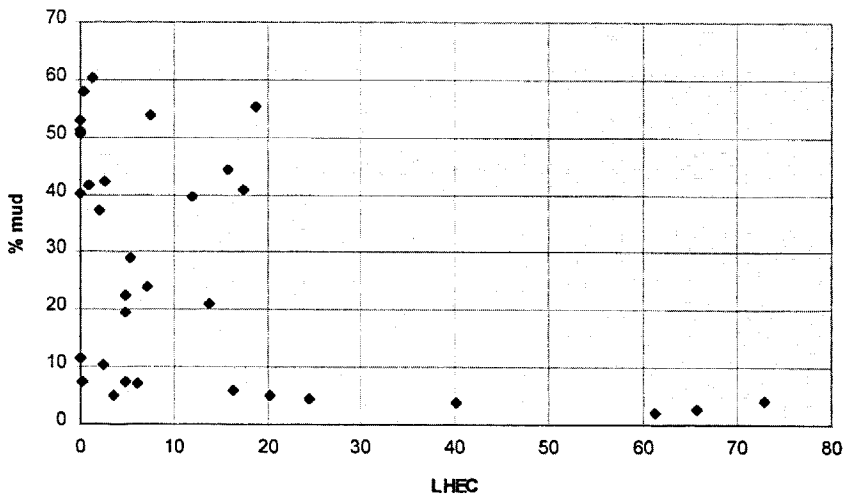


**Figure 1.5:** Correlation between the hybrid model LHEC and the observed mud content ( $\% \leq 0.063$  mm) at bed surface of the Nieuwe Merwede, the Netherlands (Wang, 1997).

Process-based models and idealised models consist of a coupled set of mathematical equations for hydrodynamics, sediment transport and bed evolution. At present, these models only exist for sand (Van Rijn, 1993) or mud (Teisson, 1997) separately. For estuaries and tidal basins,

a representative sediment size is generally used for calculating sediment transport rates, while mud content variations in time and space are neglected. Although mechanisms behind sediment segregation have been investigated separately for sand and mud, a comprehensive large-scale process-based model, in which mechanisms are brought together to explain large-scale sand-mud segregation, does not exist at present. The development of such a model is necessary to increase the physical understanding and the predictive capability concerning this phenomenon.

## 1.4 Objectives

This research aims at contributing to the understanding and modelling of large-scale sand-mud segregation in estuaries and tidal basins. Specific objectives are:

- to characterise the phenomenon of large-scale sand-mud segregation and to identify the underlying processes and mechanisms;
- to propose a model in which (part of) these processes and mechanisms are incorporated and which can be used for describing morphological behaviour including the effect of sand-mud segregation;
- to predict the trends of morphological evolution of systems including the effect of sand-mud segregation and to verify these trends with field data;

## 1.5 Approach

The research approach is visualised in Figure 1.6. First, large-scale bed composition data from Dutch systems are discussed in Chapter 2 in order to get insight into the phenomenon of large-scale sand-mud segregation and - in a later phase - for verifying the model results. Furthermore, processes and mechanisms are identified that should be included in our model. Finally, existing predictive models and concepts for bed composition modelling are summarised against the background of their applicability in our process-based model.

Following from Chapter 2, an important prerequisite for a process-based model with sand and mud is a proper erosion formulation for sand-mud mixtures. Yet, these formulations do not exist at present. Therefore, a classification for the erosion behaviour of sand-mud mixtures is developed and an erosion formulation for these mixtures is proposed in Chapter 3. Next, a process-based model is presented in Chapter 4, in which the effect of sand-mud segregation is included. The extensions to the present-day flow module, sediment transport module and bed module are discussed and its numerical implementation is described.

The behaviour of the sand-mud model is analysed and verified through experiments with a numerical model. First, three idealised situations are considered in Chapter 5: a local situation, a

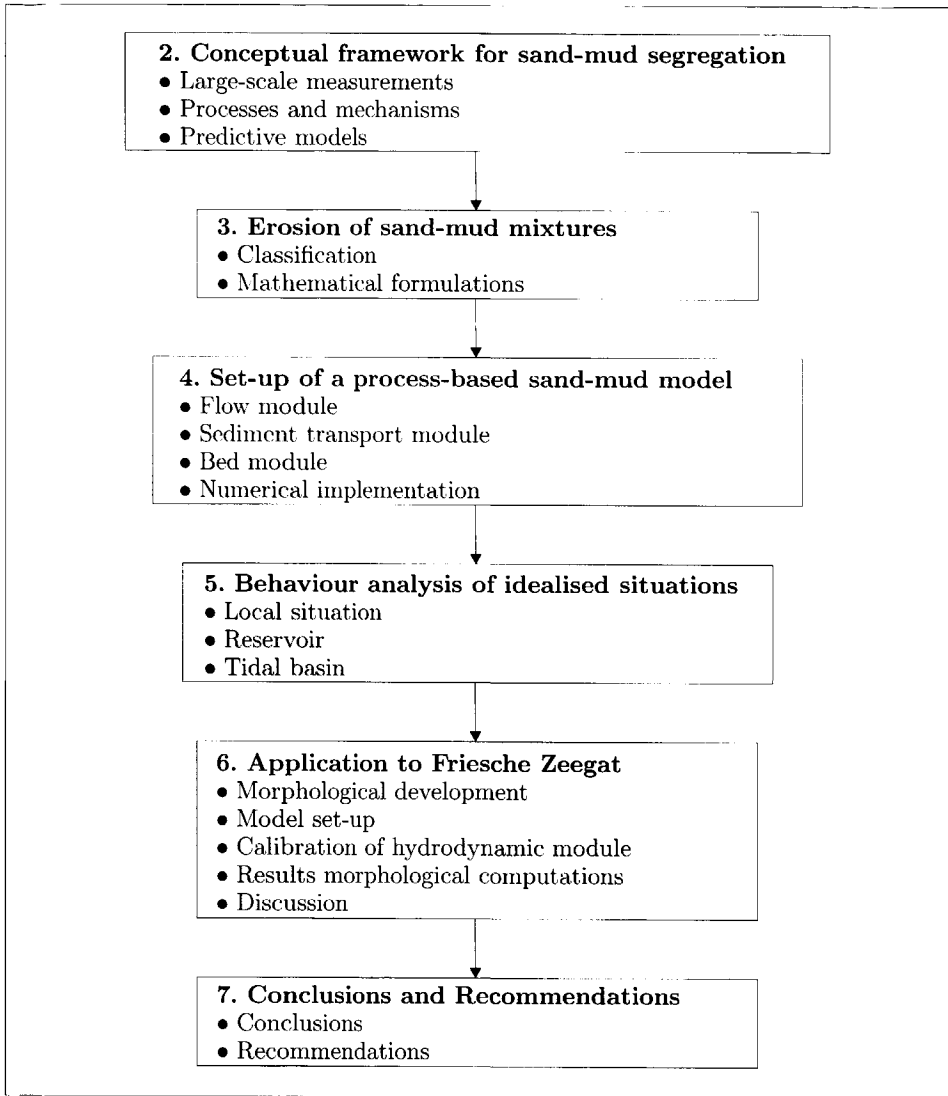


**Figure 1.6:** Graphical representation of thesis set-up.

reservoir and a tidal basin. The emphasis is on deriving parameters that govern the distribution of sand and mud in these situations. Also, the model results are compared qualitatively with field measurements. Thereafter, sand-mud segregation in the Friesche Zeegat (the Netherlands) is investigated as a realistic case in Chapter 6. The observed morphological development after the closure of the Lauwerszee (1969) is hindcasted with the model and the results are compared with field measurements.

Finally, conclusions and recommendations are summarised in Chapter 7.





## Chapter 2

# Conceptual framework for sand-mud segregation

### 2.1 Introduction

Although many studies have emphasised the phenomenon of large-scale sand-mud segregation in estuaries and tidal basins, the number of studies directly dedicated to the understanding and modelling of this phenomenon is limited. The main reason is that sand and mud were largely studied separately in preceding decades because of important differences in their behaviour in the bed as well as in the water column. Only recently, a few studies have concentrated on the behaviour of sand-mud mixtures (Torfs, 1995; Mitchener & Torfs, 1996).

A large number of studies exist that are related to sediment segregation in general, but these are scattered over different research fields. Roughly, the following classification can be made:

- **Descriptive studies:** Various sedimentological studies exist in which bed composition variations are described and qualitatively explained for specific estuaries and tidal basins. For example, De Glopper (1967) describes a large-scale bed composition survey in the Wadden Sea (the Netherlands) and qualitatively explains bed composition variations. In addition, several sedimentologists have tried to relate spatial changes in grain size distribution parameters to the sediment transport patterns. A well-known example is McLaren (1981), who deploys a method for identifying net transport paths of different sediment sizes based on changes in the mean, sorting and skewness of the measured grain size distributions (see also McLaren & Bowles, 1985).
- **Process-oriented studies:** Specific processes have been investigated separately for sand and mud (e.g. erosion, deposition) by means of laboratory or field experiments. Van Rijn (1993) and Whitehouse et al. (2000) give an extensive overview of experimental results, conceptual models and various formulations for sand beds and for mud beds, respectively. Moreover, mechanisms for net horizontal transport of either sediment fraction (e.g. tidal asymmetry) are extensively examined. Overviews of important net transport mechanisms in estuaries and tidal basins are given by Dyer (1997) and Nichols and Boon (1994), respectively.

- **Predictive model studies:** Large-scale models for estuaries and tidal basins are commonly classified into empirical, hybrid and process-based models (De Vriend, 1991b). Only a few studies have tried to relate the mud content variations to an empirical or hybrid parameter (Wang, 1996). Process-based and idealised models only exist for sand (Van Rijn, 1993) and mud (Teisson, 1997) separately and mud content variations in time and space are not presently included in these models. Only one example in the literature exists of a process-based sand-mud model (Chesher & Ockenden, 1997). On the other hand, concepts for modelling multiple sand fractions in process-based models have existed since the early 1970's and have been extensively analysed and applied in river situations (see e.g. Ribberink, 1987; Armanini, 1995).

This chapter aims to give a conceptual framework for a process-based sand-mud model (Chapter 3 and 4) and its implementation and testing in a numerical model (Chapter 5 and 6). Following the aforementioned classification, three main topics with respect to large-scale sand-mud segregation are discussed consecutively. In Section 2.2, we discuss large-scale bed composition measurements in Dutch systems, in order to gain insight into the phenomenon of interest and - in a later phase - to verify model results. Important aspects to be addressed are the availability and quality of the data, the characterisation of the bed composition and the observed sand-mud patterns. Next, we describe processes and mechanisms that are relevant to the understanding and modelling of large-scale sand-mud segregation (Section 2.3). These processes and mechanisms are to be included in a process-based model. In particular, the limited understanding of the erosion process of sand-mud mixtures has prevented this type of model development so far. Finally, the possibilities and limitations of the current large-scale models are discussed in Section 2.4. In addition, existing concepts for modelling the bed composition are summarised in preparation for the development of a process-based model with multiple sediment fractions.

## 2.2 Large-scale bed composition measurements in Dutch systems

### 2.2.1 Object and methods

#### Classification

Fine sediment particles are generally classified according to their individual grain size, with sand, silt and clay as the principal classes (see e.g. Van Rijn, 1993). Often, the grain size ( $d$ ) is expressed on a metric scale, but the  $\phi$ -scale, defined as  $\phi = -2 \log d$  ( $d$  in mm) is used as an alternative (Krumbein, 1936). The boundaries between the sediment classes are given in Table 2.1. A subdivision of the sand fraction is included in the list. Although mud is not a specific fraction in the standard sediment classifications, the term is widely used and defined as all sediment with grain size less than 0.063 mm (i.e. silt and clay).

**Table 2.1:** Sediment classification.

| Class name    | $d$ (mm)           | $\phi$       |
|---------------|--------------------|--------------|
| Sand          | $0.063 \div 2$     | $-1 \div +4$ |
| - Very coarse | $1 \div 2$         | $-1 \div 0$  |
| - Coarse      | $0.5 \div 1$       | $0 \div +1$  |
| - Medium      | $0.25 \div 0.5$    | $+1 \div +2$ |
| - Fine        | $0.125 \div 0.25$  | $+2 \div +3$ |
| - Very fine   | $0.063 \div 0.125$ | $+3 \div +4$ |
| Silt          | $0.004 \div 0.063$ | $+4 \div +8$ |
| Clay          | $< 0.004$          | $> +8$       |
| Mud           | $\leq 0.063$       | $\geq +4$    |

### Grain size distribution

The composition of a sediment sample is characterised by the distribution of grain size by percentage of weight, yielding the so-called grain size distribution (see e.g. Van Rijn, 1993). It is important to note that 'the grain size' in the silt and clay range is not well defined, because these sediment fractions are able to form aggregates or flocs in suspension. Aggregates are still present in the bed after deposition. Normally, a sediment sample is first deflocculated before the grain size distribution is determined. In this case, the grain size distribution of the individual sediment particles is obtained. If an untreated sample is analysed, the resulting grain size distribution includes part of the flocs in the bed. As a result, the distribution of an untreated sample generally underestimates the percentage of clay particles.

Important grain size distribution parameters are the sand content (%0.063 - 2 mm), silt content (%0.004 - 0.063 mm), clay content (%< 0.004 mm) and mud content (% $\leq$  0.063 mm) by dry weight of a sample. Unless otherwise stated, the 'content' of a specific sediment fraction refers to the amount of sediment by dry weight throughout this thesis. Other important characteristics, which are generally used for the sand fraction only, are the mean ( $d_m$ ) and median diameter ( $d_{50}$ ) and the sorting index ( $S_i$ ). The mean diameter is defined as  $d_m = \sum(p_i d_i)$  in which  $p_i$  is the percentage of dry weight of each fraction with grain size  $d_i$ . The median diameter is the size at which 50% by dry weight is finer. The sorting index  $S_i = \frac{1}{2} \left( \frac{d_{50}}{d_{16}} + \frac{d_{84}}{d_{50}} \right)$  and expresses the gradation within the sand fraction (Raudkivi, 1990). A sand grain size distribution with a sorting index less than about 1.35 is called uniform (and poorly sorted), whereas a distribution with a much higher sorting index is strongly non-uniform (and well-sorted).

### Sampling methods

Various sampling techniques exist for fine sediments in order to determine the bed composition (see e.g. Van Rijn, 1993). Traditionally, grabs are used for collecting a surface sample of the bed material. A so-called 'disturbed' sample with a thickness of about 10 cm is obtained with

the widely used 'Van Veen' grab. Hence, the mean composition of the upper 10 cm of the sediment bed is determined with this sampling technique. Recently, a new in-situ technique has been developed for monitoring the bed surface (De Meijer et al., 1996). This so-called MEDUSA (acronym for Multi Detector system for Underwater Sediment Activity) is trailed over the sediment bed by a vessel and measures the activity concentrations of different natural radionuclides in the sediment bed. Because sand and mud have different radiometric characteristics, MEDUSA is suitable for mapping the mud fraction by calibrating the radiometric characteristics to the mud content of several traditional samples. Van Wijngaarden et al. (2002a) state that the mean composition of the upper 30 cm of the sediment bed is determined with this technique. The absolute error in the radiometrically derived mud content is 4 - 10% compared with the mud content obtained by means of a grain size analysis.

### Analysis methods

The grain size distribution of a bed sample can be obtained by several analysis methods (see e.g. Van Rijn, 1993; Berlamont et al., 1993). Sieve analysis is an easy and reliable method and is applicable for grain sizes ranging from 0.1 mm to 50 mm. The grain size distribution is much more difficult to obtain in the silt and clay range. Techniques with different accuracy include light diffraction (e.g. Malvern), conductivity (e.g. Coulter Counter) or sedimentation of a dispersed suspension (e.g. Pipet-withdrawal tube, Sedigraph) (see e.g. Van Rijn, 1993; Berlamont et al., 1993). Different tests with a Malvern indicate that this technique strongly underestimates (up to 80%) the percentage of sediment smaller than 0.002 mm within a sample. Furthermore, the results up to grain sizes of 0.016 mm are not very accurate. Results obtained with a Coulter Counter are often inaccurate due to the possibility of floc breakage. Moreover, small vibrations and radio frequency waves in the vicinity can cause inaccurate results. Sedimentation methods give reliable results for the entire distribution. The only restriction seems to be the sample concentration which should be less than about 5 - 10 g/l in order to avoid accuracy problems.

### 2.2.2 Data inventory

An inventory is made of large-scale bed composition data for the Dutch tidal basins and estuaries. The characteristics of these measurements are summarised in Table 2.2 and the locations of these areas are shown in Figure 2.1. The inventory shows that the availability of large-scale bed composition data is scarce. Only one measurement campaign is digitally available for the Wadden Sea (RIKZ, 1998), the Scheldt estuary (McLaren, 1994) and the Haringvliet - Hollandsch Diep (Van Wijngaarden et al., 2002a, 2002b). Furthermore, the sampling year and season differ in the Wadden Sea campaign during the 1990's. The samples are mostly collected during spring, but the surveys in the Vlie and the Ems-Dollard estuary were during summer and autumn, respectively. Although the sampling area of the Molenplaat is relatively small, the data set is valuable because it gives time-dependent information about the bed composition

**Table 2.2:** Characteristics of large-scale bed composition measurements in the Netherlands (see Figure 2.1 for the area locations).

| Area                    | Resolution (m)        | Sample thickness (m) | Sampling year (month) | Sampling method | Analysis method <sup>1</sup> | Parameters                                              | Reference                               |
|-------------------------|-----------------------|----------------------|-----------------------|-----------------|------------------------------|---------------------------------------------------------|-----------------------------------------|
| Wadden Sea <sup>2</sup> | 900                   | 0.25                 | 1950 - 1955 (?)       | grab            | Pipet (?)                    | $d_{50}$ , %clay                                        | De Glopper (1967)                       |
| Ems-Dollard             | 500 - 1000            | 0.10                 | 1989 (9-12)           | grab            | Malvern (-)                  | full distribution                                       | RIKZ (1998)                             |
| Dollard                 | 500 - 1000            | 0.10                 | 1991 (9-10)           | grab            | Malvern (-)                  | full distribution                                       | Ibid.                                   |
| Lauwers, Schild         | 500 - 1000            | 0.10                 | 1996 (4-7)            | grab            | Malvern (-)                  | full distribution                                       | Ibid.                                   |
| Friesche Zeegat         | 500 - 1000            | 0.10                 | 1994 (4-7)            | grab            | Malvern (-)                  | full distribution                                       | Ibid.                                   |
| Borndiep                | 500 - 1000            | 0.10                 | 1995 (4-7)            | grab            | Malvern (-)                  | full distribution                                       | Ibid.                                   |
| Vlie                    | 500 - 1000            | 0.10                 | 1995 (5-8)            | grab            | Malvern (-)                  | full distribution                                       | Ibid.                                   |
| Eijerlandse Gat         | 500 - 1000            | 0.10                 | 1993 (4-7)            | grab            | Malvern (-)                  | full distribution                                       | Ibid.                                   |
| Marsdiep                | 500 - 1000            | 0.10                 | 1993 (4-7)            | grab            | Malvern (-)                  | full distribution                                       | Ibid.                                   |
| Scheldt estuary         | 500                   | 0.10                 | 1992 (?)              | grab            | Malvern (-)                  | full distribution                                       | Ibid.                                   |
| Molenplaat              | 125 - 250             | 0.01                 | 1995 (3,6,9,12)       | grab            | Sedigraph (+)<br>Malvern (?) | full distribution<br>%mud, %coarse<br>%fine, %very fine | McLaren (1994)<br>Thoolen et al. (1997) |
| Hollandsch Diep         | 20 & 500 <sup>3</sup> | 0.30                 | 1998 (7)              | MEDUSA          | Radiometry<br>& Malvern (+)  | %sand, %mud<br>%lutum (< 8 $\mu$ m)                     | Van Wijngaarden<br>et al. (2002a,b)     |
| Haringvliet             | 20 & 500 <sup>3</sup> | 0.30                 | 1999 (8)              | MEDUSA          | idem                         | idem                                                    | Ibid.                                   |

<sup>1</sup> The sample treatment is indicated in brackets as follows: treated (+), untreated (-), no information (?).

<sup>2</sup> A map of the intertidal area only is available with a classification for the median sand grain size and the clay content (% < 0.002 mm).

<sup>3</sup> The resolution in one cross-section was about 20 m, the distance between each cross-section 500 m.

during one year. The data quality is generally good, except maybe for the recent Wadden Sea data set (RIKZ, 1998). The samples, collected during the Wadden Sea campaign, were not deflocculated and a Malvern analysis was applied for the determination of the full grain size distribution. The clay fraction especially may be strongly underestimated.

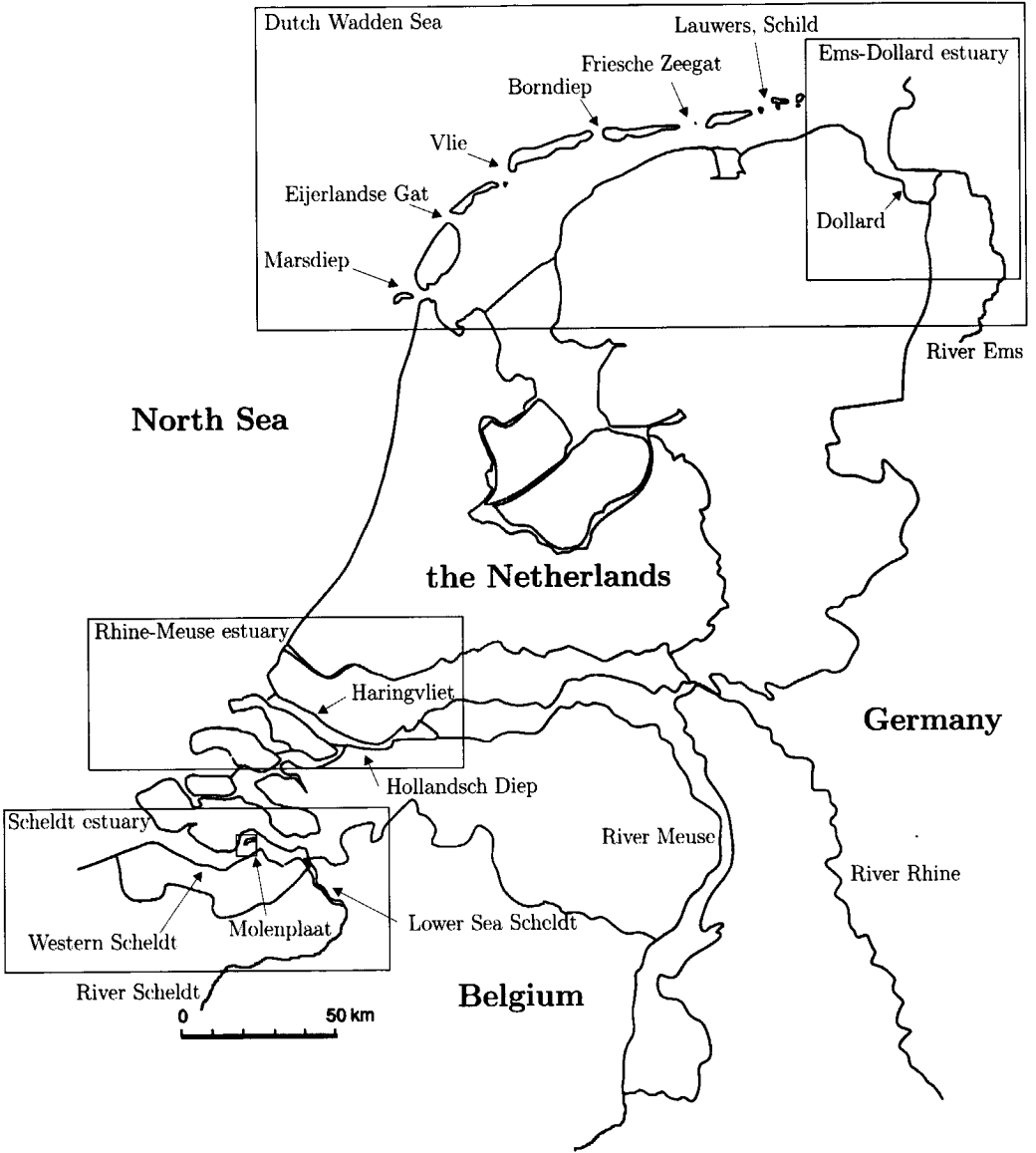


Figure 2.1: Locations of large-scale measurements in the Netherlands.

### 2.2.3 Segregation parameters

An analysis of the full grain size distribution is carried out for the different tidal inlets in the Wadden Sea, the Ems-Dollard estuary and the Scheldt estuary in order to determine the parameters for characterising sediment segregation. For this purpose, the Scheldt estuary is divided into the Lower Sea Scheldt between Rupelmonde (Belgium) and the Dutch-Belgian border, and the Western Scheldt between this border and Vlissingen (the Netherlands). This distinction is generally made based on the hydrodynamic conditions (see e.g. Verlaan, 1998). Depending on the river discharge, the sea water penetrates into the estuary towards the Dutch-Belgian border at high river discharges and towards Rupelmonde at low discharges.

**Table 2.3:** Bed composition characteristics of Wadden Sea inlets, Ems-Dollard estuary, Western Scheldt and Lower Sea Scheldt: average and standard deviation of the mean sand grain size, the sorting index and the mud content, and the clay/silt ratio with the accompanying correlation coefficient (see Figure 2.1 for area locations).

| Area              | Number of samples | Mean sand grain size ( $\mu\text{m}$ ) | Sorting index (-) | Mud content ( $\% \leq 0.063 \text{ mm}$ ) | $\frac{\% \text{clay}}{\% \text{silt}}$ | $R^2$ |
|-------------------|-------------------|----------------------------------------|-------------------|--------------------------------------------|-----------------------------------------|-------|
| Ems-Dollard       | 739               | $121 \pm 46$                           | $1.18 \pm 0.24$   | $34.0 \pm 33.1$                            | 0.25                                    | 0.85  |
| Lauwers, Schild   | 430               | $124 \pm 21$                           | $1.14 \pm 0.11$   | $14.4 \pm 15.8$                            | 0.25                                    | 0.84  |
| Friesche Zeegat   | 393               | $129 \pm 26$                           | $1.15 \pm 0.09$   | $21.1 \pm 23.1$                            | 0.21                                    | 0.85  |
| Borndiep          | 491               | $134 \pm 28$                           | $1.16 \pm 0.07$   | $15.7 \pm 19.5$                            | 0.19                                    | 0.80  |
| Vlie              | 1034              | $143 \pm 45$                           | $1.20 \pm 0.18$   | $16.4 \pm 20.3$                            | 0.18                                    | 0.85  |
| Eijerlandse Gat   | 228               | $154 \pm 33$                           | $1.19 \pm 0.09$   | $11.3 \pm 12.6$                            | 0.16                                    | 0.72  |
| Marsdiep          | 1285              | $165 \pm 52$                           | $1.25 \pm 0.18$   | $17.9 \pm 22.0$                            | 0.17                                    | 0.85  |
| Western Scheldt   | 1315              | $174 \pm 61$                           | $1.25 \pm 0.18$   | $16.4 \pm 23.9$                            | 0.24                                    | 0.80  |
| Lower Sea Scheldt | 217               | $157 \pm 93$                           | $1.27 \pm 0.23$   | $44.3 \pm 36.2$                            | 0.28                                    | 0.67  |

The results of this analysis are shown in Table 2.3. The ratio between the clay and the silt content (column 6), and the accompanying correlation coefficient (column 7) are given, as earlier work has already suggested that these might be strongly correlated in tidal systems (e.g. Pejrup, 1988; Sly, 1989). We observe that the mean sand grain size ( $d_m$ ) in all the systems can be characterised as fine or very fine sand (see also Table 2.1). Furthermore, the standard deviation of the mean sand grain size indicates that the horizontal variation in mean sand grain size is not very large in these systems. According to Raudkivi (1990), the mean sorting index ( $S_i$ ) and the small standard deviation for all systems point out that the sand fraction is nearly uniform in these systems. The mean mud content indicates that the bed composition in these systems is dominated by sand, but the standard deviation suggests that horizontal variations in mud content are present. Finally, the correlation coefficient between the clay and the silt content is high for all areas ( $R^2 > 0.8$ ) except the Lower Sea Scheldt and Eijerlandse Gat. It is striking that the clay/silt ratio for all systems varies in a narrow range between 0.16 and 0.28.

The observation of a nearly uniform sand fraction with a relatively small sand grain size seems

to be a general characteristic of estuaries and tidal basins. A nearly uniform, fine sand fraction is generally attributed to selective erosion and deposition during transport of sediment away from its source. Near the sediment source (e.g. in the upstream parts of rivers), sediments are relatively coarse and strongly non-uniform, whereas nearly uniform fine sediments are found far away from the source (e.g. near the sea).

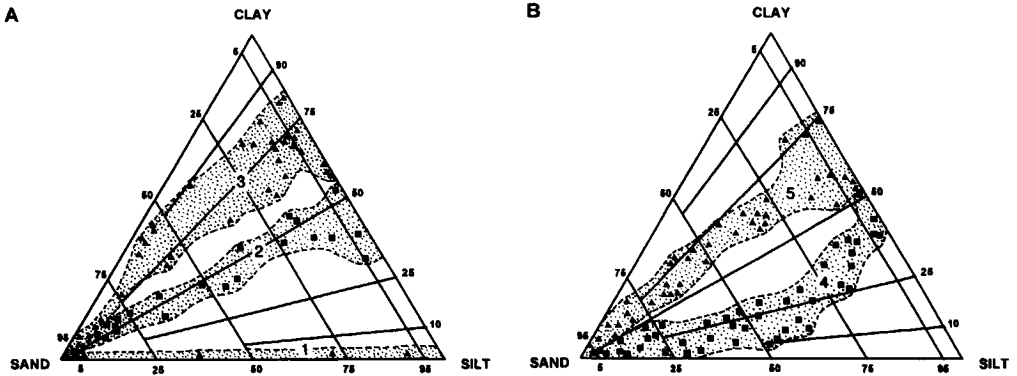


**Figure 2.2:** Sand-silt-clay diagrams: a) 1. Jiang Su, China, 2. Wadden Sea, Denmark, 3. Dyfi estuary, Wales b) 4. Minas Basin, Canada and 5. Mugu Lagoon, USA (Flemming, 2000).

Also the observed constant ratio between silt and clay is a well-known characteristic that is found in various tidal areas all over the world. For example, Flemming (2000) publishes data from five tidal areas (Jiang Su Province, China; Wadden Sea, Danmark; Dyfi estuary, Wales; Minas Basin, Canada; Mugu Lagoon, USA) (Figure 2.2) and two open shelf environments (Bering Shelf; Central gulf of Alaska Shelf) in a sand-silt-clay triangle. The more or less diagonal bands in these triangles indicate a more or less constant clay/silt ratio for each system. In addition, Sly (1989) shows data from Lake Ontario (Canada) and obtains a clear correlation between the clay and the silt content for mud content less than 80%. Pejrup (1988) puts forward that the constant ratio between silt and clay is attributed to the flocculation process. Because of flocculation, silt and clay particles stick together and these particles are therefore not subject to hydraulic sorting (cf. Merckelbach, 2000).

In conclusion, the bed composition in these systems can be characterised by a nearly uniform sand fraction and a mud fraction with a constant clay/silt ratio. Hence, the mean (or median) sand grain size and the mud content are suitable parameters for characterising sediment segregation. Herein, we limit ourselves to variations in mud content, whereas variations in the mean sand grain size are not considered. In the next subsections, large-scale sand-mud patterns are shown and qualitative explanations are discussed for the Wadden Sea, the Scheldt estuary and the Haringvliet-Hollandsch Diep.



### 2.2.4 Sand-mud patterns in the Wadden Sea

Reference is made to Van Straaten and Kuenen (1957), De Glopper (1967) and Oost (1995) for an extensive description of the Dutch Wadden Sea and the observed patterns in mud and clay content. Only the most important characteristics with respect to the distribution of sand and mud will be discussed below. Based on measurements between 1950 - 1955, De Glopper (1967) observes that areas with relatively high clay content ( $> 3\%$ ) are only found in a narrow band of 500 to 1500 meters near the dike of Groningen and Friesland, in the (former) Lauwerszce and the Dollard. In the Dollard region, the increase in clay content towards the dike is very regular. Similar tendencies in mud content are found in the mud content distribution of the 1990's (RIKZ, 1998). The mud content is relatively low ( $< 10\%$ ) for almost the entire tidal basin. Only near the borders and the watersheds, the mud content suddenly increases to high values ( $> 50\%$ ). In addition to this pattern, many patches with a locally high mud content are observed in areas with otherwise relatively low mud content (Oost, 1995).

Various authors have given different explanations for the observed sand-mud patterns in the tidal basins of the Wadden Sea. Van Straaten and Kuenen (1957) and De Glopper (1967) explain the sand-mud patterns in each tidal inlet by a decreasing energy gradient: sand is found near the mouth where tidal current velocities are high, whereas silt and clay deposit near the borders where the velocities approach zero. Various researchers also stress the role of lag effects in combination with tidal asymmetry, resulting in an increasing mud concentration in the water column and the sediment bed with increasing distance from the mouth (Van Straaten & Kuenen, 1957; Postma, 1961; Oost, 1995). Finally, Flemming and Nyandwi (1994) put forward an interesting hypothesis that - because of the land reclamation in the Middle Ages - the normal energy gradient is interrupted by dikes and areas with high mud content in these inlets cannot exist anymore (Figure 2.3). In addition to these global sand-mud patterns, Oost (1995) and Flemming and Ziegler (1995) explain the presence of many small patches of high mud content in large areas with low mud content by the presence of mussel beds. Mussels filter water and predominantly fine sediments and aggregate them into faeces and pseudo-faeces. These faeces are fairly resistant against erosion and the mud content is therefore much higher at these locations.

Nichols and Boon (1994) state that the observed pattern in the Dutch Wadden Sea tidal basins is one example of three general types in tidal basins. These patterns are shown in Figure 2.4 and the characteristics of each type are discussed below:

- Type A is a tidal basin with a muddy centre and sand along the borders. These characteristics are typical of deep, choked or restricted micro-tidal basins and a high influx of fine sediments. Only near the shore, moderate wave action hinders deposition of fine sediments or winnows fine material from the bed.
- Type B is characterised by sand in the central parts and mud along the shore. Similar to Type A, these basins are also choked or restricted with a small tidal range, but are

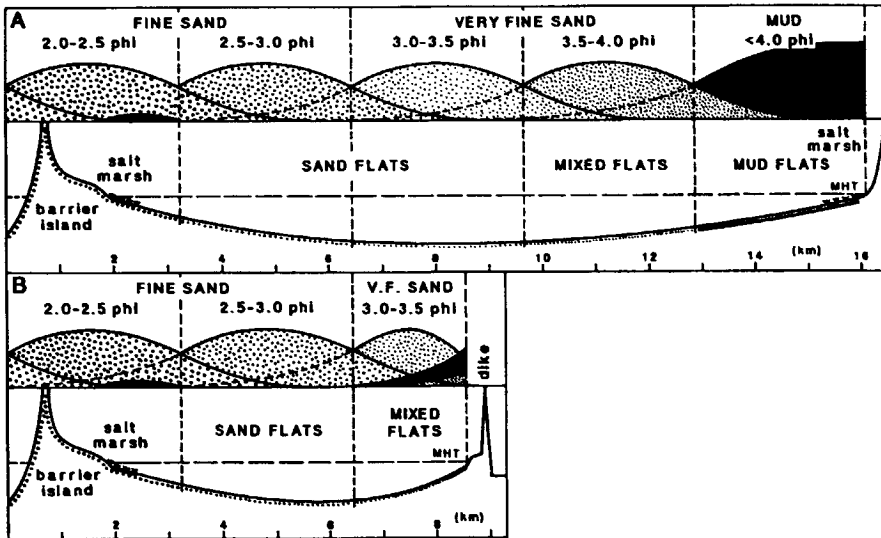


**Figure 2.3:** a) Shoreward fining in a natural natural tidal basin and b) Actual sequence observed in the tidal basin south of Spiekeroog Island (Flemming and Nyandwi, 1994).

shallow, have a low supply of fine sediments and more severe wave conditions. These waves prevent settling of fine sediments in the central parts and deposition is limited to the sheltered areas near the borders.

- Type C has a sediment pattern with coarse sand in the channels and mud on the tidal flats and near the borders. This type is found in meso- and macro-tidal systems where tidal strength and wave action decrease in the landward direction. Tidal currents predominate in the channels, whereas wave effects prevail on the flats. Sand deposits are found near the entrance and in the channels as a result of the high current velocities by the tide. Mud is mainly observed at the intertidal area of the basin with less severe hydrodynamic forcing.

Nichols and Boon (1994) argue that the tidal basins in the Dutch Wadden Sea are examples of Type C: sandy channels with muddy intertidal areas. Based on the observations however, one may also argue that the Dutch Wadden Sea has strong similarities with Type B: a sandy basin with only mud at the margins. Nevertheless, the classification indicates that different types of sand-mud patterns exist depending on the hydrodynamic strength of currents and waves on the one hand and the supply of sediment on the other hand.

### 2.2.5 Sand-mud patterns in the Scheldt estuary

RIKZ (1999) presents a map of the mud content in the upper 10 cm of the bed surface in the Scheldt estuary based on large-scale measurements in 1992 (see also Table 2.2). An increasing

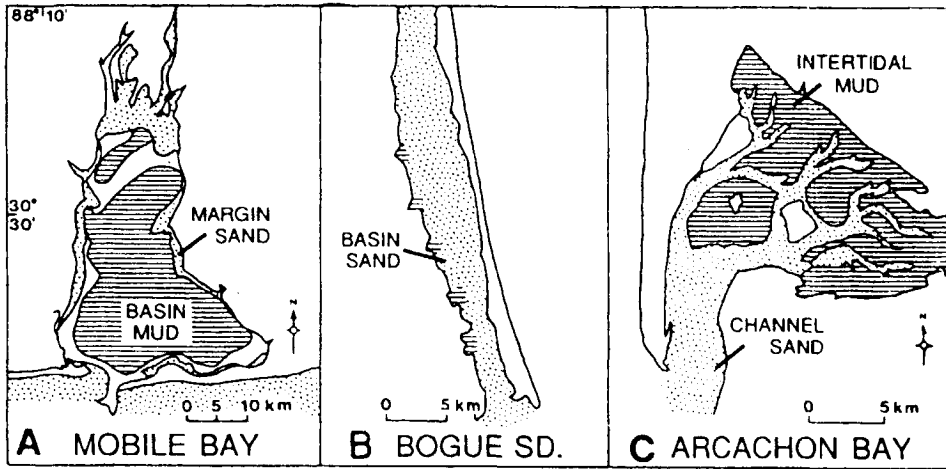


**Figure 2.4:** Types of horizontal bed composition patterns in tidal basins (Nichols and Boon, 1994).

level in mud content is observed from the estuary mouth at Vlissingen towards Antwerpen. Especially near Antwerpen, the mud content is relatively high ( $> 50\%$ ). The mud content is generally low ( $< 10\%$ ) in the channels and on the tidal flats, but is relatively high near the borders ( $> 50\%$ ). Finally, small spots of high mud content can be observed on tidal flats but also in channels.

The reader is referred to Wartel (1977) for a detailed discussion about the grain size characteristics in the Scheldt estuary. Only the main characteristics will be discussed hereafter. The strong increase in the mud content in the Lower Sea Scheldt (km 60 - 100) is explained by gravitational circulation. Between Antwerpen (km 80) and the Dutch-Belgian border (km 60), the residual currents in the lower part of the water column are at a minimum, which corresponds with the very high mud content near km 65 - 70. Van den Berg et al. (1996) explain the small spots of high mud content in deep channels as exposure of older deposits (early Holocene/Tertiary). Furthermore, they stress the role of tidal asymmetry and lag effects for both sand and mud in the long-term and large-scale morphological development of this estuary.

In addition to the aforementioned large-scale pattern, measurements at the Molenplaat in this estuary give indications of sand-mud patterns at a smaller scale (Thoolen et al., 1997). For this purpose, the measurements are interpolated to obtain maps, which show the mud content in the upper 1 cm of the sediment bed in different months in the year 1995 (Figure 2.5). The mud content shows a strong variation in time and space between March and June (Figure 2.5a-b). In March 1995, the Molenplaat is sandy with a small muddy spot in the central area, with a mud content of about 25%. Although the mud content near the edges of the flat does not change very much between March and June 1995, a strong increase in mud content is observed

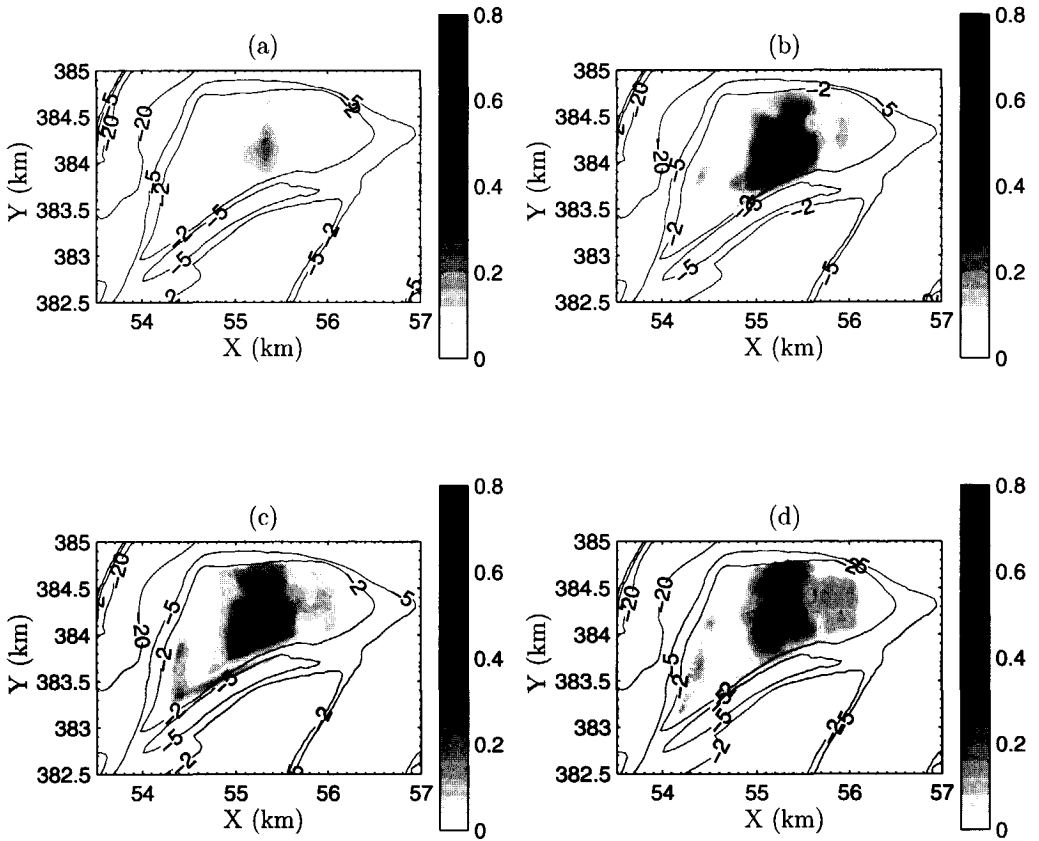


**Figure 2.5:** Mud content in the upper 1 cm of the bed at the Molenplaat (the Netherlands) in March (a), June (b), September (c) and December 1995 (d) (see Figure 2.1 for the location of the Molenplaat).

in the central part. The distributions in September and December 1995 (Figure 2.5c-d) show more or less the same pattern, but the maximum mud content in the central part appears to be significantly lower.

Various explanations can be given for the mud content differences between March and June at the Molenplaat (Figure 2.5). Firstly, the variation in wave effects is probably a driving agent behind this variation. From May to September, the wave effects are much smaller than from October to April. Hence, fines settle more easily in spring and summer, so the mud content increases. However, deposition of fines is absent during autumn and winter, because of the high wave attack. Secondly, biological activity in spring and summer (e.g. algae bloom) might also enhance mud deposition between March and June. For instance, the presence of algae can stabilise the sediment bed, whence the erosion threshold increases. As a result, a net deposition of fines may occur in this period, thus the mud content may increase. When the biological

activity decreases after the summer period, the reverse may occur, whence the bed becomes more sandy.

The question arises whether the strong seasonal variation in mud content can be related to the small sample thickness of 1 cm. Herman et al. (2001) publish data of detailed vertical mud content distributions at five locations on the same intertidal flat. Only at location 2, the vertical mud content distribution at intervals of 1 cm is measured at four moments during the period June 1996 - June 1997. Based on these data, the mean mud content for sample thickness of 1, 5 and 10 cm are shown in Figure 2.6a. Next, the standard deviation for different sample thickness during this period is determined and the result is shown in Figure 2.6b. The bed level change during this period is estimated from monthly bed level data in this area (RIKZ, 2002). The seasonal variation of the bed level is ten centimeters at the nearest data point. Notice that this variation is smaller than the maximum sample thickness in Figure 2.6b.

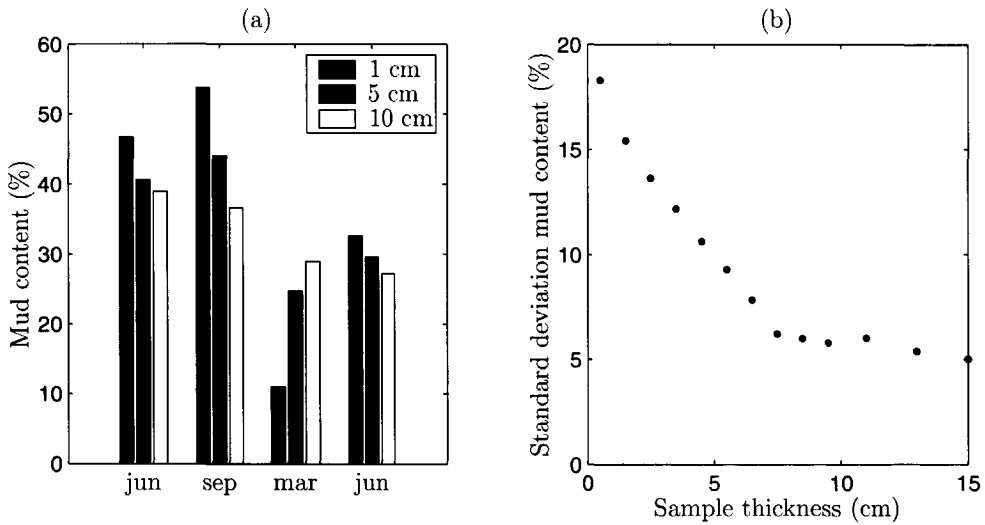


**Figure 2.6:** Mean mud content (a) and standard deviation of mud content (b) for different sample thickness at Molenplaat in the period June 1996 - June 1997.

It appears that the standard deviation monotonically decreases with increasing sample thickness (Figure 2.6). The mean mud content varies between 11 and 54% with a sample thickness of 1 cm, whereas the range is 28 - 38% with a thickness of 10 cm (Figure 2.6a). The standard deviation equals 18% at a sample thickness of 1 cm, whereas the standard deviation is about 6% for a sample thickness of 10 cm (Figure 2.6b). Although only one measurement location is considered, this result suggests that the observed seasonal variations might be connected with the small sample thickness of 1 cm.

### 2.2.6 Sand-mud patterns in the Haringvliet - Hollandsch Diep

Van Wijngaarden et al. (2002a, 2002b) present a map of the mud content in the upper 30 cm of the bed in the Haringvliet - Hollandsch Diep and describe the observed sand-mud patterns (cf. Figure 1.2). Except for the Amer, the mud content is low ( $< 15\%$ ) at the mouth of the river branches Nieuwe Merwede and Dordtse Kil. Moreover, the shallow parts of the Hollandsch Diep (former intertidal flats and shoreline) also have a low mud content ( $< 30\%$ ). The channels in the Hollandsch Diep, however, have a much higher mud content (50 - 60%). The differences in mud content between the channels and the shores are less pronounced in the Haringvliet. In this area, the mud content in the sediment bed of the channels is up to 30% with a locally high mud content up to 60%.

Van Wijngaarden et al. (2002b) also provide explanations for the sand-mud patterns in this system. Because of the closure of the Haringvliet Sluices in 1970, the sediment transport capacity has strongly decreased in the Hollandsch Diep and Haringvliet. As a result, sand and mud supplied by the rivers, accumulates in this area. Sand first settles and is therefore mainly found at the end of the river branches and in the beginning of the Hollandsch Diep, whereas mud is transported further downstream and deposits in the central part of the Hollandsch Diep area. Therefore, the bed composition in the deep channels is very muddy. Near the shores and on the former intertidal areas, settling is hindered by wind and ship waves, which results in a predominantly sandy bed. Because the flow velocities are very small in the Hollandsch Diep (5 - 10 cm/s), most of the fines have settled before reaching the Haringvliet. Hence, the accumulation of sediment in the Haringvliet is small and the sandy bed is still a result of the situation before 1970. The small areas with high mud content in the Haringvliet are old sand pits, which are now used for dumping dredged material.

## 2.3 Processes and mechanisms behind sand-mud segregation

### 2.3.1 Scale concept

Similarly to large-scale bed forms (De Vriend, 1991a), the identification of relevant processes behind large-scale sand-mud segregation is far from straightforward. Based on the qualitative explanations in the previous section, (at least) three complications can be distinguished:

- Processes behind the phenomenon of sand-mud segregation have different origin. Physical processes will generally be important (e.g. deposition, erosion), but biological processes (e.g. filter feeding), geological processes (e.g. exposure of old layers) and human activities (e.g. dredging and dumping of sediment) may also play a role.
- The processes act at various time and length scales. Relevant physical processes for sand-mud segregation are indisputably erosion and deposition in the entire system. Obviously, these processes vary at the time scale of the tidal period, but generally also exhibit

a seasonal variation. An important biological process is often the enhanced seasonal deposition of mud by filter feeders on intertidal areas.

- Interaction between different processes makes the picture even more complicated. A well-known example is the effect of biological processes (e.g. stabilization by algae) on the erosion properties of the sediment bed.

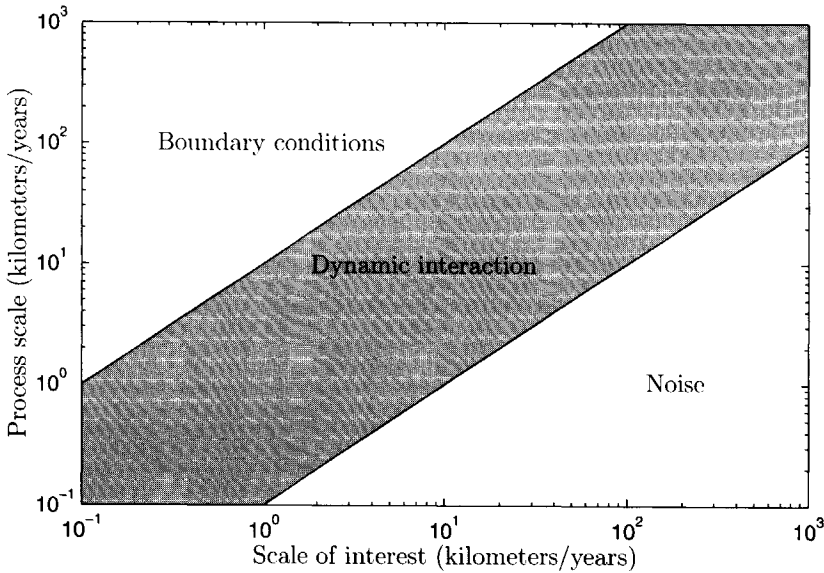


**Figure 2.7:** Primary scale relationship (After De Vriend, 1993).

To identify relevant processes, De Vriend (1991a, 1991b) introduces the so-called ‘scale concept’ (Figure 2.7). He suggests that a phenomenon of interest is likely to be related to the underlying (physical) processes on similar time and length scales. Processes on much larger scales are considered as boundary conditions and those on smaller time and length scales as noise. Noise does not mean that these processes are irrelevant, but that only the net effects of these processes are important.

Applying this concept to our scale of interest (cf. Figure 1.4), we can argue which processes should be treated as noise, a component of morphodynamic interaction or as a boundary condition:

- Deposition and erosion during a tidal period, but also filter feeding processes can be considered as noise. Although these processes act on a much smaller time and spatial scale than our scale of interest, the net effect of these processes cannot be neglected and should ideally be included in a large-scale process-based model. Hence, relevant hydrodynamic and sediment transport processes are discussed in section 2.3.2 and 2.3.3 respectively.

- Differences in residual transport of sand and mud due to tidal asymmetry is likely to be an important morphodynamic interaction process. These differences may lead to large-scale bed level and bed composition changes, and these changes will affect the flow and the residual transport of sediments again. Because several hydrodynamic and sediment transport processes are involved (e.g. tide, erosion, deposition), tidal asymmetry is called a 'mechanism' herein. Relevant mechanisms are discussed in 2.3.4.
- Important boundary conditions for large-scale sand-mud segregation are the supply of sediment from the adjacent sea or river and the mean sea water level, but also the presence of old layers. These boundary conditions are more or less constant at the time scale of interest, and are therefore not discussed herein.

### 2.3.2 Hydrodynamic processes

The bed shear stress, which is the result of the water motion (currents, waves) over the bed and the roughness of the bed surface itself, is a crucial parameter for sediment transport processes. Currents are mainly driven by tide, wind, river discharge and density differences due to salinity or sediment concentrations. Wind waves are locally generated by the wind or penetrate from the open sea into the estuary or tidal basin. The bed roughness is usually divided into form-related and grain-related roughness. In sandy environments, the bed roughness is generally dominated by bed forms that depend on the hydraulic conditions. The bed in muddy environments is usually smooth and the bed roughness is determined by the sediment particles only.

At present, the currents by tides, wind, river discharge and salinity differences are relatively well-described and modelled for tidal areas with low suspended sediment concentrations. Low sediment concentration means that the influence of the sediment on the water motion can be neglected. By the absence of a reliable roughness predictor, a bed roughness coefficient that is constant in time and space is generally applied. The behaviour of short waves (e.g. Booij et al., 1999) and high sediment concentrations (e.g. Winterwerp, 1999) in estuaries and tidal basins are less well understood. Important problems with respect to short waves are the interaction with tidal currents (e.g. wave blocking), the complicated bathymetry (e.g. flooding and drying) and different sources of wind waves (e.g. local generated wind waves and swell from the sea). Also the complicated interaction between high sediment concentrations and the turbulent water motion deserves further attention.

### 2.3.3 Vertical sediment transport processes

For low sediment concentrations, several vertical sediment transport processes can be distinguished which are important for the understanding of large-scale mechanisms. These processes are graphically represented in Figure 2.8 and are discussed consecutively:



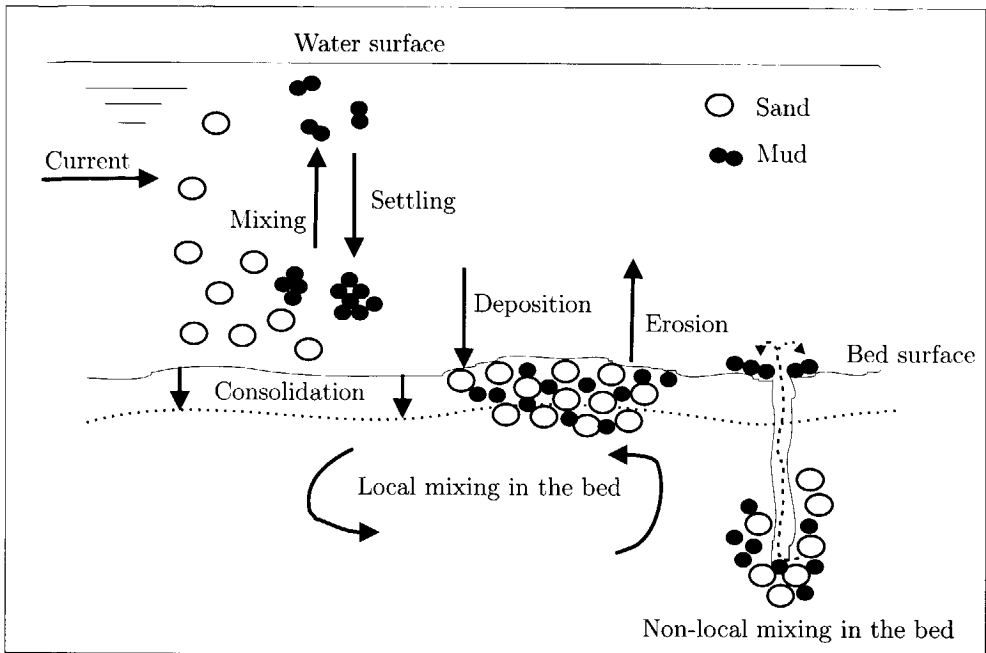


**Figure 2.8:** Vertical sediment transport processes.

### Erosion

An important distinction in erosional behaviour is made between non-cohesive and cohesive sediment beds (Raudkivi, 1990). Non-cohesive beds have a granular structure and do not form a coherent mass. The particle size and weight are the dominant parameters for erosion. However, cohesive beds form a coherent mass due to electrochemical interactions between the sediment particles. These interactions dominate the erosional behaviour, and particle size and weight are of minor importance. The transition between a non-cohesive and a cohesive bed is mainly determined by the clay content. Approximately 5 - 10% of clay minerals by dry weight are considered to be sufficient for a complete control of the bed properties (Raudkivi, 1990).

Historically, many experimental investigations have been carried out for (non-cohesive) sand beds and (cohesive) mud beds separately, in order to improve our understanding of their erosion behaviour and to find mathematical formulations for describing the erosion process. An extensive overview of experimental results, conceptual models and various erosion formulations is given by Van Rijn (1993) for (non-cohesive) sand beds and by Winterwerp (1989) and Whitehouse et al. (2000) for (cohesive) mud beds. In the erosion formulations available, the effects of biological processes on erosion properties are never explicitly accounted for, but always hidden in empirical coefficients.

Recently, several erosion experiments have clearly demonstrated that the erosion characteristics

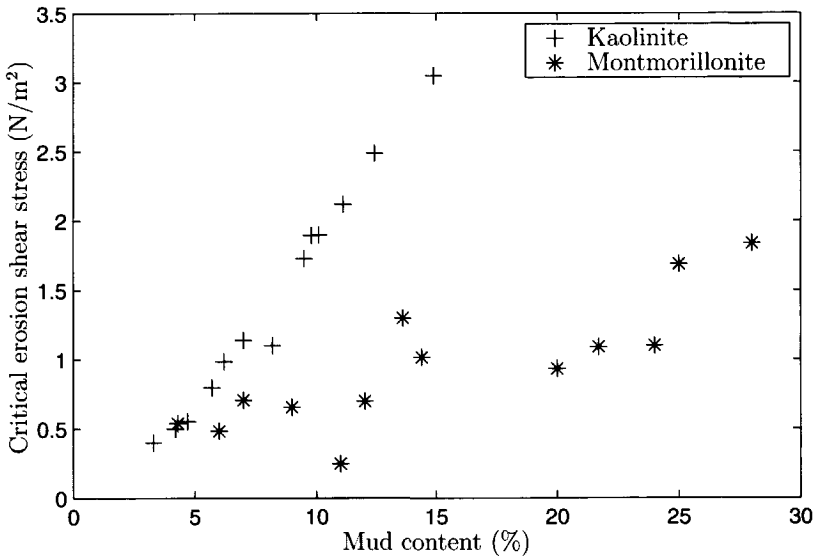


**Figure 2.9:** Effect of mud content on the critical erosion shear stress for two different sand-mud mixtures (After Torfs, 1995).

can change dramatically when a small amount of mud is added to a sand bed (e.g. Torfs, 1995) or vice versa (e.g. Williamson & Ockenden, 1993). As an example, the strong increase in critical erosion shear stress as a function of mud content for two different sand-mud mixtures is shown in Figure 2.9. The experimental results with sand-mud mixtures indicate that the erosion behaviour of these mixtures cannot be described by using the existing erosion formulations for sand or mud only. To the author's knowledge however, formulations for sand-mud mixtures do not exist at present. Such a formulation is an important prerequisite for a process-based model with sand and mud (see also Chapter 3).

### Mixing and settling in the water column

Sediment particles in the water column tend to settle downwards due to gravity, whereas the turbulent shear stress mixes the sediment particles in upward and downward directions. The interaction between these two processes results in a vertical concentration profile. The governing parameter for the shape of this profile is the dimensionless Rouse parameter  $\beta = w_s / \kappa u_*$ , where  $w_s$  is the settling velocity of a sediment particle,  $\kappa$  is Von Karman's constant and  $u_*$  is the shear velocity. For increasing  $\beta$ , the vertical concentration profile becomes less uniform.

In contrast with sand, the settling velocity and the diameter of mud can strongly vary in time and space as a result of flocculation (e.g. Van Leussen, 1994; Winterwerp, 2002). The flocculation process is mainly governed by turbulence-induced aggregation and breakup processes. On the one hand, turbulent mixing induces collision of individual particles, and aggregates of

silt and clay particles ('mud flocs') are formed. On the other hand, turbulent shear stresses also result in the break up of bonds between these mud flocs. Hence, the dominant physical parameters in the flocculation process are the turbulence intensity, the sediment concentration and the cohesive properties of the clay particles.

Recently, Winterwerp (2002) has presented a model for describing the evolution of a mud floc to its equilibrium size, in which the effects of turbulence intensity and sediment concentration are included. Important time scales for reaching the equilibrium floc size are derived. In addition, a relationship is given between the floc size and the settling velocity for mud flocs. Although a direct application of this model is not feasible for large-scale areas, because of computation time, the derived time scales can be used for estimating the possibility of strong settling velocity variations due to flocculation.

### Deposition

Deposition of sand is generally described in terms of non-equilibrium conditions for bed load and/or suspended load transport. When the actual suspended sediment concentration is higher than the equilibrium concentration, deposition occurs. For bed load transport, sedimentation occurs when a negative gradient exists in the bed load transport. Following the concept of Shields, a critical bed shear stress for sand movement is generally incorporated in the expressions for bed load transport and the equilibrium concentration. When the bed shear stress exceeds its critical value, sand particles are transported, whereas they remain at rest below this value. The critical shear stress for sand particles with a grain size of about 0.1 - 0.2 mm is about 0.15 N/m<sup>2</sup> (e.g. Van Rijn, 1993).

Krone's deposition concept is usually applied to the description of mud deposition (e.g. Van Rijn, 1993). Deposition of a mud floc occurs when the strength of a mud floc is high enough to withstand the shear stress near the bed, whereas a floc is resuspended if the bed shear stress is too large. Although the so-called critical bed shear stress for deposition strongly depends on the kind of sediment and the water properties, it generally varies between 0.05 and 0.15 N/m<sup>2</sup> (Winterwerp, 1989; Van Rijn, 1993). Based on a re-analysis of Krone's experiments, Winterwerp (2003) rejects the existence of a critical shear stress for deposition. He demonstrates that the critical shear stress for deposition should be interpreted as a critical erosion shear stress of freshly deposited sediment. This implies that Krone's concept for deposition is in fact a combined erosion-deposition formula.

Another important type of mud deposition is the production of bio-deposits by filter feeders (e.g. *Mytilus edulis*). These organisms filter sea water with suspended sediment to obtain food. Sediment particles are filtered out, the food is absorbed and the remainder is excreted as faeces (or bio-deposits). Experiments have shown that sediment particles from 2 - 5  $\mu\text{m}$  to about 100  $\mu\text{m}$  are trapped much more effectively than coarser and finer sediment particles (Oost, 1995).

### Mixing in the bed

Particles in a sediment bed can be reworked because of physical and biological mixing processes. Physical mixing in a sediment bed occurs near the bed surface by small-scale bed features such as ripples. Armanini (1995) states that this process can be considered as a diffusion process with a certain mixing coefficient. He assumes that the intensity of mixing increases with increasing velocity and decreases with increasing distance from the bed surface. As a result of physical mixing, bed composition variations in vertical direction become less pronounced.

In addition, the activity of organisms induces 'local biological mixing' of sediments in the bed, i.e. bioturbation (Figure 2.8). Organisms move through the bed and therefore mix the sediment particles. Similarly to the aforementioned physical mixing process, local biological mixing is also considered as a diffusion process (e.g. Boudreau, 1997), because the sediment fluxes are determined by the local gradients in sediment composition. An important parameter for this process is the bioturbation or mixing coefficient, and measured mixing coefficients range widely from  $10^{-2}$  to  $10^2$   $\text{cm}^2/\text{year}$ . Similar to the aforementioned physical mixing, the result of local biological mixing is that bed composition gradients become less pronounced.

Another type of mixing by biological activity is 'non-local biological mixing' (Boudreau, 1997, see also Figure 2.8). Non-local mixing is caused by organisms that transport a specific sediment fraction from one place to another in the bed. An example is the *Heteromastus filiformis*, which transports only fine sediment particles from 10 cm depth to the bed surface (Herman, 2000). This process is called non-local mixing, because the sediment fluxes within the bed do not depend on the local gradient in the content of the sediment fractions (Boudreau, 1997). Hence, it cannot be considered as a diffusion process, but rather as sources and sinks of specific sediment fractions at certain distances from the bed surface. The result of non-local mixing can be an increase of the bed composition gradients due to size specific sediment transport.

### Consolidation

Consolidation is a time-dependent process in which pore water is being driven out of the bed due to the overburden of the deposited sediment. Consequently, the bed properties (e.g. the bed density, erosion shear stress) become a function of time and depth below the bed surface. Unlike the mixing processes discussed above, the consolidation process does not affect the bed composition in the vertical direction in a moving frame with the bed level as its reference.

Toorman (1996) demonstrates that the consolidation process can be described by an advection-diffusion equation in a Eulerian reference frame. The dependent variable is the solid fraction and constitutive equations are required for the bed permeability and the effective stress between the sediment particles. Merckelbach (2000) derives constitutive equations for these variables based on a fractal description of the sand-silt-clay mixture and the obtained model results agree convincingly with measured bed density profiles of freshly deposited mud layers. In addition, he also proposes a failure criterion that related the erosion shear stress of a soft mud bed to

the effective stress and clay content by volume.

Although the process-based modelling of the consolidation process has been significantly improved in recent years (e.g. Toorman, 1996; Merckelbach, 2000), the description of the consolidation process in large-scale process-based models is still highly empirical. The sediment bed is often divided into multiple layers and empirically fitted curves for the bed density and the erosion shear stress distribution are applied (Teisson et al., 1993; Teisson, 1997). The main reasons for the empirical approach are not only a lack of information about the constitutive equations for erosive situations, but also the computational effort for solving the full consolidation equation in a large number of grid points.

### 2.3.4 Mechanisms

The most obvious mechanisms behind segregation of sand and mud are selective erosion, transport and deposition by horizontal variations in bed shear stress. For example, the critical shear stress for the initiation of motion of fine sand is about  $0.15 \text{ N/m}^2$  (e.g. Van Rijn, 1993), whereas the critical deposition shear stress for mud is generally less than  $0.15 \text{ N/m}^2$  (e.g. Winterwerp, 1989; Van Rijn, 1993). Consequently, mud can still be transported in suspension, while sand is already deposited at the bed surface. This results in segregation of sand and mud.

Other, less evident mechanisms are tidal asymmetry, gravitational circulation, spring-neap variations and seasonal variations by wind waves. These are graphically represented in Figure 2.10 and are discussed consecutively:

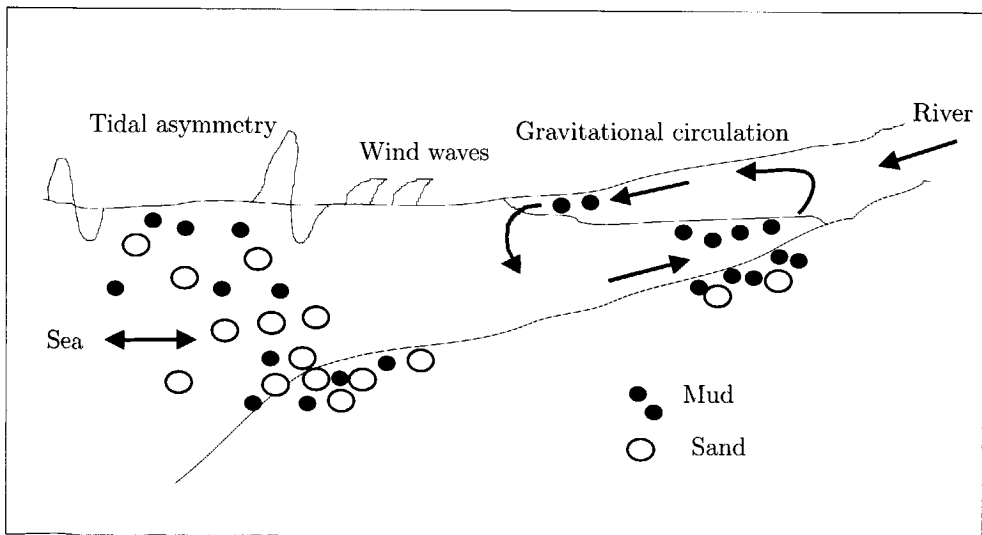
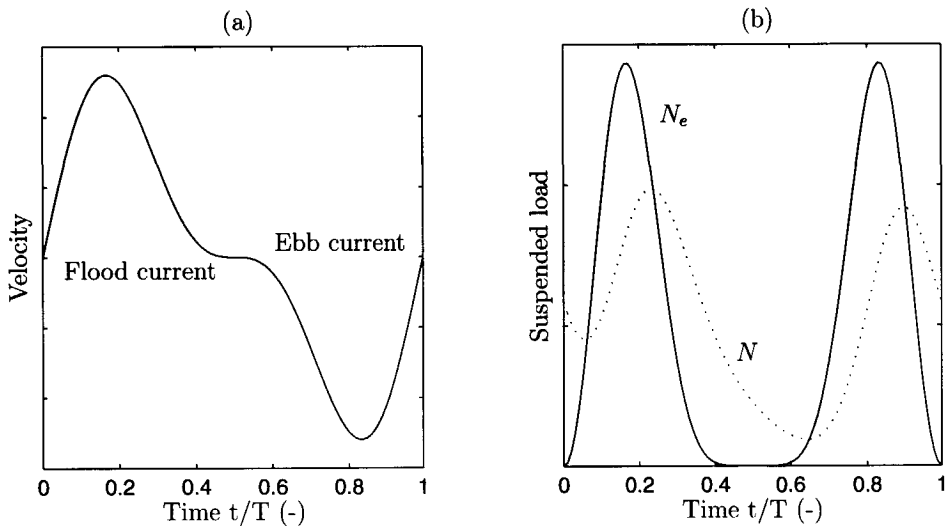


Figure 2.10: Important mechanisms for sediment segregation.

### Tidal asymmetry

The phenomenon of asymmetrical water level and velocity variations during the tide is called tidal asymmetry. The main causes are asymmetrical forcing of the water level at the mouth of a basin, non-linear bottom friction, non-linear advection of momentum, and tidal interactions with the morphology inside the estuary (Aubrey, 1986). Two important asymmetries must be distinguished: i) differences in the maximum ebb and flood velocity and ii) differences in the velocity behaviour around slack water.

The net transport of sand during a tidal period is strongly determined by the asymmetrical behaviour of the maximum current velocity. The main reason behind this is that sand transport adapts instantaneously (bed load) or almost instantaneously (suspended load) to the changing tidal current (Aubrey, 1986; Van de Kreeke & Robaczewska, 1993). When the maximum velocity during flood exceeds the maximum velocity during ebb (i.e. flood-dominated system), the net transport of sand is generally in the flood-direction and vice versa.



**Figure 2.11:** Time variations of the current velocity (a) and the equilibrium suspended load  $N_e$  and actual suspended load  $N$  (b) during a tidal cycle on an arbitrary scale (After Groen, 1967).

Unlike sand transport, the net transport of mud is mainly determined by the settling time and the current asymmetry around slack water (e.g. Postma, 1961; Groen, 1967). Groen (1967) explains the basic mechanism behind the so-called 'settling lag effect' using a detailed analysis (Figure 2.11). Fine sediment particles do not adapt instantaneously to changing flow conditions, but lag significantly behind the flow. If the slack water period at high water is much longer than at low water, the particles have longer time to settle during high water and the suspended sediment concentration after the high water period is lower than after the low water period. Therefore, less suspended sediment is transported backwards during the ebb period and a

residual flux in flood direction during one tide occurs.

Several researchers have tried to quantify the net flux of sand and mud by tidal asymmetry. Groen (1967) quantifies the residual flux for very fine suspended sediment in an alternating current with a symmetrical maximum ebb and flood currents, but with an asymmetrical behaviour around slack water. The governing parameters for the magnitude of the residual flux appear to be the ratio between the velocity amplitudes ( $\hat{u}_4/\hat{u}_2$ ) and the settling time. Dronkers (1986a) derives expressions for the residual flux of mud in a tidal current. He demonstrates that the current variation around slack water, the settling time and also the critical velocity for deposition and erosion are important parameters for the magnitude of the residual flux. Based on these expressions, he estimates the net flux of fine sediments for two tidal basins in the Netherlands, and shows that the computed residual flux is in agreement with observations, both in direction and magnitude. Finally, Van de Kreeke and Robaczewska (1993) derive an analytical expression for the net bed load transport of sand in a  $M_2$  tidal current with one overtide. The direction of transport depends only on the relative phase between the  $M_2$  and  $M_4$ -constituent of the current velocity, whereas the ratio between the velocity amplitudes determines the magnitude of the residual flux.

### Gravitational circulation

Longitudinal salinity gradients generate longitudinal pressure gradients. These gradients generate a circulation pattern in the vertical plane, known as 'gravitational circulation'. This circulation is important for sediment transport, as the near-bed residual transport direction is up-estuary (Figure 2.10). When the salinity distribution is stratified, the magnitude of the gravitational circulation can increase by a factor two at most. Gravitational circulation in estuaries especially, has been thoroughly studied, because it contributes amongst others to the presence of a turbidity maximum in estuaries (e.g. Dyer, 1994). This maximum is commonly associated with a very high mud content at the bed surface. A turbidity maximum can be characterised as follows: it is a zone in the estuary with considerably higher suspended sediment concentrations than upstream in the river or downstream in the estuary and is often located near the head of salt intrusion. The sediments in a turbidity maximum consist of fine silt and clay particles and the sediment concentrations vary from 0.1 to 10 g/l. The location of the turbidity maximum is not fixed but varies during the tide, spring-neap cycle and seasons as a result of river discharge variation.

The formation of a turbidity maximum due to gravitational circulation is shown graphically in Figure 2.10 and can be explained as follows (e.g. Dyer, 1994, 1997). Fine sediment particles from the river are transported in the downstream direction because of a residual flux by the river. Because these sediments settle due to gravity, they reach lower layers and are transported in the upstream direction by the residual flow in the lower layer to the convergence point where the residual flux has a minimum, the so-called 'null point'. Similarly to fluvial particles, sediment particles from the sea are trapped around the null point. The sediment concentration in the

water column is much higher around the null point than in the upstream and downstream areas. However, gravitational circulation is not the only mechanism which contributes to the formation of a turbidity maximum (Dyer, 1994). Tidal asymmetry in combination with lag effects between the current velocity and the suspended sediment concentration (e.g. 'settling lag') also induce residual fluxes of sediment. This so-called 'tidal pumping' of sediment appears to be a major factor in the formation of the turbidity maximum, too.

### Spring - neap variations

Various authors stress the interaction between spring-neap tide variations and the consolidation process of mud layers. Spring - neap tide variations are caused by frequency difference between the (basic) solar and lunar component of the tide ( $S_2$ - $M_2$  interaction) and have a time scale of about fourteen days. Villaret and Latteux (1992) use a simple model to analyse the system response in the case of a spring - neap tide and consolidation of a mud bed. Their analysis indicates that the (tidally averaged) concentration is lower after a neap tide than after a spring tide due to consolidation (i.e. hysteresis). Le Hir and Karlikow (1992) deduce from mud transport simulations for the Loire estuary (France) that the consolidation process influences the time lag between the hydrodynamic forcing and sediment transport. This time lag occurs at different time scales (tide, spring - neap, seasonal) and forces a residual transport. Teisson (1997) also mentions the importance of the consolidation process for long-term sediment transport modelling of estuaries. He concludes that the consolidation process introduces a new time scale between the hydrodynamics and the morphological behaviour, which complicates long-term modelling of mud transport.

### Seasonal variations

The effect of seasonal variations is also often mentioned as an important net transport mechanism of fine sediments in estuaries and tidal basins. Based on field observations, Winkelmoen and Veenstra (1980) report that large amounts of fine sediments are eroded from the tidal flats and the marshes during a few storm surges and transported seaward by the strong ebb currents. After a storm surge, the flood tide penetrates less and a seaward residual flux of fine sediments occurs. Dronkers (1986b) also stresses the role of wind waves in the long-term accumulation of fine sediments by explaining the differences between calculations and observations of the net import of mud into the Borndiep (the Netherlands). Calculations show that the net residual landward flux due to tidal asymmetry in the Borndiep area is much higher (factor 8) than the observed net import of fine sediment. Export during storm surges can be an explanation for the difference.



## 2.4 Predictive models

### 2.4.1 Empirical and hybrid models

Following the rule-of-thumb “the calmer the water, the finer the bed sediment”, several attempts have been made to empirically correlate a representative hydrodynamic parameter to the mud content at the bed surface. The most obvious parameter is the mean or maximum bed shear stress during the tide. A typical result of such a correlation is shown in Figure 2.12. WL|Delft Hydraulics (1997) concludes that a threshold in the bed shear stress exists. Above this value, the bed consists of sand with low mud content. Below this value, a large scatter in the mud content is observed, ranging from 0 to 100%. The same results are obtained when using the maximum bed shear stress and the maximum energy dissipation rate (WL|Delft Hydraulics, 1997, 1998).

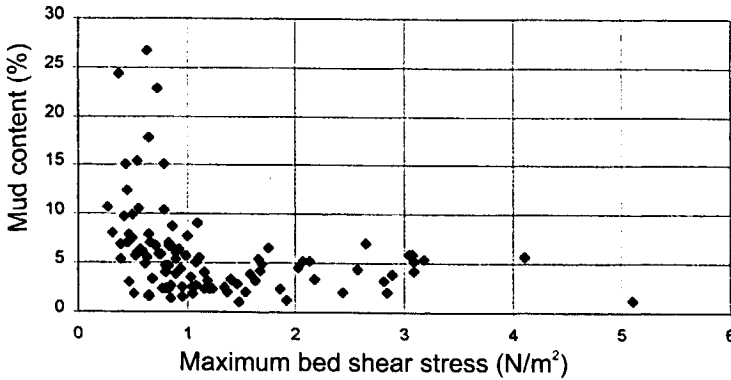


**Figure 2.12:** Correlation between the maximum bed shear stress during the tide and observed mud content at the Molenplaat, the Netherlands (WL|Delft Hydraulics, 1997).

Wang (1996) has developed the so-called hybrid parameter LHEC for predicting the mud content. In contrast to empirical parameters, a hybrid approach includes information about the basic processes influencing sediment transport. The parameter LHEC is based on the advection-diffusion equation for mud in which non-local terms are omitted. For the source and sink terms, the erosion formulation of Partheniades and the deposition formulation of Krone are used, respectively:

$$\frac{dhC_m}{dt} = M \left( \frac{\tau_b}{\tau_e} - 1 \right) H \left( \frac{\tau_b}{\tau_e} - 1 \right) - w_m C_m \left( 1 - \frac{\tau_b}{\tau_d} \right) H \left( 1 - \frac{\tau_b}{\tau_d} \right) \quad (2.1)$$

in which  $h$  is the water depth,  $C_m$  the depth-averaged mud concentration in the water column,  $t$  time,  $M$  the erosion parameter,  $\tau_b$  the bed shear stress,  $\tau_e$  the critical bed shear stress for erosion,

$H$  a Heaviside function,  $w_m$  the settling velocity for mud and  $\tau_d$  the critical bed shear stress for deposition. LHEC has been defined as the local, tidally-averaged hypothetical equilibrium concentration:

$$LHEC = \frac{1}{T} \int_0^T C_m(t) dt \quad (2.2)$$

where  $T$  is the tidal period.

Wang (1996) hypothesizes that with increasing value of LHEC, the mud content in the bed decreases. An important restriction of the applicability of LHEC is that this parameter has a finite value only when the bed shear stress during the tide is larger than the critical bed shear stress for erosion and the critical bed shear stress for deposition. Wang (1997) has tested the applicability of this parameter for the Nieuwe Merwede, a river branch in the Noordelijk Deltabekken (Figure 1.5). Comparing the measured mud content with LHEC, Wang (1997) concludes that this parameter can discriminate between definitely sandy areas ( $< 10\%$  mud content), and areas in which the mud content cannot be predicted and varies between  $0\%$  and  $100\%$ . However, a quantitative relation between LHEC and the mud content is not possible. Although more physical knowledge has been incorporated in this hybrid approach, the capability to discriminate between areas with different mud content is more or less similar to the aforementioned empirical parameters.

### 2.4.2 Process-based models

In process-based models, the system behaviour is modelled by solving a coupled system of equations for the water motion, sediment transport and bed level variation. A distinction is generally made between complex and idealised process-based models. Complex models generally solve the full system of non-linear equations, whereas the underlying equations are generally simplified (e.g. linearised) in idealised models. At present, process-based models only exist for non-cohesive (sand) and cohesive (mud) sediment transport separately. Only one example is known of a combined sand-mud model. The most important characteristics of these models are described consecutively.

#### Sand models

Van Rijn (1993) extensively describes large-scale models for sand transport and bed level variations. Basically, these models consist of a hydrodynamic module, a sediment transport module and a bed module. A graphical representation of the present-day sand models is given in Figure 2.13a.

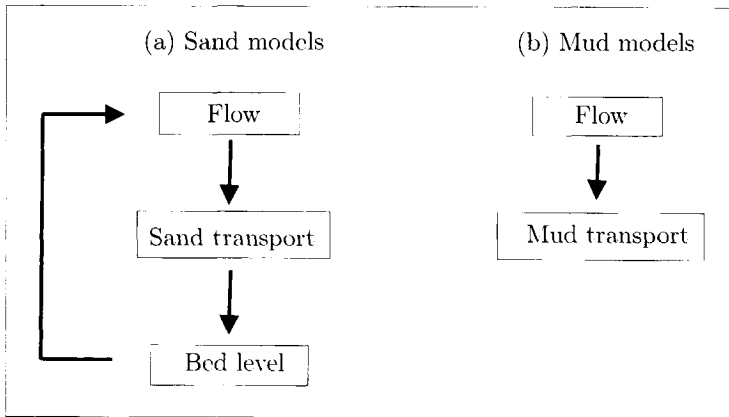


**Figure 2.13:** Present set-up of process-based & idealised models.

At present, the main characteristics and restrictions are:

- turbulence-averaged description without interaction of suspended sediment with the flow;
- depth-averaged energy balance in combination with linear wave theory for short waves;
- constant bed roughness coefficient in time and space;
- bed load transport formula based on local hydrodynamic parameters;
- advection-diffusion equation for suspended sediment transport;
- exchange of suspended sediment by using an equilibrium concentration concept near the bed;
- bed level changes by mass balance of bed load and suspended load transport;
- constant bed composition in time and space;

### Mud models

Teisson (1997) gives an overview of the large-scale models for mud. The hydrodynamic part of these models is similar to sand models and interaction between the mud concentration and the water motion is also neglected. A major difference is that a dynamic coupling between bed level changes by mud exchange and the water motion are generally not included at present. The main features of large-scale mud transport models are (Figure 2.13b):

- sediment transport by using the advection-diffusion equation;
- deposition modelled by the formula of Krone;
- settling velocity often taken as constant or given by an empirical formula, depending on the sediment concentration and/or the bed shear stress to account for flocculation effects;
- erosion modelled by the formula of Partheniades;
- consolidation effects often included by modelling a sediment bed with multiple layers;
- erosion parameters empirically fitted to consolidation curves;

### Sand-mud model

The only known application of a process-based model with both sand and mud transport is given by Chesher and Ockenden (1997). In this model, experimental results with sand-mud mixtures are used for describing the interaction between both fractions in the bed module. The following expression for the critical bed shear stress for erosion ( $\tau_e$ ) is applied:

$$\tau_e = K \rho_b^L \quad (2.3)$$

in which  $\tau_e$  is the critical bed shear stress for erosion,  $\rho_b$  the bed density and  $K$  and  $L$  are empirical coefficients. The erosion rate ( $E$ ) is prescribed by a modified Partheniades formula:

$$E = m_e (\tau_b - \tau_e) \quad (2.4)$$

in which  $E$  is the erosion rate and  $m_e$  an erosion parameter. The erosion parameter  $m_e$  and the bed density  $\rho_b$  are both given by empirical functions that depend on the sand content in the sediment bed. Consequently, the critical shear stress (eq. 2.3) and the erosion rate (eq. 2.4) are a function of bed composition. Vertical bed composition variations within the bed itself are not taken into account, and sand and mud are assumed to be completely mixed, i.e. the mixing layer concept (see Section 2.4.3). Initial sediment transport computations have been performed for a simple test case (straight channel) and the Mersey estuary (England). The transport rates of sand and mud have been calculated with and without interaction between sand and mud in the bed. The results show that the interactions cause a strong reduction in the entrainment and transport of both sand and mud. The application to the Mersey estuary also demonstrates that the tidally-averaged transport direction of mud during one tide may change by 180° when the sand-mud interactions are included.

The presented sand-mud model and its results have a number of shortcomings. Firstly, the incorporated erosion formulation does not reflect observed characteristics of erosion behaviour of sand-mud mixtures. For example, a distinction between typical non-cohesive and cohesive behaviour depending on the mud content is not incorporated. Secondly, no detailed analysis has been made of the governing parameters to explain the model results. For example, only a qualitative explanation is given for the computed reversal of the net transport direction in the Mersey estuary. It should be possible to derive dimensionless parameters which explain this behaviour. Thirdly, Chesher and Ockenden (1997) already recommend validation of the model results against field and laboratory experiments, in order to improve the presented model.

### 2.4.3 Bed composition variations in process-based models

Concepts for including time- and space-dependent bed composition variations in process-based models are well-known. Some of them are already applied for non-cohesive sediments in rivers (see e.g. Ribberink, 1987). These concepts are summarised below:

### Mixing layer concept

Hirano (1971, 1972) introduces the first so-called 'mixing layer concept' for non-cohesive sediments. A graphical sketch of this concept is given in Figure 2.14. The upper part of the bed consists of a mixing layer with a certain thickness. This layer contains a number of sediment fractions, and these fractions are completely mixed in this layer. Below the mixing layer, a sublayer exists and the composition of the sublayer may be different from the composition of the mixing layer.

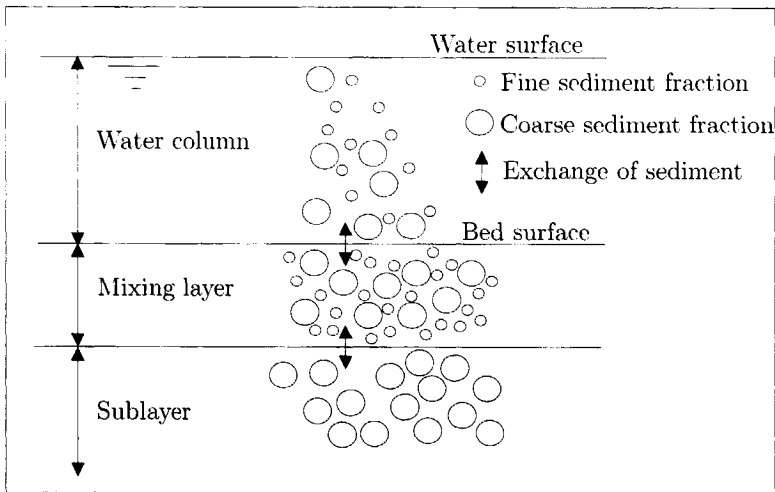


Figure 2.14: Hirano's mixing layer concept.

Vertical sediment exchange occurs between the water column and the mixing layer and between the mixing layer and the sublayer and these exchanges must be prescribed for each sediment fraction. The sediment exchange between the mixing layer and the water column depends on the gradient in the bed load transport rate and the difference between the local concentration and the equilibrium concentration at a certain reference level. The exchange of sediment between the sublayer and the mixing layer depends on the bed level change. In case of erosion, sediment with the composition of the sublayer is transported from the sublayer to the mixing layer. In case of deposition, sediment with the composition of the mixing layer is transported from the mixing layer to the sublayer. Notice that this concept only keeps track of the composition of the mixing layer, whereas the sublayer always remains unchanged.

For calculating the bed load transport rate for each sediment fraction, Einstein's similarity concept is generally applied. In this concept, the sediment bed is schematised in a number of sediment fractions. For each of these fractions, the bed load transport rate is computed with a bed load transport formula (e.g. Meyer-Peter Müller) by applying the grain size of that specific fraction. The total bed load transport rate is obtained by a summation of all bed load transport rates, which are weighted by the content of each sediment fraction in the mixing layer. The bed

level change is easily computed from the mass balance of all sediment fractions.

The similarity concept does not take into account sheltering effects of smaller grains by larger grains and (vice versa) the more exposed position of the larger grains due to the smaller grains. Therefore, the critical bed shear stress for each sediment fraction is generally corrected (Ribberink, 1987). The net effect of these corrections is that the sediment transport rate of the finer fractions decreases and the sediment transport rate of the larger fractions increases.

### **Multi-layer concept**

Ribberink (1987) extends the mixing layer concept by introducing more layers in the bed. The reason for introducing more layers is twofold. Firstly, increasing the number of layers is physically more realistic, because the bed composition below the mixing layer is not constant in time and space. Secondly, more layers also increases the numerical stability. Mathematical analysis of the one-layer system shows that the set of equations can become elliptic when fine sediment is below a coarse mixing layer. Hence, knowledge of future boundaries is needed for solving these equations which is physically unrealistic. An analysis of the two-layer approach has demonstrated that the possibility of elliptic behaviour is smaller, although a complete exclusion is not possible.

### **Continuous concept**

Armanini (1995) generalises the multi-layer concept to a continuous concept for bed composition variations. His main argument is that *“it is hard to accept, and to prove, the existence of a zone of finite thickness where instantaneous and complete mixing of all grain-size classes occurs”*. In his continuous description, the bed composition is a continuous function of the vertical coordinate within the bed. He also shows two important differences between Hirano's mixing layer concept and his continuous approach. Firstly, the mixing layer concept does not take into account the diffusive flux between the mixing layer and the sublayer. This diffusive flux can physically be explained by the existence of short-term bed fluctuations. Secondly, Hirano's model assumes a constant bed composition over a certain thickness, whereas the bed composition can vary at infinitely small distance from the bed surface in the continuous concept.

### **Probabilistic concept**

Recently, Parker et al. (2000) proposes a new conceptual framework for modelling bed composition variations. In this so-called 'probabilistic concept', the bed composition varies continuously with depth, which is similar to the continuous concept of Armanini (1995). However, the bed elevation and sediment erosion and deposition are prescribed with probability density functions instead of deterministic functions. Furthermore, no distinction is made in this concept between erosion and deposition at the bed surface, and mixing in the sediment bed itself (cf. Armanini, 1995). The probability density functions for the exchange of sediment and the bed

level fluctuations are not generally available, but should be derived from laboratory and/or field experiments. Blom et al. (2001) starts with deriving these functions for tracer particles in dune conditions and a first comparison with laboratory experiments turns out to be promising (see also Blom, 2003).

**Table 2.4:** Characteristics of the bed composition concepts for multiple sediment fractions.

|                             | Mixing-layer           | Multi-layer         | Continuous         | Probabilistic           |
|-----------------------------|------------------------|---------------------|--------------------|-------------------------|
| Reference                   | Hirano<br>(1971, 1972) | Ribberink<br>(1987) | Armanini<br>(1995) | Parker et al.<br>(2000) |
| Exchange at bed surface     | yes                    | yes                 | yes                | yes <sup>1</sup>        |
| Mixing in the bed           | no                     | no                  | yes                | yes <sup>1</sup>        |
| Deterministic/Probabilistic | deterministic          | deterministic       | deterministic      | probabilistic           |
| Stratification in the bed   | no                     | yes                 | yes                | yes                     |
| Discrete/Continuous         | discrete               | discrete            | continuous         | continuous              |

<sup>1</sup> Exchange at the bed surface and mixing in the sediment bed itself are treated as one mechanism in this concept.

Summarising, four concepts have been proposed for modelling bed composition variations: the mixing layer concept (Hirano, 1971, 1972), the multi-layer concept (Ribberink, 1987), the continuous concept (Armanini, 1995) and the probabilistic concept (Parker et al., 2000). Their characteristics are listed in Table 2.4. The applicability of these concepts strongly depends on the knowledge of the exchange processes at the bed surface and the mixing processes in the bed itself. For instance, the probabilistic concept requires probabilistic functions of the bed level variations and the exchange of the sediment fractions, whereas deterministic exchange formulations are sufficient in the mixing-layer concept. Moreover, the need for modelling vertical bed composition changes is another important factor. Except for the mixing layer concept, the bed composition concepts are able to keep track of the vertical stratification in the sediment bed. The difference between discrete and continuous descriptions seems to be less important, because the underlying continuous equations can generally be solved analytically for idealised situations only. For real-life situations, a numerical discretisation of these equations will always be necessary.

## 2.5 Conclusions

In this chapter, large-scale bed composition measurements in Dutch systems have been presented and sand-mud patterns have been discussed. Next, the relevant processes and mechanisms behind large-scale sand-mud segregation have been identified. Finally, predictive modelling tools with respect to mud content variations have been summarised and existing concepts

for modelling bed composition variations have been discussed. The following conclusions can be drawn:

### **Large-scale bed composition measurements in Dutch systems**

- Large-scale bed composition data for Dutch systems are scarce (Table 2.2). Only one measurement campaign is digitally available for the Wadden Sea, Scheldt estuary and the Haringvliet - Hollandsch Diep, respectively. Although the sampling area of the Molenplaat is relatively small, the data set is valuable because of time-dependent information about the bed composition.
- The bed composition in the Wadden Sea and the Scheldt estuary can be characterised by a nearly uniform sand fraction and a mud fraction with a constant ratio between the clay and the silt content. These characteristics appear to be present in various tidal systems all over the world.
- Horizontal sand-mud patterns are observed in the Dutch systems at different spatial scales. Differences are observed between the entrance and the borders of a tidal basin, between channels and flats and also on a tidal flat. The Molenplaat measurements clearly indicate that sand-mud patterns also show strong seasonal variations. An analysis indicates that the observed variations throughout the year are likely to be a result of the small (vertical) sampling resolution.

### **Processes and mechanisms**

- Important hydrodynamic processes affecting mud content variations are currents and short waves. At present, currents are relatively well-described and modelled for tidal areas with low suspended sediment concentrations, whereas knowledge and modelling tools for short waves and high sediment concentrations are less well-developed.
- In addition, several sediment processes are likely to be affecting horizontal segregation of sand and mud. Erosion, deposition and mixing of sediment particles in the bed are relevant processes. Consolidation and flocculation are less important, because these only affect the erosion and deposition characteristics, respectively. The main limitation for a process-based sand-mud model seems to be the absence of an erosion formulation for sand-mud mixtures.
- Several mechanisms are put forward to explain horizontal sand-mud patterns in estuaries and tidal basins. Following the rule-of-thumb “the calmer the water, the finer the bed sediment”, the most obvious explanation is horizontal bed shear stress variation. Other important mechanisms are tidal asymmetry, spring-neap variations, gravitational circulation and seasonal variations. However, important time and length scales or parameters that govern these sand-mud patterns are not available.



### Predictive models

- Various empirical models and one hybrid model exist for predicting mud content variations. These can discriminate between areas with definitely less than 10% mud content and areas in which the mud content potentially varies between 0 and 100%.
- At present, complex and idealised process-based models only exist for sand or mud individually. Only one example is known of a sediment transport model in which the interaction between sand and mud has been incorporated (Chesher & Ockenden, 1997). Shortcomings of this model include the discrepancy of the erosion formulation from observed erosion behaviour, only a qualitative analysis of the model results, and the absence of model validation against field measurements.
- Several concepts are described for including bed composition variations in a process-based model: the mixing layer concept, the multi-layer concept, the continuous concept and the probabilistic concept. In general, these concepts have only been applied for non-cohesive sediments in river situations. The applicability of these concepts mainly depends on i) the knowledge of the exchange processes at the bed surface and the mixing processes in the bed, and ii) the need for keeping track of vertical bed composition variations.

Summarising, this chapter has demonstrated the lack of understanding and predictive capabilities concerning the phenomenon of sand-mud segregation in estuaries and tidal basins. A number of processes and mechanisms have been put forward to explain the distribution of sand and mud in these systems qualitatively (see Section 2.2 and 2.3). However, these processes and mechanisms have never been brought together in a comprehensive process-based sand-mud model (see Section 2.4). Such a model is a necessary tool to integrate the relevant processes and mechanisms. The analysis of model behaviour and the verification with field data can underpin or reject the given explanations behind sand-mud segregation. Finally, the model can be used for predicting future morphological changes, including the effect on sand-mud segregation.

Based on these considerations, the development of a process-based sand-mud model and its application to tidal systems will therefore be subject of the next chapters (see also Figure 1.6). An erosion formulation for sand-mud mixtures is an important prerequisite for a process-based sand-mud model. Yet, such a formulation does not exist at present (see Section 2.3). Hence, the erosion behaviour of these mixtures and the derivation of erosion formulations are discussed in Chapter 3. Next, the set-up of a process-based sand-mud model is discussed in Chapter 4, which integrates the current knowledge of sand and mud models (see Section 2.4). The relevant processes which are incorporated in this model, are erosion, deposition and mixing in the sediment bed itself (see Section 2.3). Furthermore, the continuous concept of Armanini (1995) is applied for modelling mud content variations in time and space (see Section 2.4). In Chapter 5 and 6, the distribution of sand and mud in tidal systems is studied through experiments with the numerical sand-mud model. Important parameters that govern sand-mud segregation in these systems are derived. Also, the model results are (partly) compared with the presented field measurements from the Dutch tidal systems (see Section 2.2).



## Chapter 3

### Erosion of sand-mud mixtures

#### 3.1 Introduction

Historically, many investigations have been carried out for (non-cohesive) sand beds and (cohesive) mud beds separately to improve our understanding of the erosion behaviour. Based on these results, various conceptual models and mathematical formulations have been developed for describing the erosion process in sand and mud models. An extensive overview of these results are given by Van Rijn (1993) for (non-cohesive) sand beds and by Winterwerp (1989) and Whitehouse et al. (2000) for (cohesive) mud beds.

A major difference exists between the erosion formulations for sand and mud beds. Sand erosion is generally formulated in terms of a deviation with respect to a certain equilibrium situation. This equilibrium exists because sand deposition and erosion balance over alluvial beds, and it depends on the flow conditions and the sediment characteristics. Contrary to sand beds, the availability of mud is often limited and the flow is far from its transport capacity. Consequently, an equilibrium situation between mud deposition and mud erosion only exists in high concentrated mud suspensions. Hence, the erosion formulations for mud beds do not include a certain equilibrium, but only depend on the flow conditions and the bed properties.

Recently, several erosion experiments have demonstrated that the erosion characteristics can change dramatically when a small amount of mud is added to a sand bed (Bisschop, 1993; Torfs, 1995), or vice versa (Williamson & Ockenden, 1993). For example, Torfs (1995) measured a critical erosion shear stress that was 2 - 5 times higher than the critical shear stress for pure sand when 10% mud was added to a sand bed. Moreover, the erosion rate strongly decreased with increasing mud content. These results point out that the erosion behaviour of sand-mud mixtures cannot be described by using the existing erosion formulations for sand (Van Rijn, 1993) or mud (Winterwerp, 1989; Whitehouse et al., 2000).

Based on laboratory and field experiments, several researchers have identified a transition from non-cohesive into cohesive behaviour for increasing mud content in a sand bed. Mitchener and Torfs (1996) suggest a transition range at 3 - 15% mud content ( $\% \leq 0.063$  mm). However, other experimental data demonstrate that the transition between non-cohesive and cohesive behaviour

can be at much higher mud content. For example, Houwing (2000) reports a transition in erosion behaviour at around 20 - 30% mud content, based on field experiments in the Wadden Sea (the Netherlands).

Additionally, several authors have presented mathematical formulations for important erosion parameters. Van Rijn (1993) and Whitehouse et al. (2000) propose a relationship between the mud content and the critical erosion shear stress for mud contents less than 20%. Mitchener and Torfs (1996) suggest the use of cohesive-type erosion formulations above the critical mud content range of 3 - 15%, whereas Torfs (1995) states that the classical non-cohesive formulations for sand should be used below this range. Nevertheless, an erosion formulation for the entire mud content range, which can be applied directly in a process-based model, has not been developed yet.

In this chapter, a conceptual model is presented in which the observed erosion behaviour of sand-mud mixtures is classified (Section 3.2). Next, an erosion formulation for sand-mud mixtures is proposed for the full mud content range (Section 3.3). The classification and the formulations are validated against the results of both laboratory and field experiments. The formulations are an important prerequisite for any process-based sand-mud model.

## 3.2 Classification<sup>1</sup>

### 3.2.1 Limitations

The behaviour of sand beds under moderate flow conditions ( $< 2$  m/s) is mainly characterised by the grain size distribution. In more extreme flow regimes, the so-called 'sheetflow regime', permeability and the packing of a sand bed are also important (Bakker & Van Kesteren, 1998). A variety of bed properties influence the erosion behaviour of mud beds in natural systems (Berlamont et al., 1993). Important physical parameters for mud bed behaviour include the grain size distribution, the water content, the type of clay mineral, permeability and compressibility, but several biological (e.g. organic content) and chemical parameters (e.g. chlorinity, pH) are also important.

Although these parameters are presumably of importance for sand-mud mixtures, including all these parameters in an erosion model is beyond the present knowledge. Even for mud beds only, the influence of several parameters is only partly and qualitatively understood (Winterwerp, 1989; Whitehouse et al., 2000). Moreover, the role of chemical and biological parameters in previous erosion experiments with sand-mud mixtures was not investigated, which makes validation of these parameters impossible at present.

---

1. The contents of this section have been submitted for publication in *Continental Shelf Research* with W.G.M. van Kesteren and J.C. Winterwerp as co-authors.

Hence, several assumptions have to be made. Firstly, only physical parameters are used to describe the erosion behaviour of sand-mud mixtures. Secondly, the sediment mixture is assumed to be homogeneous with depth and in the horizontal plane. Thirdly, it is assumed that physical parameters from tests on remoulded bed samples can be used in classifying and describing the erosion behaviour of mixed sediment beds. Remoulded bed samples are samples that have lost their original structural properties, which is generally the case in laboratory experiments. Finally, only erosion behaviour under moderate flow conditions is considered.

These assumptions limit the applicability of the proposed erosion model. For example, old sediment layers that are exposed, can have a quite different erosion behaviour than remoulded samples with the same physical parameters, as a result of overconsolidation and aging effects. Also horizontal heterogeneity such as channels formed by biological activity, will affect the erosion behaviour. Nevertheless, an erosion model that is based on the principal physical parameters involved will be able to capture the change in erosion behaviour when the sand-mud ratio is changing.

### 3.2.2 Classification parameters

Fine sediments are generally classified according to their individual particle size, with sand, silt and clay as the principal classes (cf. Table 2.1). Sometimes silt and clay are treated as one sediment fraction, called mud or fines. However, it is important to note that only the clay particles within the mud fraction have cohesive properties. Therefore, a distinction between sand, silt and clay is adopted herein, and the definitions and symbols are listed in Table 3.1.

**Table 3.1:** Definitions and symbols for the fractions in the bed.

| Fraction | Grain size (mm) | Content by volume | Content by dry weight |
|----------|-----------------|-------------------|-----------------------|
| Sand     | 0.063 - 2       | $\phi_{sa}$       | $p_{sa}$              |
| Silt     | 0.004 - 0.063   | $\phi_{si}$       | $p_{si}$              |
| Clay     | < 0.004         | $\phi_{cl}$       | $p_{cl}$              |
| Water    |                 | $\phi_w$          |                       |

It has long been known that a natural sediment bed shows different erosion behaviour, depending on the composition of sand, silt, clay and water. Two important aspects will be discussed hereafter: cohesion and network structure.

#### Cohesion

Historically, an important distinction is made between non-cohesive and cohesive erosion behaviour (Raudkivi, 1990). Non-cohesive beds have a granular structure and the individual sediment particles do not stick together. The particle size and its weight are the dominant parameters for erosion. Cohesive beds form a coherent mass because of electrochemical inter-

actions between the sediment particles. These interactions dominate the erosion behaviour and the particle size and weight are of minor importance.

A sediment bed is called 'cohesive' when it exhibits a certain shear strength. It appears that for most soils a relationship exists between the remoulded shear strength and the liquidity index (Van Kesteren et al., 1997). The liquidity index ( $LI$ ) is expressed in terms of the actual water content ( $w$ ) and the Atterberg limits (Mitchell, 1976):

$$LI = \frac{w - PL}{LL - PL} \quad (3.1)$$

where  $LL$  is the liquid limit and  $PL$  the plastic limit. The liquid limit is the water content that defines the transition from plastic to liquid behaviour and the plastic limit is the water content that defines the transition from solid to plastic behaviour. The difference between the liquid limit and the plastic limit is defined as the plasticity index ( $PI$ ) and can be estimated by (Mitchell, 1976):

$$PI = A(p_{cl} - n) \quad (3.2)$$

where  $p_{cl}$  is the clay content by dry weight,  $n$  the so-called 'offset' of the clay content by dry weight and  $A$  the activity of the clay. The offset can be interpreted as a minimum clay content at which sediment shows plastic behaviour. The offset for mixtures is about 5 - 10% clay content (Mitchell, 1976). The activity is a measure for the binding capacities of the clay mineral and strongly depends on the type of clay. For example, the activity for kaolinite is about 0.5, whereas the activity for montmorillonite is between 1 and 7 (Mitchell, 1976).

The liquidity index governs the transition between non-cohesive and cohesive behaviour in the following ways. The offset can be interpreted as a critical clay content, needed for giving a natural bed cohesive properties. Dyer (1986) and Raudkivi (1990) have already stated that approximately 5 - 10% clay content by dry weight is considered to be sufficient for a natural bed to have cohesive properties, which agrees with the measured range for the offset. Furthermore, the relationship between the remoulded shear strength and the liquidity index indicates that the remoulded shear strength increases with decreasing water content (i.e. increasing bed density) for a constant clay content by dry weight. Thus, the cohesiveness of a natural sediment bed not only increases with increasing clay content by dry weight, but also with decreasing water content.

### Network structure

The erosion behaviour also depends on the network structure in a sediment bed. As an example, a sand bed without silt and clay is considered (Figure 3.1). When the volume content of sand is large, sand particles make contact with the surrounding sand particles and are able to build a

network structure (Figure 3.1a). With increasing water content, the distance between the sand particles becomes larger and the contact between the particles decreases. A critical network structure is reached at a so-called critical volume content for sand ( $\phi_{cr}$ ) (Figure 3.1b). When the water content increases further, the sand particles loose contact with the surrounding sand particles (Figure 3.1c). The volume content of sand is less than the critical volume content and the sand-water mixture behaves like a fluid (i.e. quick sand), be it with a higher viscosity because of the high sediment concentration.

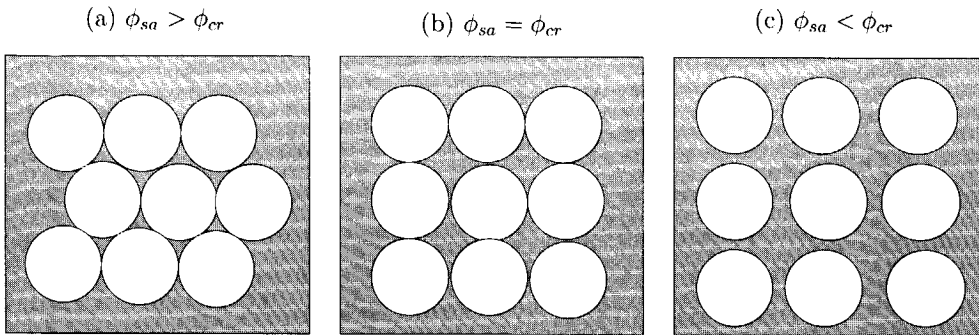


**Figure 3.1:** Network structure in a sand bed for different volume fractions of sand.

The network structure in a sediment mixture is determined by sand, silt or clay particles. In line with the above transition in network structure for sand only, differences in erosion behaviour can be expected when the network structure changes from sand-dominated in clay-dominated or silt-dominated. From fluidization experiments it is known that sand particles build a network structure if the volume content of sand ( $\phi_{sa}$ ) is more than 40 - 50% (Merckelbach, 2000). Similarly, silt particles build a bed structure if the volume content of the silt particles relative to the pore volume around the sand particles ( $\phi_{si}/(1 - \phi_{sa})$ ) is more than 40 - 50%. In other cases, the clay fraction builds the network structure if sufficient clay is present in the sediment mixture. The clay content must be higher than the aforementioned offset for building a network structure.

### 3.2.3 Classification diagram

The boundaries for the transition between a cohesive and a network structure are visualised in a sand-silt-clay triangle in which the sand, silt and clay content by dry weight are given on the axes (Figure 3.2). The horizontal solid line indicates the transition between non-cohesive (below) and cohesive (above) mixtures. As indicated in the previous section, a clay content of 5 - 10% by dry weight appears to be the transition value. This parameter is therefore set at 7% herein. The dotted lines in the left-hand corner indicate the boundary of a sand-dominated network structure for different volume fractions of water. This transition is determined by the volume content of sand:

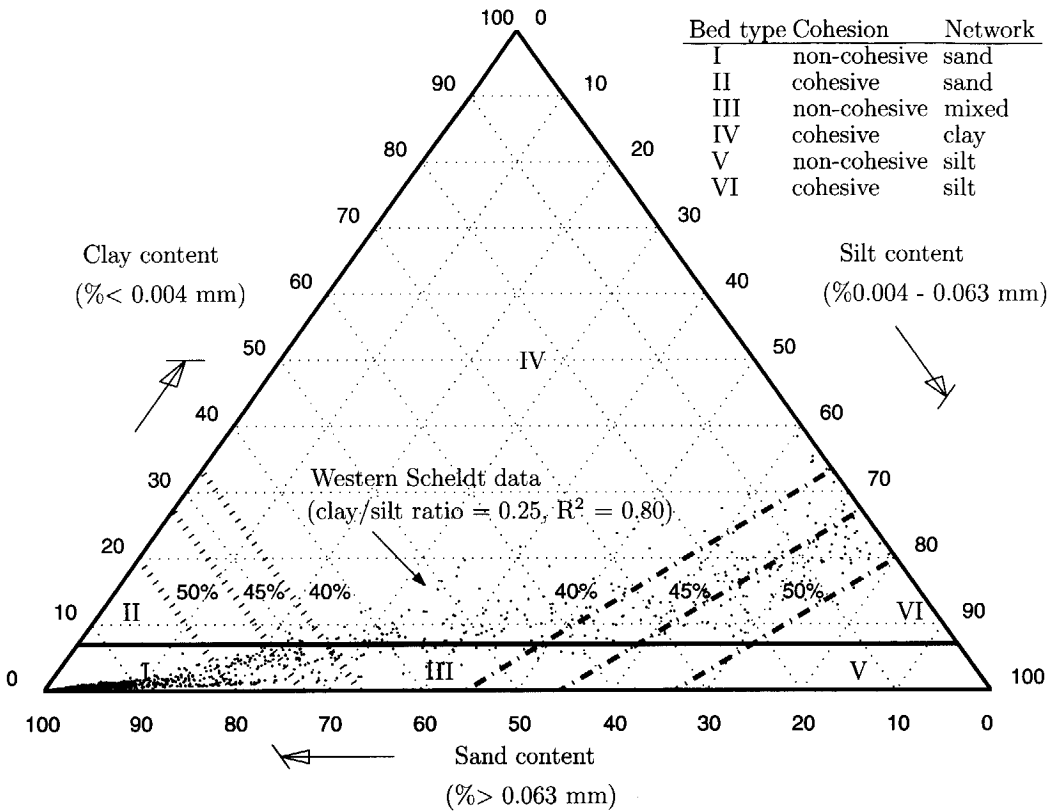


**Figure 3.2:** Sand-silt-clay triangle with six different bed types depending on the transitions for cohesion (solid line) and network structure (dotted lines). The Roman numbers in the triangle refer to various bed types with the characteristics listed in the table at the top of the figure.

$$\phi_{sa} = (1 - \phi_w)p_{sa} \tag{3.3}$$

Consequently, the position of this transition in a sand-silt-clay triangle not only depends on the volume content of sand, but also on the volume content of water. The minimum volume content of sand for a sand-dominated network structure appears to be 40 - 50% and is set at 40%. The volume fractions of water are set at  $\phi_w = 40, 45$  and  $50\%$  which are equivalent to a dry bed density of  $1590 \text{ kg/m}^3, 1458 \text{ kg/m}^3$  and  $1325 \text{ kg/m}^3$ , respectively. The dotted lines in the right-hand corner in Figure 3.2 indicate the boundary of a silt-dominated network structure for different volume fractions of water. This transition is determined by the volume content of silt relative to the pore volume around the sand particles:

$$\frac{\phi_{si}}{1 - \phi_{sa}} = \frac{(1 - \phi_w)p_{si}}{1 - (1 - \phi_w)p_{sa}} \tag{3.4}$$



Hence, the position of this transition in the sediment triangle also depends on the volume content of water. The settings of these transitions are similar to the sand-dominated transitions with  $\phi_{si}/(1 - \phi_{sa}) = 40\%$  and  $\phi_w = 40, 45$  and  $50\%$ .

Based on the transition for a cohesive and network structure, six bed types can be distinguished the sand-silt-clay triangle (Figure 3.2). Sediment beds in the lower left-hand corner and lower right-hand corner of the sediment triangle have a sand-dominated (I and II) and silt-dominated (V and VI) network structure, respectively. In the remainder, the network structure is dominated by clay if sufficient clay is present (IV). In area III none of the fractions of sand, silt or clay are large enough to build the network structure itself, and all sediment fractions contribute to the network structure. The horizontal line at a clay content of 7% divides sediment mixtures which are cohesive (II, IV and VI) or non-cohesive (I, III and V).

Several diagrams have been proposed for classifying sand-silt-clay mixtures in natural systems. Two well-known diagrams are those proposed by Shepard (1954) and Folk (1954) (see also Flemming, 2000), which are shown in Figure 3.3. The presented classification in Figure 3.2 does not coincide with the diagrams in Figure 3.3. The main reason is that the transitions used in the Shepard's and Folk's diagram (e.g. 25, 50 and 75% in Figure 3.3) are chosen more or less arbitrarily, whereas the presented transitions in Figure 3.2 have a physical background.

### 3.2.4 Experimental validation

The proposed classification is validated using experimental results from laboratory and field experiments. Several authors have investigated the transition for cohesion, but the effect of the network structure was not investigated. Therefore, experimental data from Torfs (1995) are re-analysed to establish this transition.

#### Cohesion

Murray (1977) performed laboratory experiments with three mixtures of uniform coarse sand and mud. The mud percentages for these mixtures were 0, 10 and 18% and the clay percentage were 0, 1.0 and 1.8%. No information was given on the water content or dry bed density. During these experiments the sediment transport rate of the coarse sand fraction was measured as a function of the applied bed shear stress. Because the clay content is much less than 5 - 10%, non-cohesive behaviour is expected for all the experiments. This classification agrees with Murray's observation that the coarse sand was transported as bed load and mud was easily suspended.

Alvarez-Hernandez (1990) carried out erosion experiments with mixtures of laponite clay and various sand grain sizes. It was concluded that the transition between cohesionless and cohesive behaviour occurred between 5 - 15% clay content by dry weight, depending on the sand grain size. Again, these experimental results agree well with the suggested clay content range of 5 - 10%, beyond which a sediment mixture exhibits cohesive properties.

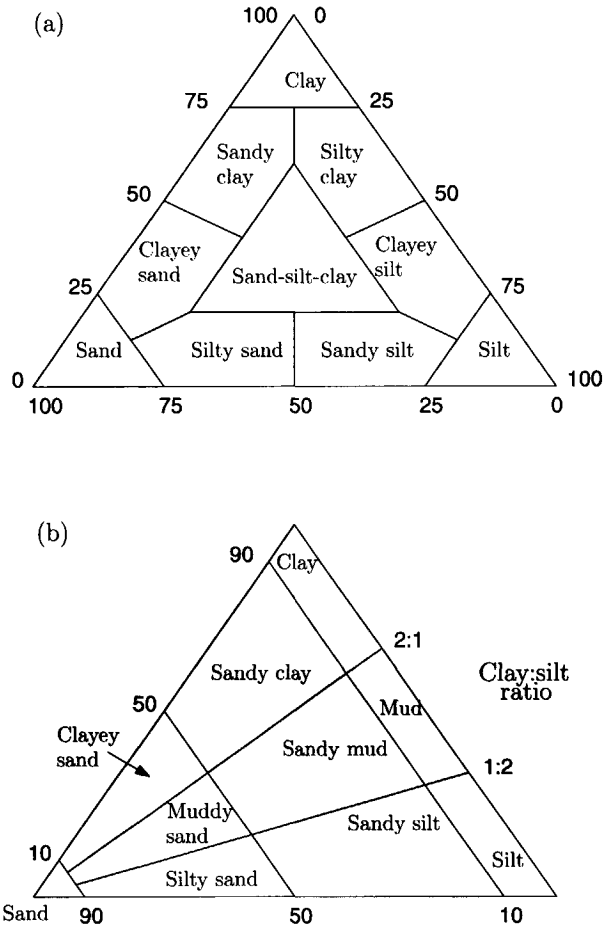


**Figure 3.3:** Classification diagrams for sand-silt-clay mixtures after Shepard (1954) (a) and Folk (1954) (b).

Torfs (1995) investigated the erodibility of artificial sand-mud and natural sand-mud mixtures. Only the artificial sand-mud mixtures with high bed density are considered herein, because only a few natural mixtures and artificial mixtures with low bed density were examined. The characteristics of these experiments are summarised in Table 3.2. Two muds of different composition were added to fine sand and the erodibility was tested for a certain mud content range by dry weight. The wet bed density was kept constant for all mixtures. Transitions from non-cohesive to cohesive behaviour were observed at a certain ‘critical mud content’. For a low mud content, ripples were observed indicating bed load transport of sand, and fine particles were washed out from the top layer. Above the critical mud content, the mixtures showed typical cohesive (mass or surface) erosion. For kaolinite mixtures the critical mud content was about 4% and an abrupt

change from non-cohesive into cohesive was observed. The montmorillonite mixtures showed typical cohesive behaviour above 13% mud content. Moreover, the montmorillonite mixtures showed a transition zone between 7 and 13% in which the behaviour could be defined neither non-cohesive nor cohesive.

**Table 3.2:** Characteristics of sand-mud mixtures used by Torfs (After Torfs, 1995).

| Sand grain size<br>(mm) | Mud type        | $p_{sa}$<br>(-) | $p_{si}$<br>(-) | $p_{cl}$<br>(-) | Mud content<br>(%) | Wet bed density<br>(kg/m <sup>3</sup> ) |
|-------------------------|-----------------|-----------------|-----------------|-----------------|--------------------|-----------------------------------------|
| 0.23                    | Kaolinite       | 0               | 0.15            | 0.85            | 0 - 15             | 1850                                    |
| 0.23                    | Montmorillonite | 0.09            | 0.49            | 0.42            | 0 - 28             | 1850                                    |

The observed transition values in mud content by Torfs (1995) from non-cohesive into cohesive behaviour can be expressed in terms of clay content by using the sand-silt-clay distribution in Table 3.2. The transition value for the kaolinite mixtures appears to be 3 - 4% clay content, and 3 - 5% clay content for the montmorillonite mixtures. Apparently, the clay content at the transition is about equal for both mixtures, whereas the mud content strongly differs. This agrees with the conceptual model. This is a further proof that the clay content, instead of the mud content, determines the transition between non-cohesive and cohesive behaviour. The relatively low value of the clay content, as compared with the suggested range of 5 - 10% in the conceptual model, can probably be explained by the relatively high bed density.

Panagiotopoulos et al. (1997) measured the critical erosion shear stress of sand-mud mixtures. Sand-mud mixtures were prepared with two different sand grain sizes and natural mud, ranging from 0 to 50% mud content. The data showed an increasing erosion threshold for both grain sizes when the mud content increased from 0 to 50%. Moreover, the increment was relatively small for a mud content less than 30% (clay content less than 10%), and much higher for a mud content between 30 and 50%. Finally, the erosion threshold was about the same for both sand grain sizes, viz. at a mud content of 50%. Panagiotopoulos et al. (1997) already stated that the transition in behaviour agreed well with the earlier proposed critical clay content of 5 - 10%.

Houwing (2000) measured the erosion rate of natural sand-mud beds in the Wadden Sea (the Netherlands). He observed a transition in erosion behaviour around 20 - 30% mud content by dry weight. According to Table 2.3, the mud content is 4 - 5 times the clay content in this area. Thus, the observed transition in mud content corresponds with 5 - 7% clay content, which again agrees well with the classification.

### Network structure

As Torfs (1995) did not mention the effect of a change in network structure with increasing mud content, a re-analysis is carried out to estimate the changes in network structure during the experiments. The wet bed density was equal to 1850 kg/m<sup>3</sup>, corresponding with a water

content  $\phi_w = 0.485$ . When a minimum volume content of sand  $\phi_{sa} = 0.45$  is assumed, a sand-dominated network structure was thus present in samples with less than 13% mud content by dry weight according to eq. (3.3). Above 13% mud content, the network structure was no longer sand-dominated. As indicated before, the transition between non-cohesive and cohesive behaviour occurred at a clay content of about 3 - 5%. These transitions and the composition of the kaolinite and montmorillonite mixtures are presented in Figure 3.4. On the horizontal axis, the mud content by dry weight is shown and on the vertical axis the clay content by dry weight. The dotted lines are the transitions of cohesion and network structure and the Roman numbers correspond with the bed types in Figure 3.2.

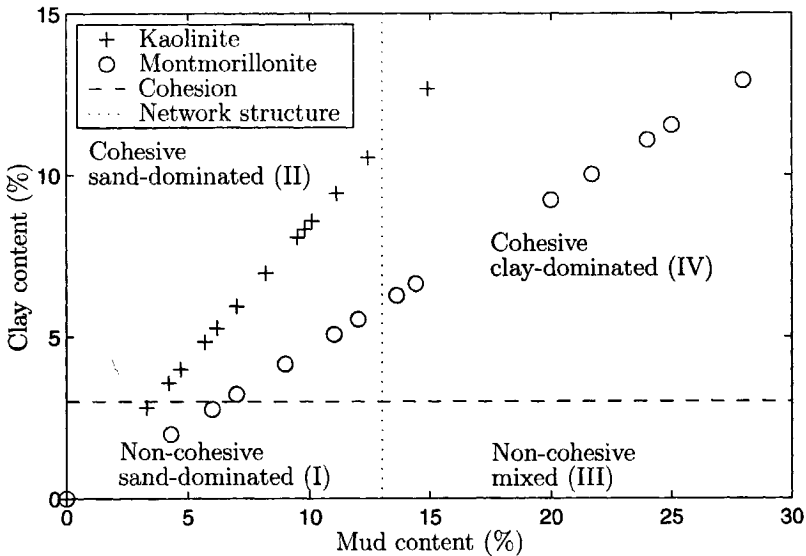


**Figure 3.4:** Transitions in cohesion and network structure for kaolinite and montmorillonite mixtures (After Torfs, 1995).

It can be concluded for the kaolinite mixtures, that the network structure was sand-dominated except for one mixture (Figure 3.4). Furthermore, the transition between non-cohesive to cohesive behaviour occurred when the network structure was still sand-dominated. This indicates that an abrupt change from non-cohesive into cohesive behaviour can be expected with increasing clay content, which is confirmed by the observations. However, the network structure for the montmorillonite mixtures changes from sand-dominated at low mud content to clay-dominated at high mud content (Figure 3.4). Meanwhile, the sediment bed also changes from non-cohesive into cohesive behaviour. This suggests a more gradual change from the non-cohesive into cohesive bed behaviour, because the network structure also changes. It probably explains the observed transition zone in bed behaviour between 7 - 13% mud content by Torfs (1995). The bed behaviour in this range could be described as neither non-cohesive nor cohesive.

### 3.2.5 Relevance of bed types in natural systems

It is not expected that all bed types distinguished in the previous sections play an important role in a specific system, because of the often observed constant ratio between clay and silt by dry weight (see Section 2.2 and Table 2.3). The data of the Western Scheldt are shown as an example in Figure 3.2. It can be observed that these data are centered around a straight line in the sand-silt-clay triangle with a constant clay/silt ratio, which limits the number of relevant bed types.

The importance of the proposed bed types can be estimated by using empirical relationships for the dry bed density and the remoulded shear strength. Based on field measurements, Allersma (1988a) proposes an empirical relationship between the sand content and the dry bed density ( $\rho_{dry}$ ):

$$\rho_{dry} = 480\alpha_c + (1300 - 280\alpha_c)p_{sa}^{0.8} \quad (3.5)$$

where  $\alpha_c$  is a consolidation coefficient, ranging from 0 (fresh deposit) - 2.4 (old deposit). A relationship between the liquidity index ( $LI$ ) and the remoulded shear strength ( $f_u$ ) is necessary to discriminate between non-cohesive and cohesive sediment mixtures:

$$f_u = 10^{0.4LI^2 - 2.3LI + 2.2} \quad 0 < LI < 2.5 \quad (3.6)$$

This relationship follows the experimental data in Van Kesteren et al. (1997) (see also Mitchell, 1976) reasonably well. A minimum value of 0.1 kN/m<sup>2</sup> is applied in eq. (3.6) for the remoulded shear strength to distinguish non-cohesive and cohesive behaviour. Furthermore, a constant value of 25% is applied for the plastic limit in eq. (3.1), the offset  $n$  for the clay content by dry weight is set at 5% and the activity  $A$  equals 3 in eq. (3.2). These values are quite common for marine deposits in the Netherlands (Van Kesteren, 2002).

Based on these relationships, the relevance of the different bed types is estimated in Figure 3.5. For convenience, the transitions are first shown separately in Figure 3.5a-c. Firstly, the empirical relationship between the sand content and the bed density (eq. 3.5) is shown in Figure 3.5a for different values of the consolidation coefficient  $\alpha_c$ . According to this relationship, natural sediment mixtures are found between these lines. Secondly, the lines in Figure 3.5b indicate the transition between non-cohesive (above) and cohesive (below) behaviour for different clay/silt ratios ( $p_{cl}/p_{si}$ ). Thirdly, the transitions in the network structure directly follow from eq. (3.3), (3.4) and (3.5) and are presented in Figure 3.5c. These transitions are drawn with the following settings: the minimum volume content for a sand-dominated and silt-dominated network structure are equal to  $\phi_{sa} = 40\%$  and  $\phi_{si}/(1 - \phi_{sa}) = 40\%$ , respectively and the clay/silt ratio  $p_{cl}/p_{si} = 0.33$ . Notice that the clay/silt ratio only affects the silt-dominated area. This area (slightly) increases for a lower ratio, whereas it diminishes for a higher ratio. Finally, the combination

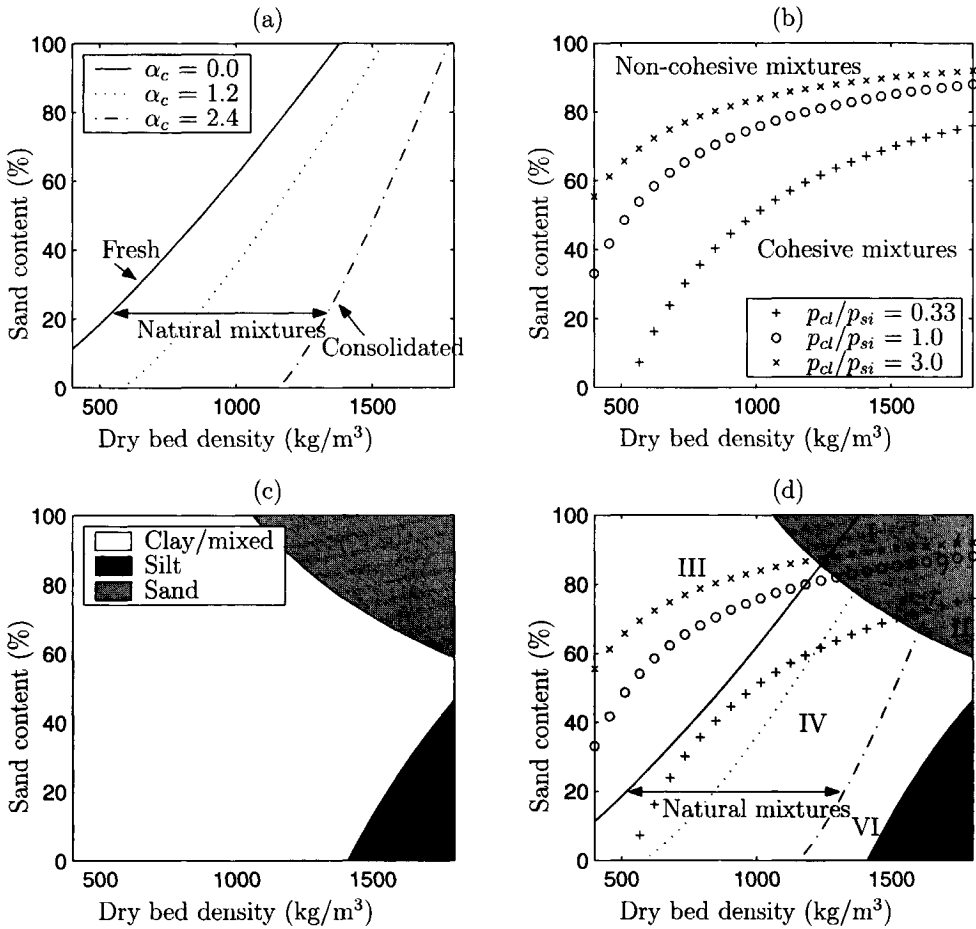


**Figure 3.5:** Estimation of relevant bed types for natural systems. See text for further explanation.

of these transitions is presented in Figure 3.5d. The Roman numbers indicate the different bed types, as defined in Figure 3.2.

Figure 3.5d shows that silt-dominated bed types fall outside the area with natural combinations of sand-silt-clay mixtures following eq. (3.5). Bed type VI is indicated, but bed type V falls outside the given range of dry bed density. Thus, only for very low clay/silt ratios, silt-dominated bed types may be important in systems for which eq. (3.5) holds. In addition, a relatively large area is covered by bed type I (non-cohesive sand-dominated) and IV (cohesive clay-dominated) for all clay/silt ratios. Finally, the importance of bed type II and III strongly depends on the clay/silt ratio. For high clay/silt ratio ( $> 3$ ), only bed type II is important while for low clay/silt ratio ( $< 0.33$ ) bed type II can be neglected. For bed type III, the opposite is true. In the next section we propose erosion formulations assuming that either type I or type IV bed occur.

### 3.3 Mathematical formulations

#### 3.3.1 Sand and mud only

The exchange at the bed boundary of pure sand beds is generally described separately for bed load transport and suspended load transport. The net sand flux from the bed into the water column ( $F_s$ ) is expressed as follows:

$$F_s = \nabla q_b + w_s(c_a - c_s) \quad (3.7)$$

where  $q_b$  is the bed load transport rate,  $w_s$  the settling velocity for sand,  $c_a$  the reference concentration and  $c_s$  the actual sand concentration near the bed surface. Thus, erosion of a sand bed occurs when a positive gradient exists in the bed load transport rate and/or the suspended sediment concentration is less than the equilibrium concentration. Several expressions exist for the bed load transport rate and the reference concentration for sand beds (Van Rijn, 1993).

The sediment exchange at mud beds is generally described by using the (Ariathurai-) Partheniades' erosion formula and Krone's deposition formula (see e.g. Van Rijn, 1993; Teisson, 1997). The net mud flux from the bed into the water column ( $F_m$ ) is classically given by:

$$F_m = E_m - D_m = M \left( \frac{\tau_b}{\tau_e} - 1 \right) H \left( \frac{\tau_b}{\tau_e} - 1 \right) - w_m c_m \left( 1 - \frac{\tau_b}{\tau_d} \right) H \left( 1 - \frac{\tau_b}{\tau_d} \right) \quad (3.8)$$

where  $E_m$  is the mud erosion flux,  $D_m$  the mud deposition flux,  $M$  is the erosion coefficient,  $\tau_b$  the bed shear stress,  $\tau_e$  the critical erosion shear stress,  $\tau_d$  the critical deposition shear stress,  $c_m$  the near-bed mud concentration,  $w_m$  the settling velocity for mud and  $H$  the Heaviside function. The Heaviside function equals 1 when the argument is larger than 0, and equals 0 when the argument is less or equal than 0.

The critical erosion shear stress is generally larger than the critical deposition shear stress in eq. (3.8). This implies that deposition and erosion are mutually exclusive, i.e. the classic cohesive sediment paradigm. This paradigm has been disputed by Sanford and Halka (1993) and very recently by Winterwerp (2003). Sanford and Halka (1993) show that models with mutually exclusive erosion and deposition fail to reproduce field data in the Chesapeake Bay, whereas the best model fit is found when assuming continuous deposition of mud, i.e. neglecting the term  $\left( 1 - \frac{\tau_b}{\tau_d} \right) H \left( 1 - \frac{\tau_b}{\tau_d} \right)$  or applying an infinitely large critical shear stress for deposition in eq. (3.8). Similarly, Winterwerp (2003) demonstrates that Krone's experiments are well-described when assuming continuous deposition of mud and applying Partheniades' erosion formula with a stochastic description of the bed shear stress (see also Winterwerp & Van Kesteren, in prep.). Both results would imply that the combination of Partheniades' erosion formula and Krone's deposition formula is basically wrong for describing the mud exchange between the bed and the water column. Nevertheless, the classic paradigm of mutually exclusive mud erosion and deposition is adopted throughout this thesis.

The expressions for sand deposition in eq. (3.7) and mud deposition in eq. (3.8) can also be applied for sand-mud mixtures when the mud concentration in the water column is well below the so-called 'gel point concentration'. The gel point concentration is the concentration beyond which sand particles get trapped in the mud matrix. Depending on the type of sediment, the gel point concentration is about 30 - 180 g/l (Winterwerp, 1999). Several experiments have shown that sand and mud behave independently in the water column under these conditions. For example, Torfs (1995) observed strong segregation of sand and mud during settling experiments for sediment concentrations below the gel point, whereas sand particles were trapped within the matrix of mud particles at higher concentrations. Hence, the deposition fluxes for suspended sand ( $-w_s c_s$ ) in eq. (3.7) and mud ( $D_m$ ) in eq. (3.8) are not reconsidered herein.

The aforementioned equations for sand and mud cannot be applied directly to the erosion of sand-mud mixtures. Obviously, the availability of a certain sediment fraction in the bed limits the erosion flux of that fraction. Besides, several erosion experiments have shown that the erosion characteristics are also affected by the mud content (Murray, 1977; Torfs, 1995; Panagiotopoulos et al., 1997). Thus, the bed load transport rate of sand ( $q_b$ ) and the erosion flux for suspended sand ( $w_s c_a$ ) in eq. (3.7) and the erosion flux for suspended mud ( $E_m$ ) in eq. (3.8) must be reconsidered for sand-mud mixtures. In Section 3.2, a useful classification was made for the erosion behaviour of sand-mud mixtures by using appropriate parameters for cohesion and network structure. At present however, the importance of the network structure is less clear than that of cohesion. Hence, erosion formulations are proposed for non-cohesive (Section 3.3.2) and for cohesive sand-mud mixtures (Section 3.3.3), but the effect of the network structure is not taken into account explicitly. Finally, the formulations are validated against experimental results (Section 3.3.4).

Beforehand, it should be emphasised that the erosion formulations in the next sections are described in terms of sand and mud, instead of the classical distinction between sand, silt and clay (cf. Table 2.1). The silt and the clay fraction are treated in one mud fraction, because the clay/silt ratio appears to be constant for a specific estuary or tidal basin (cf. Table 2.3). A special remark is made with respect to the distinction between non-cohesive and cohesive sand-mud mixtures. In general, a clay content of 5 - 10% is the governing parameter for this transition (see also Section 3.2). Because silt and clay are considered as one mud fraction, a so-called 'critical mud content' (denoted by  $p_{m,cr}$ ) is applied herein for the distinction between non-cohesive and cohesive sand-mud mixtures. So, the parameter value is always site-specific.

### 3.3.2 Non-cohesive sand-mud mixtures

#### Effects of adding mud to a sand bed

Although non-cohesive sand-mud mixtures do not have cohesive properties, several erosion experiments have shown that the erosion characteristics can change when adding (a small



amount of) mud to a sand bed. For example, Murray (1977) observed that the (horizontal) bed load transport rate decreased significantly with increasing mud content, whereas the bed behaviour was still non-cohesive. In addition, Bisschop (1993) measured a decreasing (vertical) erosion rate for increasing clay content. Finally, Panagiotopoulos et al. (1997) reported an increasing critical shear stress for sand with increasing clay (and mud) content. However, Torfs (1995) did not observe changes for low mud content and could describe the sand transport rate reasonably well with an existing formula for sand only.

Various authors have given explanations for the observed decrease in bed load transport rate or erosion rate for sand. Mitchener and Torfs (1996) suggest that the bed roughness decreases, because mud between the sand particles smooths the bed surface. As a result, the applied bed shear stress and the bed load transport rate also decrease. Panagiotopoulos et al. (1997) state that the angle of repose for the sand particles increases because mud fills the pores in between the sand particles. Consequently, the critical shear stress for sand increases and the bed load transport decreases. Bisschop (1993) puts forward that mud fills the pores in between the sand particles as a result of which the bed permeability decreases. As a consequence, the pick-up rate of sand particles (and the bed load transport rate) decreases. It should be noted that the latter effect was given little attention in most erosion experiments with sand-mud mixtures.

Several suggestions have been given for taking into account these effects in the traditional formulae for sand transport only. Mitchener and Torfs (1996) present some indicative values for the roughness of sand beds, mixed sand-mud beds and mud beds, but changes in bed roughness have never been investigated systematically. Based on laboratory experiments, Van Rijn (1993) and Whitehouse et al. (2000) propose a relationship between the critical shear stress and the mud content between 0 and 20%. The latter expression has been based on earlier work by Chesher and Ockenden (1997). Although not equivalent, these equations suggest that the critical shear stress at a mud content of 20% is a factor 3 to 5 times larger than the critical shear stress for sand only. Because the authors do not make a distinction between non-cohesive and cohesive sand-mud mixtures, it is not clear whether these equations can be applied for non-cohesive sand-mud mixtures. Finally, Bisschop (1993) presents a formula for the erosion rate in which the effect of the bed permeability is incorporated. The proposed formula is based on the Van Rijn's erosion rate formula (Van Rijn, 1984) and shows good agreement with experimental data. However, the applicability of this formula for non-cohesive sand-mud mixtures is limited because of several reasons:

- The formula was validated for relatively high current velocities ( $> 1$  m/s) and flat bed conditions only. It is not known at present if this expression can also be used for a rippled bed and low flow velocities.
- Good agreement between the formula and the experimental data could only be obtained when much higher values of the critical shear stress for sand only were applied than according to the Shields criterion.

- The relation between the (vertical) erosion rate and the (horizontal) bed load transport rate and the reference concentration for suspended sediment is not well understood, and therefore not straightforward (e.g Van Rijn, 1993).

### Critical shear stress

Because a validated expression accounting for the aforementioned effects is lacking, the critical bed shear stress is chosen herein to include all effects into one parameter. Van Rijn (1993) and Whitehouse et al. (2000) have already presented a relationship between the critical shear stress and the mud content. To investigate the applicability of these equations, both equations and experimental data from Torfs (1995) and Panagiotopoulos et al. (1997) are presented in Figure 3.6. The critical shear stress on the vertical axis is made dimensionless with the measured critical shear stress for sand only. Based on the classification in the previous section, a distinction is made between non-cohesive and cohesive mixtures.

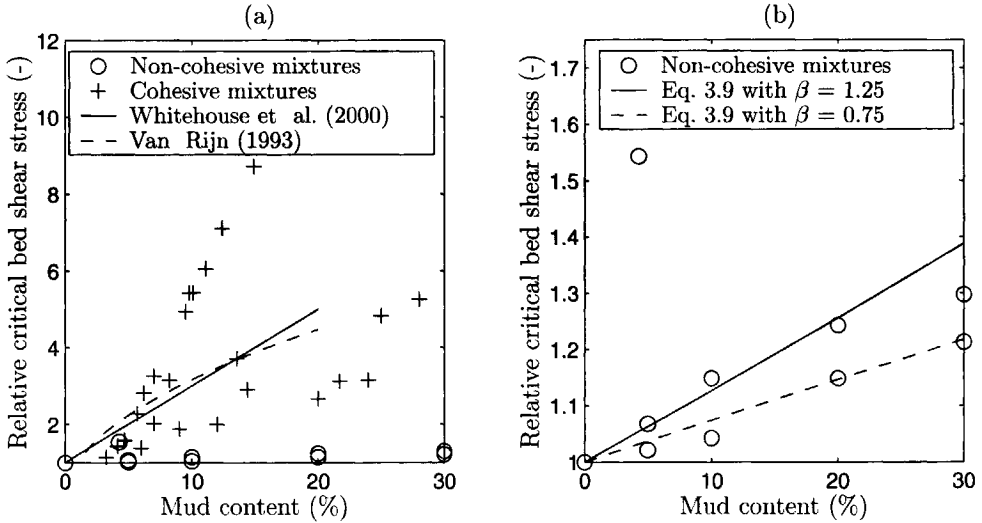


**Figure 3.6:** Comparison between experimental data and proposed equations for relationship between critical shear stress and mud content.

Figure 3.6a shows that the equations largely overestimate the effect of the mud content on the critical shear stress for non-cohesive sand-mud mixtures. Furthermore, the critical shear stress for cohesive mixtures is also not properly approximated by these equations. As the existing relationships between the mud content and the critical shear stress for non-cohesive mixtures are not appropriate, we propose the following heuristic relationship for non-cohesive beds:

$$\frac{\tau_{e,nc}}{\tau_{cr}} = (1 + p_m)^\beta \quad p_m < p_{m,cr} \quad (3.9)$$

where  $\tau_{e,nc}$  is the critical shear stress for non-cohesive sand-mud mixtures,  $\tau_{cr}$  the critical shear

stress for sand only, and  $\beta$  an empirical coefficient. The data of the non-cohesive sand-mud mixtures and eq. (3.9) for two different values of  $\beta$  are shown in Figure 3.6b. Except for one mixture, the increase in critical bed shear stress for non-cohesive mixtures is approximated reasonably well for  $\beta = 0.75 - 1.25$ . The coefficient  $\beta$  may depend on the packing of the sediment bed.

### Bed load transport rate and reference concentration

Torfs (1995) demonstrates that the existing formulations for sand transport can be applied for low mud contents. Herein, Van Rijn's equations are applied (Van Rijn, 1993), but with the modified critical shear stress (eq. 3.9) in the transport parameter  $T_{nc}$  (see also Appendix A):

$$q_b = \alpha_{b1} \Delta^{0.5} g^{0.5} d_{50}^{1.5} T_{nc}^{\alpha_{b2}} D_*^{-0.3} \quad p_m < p_{m,cr} \quad (3.10)$$

$$c_a = 0.015 \frac{d_{50}^{1.5} T_{nc}^{1.5}}{a D_*^{0.3}} \quad p_m < p_{m,cr} \quad (3.11)$$

where  $g$  is the gravitational acceleration,  $\Delta$  the specific gravity,  $d_{50}$  the median sand grain size,  $D_*$  the dimensionless grain size,  $c_a$  the reference concentration at the reference height  $a$ . The coefficients  $\alpha_{b1}$  and  $\alpha_{b2}$  depend on the parameter  $T_{nc}$ . The coefficients amount to  $\alpha_{b1} = 0.053$  and  $\alpha_{b2} = 2.1$  for  $T_{nc} < 3$ , whereas for higher  $T_{nc}$ -values  $\alpha_{b1} = 0.1$  and  $\alpha_{b2} = 1.5$ . The transport parameter  $T_{nc}$  in eq. (3.10) and (3.11) includes the modified critical shear stress according to eq. (3.9) and is defined as:

$$T_{nc} = \frac{\tau_b}{\tau_{cr}(1 + p_m)^\beta} - 1 \quad p_m < p_{m,cr} \quad (3.12)$$

Thus, the bed load transport rate in eq. (3.10) and the reference concentration in eq. (3.11) both decrease with increasing mud content when the transport parameter according to eq. (3.12) is applied. Another important implication of eq. (3.12) is that the bed shear stress at which the bed load transport rate (eq. 3.10) and the reference concentration (eq. 3.11) are equal to zero, increases with increasing mud content.

### Erosion rate for mud

An erosion formula for the mud fraction is also needed. Visual observations suggest that mud particles are easily washed out from the top layer, when the bed behaves non-cohesively (Murray, 1977; Torfs, 1995). Therefore, it seems reasonable that all mud particles between the moving sand particles are eroded. A generic erosion formula for mud is derived in Appendix A, which is a function of the bed load transport rate and the saltation length of sand particles. Applying Van Rijn's expressions (Van Rijn, 1993), the erosion rate of mud ( $E_m$ ) for non-cohesive beds is as follows:

$$E_m = \frac{\alpha_{b1}}{3} \frac{p_m}{1 - p_m} \frac{\sqrt{\Delta g d_{50}}}{D_*^{0.9}} T_{nc}^{\alpha_{b2} - 0.9} \quad p_m < p_{m,cr} \quad (3.13)$$

where  $p_m$  is the mud content at the bed surface. The erosion rate formula in eq. (3.13) has the following implications. First, the erosion rate of mud is equal to zero when the mud content at the bed surface ( $p_m$ ) equals zero, or if the bed shear stress is less than the critical bed shear stress. Furthermore, with increasing bed shear stress, the erosion rate of mud also increases. The erosion rate of mud also increases with increasing mud content in the bed due to the increasing availability of mud at the bed surface. However, it decreases due to the increasing critical shear stress. The net effect can be that the erosion flux of mud either increases or decreases with increasing mud content.

The obtained erosion formula (eq. 3.13) is comparable with the well-known Partheniades formula in eq. (3.8). The erosion coefficient  $M$  in Partheniades' formula is rewritten in eq. (3.13):

$$M_{nc} = \frac{\alpha_{b1}}{3} \frac{\sqrt{\Delta g d_{50}}}{D_*^{0.9}} \quad p_m < p_{m,cr} \quad (3.14)$$

where  $M_{nc}$  is the erosion coefficient for non-cohesive sand-mud mixtures. The value of the erosion coefficient in eq. (3.14) can be estimated for reasonable values of the sand grain size. For sand grain sizes between 100 and 200  $\mu\text{m}$ , the erosion coefficient is in the order of  $10^{-4}$  m/s or 0.1 kg/(m<sup>2</sup>s). This is several orders of magnitude larger than reported values for cohesive mud beds, which are in the order of  $10^{-3} - 10^{-5}$  kg/(m<sup>2</sup>s) (Winterwerp, 1989). The high value for the erosion coefficient in eq. (3.14) reflects that mud is easily washed out from the top layer when the bed behaves non-cohesively. The erosion of mud is limited by the availability in the top layer (eq. 3.13).

### 3.3.3 Cohesive sand-mud mixtures

Experiments with cohesive sand-mud mixtures have shown that the erosion characteristics strongly differ from non-cohesive sand-mud mixtures. Torfs (1995) observed simultaneous erosion of sand and mud from a smooth bed with no sand ripples. The erosion mode can be classified as surface or mass erosion, depending on the clay type and the bed density. These characteristics are included in formulations for the bed load transport rate of sand and the erosion fluxes of sand and mud as follows. The absence of ripples during experiments with cohesive sand-mud mixtures indicate that bed load transport of sand is not possible. Hence, we assume that sand is only transported in suspension and that the bed load transport rate for cohesive sand-mud mixtures equals zero. Williamson and Ockenden (1993) and Torfs (1995) already indicated that the erosion flux of a cohesive sand-mud bed can be described by the Partheniades' formula for cohesive mud beds. Based on these considerations, the bed load transport rate for sand, and the erosion rate of suspended sand and mud can be expressed as follows:

$$q_b = 0.0 \quad p_m > p_{m,cr} \quad (3.15)$$

$$E_s = (1 - p_m)M_c \left( \frac{\tau_b}{\tau_{e,c}} - 1 \right) H \left( \frac{\tau_b}{\tau_{e,c}} - 1 \right) \quad p_m > p_{m,cr} \quad (3.16)$$

$$E_m = p_m M_c \left( \frac{\tau_b}{\tau_{e,c}} - 1 \right) H \left( \frac{\tau_b}{\tau_{e,c}} - 1 \right) \quad p_m > p_{m,cr} \quad (3.17)$$

where  $\tau_{e,c}$  is the critical erosion shear stress and  $M_c$  the erosion coefficient for cohesive sand-mud mixtures.

For reasons of consistency, the cohesive erosion rate in eq. (3.17) and the non-cohesive erosion rate in eq. (3.13) for mud should be equal at the transition between both regions ( $p_m = p_{m,cr}$ ). Hence, the coefficient  $\alpha_{b1}$  and  $\alpha_{b2}$  in eq. (3.13) are assumed to be constant and equal to 0.075 and equal to  $\alpha_{b1} = 0.075$  and  $\alpha_{b2} = 1.9$ . The value for  $\alpha_{b2}$  is in the range of the proposed values by Van Rijn (1993) for sand beds only ( $\alpha_{b2} = 1.5 - 2.1$ ).

Furthermore, it seems unrealistic that the erosion rate for sand of a cohesive sand-mud bed (eq. 3.16) can exceed the erosion rate of a pure sand bed. When more sand would be eroded from a cohesive sand-mud bed, the sand particles will directly settle because the flow cannot keep them in suspension. Consequently, the upper limit of the sand erosion rate ( $E_s$ ) of a cohesive sand-mud bed in eq. (3.16) equals the erosion rate of a pure sand bed ( $w_{sca}$ ).

Finally, the critical erosion shear stress ( $\tau_{e,c}$ ) and the erosion coefficient ( $M_c$ ) in eq. (3.16) and (3.17) must be determined experimentally. Even for beds with only mud, the range of reported values for these parameters is very large. For natural muds, the critical erosion shear stress varies between 0.1 and 0.5 N/m<sup>2</sup> and measured erosion rates range from 10<sup>-5</sup> kg/(m<sup>2</sup>s) to 10<sup>-3</sup> kg/(m<sup>2</sup>s) Winterwerp (1989). The dependency of the erosion rate and the critical erosion shear stress on the mud content are discussed hereafter.

### Critical erosion shear stress

Laboratory and field experiments have shown that the critical erosion shear stress for cohesive mixtures can increase (Torfs, 1995; Panagiotopoulos et al., 1997), or decrease (Williamson & Ockenden, 1993) with increasing mud content (or clay content). In addition, Torfs (1995) observed for sand-mud mixtures with constant bed density, that the (linear) increase in critical shear stress strongly depends on the mud composition. Two explanations have been given for the observed dependency of the mud content with the critical shear stress. Williamson and Ockenden (1993) state that the decreasing critical shear stress could be explained by a decreasing bed density. Torfs (1995) puts forward that, with increasing mud content, more cohesive particles are present, resulting in a higher critical shear stress. She also suggests that

the higher the amount of clay in the mud fraction, the higher the increase in critical erosion shear stress.

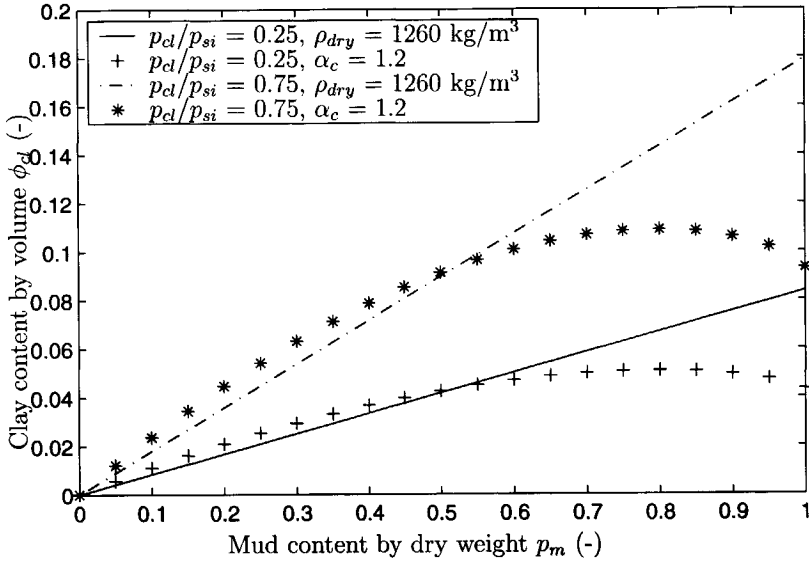


**Figure 3.7:** Clay content by volume as a function of mud content by dry weight.

These explanations suggest that the critical shear stress is likely to be proportional to the volume content (!) of clay ( $\phi_{cl}$ ). Therefore, the volume content of clay is shown in Figure 3.7 as a function of the mud content by dry weight in the sediment bed. Two situations are considered: a constant bed density ( $\rho_b = 1260 \text{ kg/m}^3$ , open symbols) and a varying bed density ( $\alpha_c = 1.2$ , closed symbols). In case of the bed density variation, the relationship of Allersma (1988a) in eq. (3.5) between the bed density and the mud content is applied with a consolidation coefficient  $\alpha_c = 1.2$ . The variation in clay content by volume in both situations is presented for two clay/silt ratios:  $p_{cl}/p_{si} = 0.25$  and  $p_{cl}/p_{si} = 0.75$ .

Figure 3.7 shows that the volume content of clay linearly increases with increasing mud content in the case of a constant bed density. Furthermore, the increase is higher for larger clay/silt ratio. Consequently, it can be expected that the critical erosion shear stress increases linearly with increasing clay content by dry weight, when the bed density is constant. This dependency is confirmed qualitatively by a re-analysis of Torfs' experiments. The critical erosion shear stress is plotted against the mud content (see also Torfs, 1995) and the clay content by dry weight in Figure 3.8. It can be observed that the increase in critical shear stress as a function of the mud content strongly differs for both mixtures, whereas the discrepancy in critical shear stress is much smaller as a function of the clay content by dry weight. The type clay mineral with a different binding capacity presumably explains this difference.

When the bed density varies however, the volume content of clay first increases and then

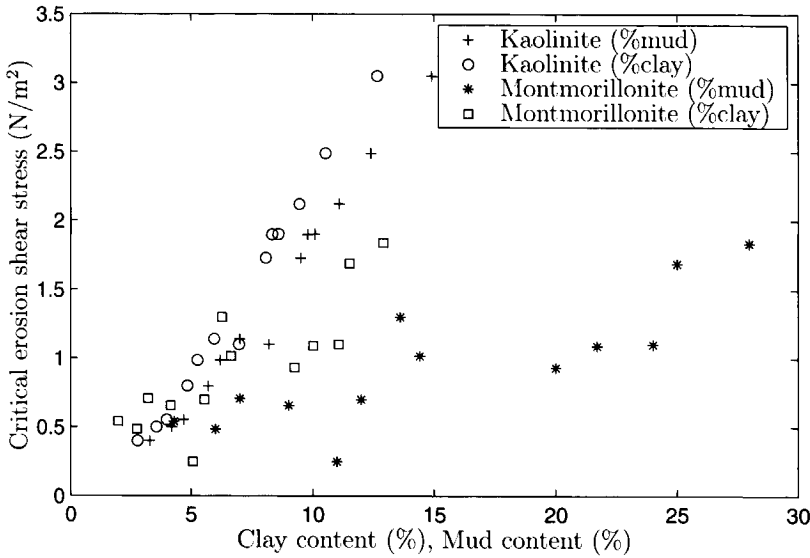


**Figure 3.8:** Re-analysis of critical erosion shear stress as a function of mud and clay content by dry weight (After Torfs, 1995).

decreases with increasing mud content (Figure 3.7). Hence, the erosion shear stress is expected to increase or decrease with increasing mud content depending on the bed density variation. This might explain qualitatively the decrease of the erosion shear stress with increasing mud content as observed by Williamson and Ockenden (1993). With increasing mud content, the bed density decreases and probably also the volume content of clay, although the clay content by dry weight increases.

In natural sediment beds, the volume content of clay varies in time and space because of consolidation. As already indicated in Section 2.3, the consolidation process is insufficiently understood, in particular for sand-mud mixtures. Hence, applying consolidation models in large-scale models is not straightforward at present. For the time being, the bed density is therefore assumed to be constant in time and space. A constant bed density and a constant clay/silt ratio in the sediment bed implies that the clay content by volume varies linearly with the mud content by dry weight (cf. Figure 3.7). Under this condition the relationship between the critical erosion shear stress for cohesive sand-mud mixtures and the mud content by dry weight is likely to be linear, too. To avoid a discrepancy with the formulation for non-cohesive mixtures, the critical erosion shear stress at the transition ( $p_m = p_{m,cr}$ ) should be equal to eq. (3.9). This results in the following expression for the critical erosion shear stress ( $\tau_{e,c}$ ) for cohesive sand-mud mixtures:

$$\tau_{e,c} = \frac{\tau_{cr}(1 + p_{m,cr})^\beta - \tau_e}{1 - p_{m,cr}}(1 - p_m) + \tau_e \quad p_m > p_{m,cr} \quad (3.18)$$

where  $\tau_e$  is the erosion shear stress of a pure mud bed. Depending on the value of  $\tau_e$ , the critical erosion shear stress increases, is constant or decreases with increasing mud content for cohesive sand-mud mixtures.

### Erosion coefficient

Various authors have presented experimental data in which the erosion parameter strongly decreases with increasing mud content (Torfs, 1995; Houwing, 2000). Other experimental data suggest that the erosion parameter increases with increasing mud content (Williamson & Ockenden, 1993). The variation in cohesive particles and bed density are both put forward to explain this behaviour. Only Van Kesteren et al. (1997) present an expression for the erosion coefficient based on theoretical considerations:

$$M = \frac{c_v}{10d_{50} \left(1 + \frac{\rho_s}{\rho_w} w_{cr}\right)} \frac{\tau_e}{f_u - \tau_e} \quad (3.19)$$

where  $c_v$  is the consolidation coefficient,  $d_{50}$  the median grain size,  $f_u$  the remoulded shear strength,  $\rho_s$  the sediment density,  $\rho_w$  the water density,  $w_{cr}$  the critical water content and  $\tau_e$  the critical erosion shear stress for mud beds. The critical water content  $w_{cr}$  is the water content at the bed surface at which the erosion process starts.

Equation (3.19) can be assessed qualitatively to determine the effects of variations in mud content. Experimental data show that the consolidation coefficient decreases and the remoulded shear strength increases logarithmically with increasing clay content (Van Kesteren et al., 1997), whereas the other parameters in eq. (3.19) are more or less constant. Thus, it is expected that the erosion coefficient also decreases logarithmically with increasing clay content. Notice that the mud content is of small importance for variations in the erosion coefficient.

Based on these qualitative dependencies, the erosion coefficient for cohesive sand-mud mixtures is assumed to decrease logarithmically towards a 'known' value for pure mud beds. To avoid discrepancies with the erosion flux for non-cohesive sand-mud mixtures (eq. 3.13), the erosion coefficient at the critical mud content ( $p_m = p_{m,cr}$ ) should be equal to  $M_{nc}/(1 - p_{m,cr})$ . Thus, the expression for the cohesive erosion coefficient ( $M_c$ ) reads as follows:

$$\log M_c = \frac{\log \left( \frac{M_{nc}}{1 - p_{m,cr}} \right) - \log M}{1 - p_{m,cr}} (1 - p_m) + \log M \quad p_m > p_{m,cr} \quad (3.20)$$

where  $M$  is the erosion coefficient for a pure mud bed. Measurements show that the erosion coefficient  $M$  ranges from  $10^{-3}$  to  $10^{-5}$  kg/(m<sup>2</sup>s) for natural mud beds in open water (Winterwerp, 1989).



### 3.3.4 Experimental validation

#### Non-cohesive sand-mud mixtures

The bed load transport formula (eq. 3.10) with the adapted transport parameter (eq. 3.12) can be compared with the experimental results of Murray (1977). During these experiments, the bed load transport rate for mixtures with a coarse sand fraction ( $d_{50} = 0.8 \text{ mm}$ ) and 0%, 10% and 18% mud content was measured. The experimental results and the accompanying bed load transport rate according to eq. (3.10) and (3.12) with  $\beta = 1.25$  are shown in Figure 3.9a.

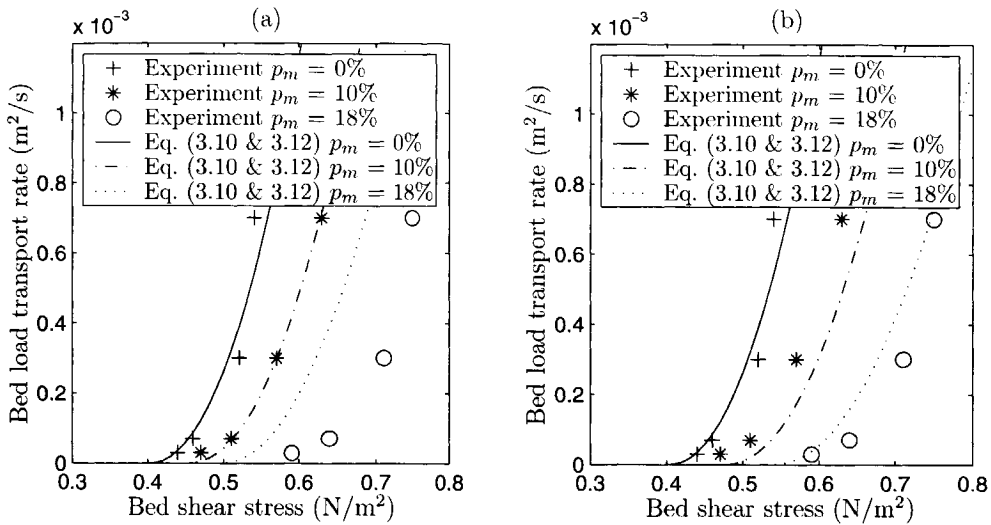


**Figure 3.9:** Comparison between Murray's experimental data and the bed load transport formula (eq. 3.10 & 3.12) with a)  $\beta = 1.25$  and b)  $\beta = 1.75$ .

A good agreement is obtained between the measurements and the bed load transport formula with  $\beta = 1.25$  for 0 and 10% mud content (Figure 3.9a). The bed load transport formula, however, overestimates the bed load transport rate for 18% mud content. Applying a somewhat larger value for  $\beta$  (e.g.  $\beta = 1.75$ , see Figure 3.9b) gives better results for the bed load transport rate. A larger value for  $\beta$  might be explained by the fact that not only the critical shear stress is higher, but also the bed roughness and permeability affects the bed load transport rate for higher mud content.

Based on experimental results, Torfs (1995) concludes that the bed load transport rate for several sand-mud mixtures with low mud content can be described properly with Van Rijn's formula for sand only. The mud content for the non-cohesive kaolinite mixtures was less than 3%, whereas the mud content of the non-cohesive montmorillonite mixtures was less than 7% during these experiments. Applying eq. (3.12) also indicates that a bed load transport formula for sand only can be used for these mixtures, because the effect on the critical shear stress is small ( $< 10\%$ ) when the mud content is less than 7%.

### Cohesive sand-mud mixtures

The proposed formulations for cohesive sand-mud mixtures can only be qualitatively compared because a data set for the entire mud content range is not available. Torfs (1995) has already shown that the erosion of cohesive sand-mud mixtures can be described with Partheniades' erosion formula. In addition, she observed that the erosion flux decreased one order of magnitude when the mud content increased from 3% to 12%. Applying the formulations proposed in the previous section would also lead to a strongly decreasing erosion flux with increasing mud content, mainly because the erosion coefficient (eq. 3.20) decreases logarithmically with increasing mud content.

## 3.4 Conclusions

In this chapter, a classification for erosion behaviour of sand-mud mixtures has been developed based on appropriate parameters for cohesion and network structure. In addition, erosion formulations for non-cohesive and cohesive sand-mud mixtures have been proposed and compared against data from laboratory and field experiments.

The following conclusions can be drawn:

- The agreement between the classification and the experimental data from laboratory experiments shows the importance of the classification. Especially, the transition between non-cohesive and cohesive behaviour at a clay content of 5 - 10% for natural sediment beds is well validated by experimental data. This also indicates that the 3 - 15% mud content range for this transition suggested by Mitchener and Torfs (1996) and Whitehouse et al. (2000) is less appropriate for this transition.
- A re-analysis of the experiments of Torfs (1995) shows that the observed differences in erosion behaviour between the kaolinite and montmorillonite mixtures can be explained by including the transitions in network structure. However, this aspect has not been given much attention in other experiments. It is recommended to study this aspect more systematically in future work.
- An estimation of the prevailing bed types in natural systems shows that the constant clay/silt ratio in a certain system determines what bed types are important. The analysis also indicates that silt-dominated bed types rarely occur in natural systems for which relationship (3.5) holds.
- Based on experimental data, a relationship between the critical shear stress and the mud content is proposed for non-cohesive sand-mud mixtures. Also an erosion equation for mud is given. The equation is similar to the well-known Partheniades formula for mud beds, but with a much larger erosion coefficient.
- Based on previous investigations, the erosion fluxes for suspended sand and mud from a cohesive bed are described by the Partheniades formula. The observed dependency of

the critical erosion shear stress and the erosion coefficient on variations in mud content are included in the proposed formulations.

- Comparison with a limited number of laboratory experiments shows that the erosion formulations can be used as a first step. It is recommended that an extensive set of erosion experiments with sand-mud mixtures is carried out to validate these formulations more precisely. Special attention should be paid to the role of the network structure.



## Chapter 4

### Set-up of a process-based sand-mud model

#### 4.1 Introduction

Currently, process-based models exist separately for sand transport (Van Rijn, 1993) and mud transport (Teisson, 1997). Basically, these models consist of a set of equations which describe the flow by currents and waves, sediment transport and bed level variations. The interaction between bed level changes and the water motion is only included in sand models at present. Obviously, the applicability of these models for the understanding and prediction of large-scale sand-mud segregation is limited. One major limitation is that temporal and spatial mud content variations in the sediment bed are not taken into account explicitly.

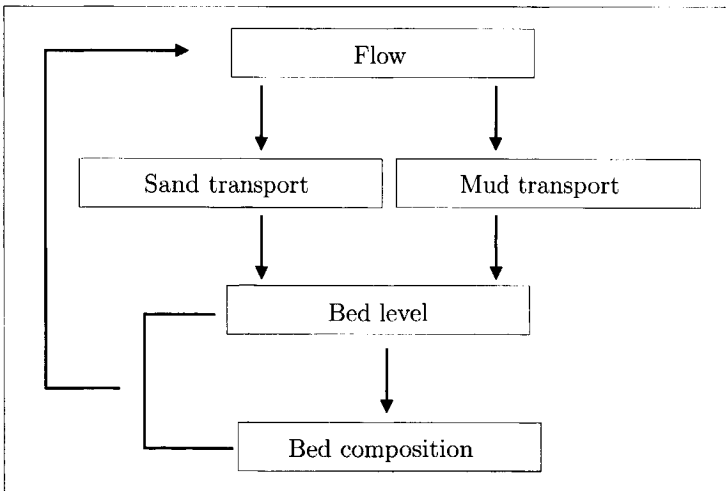


**Figure 4.1:** Set-up of the proposed sand-mud model.

In this chapter, a set of equations is proposed for a three-dimensional process-based sand-mud model with a (non-cohesive) sand fraction and a (cohesive) mud fraction. The set-up of such a process-based sand-mud model is shown in Figure 4.1. Three major extensions with respect to the aforementioned sand and mud models can be distinguished. Firstly, sand and

mud both contribute to bed level changes. Secondly, mud content variations in time and space are explicitly taken into account. Thirdly, the exchange of sediment between the bed and the water column depends on the bed composition at the bed surface.

The outline of this chapter is as follows. The flow module, the sediment transport module and the bed level and bed composition module are discussed in Sections 4.2 - 4.4, respectively. Ideally, all processes and interactions described in Chapter 2 should be included in these modules. Simplifications and assumptions, which are inevitable because of insufficient understanding of the processes, are also discussed in these sections. The erosion formulation for sand-mud mixtures derived in Chapter 3 is included in the sediment transport module. Finally, the numerical implementation of the process-based sand-mud model is discussed in Section 4.5.

## 4.2 Flow module

### 4.2.1 Equations

In principle, the present-day large-scale models for currents and short waves in estuaries and tidal basins can be applied without modifications as long as the effect of the total sediment concentration on the turbulent water motion is relatively small. This assumption is also made in the sand-mud model, because the behaviour of high-concentrated suspensions is insufficiently understood at present. Although the upper limit depends on the flow conditions, Winterwerp (2001) indicates that the effect of mud suspensions on the turbulent water motion can be neglected below several hundreds of mg/l for flow conditions normally found in estuaries and tidal basins. It seems reasonable that this limit can also be applied for sand-mud mixtures.

The three-dimensional behaviour of currents is described by a mass balance equation and three momentum equations (see e.g. Vreugdenhil, 1989; Van Rijn, 1993). Two important assumptions are made. The vertical accelerations are small with respect to the gravitational acceleration (i.e. 'shallow water approximation'). Moreover, the density variations are small with respect to the water density itself and are only maintained in the gravity term (i.e. 'Boussinesq approximation'). The dependent variables in the mass balance and momentum equations are the water level ( $\zeta$ ) and three velocity components ( $u, v, w$ ) which are shown in Figure 4.2. Currents induced by the tide, river discharge, short waves, wind and earth rotation can be modelled by solving these equations.

Short waves are described by a two-dimensional balance equation for the evolution of the action density spectrum (see e.g. Booij et al., 1999). The action density spectrum is defined as the well-known energy density spectrum divided by the relative frequency as observed in a reference frame moving with the action propagation velocity. The action balance includes important wave phenomena such as propagation, depth-induced and current-induced refraction and shoaling, wave generation by wind, wave dissipation by whitecapping and bottom friction, and non-linear

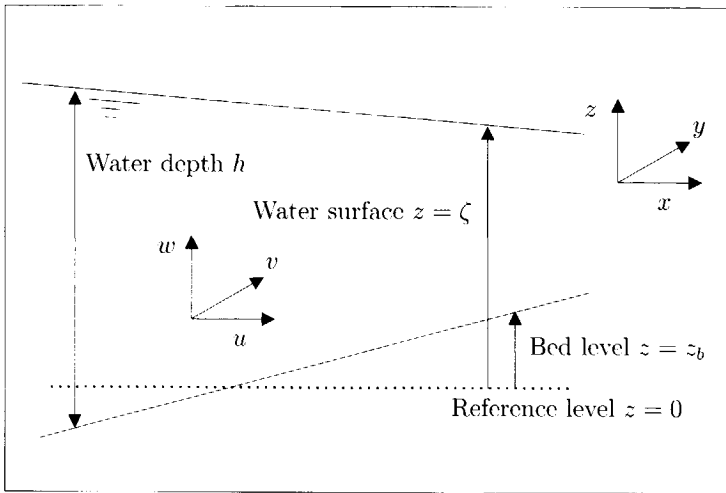


**Figure 4.2:** Definition coordinate system and flow variables.

wave-wave interactions. Pure diffraction and reflection, however, are not explicitly taken into account in the two-dimensional action balance equation.

#### 4.2.2 Parameters

Several parameters must be prescribed for solving the aforementioned equations for currents and short waves. Obviously, many of them do not change when more sediment fractions are introduced and do not require further discussion. Only the fluid mixing coefficient in both the horizontal and vertical directions and the roughness coefficient are discussed below:

##### Turbulent mixing

The existing turbulent mixing models can be applied when the total sediment concentration in the water column remains low. Herein, the horizontal fluid mixing coefficients ( $\nu_x$  and  $\nu_y$ ) are assumed constant in time and space, while an algebraic expression for the vertical fluid mixing profile ( $\nu_z$ ) is applied. For example, the well-known parabolic viscosity profile is applied for a situation with currents only. It should be noted that the use of these expressions for the mixing coefficients is not essential for the proposed model. More sophisticated turbulence models (e.g.  $k - \varepsilon$  model) can be applied as well.

##### Roughness

The bed roughness parameter is an important parameter for describing the momentum exchange between the bed and the flow by currents and/or short waves. Qualitatively, it is known that the roughness parameter for non-cohesive sediments strongly depends on the hydraulic conditions and the bed composition. Typical values for the Chézy-coefficient in natural open channel flow

range from 40 - 60  $\text{m}^{1/2}/\text{s}$  for non-cohesive sand beds, while 60 - 100  $\text{m}^{1/2}/\text{s}$  is the range for cohesive environments (Van Rijn, 1993). At present, a reliable roughness predictor, in which the effect of bed composition variations is taken into account, does not exist. Therefore, the roughness coefficient is assumed constant in time and space in this model at present.

### 4.3 Sediment transport module

#### 4.3.1 Equations

The description of sand transport is divided into bed load and suspended load transport (Figure 4.3). Bed load occurs near the bed surface and adapts instantaneously to the flow conditions, whereas suspended load is also determined by upstream conditions. The bed boundary for suspended sand transport is located at a small height above the bed level, the so-called 'reference height'. Mud is only transported in suspension at low sediment concentrations, while mud can also be transported in a layer near the bed at high concentrations (i.e. 'fluid mud'). Herein, only suspended mud is taken into account, which is mixed over the entire water column (Figure 4.3).

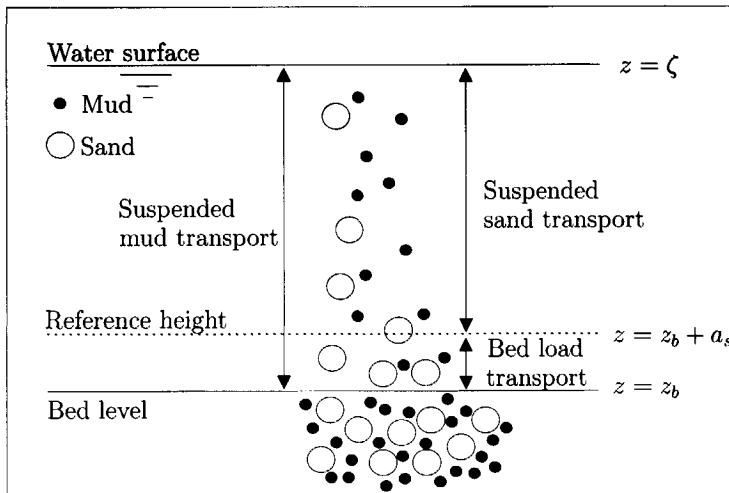


Figure 4.3: Sand and mud transport.

Suspended sand and mud transport are generally described with advection-diffusion equations (Van Rijn, 1993; Teisson, 1997). Deposition experiments for sand-mud mixtures have shown that sand and mud behave independently in the water column for mud concentrations below the so-called 'gel point' concentration or structural density (Torfs et al., 1996). Above this concentration, the mud flocs form a structure in the water column and sand particles are trapped herein. The gel point concentration ranges from 10 to 250  $\text{g}/\text{l}$  (Winterwerp, 2002).



The validity limit of the assumption that the effect of the suspended mud concentration on the turbulent water motion can be neglected, is much lower and amounts to several hundreds of mg/l (see also Section 4.2). For such low concentrations, sand and mud behave independent from each other and their concentrations can be described with two uncoupled advection-diffusion equations:

$$\frac{\partial c_s}{\partial t} + u \frac{\partial c_s}{\partial x} + v \frac{\partial c_s}{\partial y} + (w - w_s) \frac{\partial c_s}{\partial z} = \epsilon_x \frac{\partial^2 c_s}{\partial x^2} + \epsilon_y \frac{\partial^2 c_s}{\partial y^2} + \frac{\partial}{\partial z} \left( \epsilon_{z,s} \frac{\partial c_s}{\partial z} \right) \quad (4.1)$$

$$\frac{\partial c_m}{\partial t} + u \frac{\partial c_m}{\partial x} + v \frac{\partial c_m}{\partial y} + (w - w_m) \frac{\partial c_m}{\partial z} = \epsilon_x \frac{\partial^2 c_m}{\partial x^2} + \epsilon_y \frac{\partial^2 c_m}{\partial y^2} + \frac{\partial}{\partial z} \left( \epsilon_{z,m} \frac{\partial c_m}{\partial z} \right) \quad (4.2)$$

where  $c_s$  is the sand concentration,  $w_s$  the settling velocity for sand,  $\epsilon_x$  the sediment diffusivity in  $x$ -direction for sand and mud,  $\epsilon_y$  the sediment diffusivity in  $y$ -direction for sand and mud,  $\epsilon_{z,s}$  the sediment diffusivity in  $z$ -direction for sand,  $c_m$  the mud concentration,  $w_m$  the settling velocity for mud and  $\epsilon_{z,m}$  the sediment diffusivity in  $z$ -direction for mud. Because of independency between sand and mud, the settling velocity and the sediment diffusivity in the sand concentration equation do not depend on the mud concentration and vice versa. Furthermore, the sediment diffusivity coefficients in the horizontal directions are assumed to be uniform and equal for sand and mud (i.e.  $\epsilon_{x,s} = \epsilon_{x,m} = \epsilon_x$  and  $\epsilon_{y,s} = \epsilon_{y,m} = \epsilon_y$ ).

When the bed consists of sand only, the bed load transport rate for sand is formulated as a function of the grain size characteristics and the flow properties (Van Rijn, 1993). Several experiments have shown that the bed load transport rate also changes when the mud content at the bed surface varies (Murray, 1977; Torfs, 1995). An expression for the bed load transport rate in which this effect is incorporated, is derived in Chapter 3 and included in the present model set-up.

### 4.3.2 Boundary conditions

Appropriate initial and boundary conditions are needed for solving the advection-diffusion equations for suspended sand (eq. 4.1) and mud transport (eq. 4.2). These conditions are discussed below. It should be noted that in our current model set-up only the bed boundary condition essentially changes when more sediment fractions are introduced.

#### Initial conditions

The sand concentration  $c_s(t = 0, x, y, z)$  and the mud concentration  $c_m(t = 0, x, y, z)$  have to be specified at time  $t = 0$ . These concentrations are set to zero, unless otherwise stated. This condition is usually not very important because its influence will disappear after some time.

#### Inflow boundary conditions

Sand and mud concentrations have to be specified at the inflow boundaries. The equilibrium

sand concentration profile is used for sand. However, an equilibrium mud concentration profile does not exist for low mud concentrations. Therefore, a vertically uniform mud concentration profile is prescribed at the inflow boundary.

### Outflow conditions, and closed and water surface boundary conditions

The conditions used in the existing single-fraction models at these boundaries are also adequate for each sediment fraction in a multiple-sediment fraction model. A ‘weak’ condition is generally applied at outflow boundaries. This means that the first or second derivative of the concentration normal to the boundary is set to zero. The sediment fluxes across closed and water surface boundaries are set at zero.

### Bed boundary condition

The bed boundary for suspended sand transport is located at a small height above the bed level, the so-called ‘reference’ height (Figure 4.3). Two bed boundary conditions can be applied for suspended sand at this boundary: a concentration type and a gradient type (Wang, 1989). The concentration type assumes that the sediment concentration at the bed boundary adapts instantaneously to the equilibrium value, whereas the gradient type describes the upward sediment flux at the bed boundary. Herein, a gradient type boundary condition is applied, because the boundary condition for mud is also prescribed in terms of fluxes. Only the upward flux of sand is prescribed:

$$\left[ \epsilon_{z,s} \frac{\partial c_s}{\partial z} \right]_{z=z_b+a_s} = -E_s \quad (4.3)$$

where  $E_s$  is the upward flux of sand and  $a_s$  the reference height. An expression for the upward flux of sand ( $E_s$ ) is derived in Chapter 3 and it depends on the mud content at the bed surface. For practical reasons, the reference height for sand ( $a_s$ ) is set at a fixed percentage of the water depth (see e.g. Wang, 1989) and equals the thickness of the first computational cell near the bed surface in the vertical direction.

Although suspended mud transport occurs in the entire water column, the bed boundary for suspended mud cannot be located at the bed surface itself. At that point, the sediment diffusivity equals zero, so the upward flux cannot be described by the diffusion formulation. Hence, the boundary condition is assumed to be at a small distance above the bed level and the upward and downward flux are prescribed:

$$\left[ w_m c_m + \epsilon_{z,m} \frac{\partial c_m}{\partial z} \right]_{z=z_b+a_m} = D_m - E_m \quad (4.4)$$

where  $D_m$  and  $E_m$  are the mud deposition and erosion flux, respectively and  $a_m$  the distance above the bed level. Expressions for both fluxes are given in Chapter 3. Only the mud erosion

flux depends on the mud content at the bed surface. For practical reasons, the reference height for mud ( $a_m$ ) is set at a fixed percentage of the water depth and is located in the middle of the lowest computational cell in the vertical direction.

#### 4.3.3 Parameters

The advection-diffusion equations for sand (eq. 4.1) and mud (eq. 4.2) can only be solved with appropriate settings for the settling velocities and sediment diffusivity coefficients in both horizontal and vertical directions. These coefficients are discussed below:

##### Settling velocity for sand and mud

The settling velocity for sand ( $w_s$ ) is directly related to the sand grain size and is constant in time and space. The settling velocity for mud ( $w_m$ ) is not constant in time and space, because of the possibility of floc formation, and it strongly depends on turbulent intensity and the mud concentration in the water column. Recently, Winterwerp (2002) has presented a flocculation model in which these effects are incorporated. Unfortunately, the model is not applicable in our large-scale sand-mud model, because it is too complex. Given the assumption of low mud concentrations in our model, a time scale analysis of the complex model also indicated that strong variations in settling velocity are not expected during a tidal period (Van Ledden, 2000). Therefore, the settling velocity of mud is taken as constant in time and space.

##### Turbulent mixing

The horizontal sediment diffusivity ( $\epsilon_x$  and  $\epsilon_y$ ) for both sediment fractions are equal to the horizontal fluid mixing coefficients in all situations. The vertical sediment diffusivity is proportional to the vertical fluid mixing coefficient in a situation with currents only:

$$\epsilon_{z,i} = \beta_i \nu_z \quad (4.5)$$

where  $\epsilon_{z,i}$  is the sediment diffusivity of fraction  $i$  at height  $z$  above the bed,  $\beta_i$  the efficiency factor for sediment fraction  $i$ . The value  $\beta_m = 1.4$  is applied for mud which is generally used for conservative constituents and very fine particles (Winterwerp, 1999). The expression of Van Rijn (1993) is used for sand:

$$\beta_s = 1 + \left( \frac{w_s}{u_*} \right)^2 \quad (4.6)$$

The value  $\beta_s$  is limited to the range  $1 < \beta_s < 1.5$ . Notice that  $\beta_s$  in eq. (4.6) does not have a fine-grain limit ( $w_s \downarrow$ ) that is equal to the coefficient for mud ( $\beta_m = 1.4$ ).

If short waves are included, the vertical sediment diffusivity due to currents and waves is computed using Van Rijn's formulation (Van Rijn, 1993). The formulation consists of a current-

related and wave-related part. A parabolic-constant distribution is applied for the current-related diffusivity. The wave-related diffusivity is a step type distribution over the vertical, with a linear transition in between. For further details, the reader is referred to Van Rijn (1993).

## 4.4 Bed module

### 4.4.1 Equations

Exchange of sand and mud at the bed surface and consolidation of the sediment bed itself contribute to bed level changes. Herein, only deposition and erosion are taken into account, because the consolidation process of sand-mud mixtures is insufficiently understood at present. Another reason for neglecting consolidation is that this process does not directly contribute to bed composition variations. This process only indirectly affects the distribution of sand and mud by affecting the erosion properties of the sediment bed. For the time being, the bed density is assumed to be constant in time and space. This assumption also implies the mud content does not influence the bed density, even though it may fill up the pores of the sand matrix.

Under these assumptions, the bed level change directly follows from the bed load transport gradient of sand and the erosion and deposition fluxes of sand and mud (Figure 4.4):

$$(1 - \varepsilon_p) \frac{\partial z_b}{\partial t} = - \frac{\partial q_b}{\partial x} - \frac{\partial q_b}{\partial y} + D_s - E_s + D_m - E_m \quad (4.7)$$

where  $q_b$  is the bed load transport rate of sand,  $E_s$  the erosion flux of sand,  $D_s$  the deposition flux of sand,  $E_m$  the erosion flux of mud,  $D_m$  the deposition flux of mud and  $\varepsilon_p$  the bed porosity.

Bed composition variations in time and space are induced by three processes: upward and downward fluxes of sand and mud at the bed surface, physical mixing near the bed surface and (local and non-local) biological mixing processes in the sediment bed itself (see also Section 2.3.3). The processes in the sediment bed itself are generally confined in an area near the bed surface, whereas the bed composition does not change deep below the bed surface. For the time being, only physical and local biological mixing processes are taken into account, whereas non-local mixing is neglected.

The continuous concept of Armanini (1995) is chosen to include the time and space-dependent bed composition variations in our model (cf. Table 2.4). The choice of this concept is based on two reasons. Firstly, bed composition changes due to mixing processes in the sediment bed are included explicitly in this concept. These processes are likely to be very important in estuaries and tidal basins (e.g. bioturbation). Secondly, this concept prescribes the exchange and mixing processes by deterministic formulations. This is preferred to a probabilistic approach, because the knowledge of these processes in case of sand-mud mixtures is limited (cf. Chapter 3).

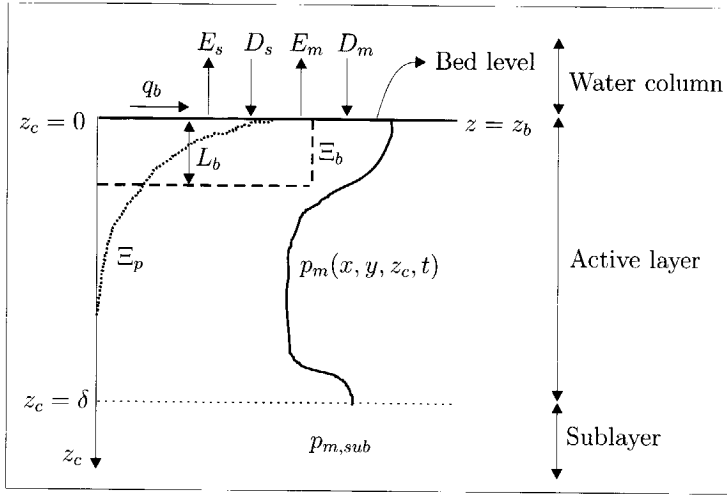


Figure 4.4: Bed level and bed composition.

According to the continuous concept, the mud content  $p_m$  below the bed surface ( $-\infty < z < z_b$ ) is described in Eulerian coordinates as follows (cf. Armanini, 1995):

$$\frac{\partial p_m}{\partial t} - \frac{\partial}{\partial z} \left( \Xi \frac{\partial p_m}{\partial z} \right) = 0 \tag{4.8}$$

where  $z$  is the vertical (Eulerian) coordinate and  $\Xi$  a mixing coefficient. From a numerical point of view, the application of the Eulerian description in eq. (4.8) is complicated. The reason is that the domain in which eq. (4.8) should be solved is not constant, because the bed level  $z_b$  varies in time. Because of this, a Lagrangian description with the bed level  $z_b$  as its reference is used in the present model set-up. Introducing a new vertical coordinate  $z_c = z + (\partial z_b / \partial t)(t - t_o)$ , the Lagrangian description of the mud content  $p_m$  below the bed surface ( $0 < z_c < +\infty$ ) reads:

$$\frac{\partial p_m}{\partial t} + \frac{\partial z_b}{\partial t} \frac{\partial p_m}{\partial z_c} - \frac{\partial}{\partial z_c} \left( \Xi \frac{\partial p_m}{\partial z_c} \right) = 0 \tag{4.9}$$

where  $z_c$  is the distance below the bed surface  $z_b$ . It should be noted that the vertical coordinate  $z_c$  in eq. (4.9) is positive in downward direction and the origin is always at the bed surface (Figure 4.4). As a result, the origin of the coordinate  $z_c$  shifts upward or downward with bed level variations in time.

Equation (4.9) consists of the following contributions. The local change in mud content at a certain distance below the bed level is given by the first term. The second term is introduced because of the Lagrangian coordinate system. The third term expresses the fluxes by physical

and/or local biological mixing in the bed. The effect of sediment exchange at the bed surface is included by a boundary condition at the bed surface, which is discussed in the next subsection.

In principle, eq. (4.9) describes bed composition variations from the bed surface towards an infinite distance down into the bed. For the numerical implementation, however, a distinction is made between an active layer with a certain thickness  $\delta$  and a sublayer (Figure 4.4). In the active layer, the mud content varies according to eq. (4.9), whereas it remains unchanged in the sublayer and is equal to  $p_{m,sub}$ . The sublayer must be chosen deep enough below the bed surface to ensure an unchanged bed composition during the entire period of interest.

In case of two sediment fractions (i.e. sand and mud), the changes in sand content in the bed follows from continuity:

$$p_s = 1 - p_m \quad (4.10)$$

where  $p_s$  is the sand content.

#### 4.4.2 Boundary conditions

The bed level equation (4.7) and the bed composition equation (4.9) can only be solved with appropriate initial conditions and boundary conditions. These conditions are discussed below.

##### Initial conditions

At time  $t = 0$  the bed level  $z_b(t = 0, x, y)$  and the mud content  $p_m(t = 0, x, y, z_c)$  have to be specified.

##### Open boundaries

The boundary condition for the bed level equation (4.7) depends on the bed load transport direction. When the bed load transport vector is directed into the model domain, a strong boundary condition is needed: the bed level is assumed to remain unchanged ( $\partial z_b / \partial t = 0$ ). When the bed load transport is directed out of the model domain, a weak boundary condition is sufficient, and  $\partial^2 z_b / \partial x \partial t = 0$  is applied herein.

Two boundary conditions are needed for solving the bed composition equation for the mud fraction (4.9): at the bed surface and at the boundary between the active layer and the sublayer. The net suspended mud flux is prescribed at the bed surface ( $z_c = 0$ ):

$$\left[ p_m \frac{\partial z_b}{\partial t} - \Xi \frac{\partial p_m}{\partial z_c} \right]_{z_c=0} = \frac{1}{1 - \epsilon_p} (E_m - D_m) \quad (4.11)$$

The boundary condition between the active layer and the sublayer ( $z_c = \delta$ ) depends on the direction of the bed level change. This boundary is an 'outflow' boundary in case of deposition

( $\partial z_b / \partial t > 0$ ), because a Lagrangian approach is applied. A weak boundary condition is then sufficient:

$$\frac{\partial z_b}{\partial t} > 0 \longrightarrow \left[ \frac{\partial p_m}{\partial z_c} \right]_{z_c = \delta} = 0 \quad (4.12)$$

In case of erosion ( $\partial z_b / \partial t < 0$ ), the boundary between the active layer and the sublayer is an 'inflow' boundary and a strong boundary condition must be prescribed. The mud content at the boundary is then equal to the mud content of the sublayer:

$$\frac{\partial z_b}{\partial t} < 0 \longrightarrow [p_m]_{z_c = \delta} = p_{m.sub} \quad (4.13)$$

where  $p_{m.sub}$  is the mud content in the sublayer. Notice that if the top level of the sublayer is deep enough below the bed surface, the bed composition will remain unaltered at this boundary. In that case, it does not make difference whether boundary condition (eq. 4.12) or (eq. 4.13) is applied.

#### 4.4.3 Parameters

The bed porosity in eq. (4.7) and the mixing coefficient in eq. (4.9) must be prescribed. These parameters are discussed below:

##### Bed porosity

The bed porosity  $\varepsilon_p$  in eq. (4.7) is constant in time and space and equals  $\varepsilon_p = 0.4$ , unless otherwise stated. Thus, consolidation effects and the filling of pores around sand particles by mud are not taken into account.

##### Mixing coefficient

The mixing coefficient  $\Xi$  in eq. (4.9) is assumed to be the sum of the physical and local biological mixing coefficient. Armanini (1995) argues that the physical mixing coefficient increases with increasing current velocity near the bed surface and decreases with increasing distance from the bed. He proposes an exponential function for this coefficient with the mean sand grain size of a sand-mixture as an important variable. This function is not directly applicable in this model, because 'the grain size' can hardly be defined in the case of mud. Therefore, a slightly different exponential function is applied (cf. Armanini, 1995):

$$\Xi_p = \alpha_p u_* h e^{-\frac{z_c}{L_p}} \quad (4.14)$$

where  $\Xi_p$  is the physical mixing coefficient,  $\alpha_p$  an empirical coefficient,  $u_*$  the shear velocity,  $h$  the local water depth and  $L_p$  the mixing length of sediment particles due to small-scale bed level

disturbances. The physical mixing coefficient distribution below the bed surface is sketched in Figure 4.4.

Armanini (1995) argues that the coefficient  $\alpha_p$  in eq. (4.14) should be a function of the Froude number, the relative roughness and the grain Reynolds number for mixtures with different sand grain sizes, whereas  $L_p$  is an appropriate length scale of the small-scale bed level fluctuations. As a first approximation, Armanini (1995) applies constant parameter values for these coefficients and compares the model results with a laboratory experiment with sand only (Ribberink, 1987). Following the expression in eq. (4.14), he derives the length scale  $L_p$  from the measured bed level fluctuations at the bed surface and the optimum setting appears to be  $L_p \cong 0.01$  m. A reasonable agreement is obtained between the computed and observed time-dependent vertical bed composition profile with  $\alpha_p \cong 10^{-6}$ . However, experimental data are not available for calibrating these coefficients in the case of sand-mud mixtures. Unless otherwise stated,  $\alpha_p = 10^{-6}$  and  $L_p = 0.10$  m are applied. The value for  $L_p$  is assumed to be reasonable for small-scale bed level disturbances in estuaries and tidal basins, whereas the calibrated value for  $\alpha_p$  by Armanini (1995) is applied without reasoning.

Local biological mixing of sediment (i.e. bioturbation) is induced by organisms that rework bed sediments. Although it is known that specific organisms mix sediments at depths of over 1 m, the major effects of bioturbation occur in the upper 10 - 15 cm of the sediment bed. Various authors have presented correlations between the bioturbation coefficient and other variables such as water depth and sedimentation velocity (see for an overview Boudreau, 1997). Middelburg et al. (1997) obtain the maximum explained variance of 43% with a relationship between the bioturbation coefficient and the water depth. Besides other factors, the remaining variance is attributed to differences in sediment properties. The mud content may be an important parameter from a physical point of view, as the mixing capacity of organisms presumably decreases with increasing cohesion between sediment particles.

Because of these uncertainties, biological mixing in the present model set-up is assumed to be constant in the area near the bed surface as a first approximation:

$$\Xi_b = \Xi_{b0} H \left( 1 - \frac{z_c}{L_b} \right) \quad (4.15)$$

where  $\Xi_{b0}$  is a biological mixing coefficient,  $L_b$  the biological mixing zone near the bed surface and  $H$  a Heaviside function. These parameters are graphically shown in Figure 4.4. The biological mixing zone is set at  $L_b = 0.1$  m, unless otherwise stated. Reasonable values for the biological mixing coefficient  $\Xi_{b0}$  appear to be  $10^{-6} - 10^{-2}$  m<sup>2</sup>/year (Boudreau, 1997).



## 4.5 Numerical implementation

### 4.5.1 Overview of extensions

The equations, described in the previous section, are implemented in Delft3D, a software package of WL|Delft Hydraulics (Roelvink & Banning, 1994). For an extensive discussion about the present model capabilities, the reader is referred to Lesser (2000) and Lesser et al. (in prep.). The extensions to the present flow, sediment transport and bed model will be briefly discussed hereafter. The numerical model set-up in the vertical direction is shown in Figure 4.5.

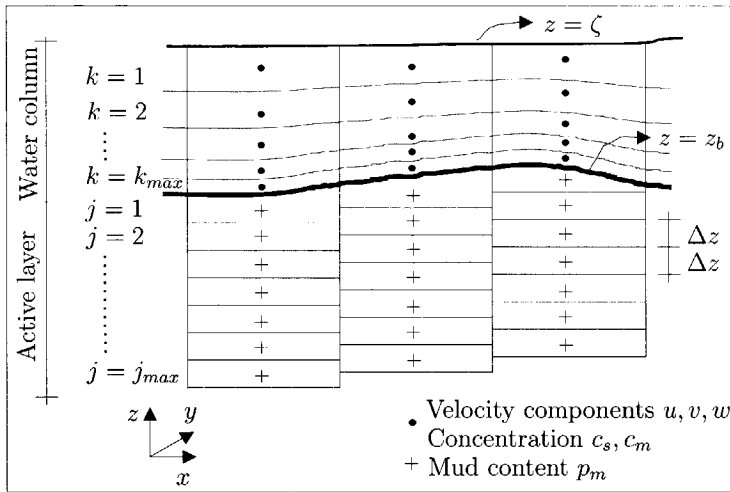


Figure 4.5: Model set-up in the vertical direction.

### Flow

The shallow water equations for currents are solved with Delft3D-FLOW (see WL|Delft Hydraulics (2001) for further details), and the short-wave model SWAN is applied for solving the action density balance equation (see WL|Delft Hydraulics (2000) for further details). The model variables are computed on an orthogonal curvilinear grid in the horizontal plane with appropriate boundary and initial conditions. A  $\sigma$ -transformation in the vertical direction is applied for the shallow water equations. The computed variables are the water level ( $\zeta$ ) and the density spectrum of the short waves ( $N$ ) for each cell with index  $(nm)$  and the current velocities with index  $(nm, k)$ . These equations are not modified for the present sand-mud model.

### Sediment transport

The suspended sand ( $c_s$ ) and mud ( $c_m$ ) concentrations are computed for each cell with index  $(nm, k)$  by solving the advection-diffusion equation for sand (eq. 4.1) and mud (eq. 4.2) with appropriate initial and boundary conditions (see WL|Delft Hydraulics (2001) for further details). The boundary condition at the bed-water interface is adapted, since it depends on the

mud content of the bed. In addition, the computation of the bed load transport rate ( $q_b$ ) is adapted.

### Bed level and bed composition

The bed level ( $z_b$ ) is computed for each cell with index ( $nm$ ) by solving the bed level equation (4.7) (see WL|Delft Hydraulics (2001) for further details). The bed composition changes are calculated by solving the advection-diffusion equation for the mud fraction (4.9). The sediment bed in each cell is divided into layers with a constant thickness ( $\Delta z$ ) and with a constant number of layers ( $j_{max}$ ). The solution procedure of the mud content in each layer with index ( $nm, j$ ) is discussed in the next subsection.

#### 4.5.2 Discretization of bed composition equation

A Crank-Nicholson numerical scheme is applied herein for the discretization of the bed composition equation (4.9) (see e.g. Vreugdenhil, 1989):

$$\frac{p_j^{n+1} - p_j^n}{\Delta t} + \theta \frac{s_{j+1/2}^{n+1} - s_{j-1/2}^{n+1}}{\Delta z} + (1 - \theta) \frac{s_{j+1/2}^n - s_{j-1/2}^n}{\Delta z} = 0 \quad (4.16)$$

where  $p_j^n$  is the mud content in layer  $j$  at time  $n$ ,  $p_j^{n+1}$  the mud content in layer  $j$  at time  $n + 1$ ,  $s_{j-1/2}^n$  the sediment flux through the upper boundary of layer  $j$  at time  $n$ ,  $s_{j+1/2}^n$  through the lower boundary of layer  $j$  at time  $n$ ,  $s_{j-1/2}^{n+1}$  the sediment flux through the upper boundary of layer  $j$  at time  $n + 1$ ,  $s_{j+1/2}^{n+1}$  through the lower boundary of layer  $j$  at time  $n + 1$ ,  $\Delta t$  the time step,  $\Delta z$  the spatial step and  $\theta$  a numerical coefficient. The numerical coefficient is set at  $\theta = 0.55$ , unless otherwise stated.

The sediment fluxes in eq. (4.16) are given as follows:

$$s_{j+1/2}^{n+1} = \frac{1}{2} u_z^{n+1/2} (p_{j+1}^{n+1} + p_j^{n+1}) - \Xi_{j+1/2}^{n+1} \frac{p_{j+1}^{n+1} - p_j^{n+1}}{\Delta z} \quad (4.17)$$

$$s_{j-1/2}^{n+1} = \frac{1}{2} u_z^{n+1/2} (p_j^{n+1} + p_{j-1}^{n+1}) - \Xi_{j-1/2}^{n+1} \frac{p_j^{n+1} - p_{j-1}^{n+1}}{\Delta z} \quad (4.18)$$

$$s_{j+1/2}^n = \frac{1}{2} u_z^{n+1/2} (p_{j+1}^n + p_j^n) - \Xi_{j+1/2}^n \frac{p_{j+1}^n - p_j^n}{\Delta z} \quad (4.19)$$

$$s_{j-1/2}^n = \frac{1}{2} u_z^{n+1/2} (p_j^n + p_{j-1}^n) - \Xi_{j-1/2}^n \frac{p_j^n - p_{j-1}^n}{\Delta z} \quad (4.20)$$

where  $u_z^{n+1/2}$  is the propagation velocity of the bed level,  $\Xi_{j-1/2}^n$  the mixing coefficient at the upper boundary of layer  $j$  at time  $n$  and  $\Xi_{j+1/2}^n$  the mixing coefficient at the lower boundary of layer  $j$  at time  $n$ . The propagation velocity of the bed level  $u_z^{n+1/2}$  is estimated by:

$$u_z^{n+1/2} = \frac{z^{n+1} - z^n}{\Delta t} \quad (4.21)$$

where  $z^n$  is the bed level at time  $n$  and  $z^{n+1}$  is the bed level at time  $n + 1$ .

The boundary conditions must be applied in the layers at the bed surface and at the boundary between the active layer and the sublayer. At the bed surface ( $j = 1$ ), the fluxes in eq. (4.18) at time  $n + 1$  and eq. (4.20) at time  $n$  are approximated as follows:

$$s_{j-1/2}^{n+1} = s_0^{n+1/2} \quad (4.22)$$

$$s_{j-1/2}^n = s_0^{n+1/2} \quad (4.23)$$

where  $s_0^{n+1/2}$  is the net bed level change by mud exchange in the time interval  $n$  and  $n + 1$ . The boundary condition at the boundary between the active layer and the sublayer ( $j = j_{max}$ ) depends on the bed level change. When the bed level change is positive ( $u_z^{n+1/2} > 0$ ), the fluxes at the lower boundary ( $j = j_{max} + 1/2$ ) in eq. (4.17) and (4.19) are equal to:

$$s_{j+1/2}^{n+1} = \frac{1}{2} u_z^{n+1/2} (p_{j_{max}}^{n+1} + p_{j_{max}}^{n+1}) \quad (4.24)$$

$$s_{j+1/2}^n = \frac{1}{2} u_z^{n+1/2} (p_{j_{max}}^n + p_{j_{max}}^n) \quad (4.25)$$

When the bed level change is negative ( $u_z^{n+1/2} < 0$ ), the mud content of the sublayer ( $p_{m,sub}$ ) is applied as a boundary condition. The fluxes at the lower boundary ( $j = j_{max} + 1/2$ ) in eq. (4.17) and (4.19) then read:

$$s_{j+1/2}^{n+1} = \frac{1}{2} u_z^{n+1/2} (p_{m,sub} + p_{j_{max}}^{n+1}) \quad (4.26)$$

$$s_{j+1/2}^n = \frac{1}{2} u_z^{n+1/2} (p_{m,sub} + p_{j_{max}}^n) \quad (4.27)$$

Substituting eq. (4.17) - (4.27) into eq. (4.16) yields a system of linear equations for the mud content at time step  $n + 1$ :

$$b_1 p_{j-1}^{n+1} + b_2 p_j^{n+1} + b_3 p_{j+1}^{n+1} = a_1 p_{j-1}^n + a_2 p_j^n + a_3 p_{j+1}^n \quad (4.28)$$

where  $b_1 \dots b_3$  and  $a_1 \dots a_3$  are coefficients for layer  $j$ . Obviously, the coefficients  $a_1$  and  $b_1$  do not exist for  $j = 1$ , whereas  $a_3$  and  $b_3$  are not defined for  $j = j_{max}$ . Equation (4.28) is easily solved by a double sweep algorithm (e.g. Vreugdenhil, 1989).

### 4.5.3 Stability and accuracy restrictions

The time step and spatial step for solving the equations cannot be chosen arbitrarily, as they are restricted by stability and accuracy conditions. The restrictions for the flow, sediment transport, bed level and bed composition model are discussed below.

#### Flow

The flow equations are solved by using the Alternating Direction Implicit method in the horizontal direction and a fully implicit integration in the vertical direction (Stelling, 1984). An important dimensionless parameter for the behaviour of the flow solution is the Courant number:

$$\sigma_f = 2\Delta t \sqrt{gh} \sqrt{\frac{1}{\Delta x^2} + \frac{1}{\Delta y^2}} \quad (4.29)$$

where  $\sigma_f$  is the Courant number for the flow,  $\Delta x$  the spatial step in x-direction,  $\Delta y$  the spatial step in y-direction and  $\Delta t$  the time step,  $g$  the gravitation acceleration and  $h$  the local water depth. Because the solution method for the unsteady flow equations is implicit, the time step and spatial step are not restricted by stability. However, Stelling (1984) demonstrates that the Courant number may not be too large for accuracy reasons and suggested a maximum value of  $4\sqrt{2}$  in case of complex geometries.

#### Sediment transport

The suspended sediment transport equations are solved in the same way as the flow equations. These equations are solved in the vertical direction by a fully implicit method, whereas the equations in the horizontal directions are solved by the Alternating Direction Implicit method. Source terms are treated explicitly, but sink terms are treated implicitly to avoid negative concentrations. Therefore, the time step and spatial step are not restricted for a stable solution, while the accuracy of the solution is determined by two components.

Firstly, the Courant number may not be too large and a value of  $4\sqrt{2}$  has been put forward as an upper limit in case of complex geometries (Stelling, 1984). The Courant number for suspended sediment transport is comparable to the Courant number for the flow in eq. (4.29), but the propagation speed is different. The propagation speed for suspended sediment transport is about equal to the horizontal flow velocity and thus much smaller than that for shallow water waves. Therefore, the time step for solving the suspended sediment transport equation can be larger than for the flow equations. Yet, for practical reasons, the time step for the suspended sediment transport equations is taken equal to the time step for the flow equations in Delft3D.

Secondly, the accuracy is also determined by the adaptation time and adaptation length of the sediment fraction. As a first approach, the depth-averaged adaptation time and length can be used for a three-dimensional computation:

$$T_i = \frac{h}{w_i} \quad (4.30)$$

$$L_i = \frac{Uh}{w_i} \quad (4.31)$$

where  $T_i$  is the adaptation time for fraction  $i$ ,  $L_i$  the adaptation length for fraction  $i$ ,  $w_i$  the settling velocity for fraction  $i$  and  $U$  the depth-averaged velocity. In order to have an accurate solution, the time and spatial step should be much smaller than the adaptation time and length scale. Because the settling velocity of sand is generally much larger than for mud, the sand fraction will determine the time and spatial step.

### Bed level

The bed level equation is solved explicitly with a time step  $N\Delta t$  where  $\Delta t$  is the time step for the flow and suspended sediment transport equation and  $N$  the so-called 'morphological factor'. A morphological factor can be applied, because the time scale for morphological changes is generally much larger than for changes in the flow (see also Latteux, 1995). To reduce the computation time, the morphological changes are scaled up each time step with the morphological factor.

The time step for the bed level equation ( $N\Delta t$ ) is restricted by stability of the computation. The maximum time step can be obtained analytically for idealised situations only. Wang (1989) derives a stability criterion for suspended sand transport above a sand bed. Similarly, an expression can be derived for suspended mud transport above a mud bed in case of erosion (Appendix B):

$$\frac{1}{1 - \varepsilon_p} \frac{Mq^2}{U_e^2 h^3} N\Delta t \leq 1 \quad (4.32)$$

where  $\varepsilon_p$  is the bed porosity,  $M$  the erosion coefficient,  $q$  the discharge per unit width,  $U_e$  the depth-averaged critical erosion velocity for mud erosion,  $h$  the local water depth,  $N$  the morphological factor and  $\Delta t$  the time step. The restrictions for sand and mud beds separately can be applied for a first estimation of the time step for the sand-mud model. During the numerical experiments, the time step is selected by trial-and-error in order to have a stable and accurate computation.

### Bed composition

The bed composition equation is solved implicitly with time step  $N\Delta t$  and spatial step  $\Delta z$ . Hence, the time and spatial step for the bed composition equation are not restricted for stability. Two dimensionless parameters are important for the accuracy of the solution: the Courant number and the Diffusion number (Vreugdenhil, 1989). These parameters are given by:

$$\sigma_c = u_z \frac{N\Delta t}{\Delta z} \quad (4.33)$$

$$\lambda_c = 2\Xi \frac{N\Delta t}{\Delta z^2} \quad (4.34)$$

where  $\sigma_c$  is the Courant number for the bed composition,  $u_z$  the propagation velocity of the bed level (eq. 4.21), and  $\lambda_c$  the Diffusion number for the bed composition. These parameters may not be too large (say less than 1) for an accurate solution and can be used as a first estimate. The time and spatial step during the numerical computations are chosen sufficiently small during the numerical experiments to have an accurate solution.

## 4.6 Summary

A process-based morphological model for sand and mud has been proposed in this chapter. The model consists of three parts: a flow module, a sediment transport module and a bed level and bed composition module. The governing equations, the boundary conditions and the model parameters have been discussed. Finally, the numerical implementation of these equations has been presented.

In summary, the set-up of these modules is as follows:

- The flow module consists of the well-known shallow water equations and the depth-averaged action balance for short waves. The influence of the suspended sediment concentration on the turbulent water motion is neglected and the roughness is invariant in space and time.
- In the sediment transport module, a distinction has been made between bed load transport of sand and suspended load sand and mud transport. Flocculation is neglected and the settling velocity of mud is constant in time and space. The erosion fluxes of suspended sand and mud at the bed surface and the bed load transport rate of sand depend on the mud content at the bed surface. These formulations have been derived in Chapter 3.
- Extensions to the present-day models have been included in the bed module. Firstly, bed level changes depend on both suspended sand and mud exchange at the bed surface and bed load transport gradients of sand. However, consolidation effects are neglected and the bed porosity is constant in time and space, at least for the time being. Secondly, the bed composition is time-dependent and non-uniform in horizontal and vertical directions by applying the concept of Armanini (1995). Bed composition variations are induced by exchange of sediment at the bed surface, physical mixing by small-scale disturbances and local biological mixing.

- 
- The proposed sand-mud model is implemented in the three-dimensional software package Delft3D from WL|Delft Hydraulics. A new routine is added for solving the bed composition equation. A Crank-Nicholson scheme is applied for the numerical discretization of this equation. Restrictions for the time and spatial step have been discussed to obtain a stable and accurate solution.





## Chapter 5

### Behaviour analysis of idealised situations

#### 5.1 Introduction

Behaviour analysis of process-based models for idealised situations has proved to be a successful way for increasing the physical understanding of morphological phenomena. A well-known example is the analysis of bed level patterns in rivers (e.g. Struiksmā et al., 1985) and tidal basins (e.g. Schuttelaars & De Swart, 2000), along coasts (e.g. Deigaard et al., 1999) and in shallow seas (e.g. Komarova & Hulscher, 2000). Despite the applied simplifications, these studies have revealed important parameters governing the behaviour of bed level features in these systems. In addition, a striking comparison has sometimes been obtained between model results and field observations (Hibma et al., 2001) or laboratory data (Struiksmā et al., 1985). Both aspects indicate the usefulness of studying model behaviour for idealised situations.

Basically, behaviour analysis of a process-based model consists of three steps:

- The first step is the application of several simplifications with respect to the geometry, the boundary conditions and the governing equations. For example, a typical schematisation for analyzing river bed morphology is a straight channel with constant width and non-erodible banks, a time-independent river discharge and linearised, depth-averaged equations.
- The next step is an analysis of the model behaviour with analytical techniques and/or numerical experiments. Well-known analytical techniques are linear or non-linear stability analysis, while examples of numerical experiments are presented by Deigaard et al. (1999) and Hibma et al. (2001).
- The final step is a verification of the model results with field and/or laboratory measurements. This step is essential, but often very difficult because of the simplifications made in the first step. Consequently, a verification with field measurements can generally be done only qualitatively, while laboratory measurements are suitable for a more quantitative comparison.

In this chapter, the present process-based sand-mud model is analysed in this way. Three idealised situations are considered with increasing complexity. First, the so-called local behaviour

is discussed in Section 5.2. This implies that only local processes are considered. Next, the analysis is extended to non-local processes in Section 5.3, for a situation with predominant deposition. Finally, in Section 5.4 a situation is considered in which erosion and deposition are both important for the morphological behaviour. Each section describes the aforementioned steps in the behaviour analysis: the model set-up and the applied simplifications, the numerical experiments and their analysis, and the verification of the model results with field measurements.

## 5.2 Local situation<sup>1</sup>

### 5.2.1 Model set-up

The set-up of the local situation is outlined in Figure 5.1. The equations for the flow, sediment transport, bed level and bed composition in this situation are as follows:

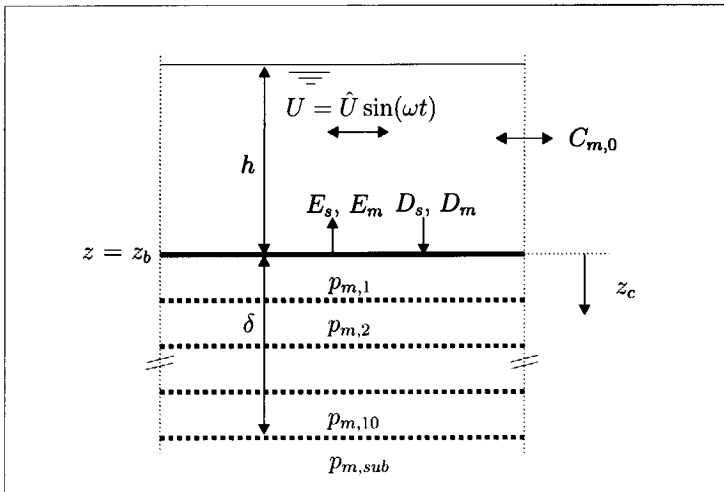


Figure 5.1: Model set-up of local approach.

#### Flow

The water depth  $h$  is taken as constant and the depth-averaged flow velocity  $U$  varies sinusoidally over the tide. The magnitude of the bed shear stress  $\tau_b$  is then given by:

$$\tau_b(t) = \hat{\tau}_b \sin^2(\omega t) \quad (5.1)$$

1. The contents of this section appeared almost completely in: *Fine Sediment Dynamics in the Marine Environment*, Proceedings of Marine Science (5), 577-594, J.C. Winterwerp and C. Kranenburg (eds.), Elsevier, Amsterdam, 2002.

with

$$\hat{\tau}_b = \rho_w \frac{g}{C^2} \hat{U}^2 \quad (5.2)$$

where  $\hat{\tau}_b$  is the bed shear stress amplitude,  $\omega$  the tidal frequency,  $t$  time,  $\rho_w$  the water density,  $g$  the gravitational acceleration,  $C$  the Chézy-coefficient and  $\hat{U}$  the velocity amplitude.

### Sediment transport

Only suspended sediment transport is taken into account, because of the local approach which basically presumes uniformity in the horizontal plane. Starting from the depth-averaged advection-diffusion equation and neglecting all non-local terms, one finds:

$$h \frac{dC_s}{dt} = E_s - D_s \quad (5.3)$$

where  $C_s$  is the depth-averaged volumetric concentration of sand,  $D_s$  the sand deposition rate and  $E_s$  the sand erosion rate.

From a physical point of view, a local approach for mud is not realistic, because the settling time is of the order of the tidal period. Consequently, horizontal transport of mud is as important as the vertical transport processes. It will be shown in the next section that the application of eq. (5.3) for the mud fraction indeed shows trivial or non-realistic results. Therefore, an extra transport term is introduced to account for horizontal advection and diffusion in a parameterized way. The mud concentration equation reads:

$$h \frac{dC_m}{dt} = E_m - D_m + k_m (C_m - C_{m,0}) \quad (5.4)$$

where  $C_m$  is the depth-averaged mud concentration,  $E_m$  the mud erosion rate,  $D_m$  the mud deposition rate,  $C_{m,0}$  the mud concentration outside the model domain and  $k_m$  a transport coefficient. The last term on the right hand side in eq. (5.4) is a transport term by which the mud concentration is affected by the concentration outside the model domain. When the inner concentration  $C_m$  is lower than  $C_{m,0}$ , it is assumed that mud is imported from outside and vice versa. Notice that this transport term is not included in the sand concentration equation (5.3).

The erosion and deposition terms in eq. (5.3) and (5.4) are prescribed by applying the equations in Chapter 4 with some modifications and simplifications. The equations for sand deposition and erosion are slightly modified because of the depth-averaged approach. The non-cohesive sand erosion flux equals  $E_s = \gamma w_s C_e$  and its deposition flux  $D_s = \gamma w_s C_s$  where  $C_e$  is the depth-averaged equilibrium concentration and  $\gamma$  a coefficient. The coefficient  $\gamma$  takes into account the vertical distribution of the velocity and concentration profile (Galappatti & Vreugdenhil, 1985). Furthermore, several simplifications are applied in the erosion and deposition formulations to

simplify the mathematical analysis. Firstly, the critical shear stress for non-cohesive erosion  $\tau_{e,nc}$  and cohesive erosion  $\tau_{e,c}$  are assumed to be independent of the mud content. Secondly, the erosion coefficient for non-cohesive ( $M_{nc}$ ) and cohesive ( $M_c$ ) erosion are assumed to be equal and independent of the mud content. Because of this, the term  $(1 - p_m)$  in the denominator of the mud erosion formula for the non-cohesive range (eq. 3.13) is omitted in order to have a continuous erosion function at  $p_m = p_{m,cr}$ . This only slightly affects the mud erosion flux in this range.

### Bed level and composition

The bed level ( $z_b$ ) and bed composition ( $p_m$ ) are governed by equation (4.7) and (4.9) in Chapter 4, respectively and are not modified herein. Constant values of the porosity  $\varepsilon_p$  and the mixing coefficient  $\Xi$  with depth and time are chosen. Furthermore, the bed composition varies in the 'active layer' with constant thickness  $\delta$ . Below, the bed has a constant mud content  $p_{m,sub}$ .

### 5.2.2 Overview of situations

The behaviour of the model variables described in the previous section can be divided into three different situations, which are shown in Figure 5.2. The bed shear stress variation ( $\tau_b$ ) in eq. (5.1) is plotted during half a tidal period and three critical shear stresses ( $\tau_{e,nc}$ ,  $\tau_{e,c}$  and  $\tau_d$ ) are indicated with horizontal lines. One could argue that another situation exists in which the maximum bed shear stress during the tide is lower than the critical shear stress for deposition. This situation, however, results in similar behaviour as situation 1 (see also next subsection).

**Table 5.1:** Overview of different situations.

| No. | Bed shear stress                                       | Deposition |     | Non-cohesive erosion |     | Cohesive erosion |     |
|-----|--------------------------------------------------------|------------|-----|----------------------|-----|------------------|-----|
|     |                                                        | Sand       | Mud | Sand                 | Mud | Sand             | Mud |
| 1   | $\tilde{\tau}_{e,nc} < 1$ and $\tilde{\tau}_{e,c} < 1$ | yes        | yes | no                   | no  | no               | no  |
| 2   | $\tilde{\tau}_{e,nc} > 1$ and $\tilde{\tau}_{e,c} < 1$ | yes        | yes | yes                  | yes | no               | no  |
| 3   | $\tilde{\tau}_{e,nc} > 1$ and $\tilde{\tau}_{e,c} > 1$ | yes        | yes | yes                  | yes | yes              | yes |

Depending on the parameter setting, non-cohesive and cohesive erosion can occur, while deposition of sand and mud is always possible during (part of) the tidal period. An overview of these possibilities is given in Table 5.1. The different situations are distinguished with the help of the dimensionless critical shear stress for non-cohesive ( $\tilde{\tau}_{e,nc} = \frac{\hat{\tau}_b}{\tau_{e,nc}}$ ) and cohesive erosion ( $\tilde{\tau}_{e,c} = \frac{\hat{\tau}_b}{\tau_{e,c}}$ ). The dimensionless critical shear stress for deposition ( $\tilde{\tau}_d = \frac{\hat{\tau}_b}{\tau_d}$ ) will also be applied later on in this chapter. Normally, the critical shear stresses are normalised by the maximum bed shear stress. Here, the reciprocal term is used, because the level of forcing can be zero. The model results are discussed for each situation in the next subsections.

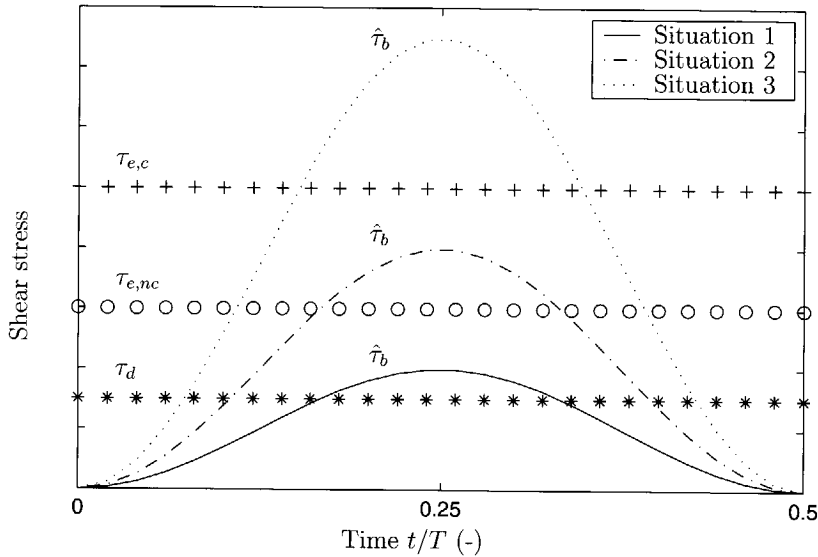


Figure 5.2: Overview of situations.

### 5.2.3 Situation 1: Deposition

Sand and mud deposition are possible during (part of) the tide in this situation, while erosion does not occur (Table 5.1). The behaviour of the various dependent variables is as follows:

#### Mud concentration

The behaviour of the depth-averaged mud concentration is governed by two time scales: a deposition time scale ( $h/w_m$ ) and a transport time scale ( $h/k_m$ ). Because the water depth is constant, the behaviour of the mud concentration is governed by the dimensionless ratio  $k_m/w_m$ . Hence, results of the mud concentration are given for different values of  $k_m/w_m$  in Figure 5.3. The mud concentration is made dimensionless by using the mud concentration outside the model domain  $C_{m,0}$ . It can be observed that the tidally-averaged mud concentration in the water column tends to a finite value for all ratios of  $k_m/w_m$ . When the ratio  $k_m/w_m$  is higher, the equilibrium value is also higher. Furthermore, the equilibrium mud concentration is always lower than the concentration outside the model domain.

The equilibrium mud concentration can be explained from a balance between the inward flux by horizontal transport and an outward flux by deposition during one tidal period. When the mud concentration is assumed to be constant during the tidal period, the equilibrium mud concentration  $C_{m,e}$  can be easily solved by integrating eq. (5.4) over the tidal period:

$$C_{m,e} = \frac{1}{\frac{w_m}{k_m} \alpha_D + 1} C_{m,0} \quad (5.5)$$

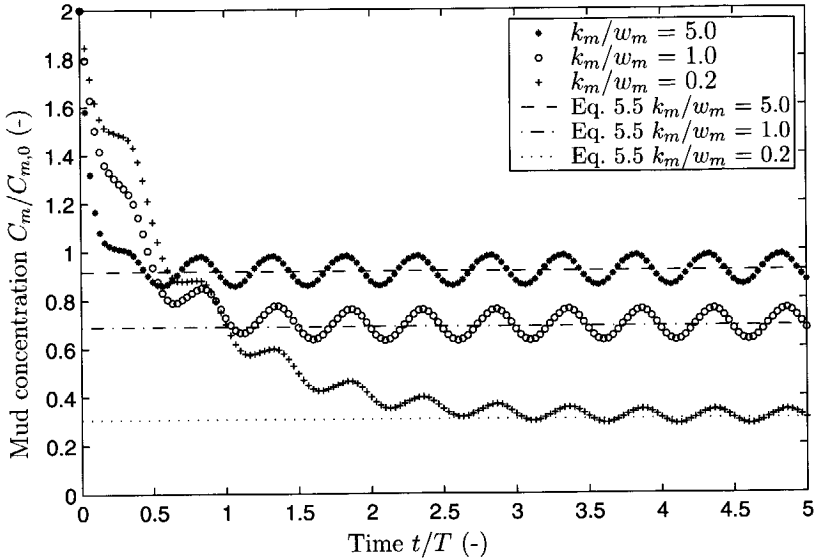


**Figure 5.3:** Mud concentration for different values of  $k_m/w_m$  with accompanying tidally-averaged equilibrium concentration according to eq. (5.5).

with

$$\alpha_D = 1 - \frac{1}{2}\tilde{\tau}_d \quad \tilde{\tau}_d < 1 \quad (5.6a)$$

$$\alpha_D = \left(1 - \frac{1}{2}\tilde{\tau}_d\right) \left(\frac{2}{\pi} \arcsin \frac{1}{\sqrt{\tilde{\tau}_d}}\right) + \frac{1}{2\pi} \sqrt{\tilde{\tau}_d - 1} \quad \tilde{\tau}_d > 1 \quad (5.6b)$$

where  $\alpha_D$  is a deposition coefficient. The analytical equations (5.6a) and (5.6b) are derived in Appendix C. Equation (5.5) is shown in Figure 5.3 for the different values of  $k_m/w_m$  and appears to be a good approximation of the numerical results. Furthermore, it follows from eq. (5.5) that the model gives a trivial solution when no horizontal transport ( $k_m = 0$ ) is included. In that case, the only flux is caused by deposition and the equilibrium mud concentration is zero. The total deposition flux then depends on the initial mud concentration.

### Sand concentration

The governing time scale for the sand concentration is  $h/w_s$ . This time scale is in general much smaller than the tidal period. If the initial sand concentration is non-zero, the sand concentration will drop very fast to zero and does not change anymore. Notice that this result differs from the mud concentration behaviour because horizontal sand exchange with the surrounding area is not included in eq. (5.3).

### Bed level

The bed level is continuously increasing because of deposition of mud particles and the absence of erosion in this situation. The speed of the bed level rise is thus determined by the equilibrium mud concentration and the settling velocity. The accretion time scale is given by:

$$T_{zb} = (1 - \varepsilon_p) \frac{\delta \left( \frac{1}{\alpha_D w_m} + \frac{1}{k_m} \right)}{C_{m,0}} \quad (5.7)$$

where  $T_{zb}$  is the time scale of accretion and  $\delta$  the total thickness of the bed layer in which the bed composition changes. This time scale expresses the time needed for sedimentation of a mud layer with thickness  $\delta$ . It is obvious that the time scale of accretion decreases for an increasing transport coefficient ( $k_m$ ), settling velocity ( $w_m$ ) and concentration outside the model domain ( $C_{m,0}$ ).

### Bed composition

Because of the continuous deposition of mud, the equilibrium composition consists of a mud bed without sand. Two time scales are important for the bed composition development: the time scale for accretion (eq. 5.7) and the mixing time scale ( $T_m$ ). The mixing time scale is given by:

$$T_m = \frac{\delta^2}{\Xi} \quad (5.8)$$

where  $\Xi$  is the mixing coefficient. The mud content at the bed surface is shown in Figure 5.4 for different ratios of  $T_{zb}/T_m$ . Furthermore, the bed composition profile is given in a fixed coordinate system at different times in Figure 5.5 for two values of  $T_{zb}/T_m$ . Herein, the depth within the bed is made dimensionless with the constant thickness of the bed layer  $\delta$ . The bed layer in which the bed composition is computed, shifts upward in time because of the fixed coordinate system and the continuous bed level rise in this situation.

It can be observed that the time needed to reach a 100% muddy bed surface is relatively long when the ratio of accretion time scale to mixing time scale is relatively large (Figure 5.4,  $T_{zb}/T_m = 5.0$ ). Moreover, the bed composition with depth is more or less constant (Figure 5.5a). For the opposite situation (Figure 5.4,  $T_{zb}/T_m = 0.2$ ) a 100% muddy bed surface is reached very fast and the bed composition shows a stratified profile (Figure 5.5b). The explanation for this behaviour is that all mud deposited on the bed surface is conserved in the upper part of the bed when the net downward flux due to deposition is much larger than the downward transport by mixing (i.e.  $T_{zb}/T_m = 0.2$ ). Consequently, a 100% muddy bed surface is reached very fast and the bed composition profile is strongly stratified. However, a relatively small deposition flux (i.e.  $T_{zb}/T_m = 5.0$ ) results in a long time span for reaching a 100% muddy bed surface and a more homogeneous bed composition profile.

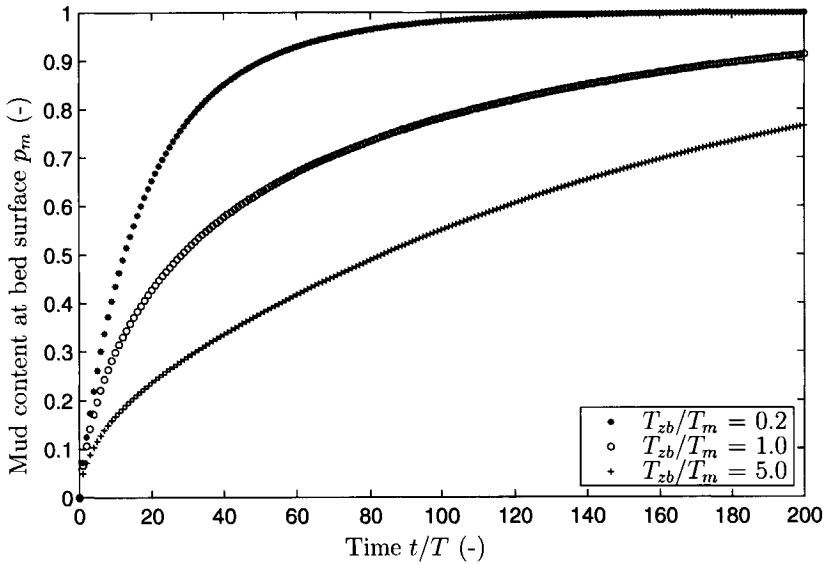


Figure 5.4: Mud content top layer for different values of  $T_{zb}/T_m$ .

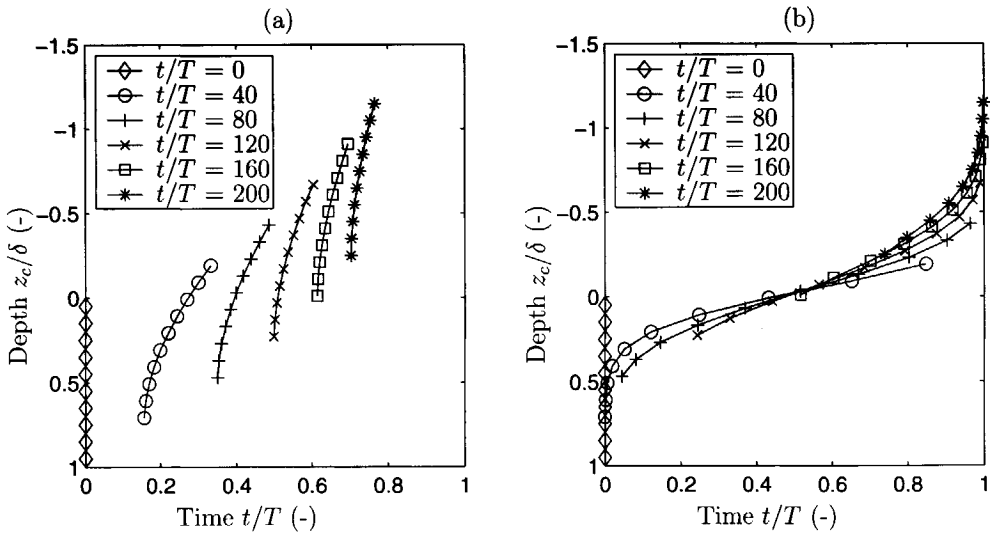


Figure 5.5: Mud content profile for a)  $T_{zb}/T_m = 5.0$  and b)  $T_{zb}/T_m = 0.2$ .

### 5.2.4 Situation 2: Deposition and non-cohesive erosion

Sand and mud deposition occur during (part of) the tide and only non-cohesive erosion of sand and mud is possible (Table 5.1). The behaviour of the various dependent variables is as follows:



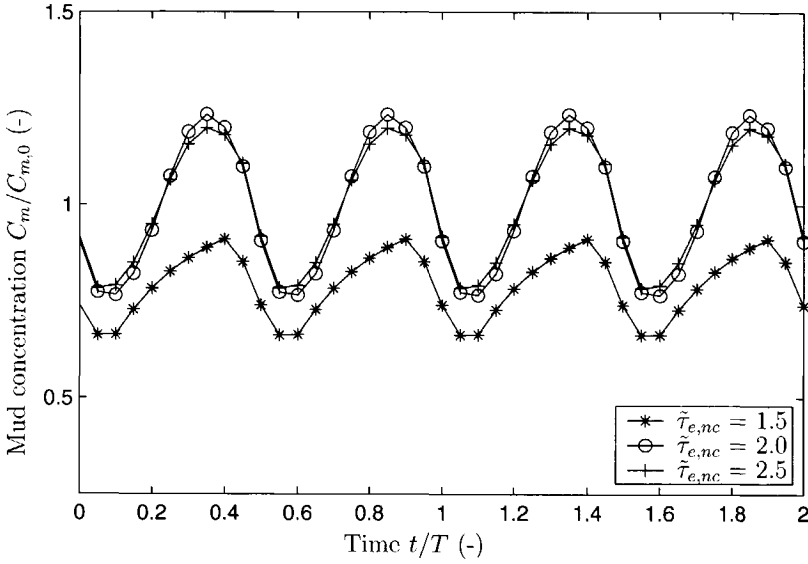


Figure 5.6: Mud concentration for different values of  $\tilde{\tau}_{e,nc}$ .

### Mud concentration

The behaviour of the mud concentration is shown for different values of  $\tilde{\tau}_{e,nc}$  in Figure 5.6. It is observed that the (tidally-averaged) mud concentration tends to the concentration outside the model domain  $C_{m,0}$  for  $\tilde{\tau}_{e,nc} = 2.0$  and  $\tilde{\tau}_{e,nc} = 2.5$ , while it is significantly lower than the concentration outside the model domain for  $\tilde{\tau}_{e,nc} = 1.5$ . The possibility of a tidally-averaged equilibrium between the erosion ( $E_m$ ) and deposition flux ( $D_m$ ) in eq. (5.4) explains this behaviour. When an equilibrium between these fluxes is reached, the tidally-averaged horizontal transport flux in eq. (5.4) equals zero. Consequently, the equilibrium mud concentration is then more or less equal to the concentration outside the model domain, and is independent of the transport coefficient  $k_m$ . Whether or not this equilibrium is reached is discussed hereafter.

### Bed level and composition

The behaviour of the bed level and bed composition is shown for different values of  $\tilde{\tau}_{e,nc}$  in Figure 5.7. The bed level and mud content tend to an equilibrium value for  $\tilde{\tau}_{e,nc} = 2.0$  and  $\tilde{\tau}_{e,nc} = 2.5$  while both variables continuously increase for  $\tilde{\tau}_{e,nc} = 1.5$ . An equilibrium bed level and mud content at the bed surface is reached when the tidally-averaged erosion ( $E_m$ ) and deposition flux ( $D_m$ ) at the bed surface are equal in eq. (5.4). When the mud content at the bed surface is assumed to be more or less constant during the tide, the equilibrium mud content at the bed surface can easily be obtained by integrating eq. (5.4) over one tidal period:

$$p_{me} = \frac{w_m C_{m,0} \alpha_D}{M \alpha_F} \quad (5.9)$$

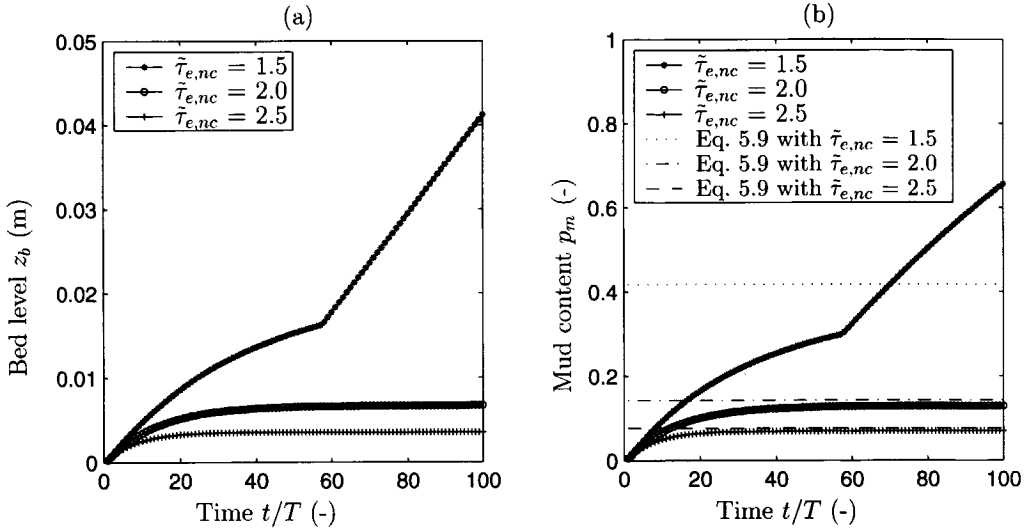


**Figure 5.7:** a) Bed level and b) Mud content with accompanying equilibrium mud content according to eq. (5.9) for different values of  $\tilde{\tau}_{e,nc}$ .

with

$$\alpha_E = 0 \quad \tilde{\tau}_e < 1 \quad (5.10a)$$

$$\alpha_E = \left( \frac{1}{2} \tilde{\tau}_e - 1 \right) \left( 1 - \frac{2}{\pi} \arcsin \frac{1}{\sqrt{\tilde{\tau}_e}} \right) + \frac{1}{2\pi} \sqrt{\tilde{\tau}_e - 1} \quad \tilde{\tau}_e > 1 \quad (5.10b)$$

where  $\alpha_E$  is an erosion coefficient and  $p_{me}$  the equilibrium mud content at the bed surface. The equations (5.10a) and (5.10b) for the erosion coefficient  $\alpha_E$  are derived in Appendix C. The deposition flux during one tide is recognised in the numerator of eq. (5.9) and the erosion flux for a 100% mud bed during one tide is observed in the denominator. Equation (5.9) is shown in Figure 5.7 for the different values of  $\tilde{\tau}_{e,nc}$ .

The magnitude of the equilibrium mud content ( $p_{me}$ ) in eq. (5.9) and the critical mud content ( $p_{m,cr}$ ) for the transition between non-cohesive and cohesive behaviour determine whether or not the equilibrium is reached in this situation. Two possibilities can be distinguished:

- $p_{me} > p_{m,cr}$   
When the equilibrium mud content is larger than the critical mud content for the transition between non-cohesive and cohesive behaviour, the non-cohesive equilibrium mud content will never be reached. An example of this situation is  $\tilde{\tau}_{e,nc} = 1.5$  in Figure 5.7. When starting with a non-cohesive bed, the mud content in the top layer tends towards

an equilibrium which is higher than the critical mud content. When the critical mud content is reached, the behaviour changes into a cohesive behaviour. Because cohesive erosion is not possible in this example, the mud content increases towards 100% and the bed level continuously increases. In fact, the situation is similar to situation 1 with only deposition and horizontal transport and no erosion.

- $p_{me} < p_{m,cr}$

When the equilibrium mud content is smaller than critical, the non-cohesive equilibrium mud content is reached. Examples of this situation are  $\tilde{\tau}_{e,nc} = 2.0$  and  $\tilde{\tau}_{e,nc} = 2.5$  in Figure 5.7. When starting with a non-cohesive bed, the mud content at the bed surface reaches the equilibrium mud content. Equation (5.9) appears to be a good approximation of the numerical result for  $\tilde{\tau}_{e,nc} = 2.0$  and  $\tilde{\tau}_{e,nc} = 2.5$ .

### 5.2.5 Situation 3: Deposition, non-cohesive and cohesive erosion

The model behaviour in situation 3 is strongly comparable to situation 2 in the previous section. The only extra possibility is cohesive erosion of sand and mud (Table 5.1). Therefore, two equilibria exist for the mud content at the bed surface (eq. 5.9), indicated with indices *nc* and *c*: a non-cohesive equilibrium ( $p_{me,nc}$ ) and a cohesive equilibrium ( $p_{me,c}$ ). Both equilibria are defined by eq. (5.9), but with a different critical erosion shear stress in the erosion coefficient  $\alpha_E$ .

**Table 5.2:** Overview of equilibria in situation 3.

| Non-cohesive equilibrium | Cohesive equilibrium | Final equilibrium             |
|--------------------------|----------------------|-------------------------------|
| $> p_{m,cr}$             | $> p_{m,cr}$         | Cohesive                      |
| $< p_{m,cr}$             | $< p_{m,cr}$         | Non-cohesive                  |
| $< p_{m,cr}$             | $> p_{m,cr}$         | Depends on initial conditions |

Similarly to situation 2, the final equilibrium in situation 3 depends on the values of the non-cohesive and cohesive equilibrium mud content compared to the critical mud content ( $p_{m,cr}$ ). Three different situations can be distinguished, which are summarised in Table 5.2. Notice that the fourth possibility ( $p_{me,nc} > p_{m,cr}$  and  $p_{me,c} < p_{m,cr}$ ) is not listed in Table 5.2, because it does not exist. Initially, the critical shear stress for non-cohesive erosion was assumed to be smaller than that for cohesive erosion (cf. Table 5.1). Consequently, the equilibrium mud content for non-cohesive erosion is always smaller than that for cohesive erosion by definition (i.e.  $p_{me,nc} < p_{me,c}$ ). This is in contradiction to the fourth possibility.

The final equilibrium for the situations in Table 5.2 can be explained as follows:

- $p_{me,nc} > p_{m,cr}$  and  $p_{me,c} > p_{m,cr}$

The non-cohesive equilibrium is never reached, because the non-cohesive equilibrium mud content is higher than the critical mud content. When the mud content is lower than

the critical mud content, the mud content increases until the non-cohesive equilibrium value is reached. When the critical mud content is reached, the equilibrium changes to the cohesive equilibrium and this is also the final equilibrium.

- $p_{me,nc} < p_{m,cr}$  and  $p_{me,c} < p_{m,cr}$   
This situation is comparable to the previous situation, but the cohesive equilibrium is never reached because its value is in the non-cohesive range. The final equilibrium is always the non-cohesive equilibrium.
- $p_{me,nc} < p_{m,cr}$  and  $p_{me,c} > p_{m,cr}$   
Both equilibria can exist and the final situation depends on the initial mud content at the bed surface. If the initial mud content is higher than critical, the cohesive equilibrium is reached. If the initial mud content is lower than the critical mud content, the non-cohesive equilibrium is reached.

### 5.2.6 Field measurements

Previously, various correlations have been made between the maximum bed shear stress and the mud content at the Molenplaat in the Western Scheldt estuary (the Netherlands) (WL|Delft Hydraulics, 1998; De Bake, 2000). These correlations show the following pattern: the mud content is always low (< 10%) for high bed shear stress, whereas the mud content varies between 0 and 100% for low bed shear stress and a useful relationship cannot be determined. Often, a sharp transition between these regimes is observed and a critical transition value can be defined.

Similarly to the correlation described above, the equilibrium mud content at the bed surface in eq. (5.9) is shown in Figure 5.8 for different values of  $w_m C_{m,0}/M$ . The maximum bed shear stress on the horizontal axis is made dimensionless with the critical erosion shear stress. It is assumed that the critical erosion shear stress for non-cohesive erosion is equal to the critical erosion shear stress for cohesive erosion. Furthermore, the critical shear stress for deposition must be known. Therefore, the equilibrium mud content is given for two ratios of  $\tau_e/\tau_d = 5$  (closed symbols) and  $\tau_e/\tau_d = 10$  (open symbols).

A sharp transition exists between a full mud bed and a full sand bed when  $w_m C_{m,0}/M = 1$  (Figure 5.8). The mud content is less than 10% beyond a dimensionless bed shear stress of about 3, whereas the equilibrium value equals 100% below a dimensionless bed shear stress of about 2. The transition becomes more gradual with increasing values of  $w_m C_{m,0}/M$ . It is important to note that when the critical shear stress for erosion in the non-cohesive and cohesive regime are not equal, the non-cohesive and cohesive equilibrium mud content are not equal. In this case, the equilibrium mud content as a function of the maximum bed shear stress is discontinuous. The discontinuity arises at the critical mud content between the non-cohesive and cohesive erosion.

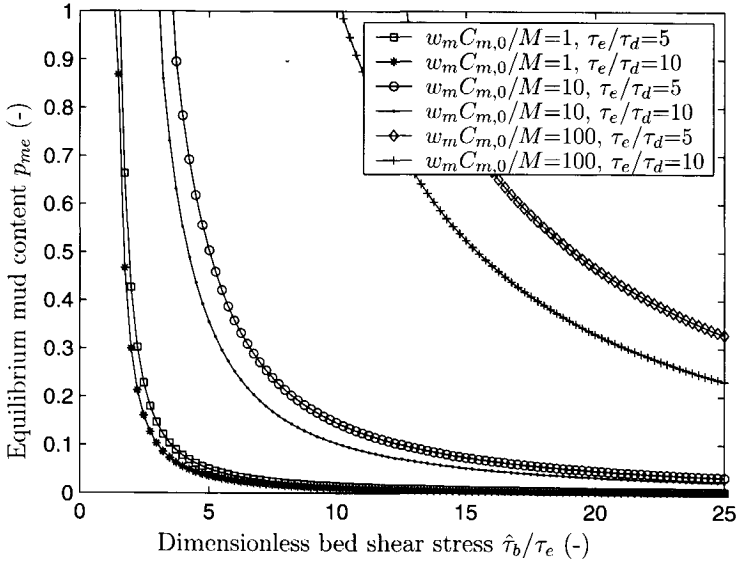


**Figure 5.8:** Equilibrium mud content for different values of  $w_m C_{m,0}/M$ .

A comparison is made between the obtained correlation by De Bake (2000) and the equilibrium mud content (eq. 5.9) derived in the present study (Figure 5.9). De Bake (2000) selected 239 samples from the data set of the Scheldt estuary in 1992 (see for details Table 2.2). The selected samples covered the domain of a detailed two-dimensional flow model around the Molenplaat (see for location Figure 2.1). The maximum bed shear stress during an average tide was computed with the flow model, and the obtained correlation with the observed mud content in the sampling points is shown in Figure 5.9. Notice that the mean sand grain size of these sampling points is  $170 \mu\text{m}$  and the accompanying critical bed shear stress for sand only equals  $\tau_{cr} = 0.15 \text{ N/m}^2$ . The equilibrium mud content in Figure 5.9 is computed by applying typical values for the parameters in the Westerchelde area:  $w_m = 0.001 \text{ m/s}$ ,  $M = 0.4 \times 10^{-7} \text{ m/s}$  ( $\simeq 1 \times 10^{-4} \text{ kg}/(\text{m}^2\text{s})$ ),  $C_{m,0} = 4 \times 10^{-5}$  ( $\simeq 100 \text{ mg/l}$ ),  $\tau_e = 0.5 \text{ N/m}^2$  and  $\tau_d = 0.15 \text{ N/m}^2$ . Thus, the important parameter  $w_m C_{m,0}/M$  has a value of about 1.

The equilibrium mud content derived in the present study appears to envelope the data of the mud content at almost all locations (Figure 5.9). Only a few samples have a mud content higher than the equilibrium mud content with respect to the total number of samples ( $N = 239$ ). The sharp transition between a full mud bed and a full sand bed in this area is likely to be related with the low value of  $w_m C_{m,0}/M$ . Let us assume that the settling velocity  $w_m$  and the erosion coefficient  $M$  are mud properties, which do not vary too much in tidal systems. This implies that the observed sharp transitions between sandy and (potentially) muddy areas only exist in systems with low mud concentrations ( $c_m < 100 \text{ mg/l}$ ). Based on the results, the transitions are expected to be more gradual for higher values of the mud concentration (cf. Figure 5.8).

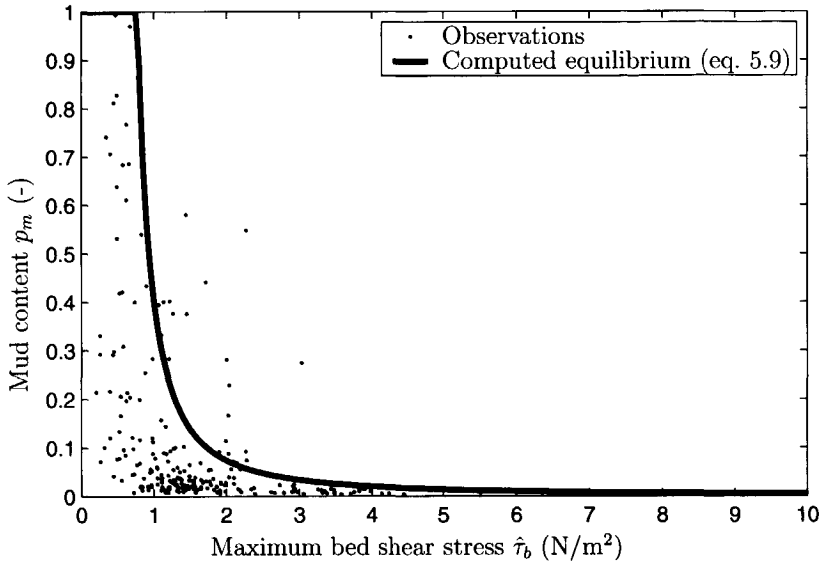


**Figure 5.9:** Correlation between observed mud content and maximum bed shear stress (De Bake, 2000) and derived equilibrium mud content (eq. 5.9) against maximum bed shear stress for Molenplaat area (the Netherlands).

Several explanations can be given for the observed large scatter in areas with a low bed shear stress (Figure 5.9):

- The relatively long time scale for reaching the equilibrium mud content suggests that the measured mud content at the sample points is probably not at equilibrium, but evolving towards that equilibrium. When mixing in the sediment bed itself is neglected, the time scale for reaching a 100% mud bed from an initial sand bed can be estimated by using the time scale of accretion  $T_{zb}$  (eq. 5.7) only. Characteristic parameter values are:  $\delta = 0.10$  m,  $\varepsilon_p = 0.4$ ,  $w_m = k_m = 1 \times 10^{-3}$  m/s,  $C_{m,0} = 4 \times 10^{-5}$  ( $\simeq 100$  mg/l) and  $\alpha_D = 0.5$ , resulting in  $T_{zb} \simeq 2$  months. The estimated time span for reaching the equilibrium mud content implies that the measured mud content at a single site not only depends on the actual hydrodynamic conditions, but also on the hydrodynamic conditions in previous months. The equilibrium mud content can be seen as the upper limit for the mud content in a particular area.
- The scatter can also be caused by differences between the real bed shear stress profile and water depth during the tide and the assumed bed shear stress profile (eq. 5.1) and constant water depth in the present model. Especially for the intertidal areas, the bed shear stress and water depth can be quite different from the assumed hydrodynamical situation due to flooding and drying.

## 5.3 Reservoir<sup>1</sup>

### 5.3.1 Model set-up

The southern part of the Rhine-Meuse estuary in the Netherlands (Figure 5.10) is used as reference for the idealised model study in this section. In 1970 the Haringvliet Sluices, indicated in Figure 5.10, came into operation to protect the hinterland under high storm surge conditions, as well as to manage the navigation depth and salt intrusion in the Rotterdam harbour under low river discharge conditions. Due to the construction of these sluices, the water motion in the southern part of the Rhine-Meuse estuary (from west to east: Haringvliet, Hollandsch Diep, Nieuwe Merwede, Boven Merwede, Amer, Bergsche Maas) was completely changed (Haring, 1977, 1978). The tidal current changed into unidirectional flow under all discharge conditions in the river branches Nieuwe Merwede and Bergsche Maas. Furthermore, the maximum current velocities decreased significantly in the entire southern area and an enormous amount of sand and mud has been deposited in the various branches in the last few decades (Allersma, 1988b; Van Dreumel, 1995).

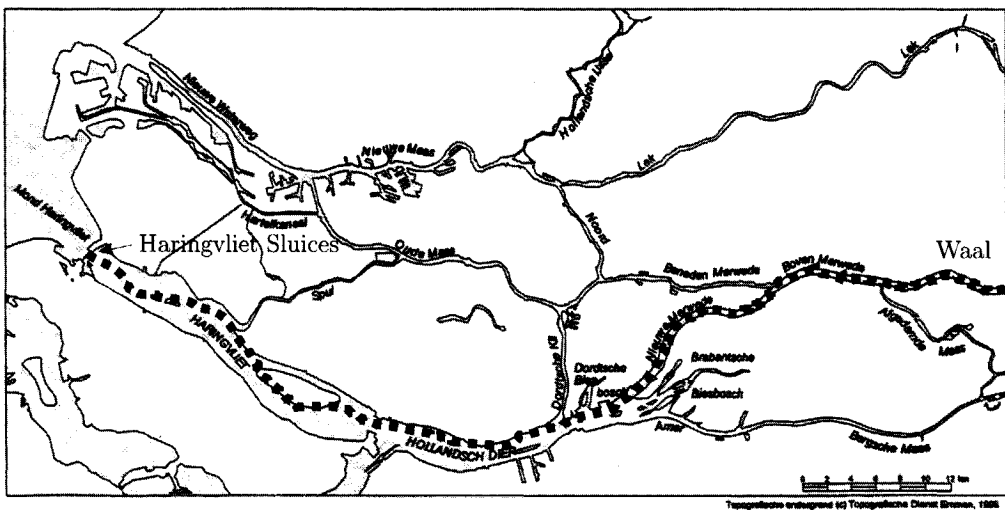


**Figure 5.10:** Rhine-Meuse estuary (the Netherlands) with the southern axis along the dotted line.

It is beyond the present model capabilities to initiate the process-based sand-mud model with the initial geometry of the southern part of the Rhine-Meuse estuary and compute the bed level and bed composition development with realistic boundary conditions. Therefore, the complexity of the geometry and boundary conditions is strongly simplified. The area is considered as

1. The contents of this section appeared almost completely in: Proceedings 2nd IAHR symposium on River, Coastal and Estuarine Morphodynamics Conference (pp. 505-514), ed. by S. Ikeda, Obihiro, Japan, 2001. with Z.B. Wang as co-author.





exponential profile. When the initial water level slope is assumed to be equal to the equilibrium bed level slope ( $i_{be}$ ), the initial bed level is given by:

$$z_b(x, t = 0) = i_{be}(L - x) - h_e - (h_1 - h_e)e^{-\frac{L-x}{L_a}} \quad (5.11)$$

where  $L_a$  is a characteristic length of the initial bed level profile. A length  $L_a = 20,000$  m is required to approach the equilibrium situation at the upstream boundary. The initial bed level according to eq. (5.11) is shown in Figure 5.11.

### Boundary conditions

The flow at the upstream boundary is driven by a constant discharge ( $Q = 1500$  m<sup>3</sup>/s) and the water level at the downstream boundary is kept constant ( $\zeta = 0.0$  m). At the upstream boundary, an equilibrium sand concentration profile is applied for suspended sand transport. In addition, a uniform mud concentration profile with a mud concentration  $c_{m,0} = 0.05$  kg/m<sup>3</sup> is prescribed for suspended mud transport. Thus, we have a realistic total annual mud load of  $2.4 \times 10^9$  kg/year (Van Dreumel, 1995). Furthermore, the bed level remains unchanged at this boundary. The initial bed and the bed of the sublayer are assumed to be composed of sand only.

### Physical Parameters

The settings of the various physical parameters for the so-called ‘reference computation’ are summarised in Table 5.3. These settings are representative for the area under consideration. Two remarks are made with respect to the reference settings in Table 5.3:

- The sand grain size ( $d_{50}$ ) is used to calibrate the annual sand transport load at the upstream boundary. The estimated annual sand load equals  $1.05 \times 10^9$  kg/year by dry weight (Van Dreumel, 1995). The application of  $d_{50} = 300$   $\mu\text{m}$  with Van Rijn’s transport formulas for bed load and suspended load results in an annual sand load of  $1.1 \times 10^9$  kg/year. This grain size is smaller than observed in the Waal, but is a reasonable value for the more downstream branches Boven-Merwede and Nieuwe Merwede (Van Dreumel, 1995).
- The critical shear stress and the erosion coefficient for non-cohesive erosion ( $\tau_{e,nc}$ ,  $M_{e,nc}$ ) and cohesive erosion ( $\tau_{e,c}$ ,  $M_{e,c}$ ) are assumed to be independent of the mud content. Furthermore, the critical mud content ( $p_{m,cr}$ ) is set at 30%. Although no specific measurements are available of this area, this parameter value is valid in nearby tidal systems in the Netherlands (see Table 2.3). Because the morphological behaviour is dominated by deposition in this situation, these parameter settings hardly affect the computational results.

In addition to the reference computation, several sensitivity computations are carried out. The morphological behaviour is dominated by deposition in the reservoir. Therefore, only parameters

**Table 5.3:** Parameter settings of the reference computation.

| Description                      | Symbol          | Value     | Unit        |
|----------------------------------|-----------------|-----------|-------------|
| Chézy-coefficient                | $C$             | 50        | $m^{1/2}/s$ |
| Horizontal fluid mixing          | $\nu_x, \nu_y$  | 100       | $m^2/s$     |
| Sand grain size                  | $d_{50}$        | 0.0003    | $m$         |
| Settling velocity sand           | $w_s$           | 0.043     | $m/s$       |
| Settling velocity mud            | $w_m$           | 0.0005    | $m/s$       |
| Critical mud content             | $p_{m,cr}$      | 0.3       | –           |
| Critical erosion shear stress:   |                 |           |             |
| - Non-cohesive erosion           | $\tau_{e,nc}$   | 0.25      | $N/m^2$     |
| - Cohesive erosion               | $\tau_{e,c}$    | 0.25      | $N/m^2$     |
| Erosion coefficient:             |                 |           | $m/s$       |
| - Non-cohesive erosion           | $M_{e,nc}$      | $10^{-6}$ | $m/s$       |
| - Cohesive erosion               | $M_{e,c}$       | $10^{-6}$ | $m/s$       |
| Critical deposition shear stress | $\tau_d$        | 0.15      | $N/m^2$     |
| Bed porosity                     | $\varepsilon_p$ | 0.40      | –           |
| Biological mixing coefficient    | $\Xi_b$         | 0.0       | $m^2/s$     |
| Physical mixing length           | $L_p$           | 0.25      | $m$         |
| Physical mixing coefficient      | $\alpha_p$      | $10^{-6}$ | –           |

are varied, which determine the deposition of sand and mud significantly. The parameters chosen are the sand grain size ( $d_{50}$ ), the settling velocity for mud ( $w_m$ ), the critical deposition shear stress ( $\tau_d$ ) and the mud concentration at the upstream boundary ( $c_{m,0}$ ).

### Numerical parameters

The horizontal grid size  $\Delta x = 500$  m. The water column is divided into five layers with a logarithmic spacing. The bed consists of 200 layers with a constant grid size  $\Delta z = 0.10$  m. Notice that this large number of layers is chosen for output purposes only. From a physical point of view, the number of layers can be chosen much smaller, because bed composition changes are only expected near the bed surface. The computational time step is set to  $\Delta t = 60$  s for the water motion and the suspended sediment transport. The time step in the bed level and bed composition computations is  $N\Delta t$  and  $N = 500$  is applied herein after trial-and-error.

The simulation time is set at a characteristic time span for the morphological behaviour in the present model set-up (Figure 5.11). A characteristic time span in this case is the time needed to fill the total volume between the initial bed level and the equilibrium bed level with sand and mud. This so-called ‘morphological time scale’ can be estimated as follows. The total volume can be computed by integrating the third term at the right hand side of eq. (5.11) over the basin length  $L$ , and adding the constant width  $B$  and the bed density  $\rho_b = (1 - \varepsilon_p)\rho_s$ . The total

volume divided by the supplied annual volume of sand and mud at the upstream boundary gives an estimation of the morphological time scale  $T_m$ :

$$T_m = \frac{(1 - \varepsilon_p)\rho_s B L_a (h_1 - h_c) \left(1 - e^{-\frac{L}{L_a}}\right)}{V_s + V_m} \quad (5.12)$$

where  $V_s$  is the annual sand load and  $V_m$  the annual mud load by dry weight. Application of the previously given parameter values results in a morphological time scale  $T_m \cong 175$  years for the reference computation.

### 5.3.2 Results

#### Reference computation

The results of the reference computation are shown in Figure 5.12. Two characteristic morphological phenomena are observed: a sand wave and a mud wave, both propagating downstream. The sand deposition wave gradually increases in the downstream direction and has a front at the downstream side. The mud wave has a clear onset at  $x/L \simeq 0.65$  (Figure 5.12b). Upstream from this onset, no mud deposition takes place. Downstream from the onset, mud deposition first increases, reaches a certain maximum and then decreases in the downstream direction. As a result of these propagating deposition waves, the bed level after 30 years is characterised by a sand deposition area in the upstream reach and a mud deposition area more downstream, whereas the bed level changes are relatively small in between (Figure 5.12c). After that, the sand wave reaches the onset of mud deposition and covers the earlier deposited mud layer. After 150 years, the bed level has a constant bed slope for almost the entire basin. The mud content at the bed surface (Figure 5.12d) shows a strong similarity with the bed level changes by mud deposition (Figure 5.12b). Initially, the mud content at the bed surface suddenly increases to 100% downstream from the onset for mud deposition, but remains low upstream and far downstream from the onset. The area with high mud content shifts in the downstream direction over time. The final composition profile at the bed surface is very sandy for almost the entire basin with only a small muddy area near the downstream end of the basin.

#### Sensitivity computations

The bed level changes by sand and mud for a five year simulation period are shown in Figure 5.13, for the various sensitivity computations. The results show the following characteristics with respect to the reference computation:

- The bed level changes by sand deposition are higher and lower for a smaller and larger sand grain size, respectively (Figure 5.13a).
- The bed level change by mud deposition has a very pronounced maximum for a higher settling velocity, whereas the mud wave is much flatter for a lower settling velocity (Figure 5.13b).

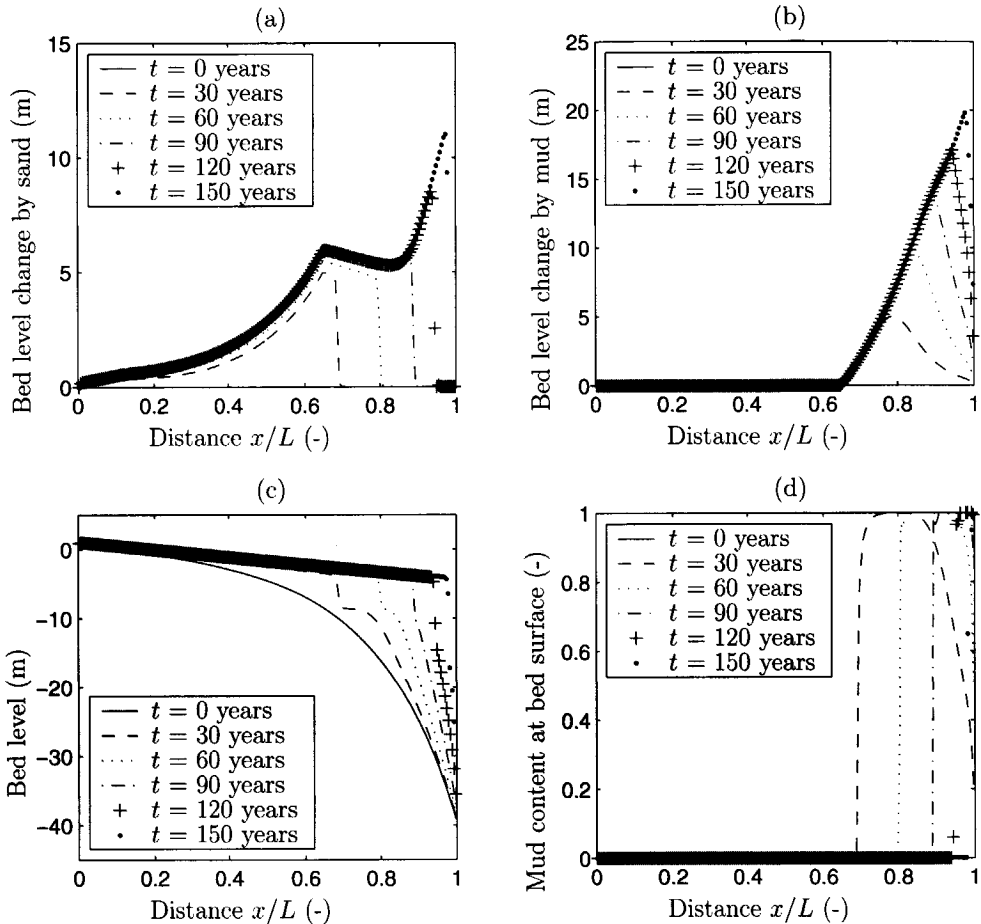


**Figure 5.12:** Results reference computation: a) bed level changes by sand deposition, b) bed level changes by mud deposition, c) bed level development and d) mud content at bed surface for time intervals of 30 years.

- The onset of mud deposition area shifts in the downstream/upstream direction when the critical shear stress for deposition decreases/increases. In a similar way, the location of the maximum mud deposition shifts in downstream/upstream direction (Figure 5.13c).
- The bed level changes by mud deposition are strongly affected by the upstream mud concentration. With increasing/decreasing mud concentration, the bed level changes are considerably higher/lower. However, the onset and the form of the deposition wave do not seem to be affected by the upstream boundary concentration (Figure 5.13d).

The bed level and bed composition profile at the end of the sensitivity computations are quite similar to the reference computation and not shown herein (see Van Ledden, 2001). The bed level has a constant bed slope for almost the entire basin and the bed surface is sandy for

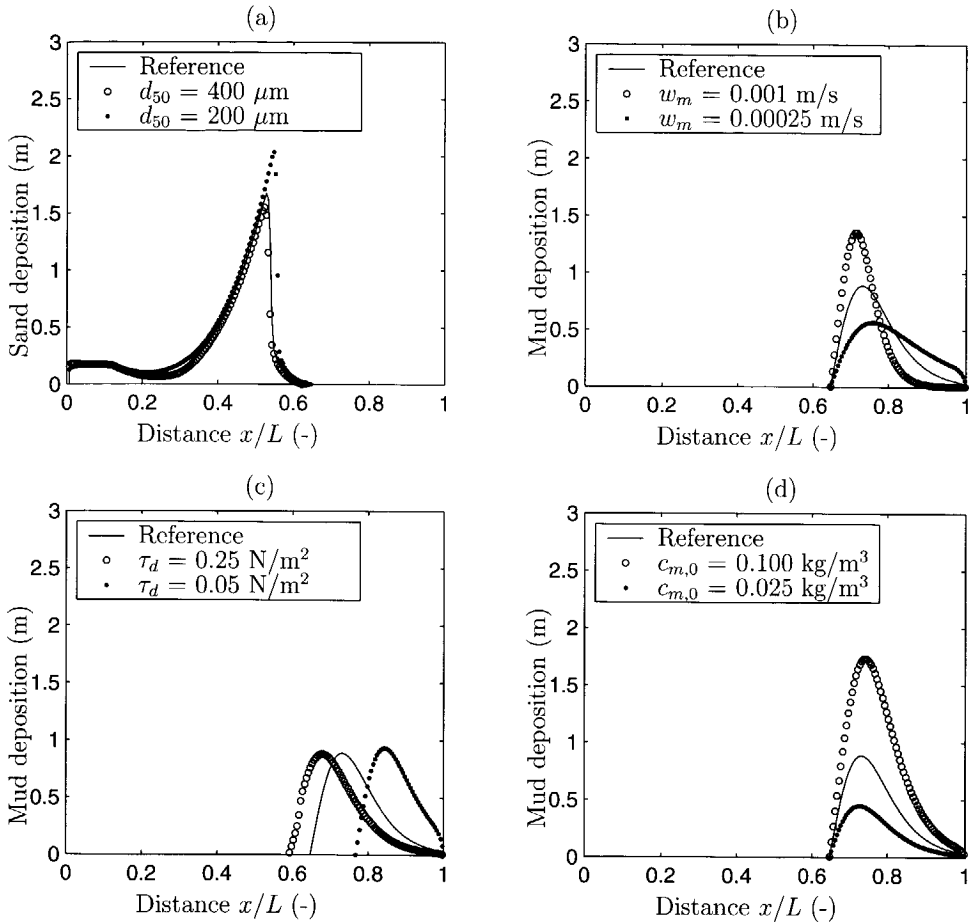


**Figure 5.13:** Results sensitivity computations: a) sand grain size, b) settling velocity of mud, c) critical shear stress for mud deposition and d) upstream mud concentration.

almost the entire basin with only a very muddy region near the downstream boundary. Below the bed surface, a thick mud layer is still present. The morphological time scale for reaching the equilibrium situation, however, is strongly affected when the parameter setting is changed. It decreases with a smaller sand grain size, a higher settling velocity for mud, a higher critical shear stress for mud deposition and a higher mud concentration at the upstream boundary.

### 5.3.3 Analysis

The results in the previous section showed two characteristic morphological phenomena: a sand wave and a mud wave propagating in the downstream direction. These are discussed below.

### Sand wave

The occurrence of the sand wave was expected and is only discussed briefly. The total transport rate of sand at the upstream side of the basin ( $x/L < 0.2$ ) is nearly uniform because of the more or less uniform water motion in this area. Therefore, the bed level is about constant in time. Further downstream, the water depth increases and the velocity decreases. Consequently, the horizontal sand transport rate decreases in the downstream direction, resulting in an increasing bed level in time. The accretion continues until the total sediment transport rate is equal to the total sand transport rate upstream. This implies that the initial water depth decreases until it is equal to the equilibrium water depth.

### Mud wave

The behaviour of the mud wave calls for a more detailed discussion. The onset for mud deposition ( $x_d$ ), the initial depth-averaged mud concentration ( $C_m$ ), the initial mud deposition rate ( $D_m$ ) and the initial distance of the maximum deposition rate relatively to the onset ( $\tilde{x}_m$ ) can be approximated as follows (Appendix D):

$$\frac{x_d}{L} = 1 + \frac{L_a}{L} \ln \left( \frac{h_d - h_e}{h_1 - h_e} \right) \quad (5.13)$$

$$\frac{C_m(\tilde{x})}{C_{m0}} = e^{-\frac{1}{L_m} \frac{\tilde{x}^2}{\tilde{x} + L_d}} \quad (5.14)$$

$$\frac{D_m(\tilde{x})}{w_m C_{m0}} = \left( 1 - \frac{1}{(1 + \tilde{x}/L_d)^2} \right) e^{-\frac{1}{L_m} \frac{\tilde{x}^2}{\tilde{x} + L_d}} \quad (5.15)$$

$$\tilde{x}_m = \frac{1}{2} \sqrt{2} \sqrt{L_m L_d} \quad (5.16)$$

where  $\tilde{x}$  is the position along the basin relative to the onset  $x_d$  (i.e.  $\tilde{x} = x - x_d$ ),  $h_d$  the water depth at the onset for mud deposition. The length scales  $L_m$  and  $L_d$  are defined as follows:

$$L_m = \frac{q}{w_m} \quad (5.17)$$

$$L_d = \frac{q}{i_{t0} U_d} \quad (5.18)$$

The first length scale ( $L_m$ ) expresses the distance covered by the flow while the mud settles from the water surface to the bed. It is comparable to the well-known 'settling length scale' for suspended sand, but is generally much larger. The second length scale ( $L_d$ ) contains the ratio between the flow discharge per unit width ( $q$ ) and the critical depth-averaged velocity for deposition ( $U_d$ ) which equals the water depth at the onset of mud deposition ( $h_d$ ). The length

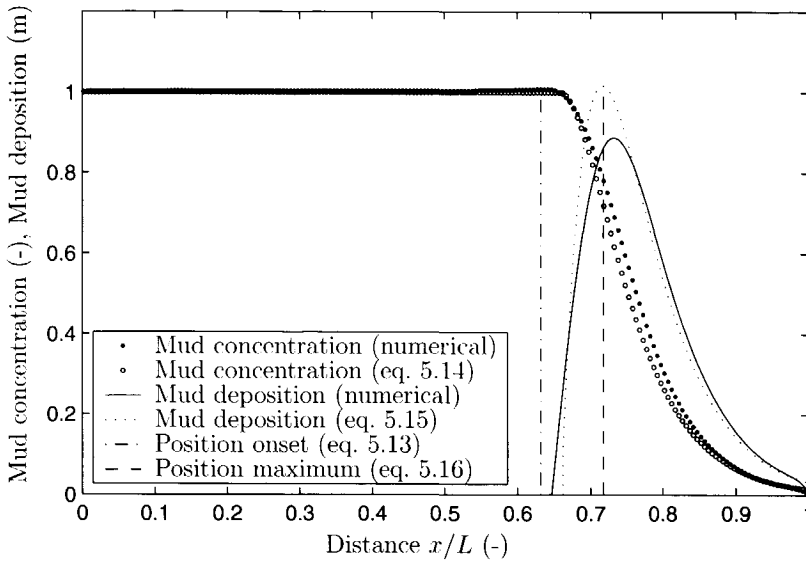


**Figure 5.14:** Comparison between numerical results after 5 years and analytical expressions for initial situation.

scale  $L_d$  expresses the distance from the onset at which the water depth is twice that at the onset. This length scale is called the ‘flow length scale’.

The presented analytical expressions are compared with the numerical results after five years in Figure 5.14. The depth-averaged mud concentration on the vertical axis is made dimensionless with the upstream mud concentration  $c_{m,0}$ . Furthermore, the analytical bed level change by mud deposition is computed by assuming a constant mud deposition rate according to eq. (5.15) during the first five years. The analytical expressions for the position of the onset (eq. 5.13) and the maximum mud deposition (eq. 5.16) are also indicated. Finally, it should be noted that the numerical onset for mud deposition is applied in the analytical expressions for the mud concentration and the mud deposition, because eq. (5.13) slightly underestimates the onset for mud deposition in the numerical results.

Because the analytical expressions agree well with the numerical results in Figure 5.14, the derived expressions are used for explaining the observed mud deposition wave with a maximum at a certain distance from the onset. Three areas are distinguished:

- **‘Flow limited’** for  $\tilde{x} \ll \tilde{x}_m$

Far upstream from the maximum mud deposition, the second term in eq. (5.15) is almost equal to zero, whereas the first term in eq. (5.15) is almost equal to unity. This implies that mud deposition is mainly limited by the flow velocity in this area, whereas the mud concentration is more or less equal to the mud concentration upstream. Hence, mud deposition in this area is called ‘flow limited’.

- **‘Supply limited’ for  $\tilde{x} \gg \tilde{x}_m$**   
 Far downstream from the maximum mud deposition rate, the first term in eq. (5.15) is almost equal to zero, whereas the second term in eq. (5.15) approaches unity. Thus, the mud concentration in the water column is very small because of upstream mud deposition, whereas the flow velocity is much smaller than the critical deposition velocity. Mud deposition in this area is therefore limited by the upstream mud supply.
- **‘Maximum’ for  $\tilde{x} \approx \tilde{x}_m$**   
 In the vicinity of the maximum, the first and the second term in eq. (5.15) are much larger than zero, but smaller than unity. The flow velocity is thus low enough and the mud concentration in the water column high enough for reaching a maximum mud deposition rate.

**5.3.4 Field measurements**

A comparison is made between the model results and existing field data for the various branches along the dotted line in Figure 5.10. Based on sediment balances by Allersma (1988b), Van Dreumel (1995) and Visser (2000), an estimation of the sand and mud deposition/erosion rates per unit area is made for the periods 1971 - 1982 and 1982 - 1992 (Figure 5.15). To enable a comparison with the sediment balances, the computed mean bed level changes by sand and mud separately are shown in Figure 5.16 between 0 and 10 years and between 10 and 20 years after the start of the computation.

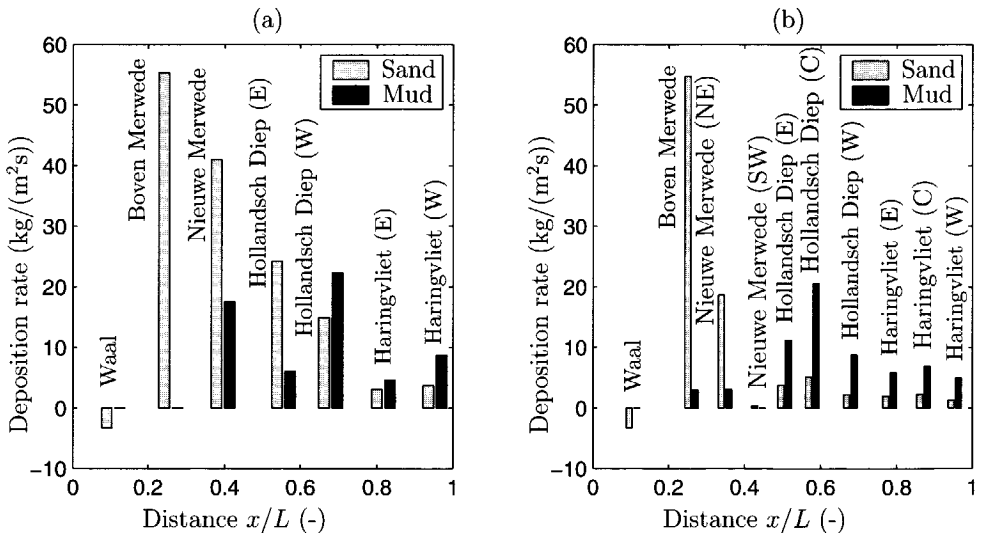


**Figure 5.15:** Sediment balances during the periods a) 1971 - 1982 and b) 1982 - 1992 (see Figure 5.10 for locations of branches).



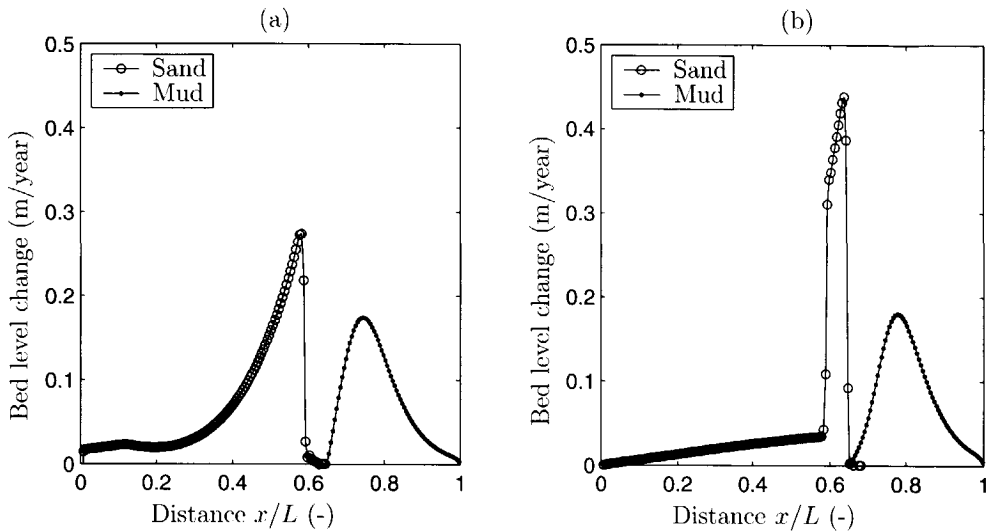


**Figure 5.16:** Bed level change by sand and mud between a) 0 - 10 years and b) 10 - 20 years after the start of the reference computation.

Several similarities as well as discrepancies are observed when the the model results in Figure 5.16 and the field data in Figure 5.15 are compared:

- The model results predict two initial deposition areas: a sand deposition area in the upstream areas and a mud deposition area more downstream. This pattern is also observed in the field data especially during the period 1982 - 1992. Sand deposition dominated at the Boven-Merwede and the north-cast part of the Nieuwe Merwede, whereas mud deposition was dominant in the Hollandsch Diep and Haringvliet area.
- A zone without sand and mud deposition between the aforementioned deposition areas of sand and mud is observed in the model results. The southwest part of the Nieuwe Merwede may indicate this behaviour. Sand and mud deposition were both very small compared with upstream and downstream areas. However, the sediment balance over the period 1971 - 1982 does not show this phenomenon.
- A characteristic mud deposition pattern is found from the model with a maximum mud deposition rate. During the period 1982 - 1992, the field data also suggest a maximum mud deposition area in the central part of the Hollandsch Diep area. Upstream as well as downstream the mud deposition is much lower. Although less clear, this pattern is also observed in the period 1971 - 1982.

Because of the correspondance between the model results and the field measurements, the presented model analysis is applied to give some indications and/or explanations for the observed sand-mud patterns. Firstly, the intense mud deposition in the Hollandsch Diep is probably caused by two interacting factors. On the one hand, the current velocities are low, so mud

deposition is possible. On the other hand, the mud concentration is still high because of the absence of mud deposition in the upstream area. Both factors cause high mud deposition in this section. Secondly, the relatively small mud deposition in the Haringvliet area is mainly limited because of the low mud concentration in the water column ('supply limited'), whereas small mud deposition in the upstream river branches Boven-Merwede and Nieuwe Merwede is mainly a result of the high current velocities ('flow limited'). Consequently, the mud content in the bed is relatively low in both areas, but for different physical reasons.

The observed discrepancies between the observed sand-mud patterns (Figure 5.15) and the model results (Figure 5.16) could be due to several causes:

- **Idealisations in set-up of the model**

River discharge variations and the effect of short waves are not taken into account in the present model. The effect of high river discharges has probably induced the observed sand sedimentation in the Hollandsch Diep and Haringvliet. Another explanation for the net sand sedimentation in these branches is erosion of the nearby banks and intertidal flats by short waves. After construction of the Haringvliet Sluices, the effect of short waves in these areas has relatively increased due to the reduction of the tidal current velocities. Hence, erosion of these banks and flats occurred and the eroded sediment was deposited nearby in the deeper channels. The sediment balances are based on depth soundings from areas with a navigable water depth, say  $> 2$  m. Thus, bed level changes at the intertidal areas are generally not taken into account in the sediment balances. When sand erodes from the nearby banks and deposits in the deeper channels, net sand deposition is detected in the sediment balances.

- **Uncertainties in the sediment balances**

These balances are based on depth soundings, dredging data, bed composition measurements and bifurcation relationships for the distribution of sand and mud transport. The bed composition measurements play a key role in the determination of the deposited and/or eroded sand and mud volume. Often, the mean mud content of the upper ten or twenty centimeters is chosen to be representative of the ratio between the deposited/eroded mud volume and the total deposited/eroded sand and mud volume. It is questionable if this parameter is representative, because the mud content can be strongly stratified near the bed surface. This suggests that the mean bed composition does not always correspond with the actual deposition conditions. A good example is the Haringvliet in which the mean bed composition in the upper layer is still relatively sandy, whereas the model results suggest only mud deposition.

Finally, the model results also give indications of the future development of the area if the boundary conditions are not changed. The results suggest that the sand wave will travel in downstream direction and cover the earlier deposited mud layers in the Hollandsch Diep. Furthermore, the mud deposition area will also shift downstream and the Haringvliet will become

more muddy in a later stage. After a long time (in the order of one century), this area is also covered with a sand layer. Notice that also the water levels gradually increase in the Hollandsch Diep and Haringvliet due to ongoing deposition of sand and mud. The final equilibrium is a 'river situation' with a more or less constant cross-sectional area. The mud concentration will be more or less constant along the basin and no further mud deposition will take place. The bed composition near the bed surface will be completely sandy. Further below the bed surface, mud layers covered with sand will be still present. Without human intervention the predicted future development will presumably give rise to several management problems in the Haringvliet and Hollandsch Diep. For instance, the gradual increase in the water level may reduce the safety of the surroundings areas. In the long term, severe sedimentation near the downstream boundary may be a serious threat to the functioning of the Haringvliet Sluices.

## 5.4 Tidal basin<sup>1</sup>

### 5.4.1 Model set-up

The tidal basins in the Wadden Sea are taken as a reference in this idealised case. They consist of a complex pattern of channels and shoals. Besides the complex bed level variations, these systems also show interesting mud content variations in horizontal and vertical directions. Flemming and Ziegler (1995) present an example of the horizontal sand-mud distribution in the German Wadden Sea near Spiekeroog (Figure 1.3c). The mud content at the bed surface in a large part of the tidal basin is relatively low (< 5%), whereas muddy deposits (20 - 50%) are only found in a small area near the dike.

#### Geometry

A strongly simplified geometry is considered (Figure 5.17). The shape of the tidal basin is assumed to be rectangular with length  $L = 20,000$  m. The sea side is located at  $x = 0$ , the land side boundary is at  $x = L$ . The banks are fixed, whereas the bed is erodible. The initial water depth is denoted as  $h_0$ , the bed level as  $z = z_b$  and the water level as  $z = \zeta$ . The initial water depth equals  $h_0 = 5$  m.

#### Boundary conditions

The water motion is forced by an external tidal motion at the sea side. Only the most important tidal component is taken into account:

$$\zeta(t) = \hat{\zeta}_2 \cos(\omega t) \quad (5.19)$$

---

1. The contents of this section will appear in: Ocean Dynamics, Proceedings of Physics of Estuaries and Coastal Seas Conference, H. Burchard et al. (eds.), 2003, with Z.B. Wang, J.C. Winterwerp & H.J. De Vriend as co-authors.

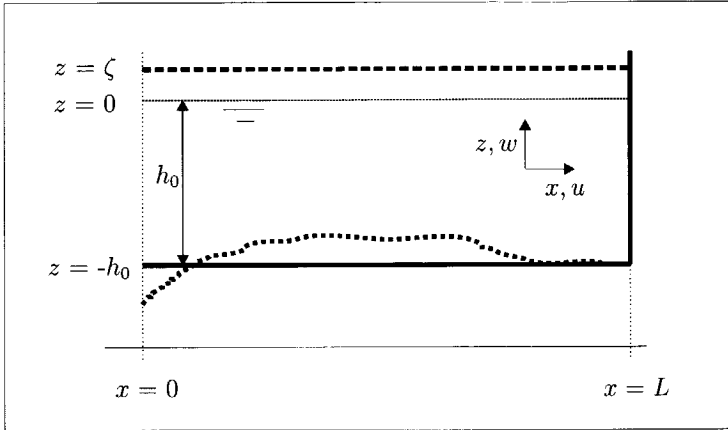


**Figure 5.17:** Model set-up of the tidal basin.

where  $\zeta$  is the water level,  $\hat{\zeta}_2$  the tidal amplitude of the  $M_2$ -tide,  $\omega$  the frequency  $M_2$ -tide. The tidal amplitude of the  $M_2$ -tide equals  $\hat{\zeta}_2 = 1.5$  m and the tidal frequency  $\omega = 1.4 \times 10^{-4} \text{ s}^{-1}$ . The mud concentration at the entrance is set at a constant value  $c_{m,0} = 0.05 \text{ kg/m}^3$  and the initial bed composition and the composition of the sublayer is 100% sand. All other boundary and initial conditions do not differ from the default settings discussed in Chapter 4.

### Physical parameters

The settings for the physical parameters for the reference computation are summarised in Table 5.4. It should be noted that the critical shear stress and the erosion coefficient for non-cohesive erosion and cohesive erosion are assumed to be independent of the mud content. In addition to the reference computation, several computations with different parameter settings are carried out to investigate the sensitivity of the model behaviour. One computation is a situation in which only sand determines the morphological behaviour. Furthermore, the sand grain size  $d_{50}$ , the settling velocity for mud  $w_m$ , the critical shear stress for deposition  $\tau_d$  and the mud concentration at the sea boundary  $c_{m,0}$  are increased and decreased within a realistic range in the other sensitivity computations.

### Numerical parameters

The horizontal grid size is equal to  $\Delta x = 250$  m and the time step for the water motion and the suspended sediment transport is set at  $\Delta t = 60$  s. The water column is divided into five layers with a logarithmic spacing and the sediment bed consists of 100 layers of  $\Delta z = 0.10$  m thickness and with a constant grid size. Notice that the large number of layers is chosen for output purposes only. The number of layers could be much smaller from a physical point of view, because bed composition changes are only expected near the bed surface. The time step in the bed level and bed composition computation is  $N\Delta t$  where  $N$  is the morphological factor.

**Table 5.4:** Settings of physical parameters reference computation.

| Description                      | Symbol          | Value     | Unit                      |
|----------------------------------|-----------------|-----------|---------------------------|
| Chézy-coefficient                | $C$             | 50        | $\text{m}^{1/2}/\text{s}$ |
| Horizontal fluid mixing          | $\nu_x, \nu_y$  | 10        | $\text{m}^2/\text{s}$     |
| Sand grain size                  | $d_{50}$        | 150       | $\mu\text{m}$             |
| Settling velocity sand           | $w_s$           | 0.016     | $\text{m}/\text{s}$       |
| Settling velocity mud            | $w_m$           | 0.0005    | $\text{m}/\text{s}$       |
| Critical mud content             | $p_{m,cr}$      | 0.3       | —                         |
| Critical erosion shear stress:   |                 |           |                           |
| - Non-cohesive erosion           | $\tau_{e,nc}$   | 0.25      | $\text{N}/\text{m}^2$     |
| - Cohesive erosion               | $\tau_{e,c}$    | 0.25      | $\text{N}/\text{m}^2$     |
| Erosion coefficient:             |                 |           |                           |
| - Non-cohesive erosion           | $M_{nc}$        | $10^{-6}$ | $\text{m}/\text{s}$       |
| - Cohesive erosion               | $M_c$           | $10^{-6}$ | $\text{m}/\text{s}$       |
| Critical deposition shear stress | $\tau_d$        | 0.10      | $\text{N}/\text{m}^2$     |
| Bed porosity                     | $\varepsilon_p$ | 0.40      | —                         |
| Physical mixing length           | $L_p$           | 0.25      | $\text{m}$                |
| Physical mixing coefficient      | $\alpha_p$      | $10^{-6}$ | —                         |
| Biological mixing coefficient    | $\Xi_b$         | 0.0       | $\text{m}^2/\text{s}$     |

By trial-and-error  $N = 70.55$  is chosen herein. This morphological factor implies that ten tidal periods on the hydrodynamic time scale correspond with one year on the morphological time scale.

The simulation time for each computation is chosen as follows. Figure 5.18a shows the mean bed level change of sand and mud in time and the bed level at five moments during the reference computation. It is observed that the total bed level change (i.e. sand and mud) after 120 years is much smaller than in the beginning. Moreover, the total bed level change is almost entirely attributed to mud deposition, as the bed level changes by sand are negligible. After 120 years, the bed level at the land boundary appears to be more or less equal to the mean water level (Figure 5.18b). Although, strictly speaking, an equilibrium state (i.e. bed level change equal to zero for entire basin) is not reached, a quasi-equilibrium is obtained with predominantly mud deposition. Obviously, the time span for reaching this quasi-equilibrium changes when sediment parameters or forcing parameters are varied in the sensitivity computations. Because the main interest is a comparable situation with respect to the reference computation, the simulation time of all computations is chosen as the time span in which the bed level at the land boundary reaches the mean water level. Under this condition, the simulation time for the reference computation then equals  $T_m = 115$  years, where  $T_m$  is denoted as the ‘morphological time scale’ of the tidal basin.

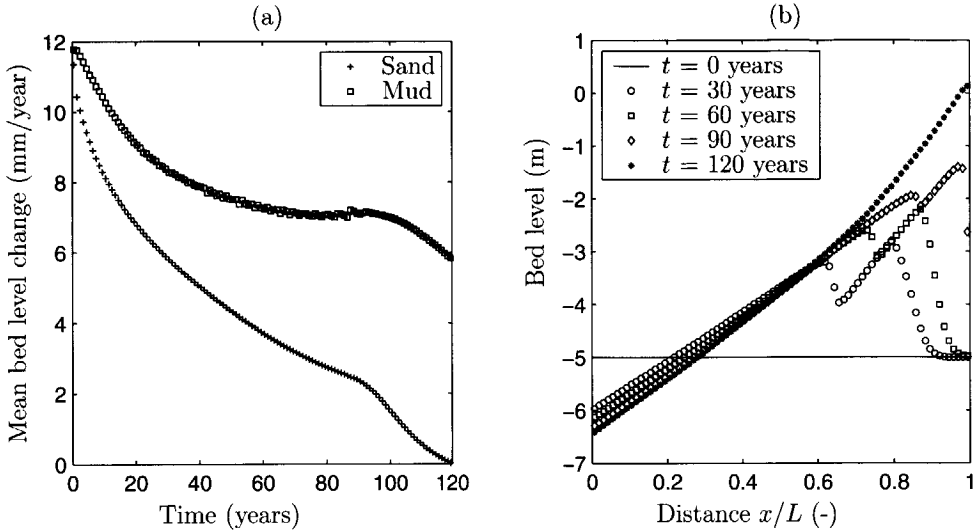


**Figure 5.18:** a) Mean bed level change by sand and mud and b) bed level profiles at different moments during reference computation.

### 5.4.2 Results

An overview of the mean bed level changes by sand and mud in the various computations is given in Table 5.5. Two situations are distinguished: the initial situation just after the start of the computation and the end situation when the bed level at the land boundary reaches the mean water level. The morphological time scale  $T_m$  is the time span for reaching this end situation. Table 5.5 shows that the initial mean bed level changes by sand and mud are larger than those in the end situation. Furthermore, the mean bed level changes by mud are much larger than the changes by sand at the end of the computation. Thus, a quasi-equilibrium is obtained for the various computations with mud deposition only. In the following, the results of the reference computation with sand and mud and the various sensitivity computations are discussed.

#### Reference computation

The results of the reference computation are shown in Figure 5.19 and the following behaviour is observed. Initially, two sedimentation waves are observed (Figure 5.19a-b at  $t/T_m = 0.2$ ): a propagating sand wave near the sea boundary and a mud wave more landwards. After some time, the mud wave is covered by a sand layer and mud deposition is located increasingly towards the land boundary. A slightly concave bed level profile is obtained at the end of the computation (Figure 5.19c at  $t/T_m = 1.0$ ). At that moment, the bed surface is very sandy over almost the entire basin with only a very small muddy area near the head of the basin (Figure 5.19d at  $t/T_m = 1.0$ ).

**Table 5.5:** Results reference computations and various sensitivity computations: Mean bed level changes due to sand and mud in the initial situation and in the end situation, and the morphological time scale  $T_m$ .

| Computation                      | Mean bed level change (mm/year) |      |               |      | Morphological<br>time scale |
|----------------------------------|---------------------------------|------|---------------|------|-----------------------------|
|                                  | Initial situation               |      | End situation |      |                             |
|                                  | Sand                            | Mud  | Sand          | Mud  | $T_m$ (years)               |
| Reference computation            | 11.4                            | 11.8 | 0.3           | 6.2  | 115                         |
| Only sand <sup>1</sup>           | 11.4                            | -    | 0.1           | -    | 600                         |
| $d_{50} = 200 \mu\text{m}$       | 11.3                            | 11.3 | 0.3           | 6.0  | 119                         |
| $d_{50} = 100 \mu\text{m}$       | 13.9                            | 12.4 | 0.2           | 6.2  | 114                         |
| $\tau_d = 0.15 \text{ N/m}^2$    | 11.3                            | 13.8 | 0.4           | 8.4  | 97                          |
| $\tau_d = 0.05 \text{ N/m}^2$    | 11.4                            | 8.1  | 0.1           | 3.2  | 170                         |
| $w_m = 0.001 \text{ m/s}$        | 11.2                            | 21.1 | 0.5           | 11.5 | 75                          |
| $w_m = 0.00025 \text{ m/s}$      | 11.4                            | 6.2  | 0.1           | 3.2  | 175                         |
| $c_{m,0} = 0.075 \text{ kg/m}^3$ | 11.3                            | 17.6 | 0.4           | 9.0  | 87                          |
| $c_{m,0} = 0.025 \text{ kg/m}^3$ | 11.4                            | 6.0  | 0.1           | 3.2  | 180                         |

<sup>1</sup> The bed level at the end of the tidal basin after 600 years is not equal to the mean water level, but still 50 cm below this level.

### Sensitivity computations

The bed level and bed composition profiles are shown in Figure 5.20 for the various sensitivity computations. It can be concluded that all computations have a more or less linear bed level profile at the end of the computation. In addition, the mud content profile at the end of the computations all show a similar pattern: the mud content is very low for almost the entire tidal basin, but suddenly increases near the land boundary, reaching high values at the boundary. However, the morphological time scale for reaching the quasi-equilibrium profile strongly differs for these computations. According to Table 5.5 the morphological time scale decreases with decreasing sand grain size ( $d_{50}$ ), increasing settling velocity ( $w_m$ ), mud concentration ( $c_{m,0}$ ) and critical shear stress for deposition ( $\tau_d$ ).

#### 5.4.3 Analysis

The observed morphological behaviour described in the previous section shows two distinct situations: the initial situation and the quasi-equilibrium situation after a long period (in the order of a century). Initially, a sand deposition area near the sea boundary and a mud deposition area more landward are observed. The mud content at the bed surface remains very sandy near the sea boundary. Further landwards, the mud content increases to high values, but decreases again towards the head of the basin. After a long period, a more or less linear bed level profile is found and the entire basin is very sandy with only a very small muddy area near the land boundary. Both situations are analysed hereafter.

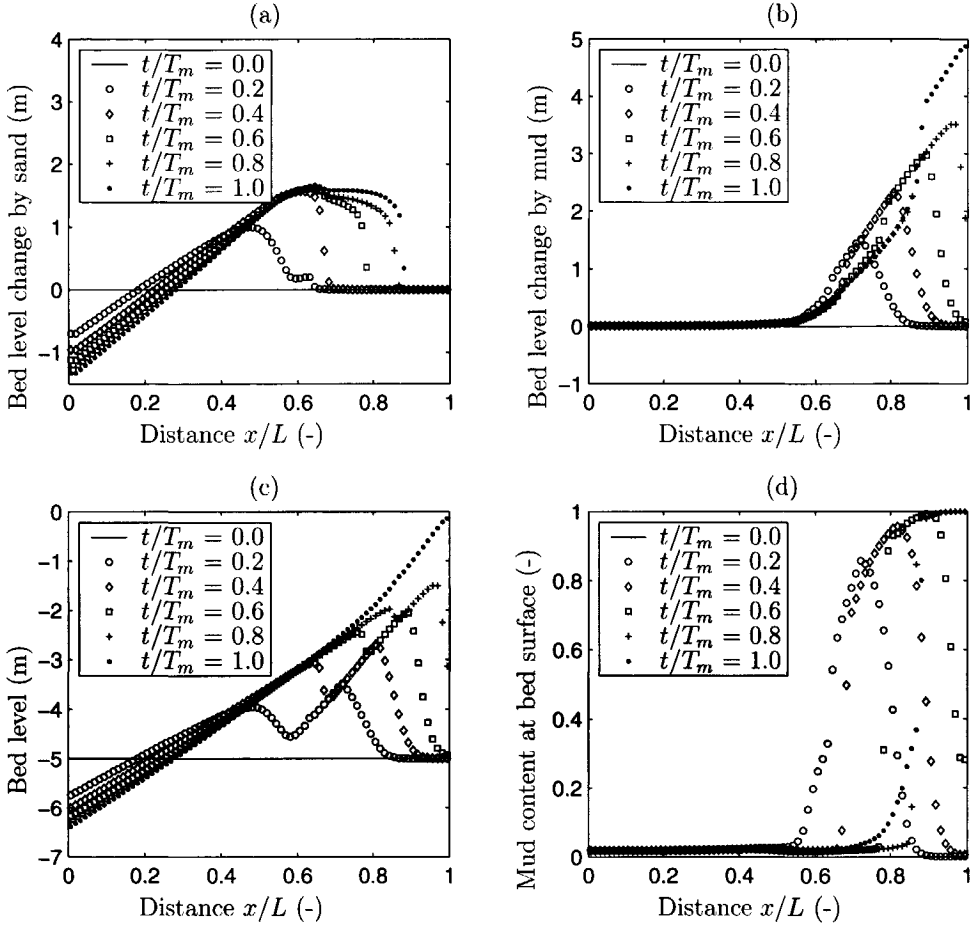


**Figure 5.19:** Results reference computation: a) Bed level changes by sand deposition, b) bed level changes by mud deposition, c) bed level development and d) mud content at bed surface with a morphological time scale  $T_m = 115$  years.

### Initial situation

The initial situation can be explained by considering the initial bed shear stress through the tidal cycle and along the basin, which can be approximated if the water level is assumed to be horizontal:

$$\tau_b(x, t) = \frac{(1 - x/L)^2}{1 + \left(\frac{\hat{\zeta}_2}{h_0}\right) \cos(\omega t)} \hat{\tau}_b \sin^2(\omega t) \quad (5.20)$$

$$\hat{\tau}_b = \frac{\rho_w g}{C^2} \left( \frac{\omega \hat{\zeta}_2 L}{h_0} \right)^2 \quad (5.21)$$



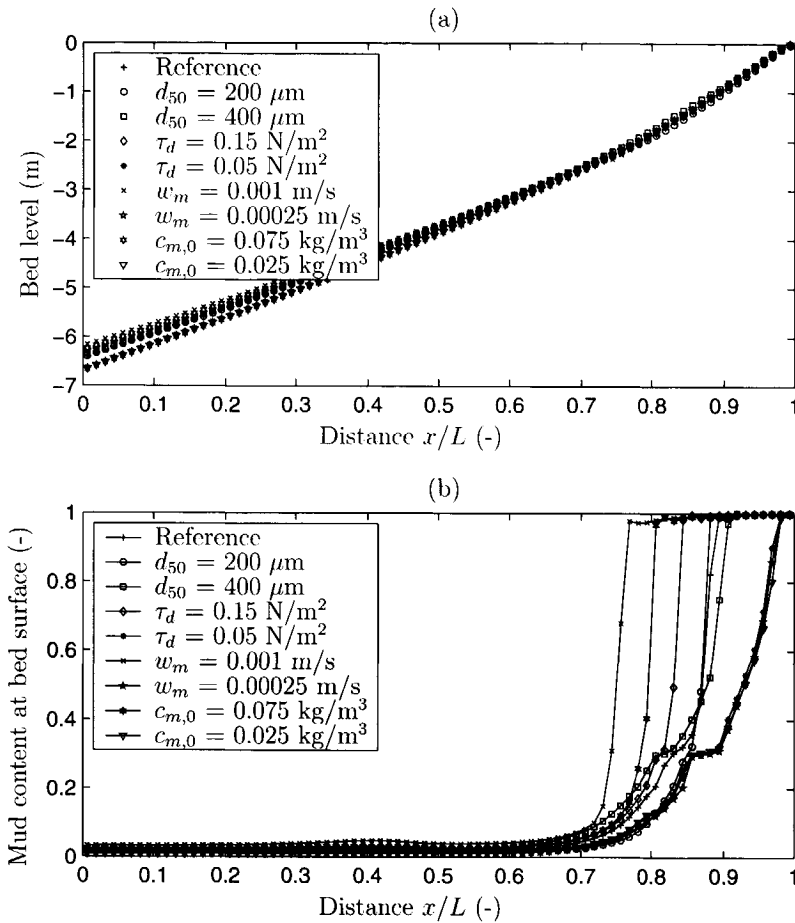


**Figure 5.20:** a) Bed level profile and b) mud content at bed surface after morphological time scale  $T_m$  for sensitivity computations.

where  $\tau_b$  is the bed shear stress,  $\hat{\tau}_b$  the bed shear stress amplitude at the entrance,  $\rho_w$  the water density,  $g$  the gravitational acceleration and  $C$  the Chézy-coefficient. As an example, the numerical bed shear stress variation and the analytical expression (eq. 5.20) at location  $x/L = 0.25$  are shown in Figure 5.21a. The agreement is good enough to conclude that the analytical expression can be used as a first-order estimate of the magnitude of the maximum bed shear stress. However, the asymmetry in the high and low water period, and the asymmetry in maximum bed shear stress during ebb and flood are not found with the analytical expression. In the numerical results, the ebb period appears to be much longer than the flood period and the maximum bed shear stress during flood is higher than during ebb. Furthermore, the period around high water is much longer than the period around low water.

The sand deposition wave has been expected because of previous investigations with short

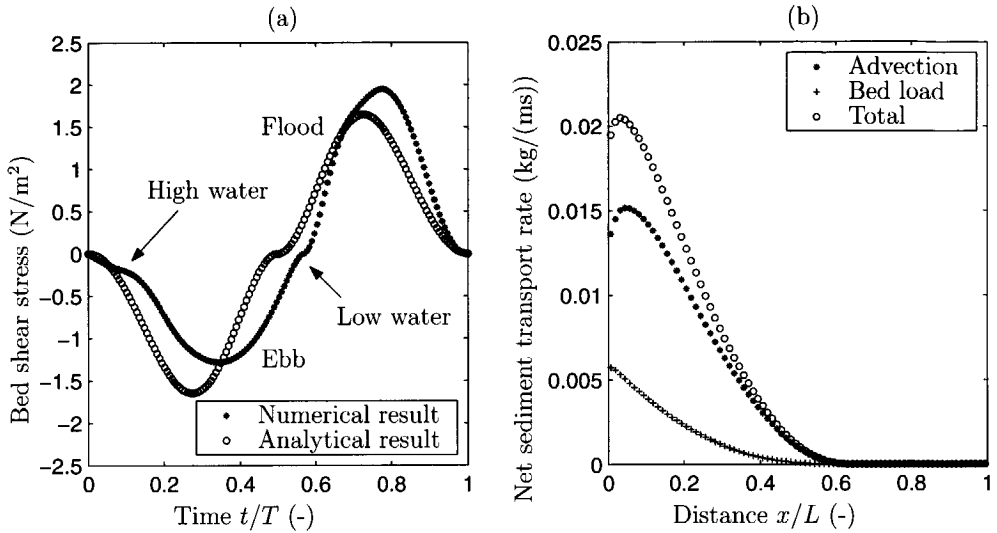


**Figure 5.21:** a) Bed shear stress variation during tidal period at  $x/L = 0.25$ . b) Initial net advective suspended load, bed load, and total transport rate of sand along tidal basin.

tidal basins (cf. Van Dongeren & De Vriend, 1994; Schuttelaars & De Swart, 1996) and is therefore only briefly discussed. The initial sand deposition wave can be explained by considering the gradients in the net (i.e. tidally-averaged) total sand transport rate, because a gradient determines whether sand erosion or deposition occurs. A positive gradient causes erosion, while a negative gradient induces deposition. The net total sand transport rate consists of two important contributions herein: bed load and advective suspended load. These contributions and the total sand transport rate are shown in Figure 5.21b. Transport of sand by diffusion is two orders of magnitude smaller than transport by advection, and is therefore not shown.

The behaviour of the net total sand transport rate is qualitatively explained as follows (Figure 5.21b). The maximum bed shear stress is initially larger during flood than during ebb. Thus, the net bed load transport rate is directed in positive  $x$ -direction. Obviously, it decreases with increasing distance from the sea, because the bed shear stress amplitude decreases. The asymmetry in the maximum bed shear stress also causes a net suspended load transport rate in positive  $x$ -direction, because the reference concentration is determined by the bed shear stress. Moreover, the net suspended load transport rate is also determined by lag effects. As already pointed out, the high water period is longer than the low water period. Thus, the sediment concentration will be lower after high water than after low water, and this also induces a net suspended sand transport flux in positive  $x$ -direction. Finally, the observed erosion near the entrance of the basin is likely to be caused by the boundary condition for suspended sand transport. The sand concentration is set to the equilibrium sand concentration at  $x = 0$  for inflow conditions, while a weak boundary condition is applied for outflow. This boundary condition

does not fit perfectly to the interior area and results in a smaller net suspended sand transport rate at the boundary.

The formation of the initial mud deposition wave is less obvious and will therefore be discussed more extensively (Figure 5.22). Previously, the maximum bed shear stress during the tidal period ( $\hat{\tau}_b$ ) and the critical shear stress for mud deposition ( $\tau_d$ ) and mud erosion ( $\tau_e$ ) appeared to be important parameters for the observed behaviour (Section 5.2). These shear stresses are shown as a function of distance  $x/L$  in Figure 5.22 by applying the analytical expression for the maximum bed shear stress (eq. 5.20) and the settings for the critical shear stresses (Table 5.4). Three different areas can be distinguished in Figure 5.22, based on these shear stresses. The initial behaviour of mud deposition can be explained as follows in these areas:

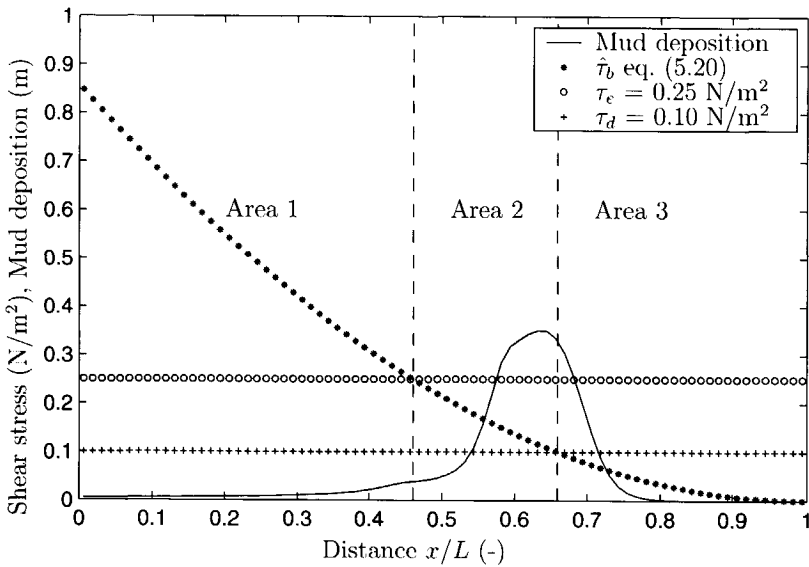


**Figure 5.22:** Bed level change by mud deposition after five years, maximum bed shear stress during the tidal period, critical bed shear stress for erosion and mud deposition and bed level change by mud deposition along the tidal basin.

- Area 1: Mud erosion and deposition during part of the tide**

Mud deposition and erosion are both possible during the tide in area 1 (Figure 5.22), because the maximum bed shear stress is higher than the critical shear stress for erosion and deposition. However, net mud deposition in this area is very small. This effect can be explained when the dimensionless parameter  $w_m c_{m,0}/M$  is considered (see also Section 5.2). This parameter can be interpreted as the ratio between the maximum deposition flux ( $w_m c_{m,0}$ ) and the erosion flux for a 100% mud bed ( $M$ ). Herein, the dimensionless parameter  $w_m c_{m,0}/M \simeq 10^{-2}$  when the reference parameter settings are applied, indicating that the erosion flux is much larger than the deposition flux. Because of the

dominance of erosion in area 1, bed level changes due to mud deposition are very small there (Figure 5.22).

- **Area 2: Only mud deposition during part of the tide**

Only mud deposition occurs during part of the tidal period in area 2, because the bed shear stress does not exceed the critical shear stress for mud erosion (Figure 5.22). Hence, strong mud deposition is observed in this area (Figure 5.22). The bed level change due to mud deposition first increases and then decreases again in this area. Qualitatively, this effect can be explained as follows: with increasing distance from area 1, the time for mud deposition during the tidal period increases and mud deposition is enhanced. Simultaneously, the mud concentration in the water column decreases with increasing distance from area 1, because of ‘upstream’ mud deposition, resulting in less mud deposition. The interaction of both effects results maximal mud deposition at a certain distance from area 1, followed by a decrease.

- **Area 3: Mud deposition during entire tidal period**

The mud concentration in the water column is very low in this area, because of mud deposition during the entire tidal period. Moreover, the supply of mud from ‘upstream’ is also limited because of mud deposition in area 2. Therefore, the initial bed level changes as a result of mud deposition are small in this area (Figure 5.22).

### Quasi-equilibrium situation

The bed shear stress distribution in the quasi-equilibrium situation can be estimated as follows while assuming a linear bed level profile and a horizontal water level:

$$\tau_b(t) = \hat{\tau}_b \sin^2(\omega t) \quad (5.22)$$

$$\hat{\tau}_b = \frac{\rho_w g}{C^2} \left( \frac{\omega \hat{\zeta}_2 L}{h_*} \right)^2 \quad (5.23)$$

where  $\tau_b$  is the bed shear stress,  $h_*$  the water depth at the entrance and  $\hat{\tau}_b$  the bed shear stress amplitude. Equation (5.22) shows that the bed shear stress only varies with time, but does not depend on the position along the basin ( $x/L$ ) anymore, indicating a uniform bed shear stress throughout the entire basin. Equation (5.22) is only valid when the tidal amplitude is much smaller than the water depth ( $\hat{\zeta}_2 \ll h_*$ ). With increasing distance from the sea boundary, the water depth decreases and near the land boundary the bed even falls dry during part of the tidal period. Thus, the analytical bed shear stress profile is not valid near the head of the basin. The numerical bed shear stress deviates from the uniform profile and decreases towards zero at the land boundary ( $x/L = 1.0$ ).

The bed level and the bed composition profile near the end of the computation can be explained qualitatively as follows. To achieve an equilibrium bed level profile for sand only, the derivative of the tidally-averaged total sand transport rate along the tidal basin should be equal to zero. Because the sand transport rate is strongly related to the bed shear stress, a more or less uniform tidally-averaged bed shear stress is found in this condition. Equation (5.22) indicates that the bed shear stress is more or less uniform when the bed level has a linear profile. The uniform bed shear stress amplitude ( $\approx 0.5 \text{ N/m}^2$ ) for this quasi-equilibrium bed level profile is still much larger than the critical shear stress for mud erosion ( $\tau_c = 0.25 \text{ N/m}^2$ ). Furthermore, the dimensionless parameter  $w_m c_{m,0}/M$  is much smaller than 1. These parameters indicate that the mud erosion capacity is much larger than mud deposition capacity, resulting in a sandy bed surface. Near the head of the tidal basin however, the bed shear stress decreases towards zero. In this area, continuous mud deposition occurs because the maximum bed shear stress is relatively low. Consequently, the bed surface is very muddy.

#### 5.4.4 Previous investigations on short tidal basins

Various authors have investigated the morphological behaviour of an idealised short tidal basin (e.g. Van Dongeren & De Vriend, 1994; Schuttelaars & De Swart, 1996). An important assumption in these studies is that the bed consists of fine sand only. Van Dongeren and De Vriend (1994) investigate a short tidal basin with a flood-dominant tidal forcing and bed load transport only. They obtain a linear bed level profile that can be considered as a quasi-equilibrium state. Because of the continuous net influx of sand, the channel is completely filled with sand in the long term. Schuttelaars and De Swart (1996) extend this analysis by also considering suspended load transport and different combinations of tidal forcing. They derive analytical bed level equilibria with different characteristics which are summarised in Table 5.6.

**Table 5.6:** Equilibrium bed level profiles for short tidal basins (Schuttelaars & De Swart, 1996).

| Transport mode            | Forcing    |                   |
|---------------------------|------------|-------------------|
|                           | $M_2$      | $M_2 + M_4$       |
| Bed load                  | horizontal | linear            |
| Suspended load:           |            |                   |
| - only advection          | linear     | no equilibrium    |
| - only diffusion          | linear     | linear            |
| - advection and diffusion | linear     | concave or convex |

Two remarks can be made with respect to the equilibria in Table 5.6 (see also Schuttelaars & De Swart, 1996). Firstly, a linear bed level profile appears to be a solution for an  $M_2$ -tide in combination with advective suspended transport only, but this result is of limited value since it cannot be reached from arbitrary initial conditions. In the case of  $M_2 + M_4$  in combination

with advective suspended transport only, the system appears to be importing or exporting sediment, depending on the phase difference between  $M_2$  and  $M_4$ . No equilibrium state can be found. Secondly, the phase difference between the tidal components determines whether the bed level profile is concave or convex in the case of  $M_2 + M_4$  in combination with advective and diffusive suspended load. In addition, the bed level profiles are more concave/convex when diffusive transport is less important.

A comparison between the analytical results of Schuttelaars and De Swart (1996) for sand only and the results in the previous sections is interesting because of the inclusion of mud in the present study. Except for the number of sediment fractions, the main differences in model set-up are summarised in Table 5.7. Despite these differences, the bed level profiles in the present study strongly correspond to the previously derived equilibria for an  $M_2$ -tide with only suspended sand transport (Table 5.6). Regardless of the parameter settings, all bed level profiles in the present study tend towards a slightly concave (quasi-)equilibrium bed level profile (cf. Figure 5.20).

The small differences between both approaches are explained by the differences in model set-up (Table 5.7):

- Schuttelaars and De Swart (2000) show that for sand only a slightly concave equilibrium profile instead of a linear profile has to be expected when the full momentum equation for the flow is taken into account.
- A formal equilibrium state is not likely to be found, because of the flow condition at the land boundary (see also Van Dongeren & De Vriend, 1994). The current velocity always tends to zero at the land boundary. Consequently, net mud and sand deposition will continue in this area and the tidal basin length will shorten. As a result, the bed shear stress in the entire tidal basin will decrease and deposition will further be enhanced. The final situation is presumably a complete fill of the main channel with sand and mud.

**Table 5.7:** Differences between model set-up of Schuttelaars & De Swart (1996) and present model.

| Item                           | Schuttelaars & De Swart, 1996  | Present model                                 |
|--------------------------------|--------------------------------|-----------------------------------------------|
| Dimensions                     | one-dimensional                | two-dimensional                               |
| Flow condition at $x = L$      | $q = 0$                        | $u = 0$                                       |
| Momentum equation flow         | $\partial\zeta/\partial x = 0$ | full equation                                 |
| Bed level condition at $x = 0$ | $\partial z_b/\partial t = 0$  | $\partial z_b/\partial t = 0$ for inflow only |

The strong similarity in equilibrium bed level profile for sand only (Schuttelaars & De Swart, 1996) and for sand-mud mixtures has two opposing implications. On the one hand, it indicates that the presence of mud itself does not affect the equilibrium bed level profile significantly for the investigated parameter settings. Mud is an extra sediment supply, whereas the equilibrium bed level profile is determined by the sand fraction. On the other hand, the presence of mud drastically decreases the morphological time scale for reaching this equilibrium. For instance,

the time scale for the reference computation with sand and mud is 115 years, while the time scale for a comparable situation with only sand is more than 600 years.

At least two effects explain the decrease in time scale for the morphological adaptation when mud is taken into account. The introduction of mud increases the availability of sediment for the morphological adaptation and therefore shortens the morphological time scale. Furthermore, the morphological changes near the head of the basin are strongly enhanced. Near the head of the basin, the sand transport flux approaches zero because of the low flow velocities. Consequently, the morphological adaptation in case of sand only is very slow in this area. However, the trap efficiency of mud is very high due to the low flow velocities. Hence, the morphological adaptation near the head of the basin is much faster, resulting in a shorter morphological time scale of the system.

#### 5.4.5 Field measurements

The model can be validated further against field data, even though the model contains numerous simplifications. Schuttelaars and De Swart (1996) already mention that O'Brien's well-known semi-empirical linear relationship between the cross-sectional flow area and the tidal prism is reproduced by the linear bed level equilibrium for sand only. The present study suggests that the presence of mud does not change this (quasi-)equilibrium bed level profile for the Wadden Sea basins and the same relationship is therefore applicable in case of sand and mud.

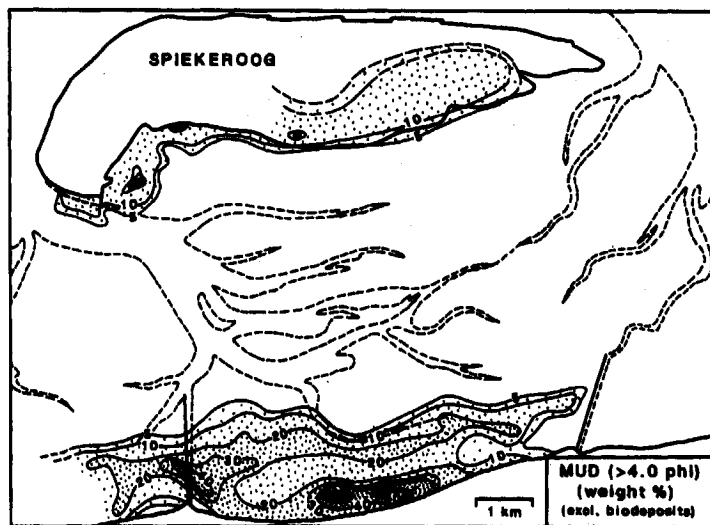


**Figure 5.23:** Mud distribution ( $\% \leq 0.063$  mm) in Spiekeroog area, Wadden Sea (Flemming and Ziegler, 1995).

Another validation of the model results is a comparison with field data from the Wadden Sea. As an example, Figure 5.23 shows the mud content ( $\% \leq 0.063$  mm) at the bed surface in the German Wadden Sea near Spiekeroog. The relatively low mud content in almost the entire area, with only a small stretch with a high mud content near the dike, is not unique. It has also been observed in the Dutch Wadden Sea (e.g. De Glopper, 1967). Qualitatively, the model results in the present study predict a similar trend in the mud distribution along the tidal basin as the mud distribution in the area near Spiekeroog: the mud content is low for the larger part of the tidal basin and suddenly increases to high values near the dike at the head of the basin.

The analysis puts forward the following explanation of the observed mud content pattern in these short tidal basins. When the tidal basin has an equilibrium bed level profile, the bed shear stress is more or less uniform along the entire tidal basin and only decreases to zero near the land boundary. Because the maximum bed shear stress during the tide is much higher than the critical erosion shear stress for mud erosion and deposition, both processes occur in almost the entire basin during the tidal period. The dimensionless parameter ( $w_m c_{m,0}/M$ ) is small for these areas, indicating the dominance of mud erosion. Consequently, the mud content at the bed surface is very low for almost the entire basin. Only near the head of the basin, the bed shear stress decreases towards zero. Net mud deposition is possible in this area and a high mud content is found in a small area near the head of the basin.

## 5.5 Conclusions

The process-based model has been analysed for three idealised situations in this chapter: a local situation, a reservoir and a tidal basin. In general, it can be concluded that the process-based sand-mud model increases the understanding of the observed sand-mud patterns significantly. The following specific conclusions can be drawn for the different situations:

### Local situation

The local behaviour of the presented model has been analysed by omitting all non-local terms in the governing equations. In the mud concentration equation, however, a parameterized horizontal transport term has been included to avoid trivial solutions.

- An expression for the equilibrium mud content at the bed surface is found when both deposition and erosion occur during the tidal period. In this equation, the settling velocity for mud ( $w_m$ ), the (depth-averaged) mud concentration outside the model domain ( $C_{m,0}$ ) and the erosion rate ( $M$ ) form an important dimensionless parameter ( $w_m C_{m,0}/M$ ). This parameter expresses the ratio between the deposition and erosion flux capacity.
- In earlier studies, correlations between the maximum or mean shear stress and the mud content often show the following characteristic picture. A critical shear stress seems to exist, below which the mud content varies between 0 and 100%. Above this value,



the mud content is always low. According to the analysis, the sharp transition between areas with a very low mud content and other areas depends on the aforementioned dimensionless parameter ( $w_m C_{m,0}/M$ ). The transition is sharp for low values ( $w_m C_{m,0}/M < 10$ ), whereas the transition becomes more and more gradual for higher values. The observed sharp transition in field data in earlier studies follows from the low value of the dimensionless parameter for these areas.

- The analysis provides two explanations for the variation in mud content between 0 and 100% at sample sites with low bed shear stress. Firstly, the actual mud content at the sample site is probably not in equilibrium due to relatively large adaptation time scales. Secondly, the scatter is probably caused by the difference between the actual hydrodynamic situation and the assumed sinusoidal velocity profile and the constant water depth.

### Reservoir

The morphological behaviour of a former estuary in which the tide was eliminated, has been analysed. This so-called reservoir is qualitatively comparable with the southern area of the Noordelijk Deltabekken (the Netherlands) in which sand and mud was deposited after the construction of the Haringvliet Sluices in 1970.

- The results show a sand and a mud deposition wave, both propagating downstream. The mud deposition wave has a characteristic form which strongly depends on two adaptation length scales: a 'settling length scale' and a 'flow length scale'. The expression for the settling length scale is equal to the well-known adaptation length scale for suspended sand transport. The 'flow length scale' depends on the actual bed level slope and the critical velocity for mud deposition.
- The results are only qualitatively comparable to field data of the Rhine-Meuse estuary, the Netherlands. Several morphological characteristics found with the numerical model are also observed in the sediment balances for sand and mud during the period 1970 - 1992. Based on the model analysis, physical explanations are given for observed deposition patterns of sand and mud.

### Tidal basin

The tidal basins in the Dutch and German Wadden Sea have been taken as a reference for investigating the behaviour of short tidal basins with sand and mud. A rectangular short tidal basin without tidal flats has been investigated with an  $M_2$ -tide at the sea boundary.

- The morphological development (i.e. bed level and bed composition) reveals two initial deposition waves: a sand wave near the entrance of the basin and a mud deposition wave more landward. A quasi-equilibrium state with predominantly mud deposition is found after a long period (in the order of a century): the bed level is more or less linear and the bed surface is sandy for almost the entire basin with a small muddy area near the land boundary. Realistic variations in the parameter setting do not change the

aforementioned morphological development qualitatively, but affect the time scale for reaching this (quasi-)equilibrium drastically.

- An analysis of the observed morphological development has revealed important (dimensionless) parameters, which govern the observed morphological behaviour. Again, the ratio between the mud deposition and erosion flux ( $w_m c_{m,0}/M$ ) is an important parameter. The typical mud content pattern in the quasi-equilibrium situation is found because the value of this ratio is much smaller than unity.
- A comparison with previous studies on short tidal basins indicates that the presence of mud does not change the equilibrium bed level profile for the applied parameter settings. The only effect on the morphological behaviour is a decreasing morphological time scale when mud is included. A qualitative validation with field data reveals that the obtained bed level and bed composition profiles are realistic. The strong separation between a large sandy area and a small muddy area near the head of the basin is also observed in the Dutch and German Wadden Sea.

## Chapter 6

### Application to Friesche Zeegat

#### 6.1 Introduction

A process-based sand-mud model has been developed and its application to several idealised situations was described in the previous chapters. An important extension compared with the existing process-based models is that mud content variations in time and space are taken into account in this model. In general, a good qualitative comparison has been obtained between observed and modelled large-scale behaviour in natural systems with sand and mud. Furthermore, the analysis has revealed important parameters which determine the observed distribution of sand and mud.

A major drawback of idealised situations is that model results can hardly be compared quantitatively with existing field data. Obviously, the simplifications in the geometry and boundary conditions are the major causes of this limitation. Consequently, the predicted results of bed level and bed composition variations in time and space (i.e. morphological response) can only be interpreted in a qualitative way. In real-life situations, however, a realistic prediction of the magnitude and the time scale of this response is generally very important to assess the short-term and long-term impacts.

In this chapter, the process-based sand-mud model is applied to the Friesche Zeegat (the Netherlands) to investigate its predictive capabilities in a more quantitative way. A substantial amount of sand and mud has been deposited in this system after a partial closure of the basin in 1969. First, the observed morphological response in the period 1970 - 1994 is briefly discussed in Section 6.2 with special emphasis on the distribution of sand and mud. Next, an overview of the model set-up is given in Section 6.3. The calibration and verification of the hydrodynamic module against field data from the 1990's are described in Section 6.4. Unfortunately, the sediment transport module and bed module could not be calibrated by lack of data. Thereafter, long-term morphological computations are performed for a simulation period of 25 years with the initial bathymetry of 1970. The results of these computations are presented in Section 6.5 and compared with the observed long-term morphological development. Finally, the similarities and discrepancies between observed and modelled behaviour are discussed in Section 6.6.

## 6.2 Morphological development

### 6.2.1 Area description

The Friesche Zeegat is a tidal basin, situated in the Dutch Wadden Sea between the barrier islands Ameland and Schiermonnikoog (Figure 6.1). The area consists of two smaller systems: Pinkegat and Zoutkamperlaag. These are separated by a supratidal shoal (Engelsmanplaat) with a massive and relatively stable clay body underneath. The common large-scale morphological elements can be distinguished in both systems: the ebb-tidal delta, the inlet throat and the basin with a large intertidal area.

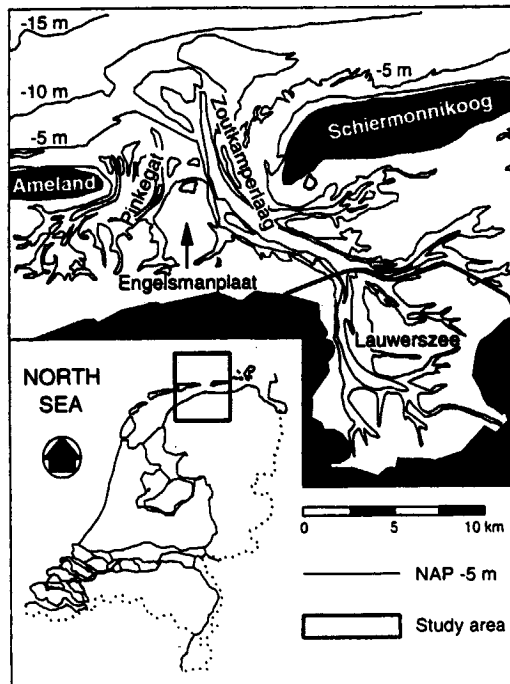


**Figure 6.1:** Friesche Zeegat in the northern part of the Netherlands (Wang et al., 1995).

The hydrodynamic and sedimentological characteristics of the Friesche Zeegat and the adjacent coast can be summarised as follows (see e.g. Oost, 1995; Biegel & Hoekstra, 1995). It is a mixed-energy coast, indicating that tidal currents and short waves are hydrodynamic forcings of more or less comparable strength. The tide is semi-diurnal with an amplitude of about 1 m. Short waves near the barrier islands and the ebb-tidal delta are predominantly determined by the wave conditions at the adjacent North Sea. The yearly-averaged significant wave height offshore equals 1.2 m with a peak period of about 5 s. Waves in the basin are mainly locally generated and the wave characteristics are determined by the wind speed and direction, the

fetch and the water depth. The average wind speed is about 8 m/s, the dominant wind direction is southwest and the mean wave height is less than 0.5 m. The bed mainly consists of sand with a mean sand grain size between 0.1 - 0.2 mm. Mud is mostly found in the intertidal areas and along the borders of the basin.

The closure of the Lauwerszee in 1969 reduced the tidal prism of the Zoutkamperlaag with about 30% from  $305 \times 10^6$  to  $200 \times 10^6$  m<sup>3</sup> (Figure 6.1). To adjust to the new hydrodynamic conditions, a large amount of sediment has been deposited in the basin of the Zoutkamperlaag in the decades following the closure. Various authors already discussed this morphological adaptation in detail (see Oost, 1995; Biegel & Hoekstra, 1995). These studies have mainly focused on the observed bed level changes in the ebb tidal delta and in the basin. Little attention, however, has been paid to changes in bed composition. Hence, the availability of data and the observed morphological response in the Zoutkamperlaag are discussed consecutively in the next subsections, with special emphasis on the bed composition.

### 6.2.2 Data availability

The morphological development of the Zoutkamperlaag is well-documented. A distinction is made between bed level and bed composition data, as discussed below.

#### Bed level data

Interpolated bed level data are digitally available for the successive years 1927, 1949, 1958, 1967, 1970, 1975, 1982, 1987 and 1994 (Oost, 1995; Van den Boogert, 2001). Depth soundings were interpolated and the bed level data have a spatial resolution of  $90 \times 90$  m. The interpolation method was based on inverse distance interpolation, but the local topography was also taken into account by weighting factors. The depth error over large areas for the various data sets is estimated at  $\pm 20 - 30$  cm in the period 1927 - 1967 and  $\pm 3$  cm after 1967 (Oost, 1995).

#### Bed composition data

Two maps are available with the bed composition of the bed surface (see also Table 2.2). De Glopper (1967) presents a map with the clay content of the upper 25 cm of the intertidal area in the period 1950 - 1955. No information is available of the composition in the channels in that period. In addition, the bed composition of the upper 10 cm was determined in the entire Friesche Zeegat and the adjacent coast between April and June 1994 (RIKZ, 1998).

Sixteen core descriptions are available with detailed information of the vertical bed composition profile (Van der Spek, 2001). These cores were taken in and along the main channel of the Zoutkamperlaag in the period 1980 - 1982 and 1986. The descriptions contain core number, the coordinates of the location, the sampling date, the bed level below mean sea level, the core length and a detailed description of the lithology. This description includes the mean sand grain size, the silt content, the clay content and the thickness of each separate layer.

### 6.2.3 Morphological response

#### Bed level changes

Oost (1995) determined the net sedimentation and erosion in the ebb-tidal delta and the basin in successive periods between 1927 and 1987. Biegel and Hoekstra (1995) carried out a similar analysis for the period 1970 - 1987. These studies used slightly different definitions with respect to the spatial extent of the ebb-tidal delta and the basin, but the resulting differences are small. The definition and the results of Oost (1995) are used herein and the net sedimentation and erosion in the period 1987 - 1994 is calculated in addition. The net volume changes in the ebb-tidal delta and basin in the successive periods between 1927 and 1994 are listed in Table 6.1.

**Table 6.1:** Net deposited (+)/eroded (-) volume and annual deposition (+)/erosion (-) rate in the ebb-tidal delta and the tidal basin of the Zoutkamperlaag in the period 1927 - 1994 (see also Oost, 1995). The data are corrected for sand extraction by dredging, except for the period 1987 - 1994. The closure of the Lauwerszee was in 1969.

| Period            | Ebb-tidal delta (94 km <sup>2</sup> )                  |                          | Tidal basin (130 km <sup>2</sup> )                     |                          |
|-------------------|--------------------------------------------------------|--------------------------|--------------------------------------------------------|--------------------------|
|                   | Net volume change<br>(10 <sup>6</sup> m <sup>3</sup> ) | Annual rate<br>(cm/year) | Net volume change<br>(10 <sup>6</sup> m <sup>3</sup> ) | Annual rate<br>(cm/year) |
| 1927 - 1949/50    | +15.1                                                  | +0.9                     | +12.3                                                  | +0.5                     |
| 1949/50 - 1957/58 | -13.7                                                  | -2.3                     | -13.7                                                  | -1.3                     |
| 1957/58 - 1965/66 | -11.6                                                  | -2.3                     | +1.7                                                   | +0.2                     |
| 1965/66 - 1970    | -5.9                                                   | -1.6                     | +10.0                                                  | +2.1                     |
| 1970 - 1975       | -9.8                                                   | -2.1                     | +14.8                                                  | +2.3                     |
| 1975 - 1979       | +0.4                                                   | +0.1                     | +10.7                                                  | +2.1                     |
| 1979 - 1982       | -10.0                                                  | -3.5                     | +4.3                                                   | +1.1                     |
| 1982 - 1987       | -6.6                                                   | -1.4                     | +3.8                                                   | +0.6                     |
| 1987 - 1994       | -1.4                                                   | -0.2                     | +8.1                                                   | +0.9                     |
| 1970 - 1994       | -27.4                                                  | -1.2                     | +41.7                                                  | +1.3                     |

It needs to be realised that the net volume changes in Table 6.1 are uncertain, because the underlying bed level data include measurement and interpolation errors. For instance, a systematic error of 3 cm in the bed level results in a volume error of  $2.7 \times 10^6 \text{ m}^3$  and  $3.9 \times 10^6 \text{ m}^3$  in the ebb-tidal delta and the tidal basin, respectively. The order of magnitude of these error estimates is comparable with the net volume changes in Table 6.1. So, the volume changes should be interpreted with care.

Oost (1995) extensively discusses the observed bed level changes in the ebb-tidal delta and the tidal basin of the Zoutkamperlaag in the period 1927 - 1987, whereas Biegel and Hoekstra (1995) only investigate the period 1970 - 1987. The main conclusions from both studies are (see also Table 6.1):

- Net erosion of the ebb-tidal delta occurred after 1950, except for the period 1975 - 1979. The total net erosion was equal to  $26 \times 10^3 \text{ m}^3$  during the period 1970 - 1987. The erosion in that period was mainly confined between -4 and -12 m NAP, whereas sedimentation was found above and below this zone.
- Net sedimentation was mostly found in the basin in the period 1927 - 1987, except in the period 1949/50 - 1957/58. The net result over the period 1927 - 1966 was only a slight sedimentation of  $0.3 \times 10^6 \text{ m}^3$ . These small changes are in contrast with the strong sedimentation in the period 1966 - 1970, probably as a result of the gradual closure of the Lauwerszee. Between 1970 - 1987, a net sedimentation of  $33.5 \times 10^6 \text{ m}^3$  occurred in the basin, with the highest sedimentation rate in the 1970's. The strongest sedimentation was observed in the deeper channels between -5 and -15 m NAP. Although the intertidal areas eroded during the early 1970's, net deposition occurred for the entire period 1970 - 1987.
- The difference of  $+7.6 \times 10^6 \text{ m}^3$  between the net sedimentation in the basin and the net erosion of the ebb-tidal delta in the period 1970 - 1987 indicates that the ebb-tidal delta and the basin were not a closed sedimentary system in that period. Oost (1995) suggests that the difference is probably explained by mud that is carried into the basin in suspension. Another likely source of sediment is sand from adjacent coastal areas (Biegel & Hoekstra, 1995).

The aforementioned trends in bed level changes between 1970 and 1987 are also found in the period 1987 - 1994 (Table 6.1). The erosion of the ebb-tidal delta still continues, although at a much smaller rate than in the previous periods. Net sedimentation continued in the basin in the period 1987 - 1994. The sedimentation rate is even somewhat higher than in the previous period 1982 - 1987, but smaller than the one in the first decade after closure of the Lauwerszee. This indicates that the morphological adaptation process still continues in the period 1987 - 1994. The difference of  $+14.3 \times 10^6 \text{ m}^3$  between the net erosion in the ebb-tidal delta ( $-27.4 \times 10^6 \text{ m}^3$ ) and the net sedimentation in the basin ( $+41.7 \times 10^6 \text{ m}^3$ ) in the period 1970 - 1994 again suggests that Zoutkamperlaag is not a closed sedimentary system. Sediment sources, which explain this difference, are mud import from the North Sea (Oost, 1995) and/or sand import from adjacent coastal areas (Biegel & Hoekstra, 1995).

### Bed composition changes

De Glopper (1967) classifies the composition of the bed surface of the intertidal area in the period 1950 - 1955 mostly as sandy with low clay content (< 3%). The clay content, however, is found to be high (5 - 25%) in a small stretch near the dike. Notice that the corresponding mud content is considerably higher than the clay content in this area (Table 2.3). At the intertidal area, the bed composition in 1994 shows similar characteristics (RIKZ, 1998). Furthermore, the mud content is high at two locations in the main channel of the basin. A small spot with high mud content is observed near the Engelsmanplaat and a larger area is found in the vicinity

of the former Lauwerszee. The ebb-tidal delta and the adjacent coasts of the barrier islands predominantly have a low mud content (< 5%), but the mud content is clearly higher in the deeper offshore parts (10 - 30%).

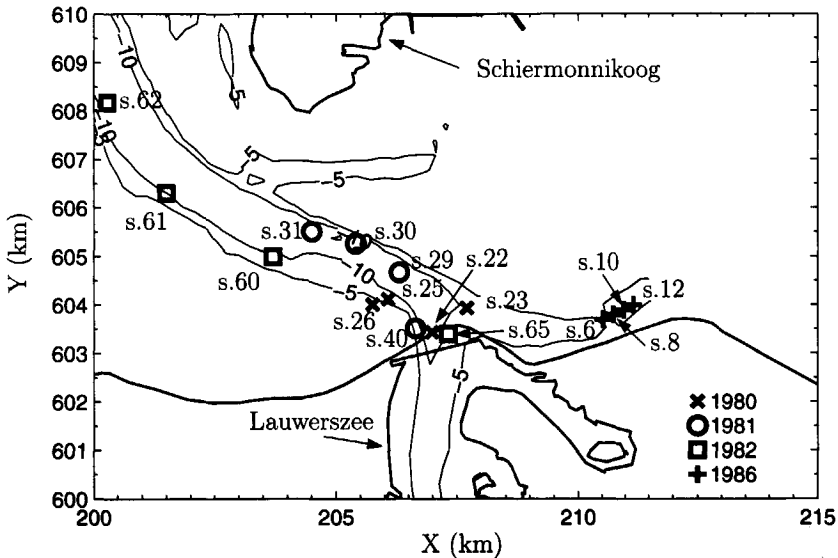


**Figure 6.2:** Locations and sampling year of the cores in the basin of the Zoutkamperlaag based on data of Van der Spek (2001).

Additional to the information of the surface composition, sixteen core descriptions are available with detailed information of the vertical bed composition profile (Van der Spek, 2001). The locations of these cores and nine profiles (s.62, s.60, s.31, s.30, s.29, s.26, s.40, s.22, s.65) are presented in Figure 6.2 and Figure 6.3, respectively. The other seven cores are not shown in Figure 6.3, because they consist of sand only (s.6, s.8, s.10 and s.12, s.23), or because no significant sedimentation occurred at the locations (s.25, s.61). The vertical axis in Figure 6.3 indicates the depth in meters with respect to the bed levels at the time of sampling. If available, the mud content of a layer is given at the left part of each bar. The grey colors also indicate the mud content. Furthermore, the bed level in 1967, 1970, 1975, 1979, 1982, 1987 and 1994 are indicated in the cores with dotted lines. They are obtained from the digital bed level maps and give a rough estimate of the bed level development at the location of the core. For instance, the bed levels in core s.62 indicate strong accretion of about 6 m in the period 1967 - 1982, slight erosion in the period 1982 - 1987 and a relatively stable period between 1987 and 1994 (Figure 6.3).

The bed composition profiles in the cores show three important characteristics (Figure 6.3, see Figure 6.2 for locations). Many cores show an abrupt increase in mud content around the bed level of 1967/1970 (e.g. s.60, s.31, s.30, s.29): the mud content changes from very low (< 20%) to



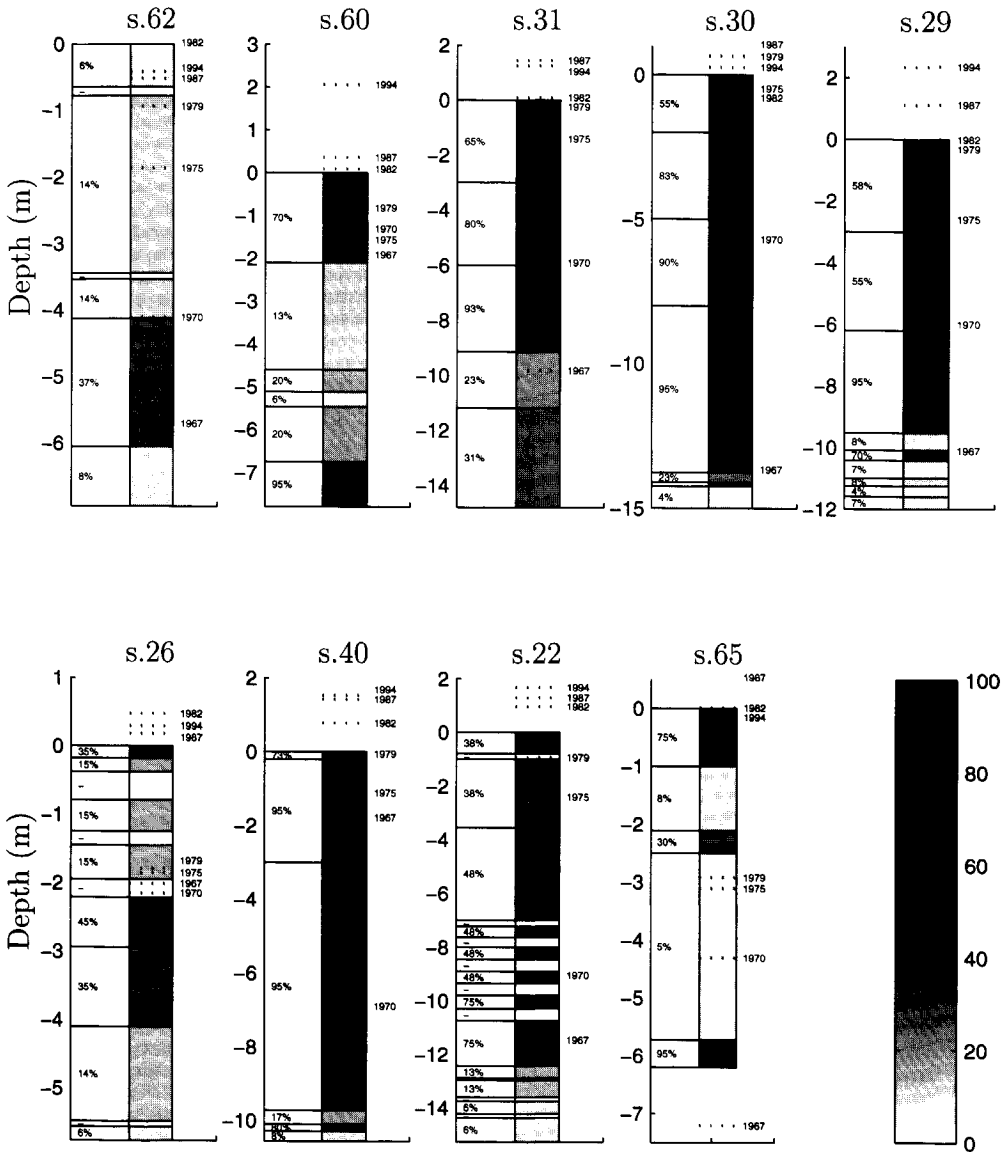


Figure 6.3: Lithology of the cores with the mud content and the bed level in various years based on data of Van der Spek (2001) (see Figure 6.2 for locations).

very high values (75 - 95%). Moreover, the mud content gradually decreases in upward direction at most core locations (e.g. s.62, s.31 and s.30). For instance, the mud content in core s.62 is equal to 37% between 1967 and 1970, 14% between 1970 and 1979 and 6% in 1982. Finally, the cores also demonstrate an increasing mud content along the main channel in the direction of

the former Lauwerszee. For instance, the mud content around the bed level of 1967/1970 varies from 37% (s.62) to 95% (s.30, s.29, s.40). Around the bed level of 1980, the mud content shows a similar trend, but the mud content is lower. The bed composition at the surface of the core s.62 has a low mud content (6%), whereas the mud content near the Lauwerszee (s.29, s.40, s.22) is still considerable and ranges between 38 and 73%.

There are, however, a few exceptions on this general pattern: core s.23 at the entrance and the cores s.6 - s.12 in the channel towards the eastern watershed (Figure 6.2). These cores do not show the abrupt change in mud content around the bed level of 1967/1970, but consist of sand only and are therefore not given in Figure 6.3. A possible explanation for these exceptions is that the watershed shifted towards the East after the closure of the Lauwerszee, as suggested by Oost (1995). As a consequence, the small channels west of the watershed became deeper, migrated and also new channels were formed. The channel itself also deepened and migrated towards the south. The strong morphological activity suggests relatively high current velocities and the absence of favourable conditions for mud deposition.

### 6.3 Model set-up

The process-based sand-mud model in Chapter 4 is applied to hindcast the bed level and bed composition development in the period 1970 - 1994 (see Section 4.5 for details of the numerical model). In the present case, the effect of short waves on the bed shear stress is taken into account, whereas wave-current interactions are neglected (cf. Wang et al., 1995). For this purpose, the wave height and wave period distribution in the Friesche Zeegat are computed at ten moments during the tidal cycle before the long-term computation is started. During the long-term computation itself, the actual wave height and wave period is obtained by a linear interpolation of the wave fields. These parameters and the actual water depth are used to compute the bed shear stress by waves in each grid point. Notice that the wave height and wave period distribution are not updated during the long-term computation. The numerical grid and the bathymetry, the boundary and initial conditions, and the parameter settings are discussed in the following sections.

#### 6.3.1 Computational grid and bathymetry

Hibma (1999) has made a numerical grid for the Friesche Zeegat with the topography of 1991. For our purpose, this model is extended towards the south in order to include the former Lauwerszee. Furthermore, the eastern model boundary is shifted slightly towards the east, in order to have a better representation of the watershed in this area. This has resulted in a horizontal grid of  $105 \times 93$  cells of 250 - 600 m size (Figure 6.4). The topography just after closure is generated with depth soundings from 1970. The soundings from this year do not cover

the entire model domain near the eastern, western and northern boundary at the North Sea. There the bed topography is based on the bed level information from 1991. In vertical direction, five layers are applied in the water column with a resolution that decreases towards the water surface. The sediment bed is divided into fifty layers with a constant thickness of 0.05 m.

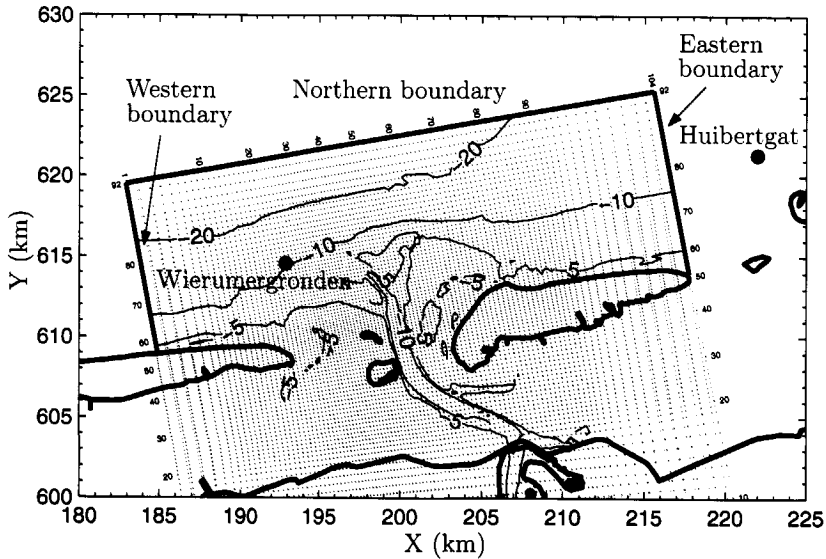


Figure 6.4: Numerical grid with the open boundaries at the North Sea.

### 6.3.2 Open sea boundary conditions

#### Hydrodynamics

The water level is prescribed along the open boundary for the flow computations. Wang et al. (1995) have examined which tidal constituents are important for the residual sediment transport is tidal inlet. They conclude that the boundary condition at the North Sea can be composed of the semi-diurnal ( $M_2$ ) and the quarter-diurnal tide ( $M_4$ ), in addition to the mean water level ( $M_0$ ). The effect of a spring-neap cycle, however, was not considered. In our model set-up, we also limit ourselves to the  $M_0$ ,  $M_2$  and  $M_4$  tidal constituents. The possible effect of a spring-neap cycle on the long-term morphological behaviour is investigated in a sensitivity computation (see Section 6.5.4).

The characteristics of the  $M_0$ ,  $M_2$  and  $M_4$  tidal constituents are derived from data at two water level stations (Wierumergronden and Huibertgat) near the eastern and western model

**Table 6.2:** Water level amplitudes and phases of tidal constituents at Wierumergronden, Huibertgat, Western and Eastern model boundary (see Figure 6.4 for locations).

| Station | Wierumergronden   |               | Huibertgat        |               | Western boundary  |               | Eastern boundary  |               |
|---------|-------------------|---------------|-------------------|---------------|-------------------|---------------|-------------------|---------------|
|         | $\hat{\zeta}$ (m) | $\varphi$ (°) | $\hat{\zeta}$ (m) | $\varphi$ (°) | $\hat{\zeta}$ (m) | $\varphi$ (°) | $\hat{\zeta}$ (m) | $\varphi$ (°) |
| $M_0$   | 0.006             | -             | -0.036            | -             | 0.019             | -             | -0.028            | -             |
| $M_2$   | 0.951             | 260.070       | 1.029             | 277.390       | 0.928             | 254.87        | 1.014             | 274.21        |
| $M_4$   | 0.097             | 7.740         | 0.087             | 29.710        | 0.099             | 1.14          | 0.089             | 25.68         |

boundary (Table 6.2, see Figure 6.4 for locations). The amplitudes and phases are interpolated/extrapolated linearly towards the eastern/western boundary and are taken constant along these boundaries. Along the northern boundary, the tidal characteristics vary linearly between the prescribed values at the eastern and western boundary.

Along the open boundaries at the North Sea, long-term representative values are imposed for the short wave conditions (Figure 6.4). The wave height, wave period and wave direction are given at the North Sea boundaries together with a constant wind velocity and wind direction in the entire model domain. Realistic long-term mean values are: significant wave height  $H_s = 1.2$  m, peak period  $T_p = 5$  s, wave direction  $\theta_{wave} = 315^\circ$  (NW), wave spreading  $\theta_{spreading} = 30^\circ$ , wind velocity  $U_w = 8$  m/s and wind direction  $\theta_{wind} = 225^\circ$  (SW) (see e.g. Oost, 1995; Dunsbergen, 1995). Default settings are used for all other parameters in the short-wave model SWAN (WL|Delft Hydraulics, 2000).

### Sediment transport

An equilibrium sand concentration profile is applied for suspended sand transport at open boundaries where inflow occurs. The magnitude of the equilibrium sand concentration strongly depends on the mean sand grain size, which is discussed in the next subsection. Visser (1993) presents maps of the long-term, depth-averaged mud concentration distribution in the North Sea. The mud concentration near the Dutch coast appears to be low offshore (5 - 10 mg/l), but strongly increases in a narrow strip of 5 - 10 km near the coast up to a mud concentration of about 100 mg/l. Because the northern model boundary is located at approximately 10 km off the coast, a vertically uniform mud concentration profile is prescribed at all open boundaries with a constant value  $c_{m,0} = 50$  mg/l (Figure 6.4). Additionally, one sensitivity computation is carried out in which the mud concentration along the eastern and western boundary linearly varies between  $c_{m,0} = 50$  mg/l onshore and  $c_{m,0} = 10$  mg/l offshore.

### Bed level and bed composition

The bed level at an open boundary is kept fixed when inflow occurs. The mud content deep down in the bed also needs to be specified and is set at  $p_{m,sub} = 0$ . The influence of this condition is negligible, because the location of this boundary is far below the bed surface.

**Table 6.3:** Settings of physical parameters reference computation.

| Description                      | Symbol          | Value     | Unit        |
|----------------------------------|-----------------|-----------|-------------|
| Manning coefficient              | $n$             | 0.021     | $s/m^{1/3}$ |
| Horizontal fluid mixing          | $\nu_x, \nu_y$  | 10        | $m^2/s$     |
| Sand grain size                  | $d_{50}$        | 0.00014   | $m$         |
| Settling velocity sand           | $w_s$           | 0.015     | $m/s$       |
| Settling velocity mud            | $w_m$           | 0.0005    | $m/s$       |
| Critical mud content             | $p_{m,cr}$      | 0.3       | –           |
| Critical erosion shear stress:   |                 |           |             |
| - Non-cohesive erosion           | $\tau_{e,nc}$   | 0.25      | $N/m^2$     |
| - Cohesive erosion               | $\tau_{e,c}$    | 0.5       | $N/m^2$     |
| Erosion coefficient:             |                 |           |             |
| - Non-cohesive erosion           | $M_{nc}$        | $10^{-4}$ | $m/s$       |
| - Cohesive erosion               | $M_c$           | $10^{-8}$ | $m/s$       |
| Critical deposition shear stress | $\tau_d$        | 0.15      | $N/m^2$     |
| Bed porosity                     | $\varepsilon_p$ | 0.40      | –           |
| Physical mixing length           | $L_p$           | 0.10      | $m$         |
| Physical mixing coefficient      | $\alpha_p$      | $10^{-6}$ | –           |
| Biological mixing coefficient    | $\Xi_b$         | 0         | $m^2/s$     |

### 6.3.3 Initial conditions

The initial current velocity, water level and suspended sediment concentrations are set to zero ('cold start'). These initial conditions for the water motion and the sediment transport are not important, because their influence vanishes before the morphological computation starts. As already mentioned in the previous section, the initial bathymetry is based on depth soundings in 1970. Information on the initial bed composition at the bed surface is scarce, whereas no information exists on the bed composition below the bed surface. The bed composition map in the period 1950 - 1955 presented by De Glopper (1967) suggests that almost the entire intertidal area has a low mud content between 0 and 10% at the bed surface, and high mud contents are only observed near the borders of the basin. Hence, the reference computation is started with a full sand bed and one sensitivity computation is carried out with more initial variation in bed composition.

### 6.3.4 Parameter settings

The parameter settings of the reference computation are summarised in Table 6.3. Several remarks are made:

- The roughness parameter is used for calibration of the water level and currents. It appears

that a Manning coefficient  $n = 0.021 \text{ s/m}^{1/3}$  is the optimum setting (see Section 6.4). The horizontal fluid mixing coefficients are set at  $\nu_x = \nu_y = 10 \text{ m}^2/\text{s}$ , but these settings are generally not very important.

- The mean sand grain size varies between 120 and 160  $\mu\text{m}$  in the inlet area (Biegel & Hoekstra, 1995) and is set at  $d_{50} = 140 \mu\text{m}$ . The corresponding settling velocity  $w_s = 0.015 \text{ m/s}$ .
- In general, the transition between non-cohesive and cohesive behaviour appears to be at a clay content of 5 - 10% (see also Chapter 3). The critical mud content ( $p_{m,cr}$ ) applied in the model, is determined by the specific clay/silt ratio in this area. This ratio appears to be 0.21 (see Table 2.3) and the critical mud content is therefore set at  $p_{m,cr} = 30 \%$ .
- Specific measurements of the critical shear stress for deposition, the settling velocity for mud, the erosion coefficients and the mixing coefficients of the sediment bed are not available. Typical values for Dutch systems in general are applied for these coefficients (see Winterwerp, 1989; Van Rijn, 1993), except for the mixing coefficients in the sediment bed. The default settings are used for the physical mixing coefficients (see also Section 4.4), whereas biological mixing is not taken into account.

## 6.4 Calibration and verification of the hydrodynamic module

### 6.4.1 Flow

Van de Kreeke and Louters (1996) present water level and current velocity measurements at various stations in the Friesche Zeegat during the period September 24 - November 18, 1992 (Figure 6.5). The current velocity was obtained at 1.5 m above the bed, except at the location Meetpaal. There, the measurement height was 0.26 and 2.36 m above the bed. Based on these data, Van de Kreeke and Dunsbergen (2000) derive the amplitudes and phases of the water level and current velocity at these stations. The water level  $\zeta$  and the current velocity vector  $\mathbf{u}$  are defined as follows:

$$\zeta = \hat{\zeta}_2 \cos(\omega t - \varphi_2) + \hat{\zeta}_4 \cos(2\omega t - \varphi_4) \quad (6.1)$$

$$\mathbf{u} = \hat{\mathbf{u}}_2 \cos(\omega t - \varphi_2) + \hat{\mathbf{u}}_4 \cos(2\omega t - \varphi_4) \quad (6.2)$$

where  $\hat{\zeta}_2$  is the water level amplitude of  $M_2$ ,  $\omega$  the frequency of  $M_2$ ,  $\varphi_2$  the phase of  $M_2$ ,  $\hat{\zeta}_4$  is the water level amplitude of  $M_4$ ,  $\varphi_4$  the phase of  $M_4$ ,  $\hat{\mathbf{u}}_2$  the current velocity amplitude of  $M_2$  and  $\hat{\mathbf{u}}_4$  the current velocity amplitude of  $M_4$ . The relative phase difference  $\psi$  between the  $M_2$ -constituent and  $M_4$ -constituent of the water level (eq. 6.1) and the current velocity (eq. 6.2)

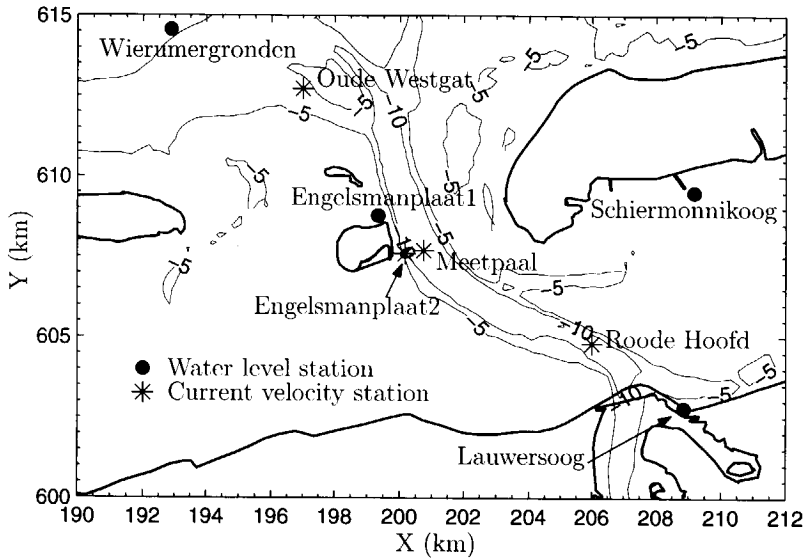


**Figure 6.5:** Water level and current velocity stations in the Friesche Zeevat.

is also considered in this chapter. With help of the transformation  $\omega t' = \omega t - \varphi_2$ , the relative phase difference in eq. (6.1) and (6.2) is defined as  $\psi = \varphi_4 - 2\varphi_2$ .

The roughness coefficient in the flow computations is calibrated against the observed water level characteristics at the water level stations (Figure 6.5). For this purpose, two-dimensional horizontal flow computations were carried out with Manning coefficients, varied within a realistic range to determine the mean discrepancy in amplitude and phase (Figure 6.6). The mean discrepancy is defined as  $\frac{1}{N} \sum |1 - \frac{x_{mod}}{x_{obs}}|$ , where  $N$  is the number of stations, and  $x_{mod}$  and  $x_{obs}$  are the modelled and observed value of parameter  $x$ , respectively. Figure 6.6 shows that the application of  $n = 0.020 - 0.022 \text{ s/m}^{1/3}$  gives a minimum in the mean discrepancy of the amplitude and phase of the  $M_2$ -constituent and the amplitude ratio between the  $M_4$ - and  $M_2$ -constituent. The mean discrepancy in the relative phase, however, slightly increases with increasing roughness coefficient. Based on these computations, the roughness coefficient is set at  $n = 0.021 \text{ s/m}^{1/3}$ : the observed and modelled water level characteristics are summarised in Table 6.4. The agreement between observed and modelled tidal characteristics is fair, except for the  $M_2$ -amplitude and  $M_4$ -phase at Schiermonnikoog. The small entrance channel towards the harbour of Schiermonnikoog is presumably not well represented in the model topography, which results in a poor representation of the tidal propagation in this area.

The flow results with the calibrated roughness coefficient ( $n = 0.021 \text{ s/m}^{1/3}$ ) are compared with the measured current velocity amplitudes and phases at five current velocity stations (Figure 6.5). For this purpose, the computed velocity at the measurement height is obtained from the

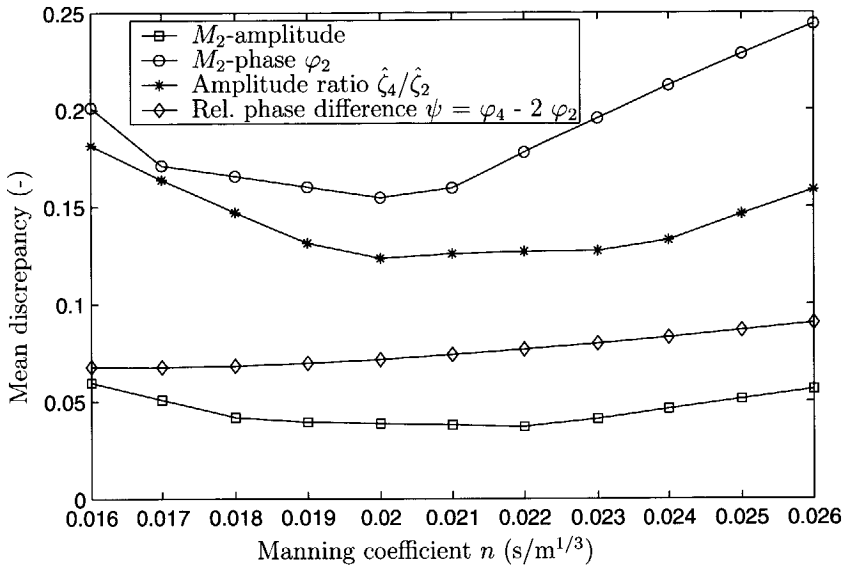


**Figure 6.6:** Mean discrepancy between the observed and modelled water level characteristics for various Manning coefficients. See text for the definition of the mean discrepancy.

**Table 6.4:** Water level measurements and model results with a Manning coefficient  $n = 0.021 \text{ s/m}^{1/3}$  (see Figure 6.5 for locations).

| Station         | $\hat{\zeta}_2$ (m) |       | $\varphi_2$ ( $^\circ$ ) |       | $\hat{\zeta}_4$ (m) |       | $\varphi_4$ ( $^\circ$ ) |       |
|-----------------|---------------------|-------|--------------------------|-------|---------------------|-------|--------------------------|-------|
|                 | meas.               | model | meas.                    | model | meas.               | model | meas.                    | model |
| Wierumergronden | 0.93                | 0.98  | 0                        | 0     | 0.08                | 0.10  | 207                      | 212   |
| Engelsmanplaat1 | 0.99                | 1.02  | 16                       | 12    | 0.09                | 0.11  | 233                      | 239   |
| Schiermonnikoog | 1.03                | 0.98  | 27                       | 33    | 0.11                | 0.10  | 230                      | 273   |
| Lauwersoog      | 1.04                | 1.06  | 22                       | 22    | 0.11                | 0.12  | 226                      | 231   |

computed depth-averaged velocity in each station by assuming a logarithmic velocity profile. Next, the amplitudes and phases of the  $M_2$ -tide and  $M_4$ -tide along the major (or principal) and minor axis of the tidal current ellipse are determined for each station. In this analysis, the velocities are positive in the flood direction and the direction of the major axis is defined as the angle between the major axis and the south-north direction, taken positive in the clockwise direction (cf. Van de Kreeke & Dunsbergen, 2000). The direction, the amplitude and the phase of the current velocity along the major axis and the current velocity amplitude along the minor axis are presented in Table 6.5 for the  $M_2$ -tide and in Table 6.6 for the  $M_4$ -tide.

It follows from Table 6.5 that the observed direction and the  $M_2$ -amplitude and  $M_2$ -phase of the major axis of the tidal ellipse show good agreement with the model results. Furthermore, the velocity amplitudes at the minor axis have the same order of magnitude as the observed



**Table 6.5:** Current velocity measurements and model results of  $M_2$ -constituent with a Manning coefficient  $n = 0.021 \text{ s/m}^{1/3}$  (see Figure 6.5 for locations).

| Station         | Major axis                                           |       |                                |       |                                   |       | Minor axis                     |       |
|-----------------|------------------------------------------------------|-------|--------------------------------|-------|-----------------------------------|-------|--------------------------------|-------|
|                 | Direction w.r.t. North<br>clockwise (+) ( $^\circ$ ) |       | Amplitude<br>$\hat{u}_2$ (m/s) |       | Phase<br>$\varphi_2$ ( $^\circ$ ) |       | Amplitude<br>$\hat{u}_2$ (m/s) |       |
|                 | meas.                                                | model | meas.                          | model | meas.                             | model | meas.                          | model |
| Oude Westgat    | 113                                                  | 114   | 0.54                           | 0.67  | 276                               | 283   | 0.006                          | 0.035 |
| Engelsmanplaat2 | 160                                                  | 161   | 0.77                           | 0.80  | 275                               | 297   | 0.006                          | 0.008 |
| Meetpaal1       | 158                                                  | 169   | 0.34                           | 0.34  | 268                               | 286   | 0.004                          | 0.004 |
| Meetpaal2       | 161                                                  | 169   | 0.51                           | 0.46  | 267                               | 286   | 0.001                          | 0.005 |
| Roode Hoofd     | 113                                                  | 112   | 0.64                           | 0.70  | 273                               | 295   | 0.002                          | 0.004 |

**Table 6.6:** Current velocity measurements and model results of  $M_4$ -constituent with a Manning coefficient  $n = 0.021 \text{ s/m}^{1/3}$  (see Figure 6.5 for locations).

| Station         | Major axis                                           |       |                                |       |                                   |       | Minor axis                     |       |
|-----------------|------------------------------------------------------|-------|--------------------------------|-------|-----------------------------------|-------|--------------------------------|-------|
|                 | Direction w.r.t. North<br>clockwise (+) ( $^\circ$ ) |       | Amplitude<br>$\hat{u}_4$ (m/s) |       | Phase<br>$\varphi_4$ ( $^\circ$ ) |       | Amplitude<br>$\hat{u}_4$ (m/s) |       |
|                 | meas.                                                | model | meas.                          | model | meas.                             | model | meas.                          | model |
| Oude Westgat    | 114                                                  | 121   | 0.04                           | 0.04  | 60                                | 87    | 0.01                           | 0.01  |
| Engelsmanplaat2 | 149                                                  | 119   | 0.06                           | 0.04  | 48                                | 105   | 0.00                           | 0.00  |
| Meetpaal1       | -                                                    | -     | <0.001                         | 0.02  | -                                 | -     | -                              | -     |
| Meetpaal2       | -                                                    | -     | <0.001                         | 0.02  | -                                 | -     | -                              | -     |
| Roode Hoofd     | 112                                                  | 123   | 0.06                           | 0.03  | 45                                | 53    | 0.02                           | 0.01  |

amplitudes except at station Oude Westgat. The observed velocity characteristics of the  $M_4$ -tide are also well represented by the flow model (Table 6.6). The order of magnitude of the velocity amplitudes at the major axis agree, except for station Meetpaal. The agreement in the phase of the  $M_4$ -constituent is also reasonable, except for station Engelsmanplaat2.

The relative phase differences between  $M_2$  and  $M_4$  of the water level in eq. (6.1) and the current velocity in eq. (6.2) are of special importance, because these parameters determine the type of tidal asymmetry. The relative phase difference in eq. (6.1) and (6.2) is defined as  $\psi = \varphi_4 - 2\varphi_2$ . The water level rise is faster than its fall for a relative phase difference between  $180^\circ$  and  $360^\circ$  and the maximum ebb velocity is higher than the maximum flood velocity for a relative phase difference between  $90^\circ$  and  $270^\circ$ . The observed and modelled relative phase differences of the water level and current velocity at the different stations are summarised in Table 6.7. It can be concluded that the relative phase difference of the water level and current velocity is well represented with the flow model. The model results indeed indicate that the water level rise is faster than its fall at the North Sea, whereas water level variation is more or less symmetric in the basin (cf. Van de Kreeke & Dunsbergen, 2000). Furthermore, the ebb-dominance of

**Table 6.7:** Measured and modelled relative phase difference  $\psi = \varphi_4 - 2\varphi_2$  between  $M_2$  and  $M_4$  tidal constituents of the water level and current velocity (see Figure 6.5 for locations).

| Water level     |       |       | Current velocity |       |       |
|-----------------|-------|-------|------------------|-------|-------|
| Station         | meas. | model | Station          | meas. | model |
| Wierumergronden | 207   | 212   | Oude Westgat     | 228   | 240   |
| Engelsmanplaat1 | 201   | 215   | Engelsmanplaat2  | 218   | 231   |
| Schiermonnikoog | 176   | 207   | Meetpaal         | -     | 40    |
| Lauwersoog      | 182   | 186   | Roode Hoofd      | 219   | 182   |

the current velocity at Oude Westgat, Engelsmanplaat2 and Roode Hoofd is also found in the model results (cf. Van de Kreeke & Dunsbergen, 2000). The model results suggest flood-dominance at station Meetpaal, but the relative phase difference could not be determined from the observations, because the current velocity amplitude of the  $M_4$ -constituent was negligible (see also Table 6.6).

The flow model is verified with historical water level data from the year 1971 (Van de Kreeke & Louters, 1996). Based on this data, Van de Kreeke and Louters (1996) have determined the water level characteristics at Schiermonnikoog and Lauwersoog. Unfortunately, the water level characteristics in 1971 are not known at Wierumergronden. The water level analysis of the years 1985, 1990 and 1995 indicated that the water level characteristics hardly changed in this station. It is assumed that the characteristics for 1985 in this station are representative for the year 1971, too.

**Table 6.8:** Measured and modelled water level characteristics in 1970/1971 with a Manning coefficient  $n = 0.021 \text{ s/m}^{1/3}$  and a bathymetry of 1970 (see Figure 6.5 for locations).

| Station         | $\hat{\zeta}_2$ (m) |       | $\varphi_2$ ( $^\circ$ ) |       | $\hat{\zeta}_4$ (m) |       | $\varphi_4$ ( $^\circ$ ) |       |
|-----------------|---------------------|-------|--------------------------|-------|---------------------|-------|--------------------------|-------|
|                 | meas.               | model | meas.                    | model | meas.               | model | meas.                    | model |
| Wierumergronden | 0.95                | 0.98  | 0                        | 0     | 0.10                | 0.10  | 207                      | 212   |
| Schiermonnikoog | 1.03                | 1.00  | 22                       | 29    | 0.10                | 0.11  | 232                      | 263   |
| Lauwersoog      | 1.05                | 1.07  | 14                       | 16    | 0.09                | 0.12  | 218                      | 216   |

The computed and observed water level characteristics in 1970/1971 are listed in Table 6.8. The results demonstrate that the measured water level characteristics at Wierumergronden, Lauwersoog and Schiermonnikoog in 1971 are reasonably well predicted with the flow model. The good agreement at Wierumergronden is not surprising, because the bathymetry in the North Sea in 1970 is the same as in the calibration computations. The results at Lauwersoog and Schiermonnikoog are a better indication of the predictive capabilities of the flow model, because the bathymetry in the basin in 1970 strongly differs from that during calibration. Except for the  $M_4$ -amplitude, the observed and computed tidal characteristics at Lauwersoog agree very well. The agreement in the  $M_2$  and  $M_4$ -amplitude at Schiermonnikoog is also good,

but the phases of these tidal constituents are poorly reproduced. The poor representation of the tidal propagation in this area was already found and discussed in the calibration computations with the bathymetry of 1992 (cf. Table 6.4). Although the absolute prediction of the  $M_2$ -phase at Schiermonnikoog is not correct, the observed increase in the  $M_2$ -phase ( $+5^\circ$ ) between 1971 and 1992 is approximated rather well by the flow model ( $+4^\circ$ ). Unfortunately, the observed ( $-2^\circ$ ) and modelled ( $+10^\circ$ ) change in the  $M_4$ -phase does not agree.

In conclusion, the computed water level and current velocity characteristics show rather good agreement with the observations. Unfortunately, the flow characteristics can only be compared to observations in the deep main channel of the Zoutkamperlaag, as no measurements are available at the intertidal area. Consequently, the performance of the flow model is not known in these areas. Yet, the agreement between observations where available and model results is considered good enough to have confidence in the whole model to be applied for the long-term morphological computations in Section 6.5.

#### 6.4.2 Short waves

Dunsbergen (1995) describes a data set that is used herein to verify the short wave computations for the Friesche Zeegat area. It includes the wind characteristics from station Huibergat and the wave characteristics at six stations on October 9, 1992 (Figure 6.7). The wave and wind characteristics are known (almost) simultaneously at five moments during this day (0600hr, 0900hr, 1200hr, 1600hr and 2300hr). A wave computation is performed with a realistic flow pattern for each of these moments to predict the significant wave height and peak period in the wave stations. The measured wave conditions in station Schiermonnikoog Noord and the wind conditions in Huibergat are used as boundary conditions for the short-wave model (Table 6.9).

**Table 6.9:** Boundary conditions short wave computations at different moments during the tidal period (see Figure 6.7 for locations).

| Time                 | Schiermonnikoog Noord |           |                              |                                   | Huibergat      |                              |
|----------------------|-----------------------|-----------|------------------------------|-----------------------------------|----------------|------------------------------|
|                      | $H_s$ (m)             | $T_p$ (s) | $\theta_{wave}$ ( $^\circ$ ) | $\theta_{spreading}$ ( $^\circ$ ) | $U_{10}$ (m/s) | $\theta_{wind}$ ( $^\circ$ ) |
| 0600 hr              | 2.24                  | 6.7       | 328                          | 31                                | 11             | 320                          |
| 0900 hr              | 2.55                  | 8.3       | 341                          | 25                                | 10             | 345                          |
| 1200 hr              | 3.31                  | 10.0      | 341                          | 23                                | 12             | 340                          |
| 1600 hr <sup>1</sup> | 3.47                  | 10.0      | 339                          | 24                                | 13             | 340                          |
| 2300 hr <sup>1</sup> | 2.92                  | 11.1      | 338                          | 27                                | 9.5            | 30                           |

<sup>1</sup> Because no information was available at 1600 hr and 2300hr, the measured wave characteristics in Schiermonnikoog Noord at 1500hr and 0000hr are applied, respectively.

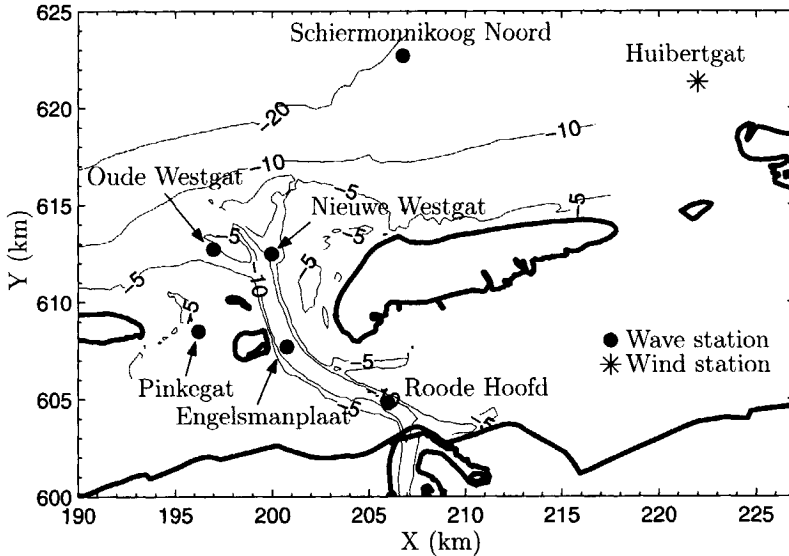


**Figure 6.7:** Wave and wind stations during measurement campaign 1992 (Dunsbergen, 1995).

Figure 6.8 presents the comparison between the observed and predicted significant wave height  $H_s$  and peak period  $T_p$  together with the correlation coefficient  $R^2$ . It can be concluded that the predicted significant wave height corresponds well with the observed wave height (Figure 6.8a). The agreement between the observed and modelled peak period is somewhat less convincing (Figure 6.8b). Notice that the wave model systematically underestimates the observed peak period for this case. Ris et al. (1999) draw a similar conclusion and attribute this discrepancy to errors in the process-formulations, the bathymetry, the driving wind field, the wind- and wave-setup and the current field.

Summarising, the agreement between between the measured and computed significant wave height and peak period is rather good. An important restriction is that the computed wave characteristics are only compared with observations in the channels. So, the performance of the short-wave model in the intertidal area is not known. Nevertheless, we have confidence that the short wave results are good enough for the long-term morphological computations in Section 6.5.

## 6.5 Results morphological computations

### 6.5.1 General

This section presents the results of the long-term computations in the Friesche Zeegat in the period 1970 - 1994. The emphasis is on the comparison between the observed and the computed

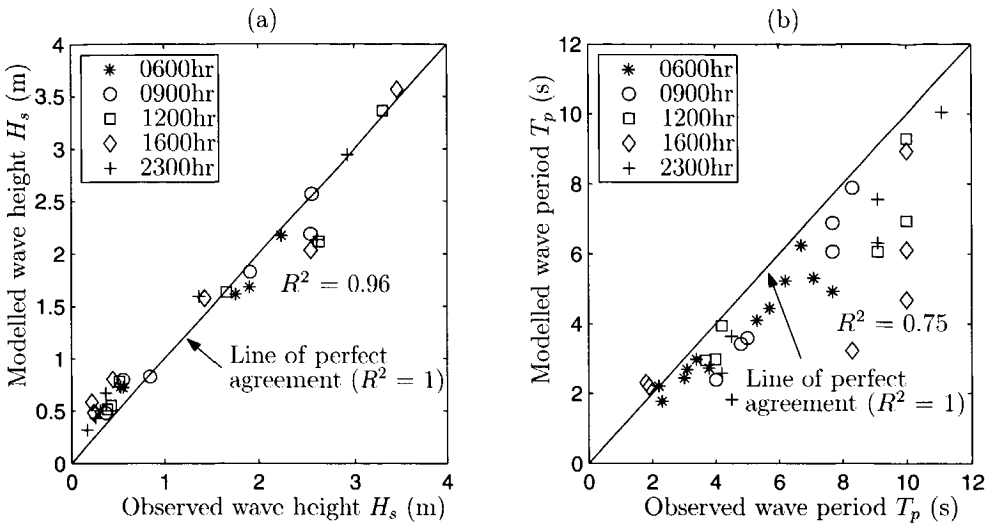


**Figure 6.8:** Comparison between observed and predicted significant wave height (a) and peak period (b) in the Friesche Zeegat at October 9, 1992.

bed level and bed composition changes (i.e. morphological response) in the Zoutkamperlaag. The observed changes were described in Section 6.2.3 and a distinction was made between the ebb-tidal delta and the tidal basin (see also Oost, 1995; Biegel & Hoekstra, 1995). This distinction is also maintained in the present section and the comparison between observations and model results is described consecutively for the ebb-tidal delta in Section 6.5.2 and the tidal basin in Section 6.5.3. Finally, the sensitivity of the results in the tidal basin are investigated in Section 6.5.4. It is noted that the present Section 6.5 only gives an overview of similarities and discrepancies between the observed and modelled morphological behaviour. A discussion of the model performance is given in Section 6.6.

### 6.5.2 Ebb-tidal delta

The observed and computed total bed level change in the period 1970 - 1994 are shown in Figure 6.9a and Figure 6.9b, respectively. It is noted that these changes are due to sand and mud erosion and deposition, i.e. the 'total' bed level changes. The spatial extent of the ebb-tidal delta according to Oost (1995) is indicated in this figure. For this area, the observed and computed total volume change, and the computed contribution of sand and mud are shown in Figure 6.10a. The observed and computed total volume change as a function of depth are shown in Figure 6.10b. Based on these results, an overview of the similarities and differences between the observed and modelled behaviour of the ebb-tidal delta will now be discussed.

Qualitatively, the computed bed level changes in the ebb-tidal delta resemble the observations to some extent, but several important differences are also observed (Figure 6.9). Important

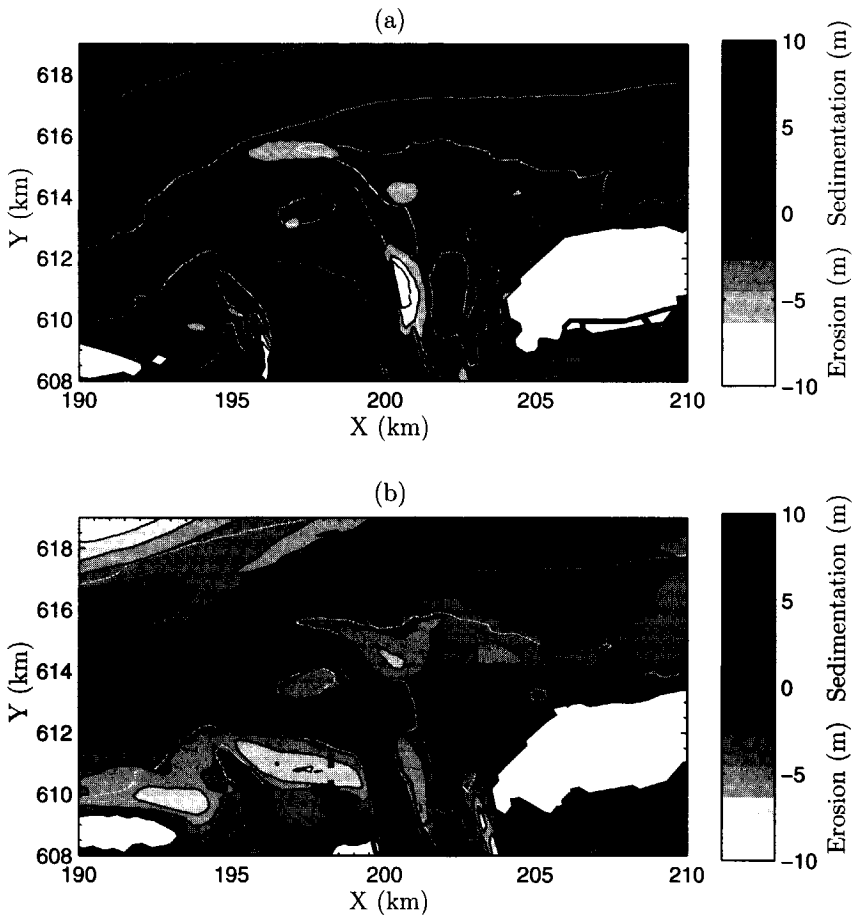


**Figure 6.9:** Observed (a) and computed (b) bed level change in the ebb-tidal delta of the Zoutkamperlaag in the period 1970 - 1994. The black dotted line indicates the spatial extent of the ebb-tidal delta according to Oost (1995).

similarities are the strong sedimentation in the deep entrance channel of the Zoutkamperlaag and the erosion in the shallow areas of the ebb-tidal delta. However, two important differences are found. The computed strong sedimentation at the north side of the ebb-tidal delta is not observed. Furthermore, the observed strong sedimentation near the westernmost tip of Schiermonnikoog is not found in the model results.

The quantitative comparison of the total volume change in time shows a striking difference (Figure 6.10a). The model suggests substantial deposition in the ebb-tidal delta directly after closure of the Lauwerszee. After five years, the ebb-tidal delta starts eroding and this process

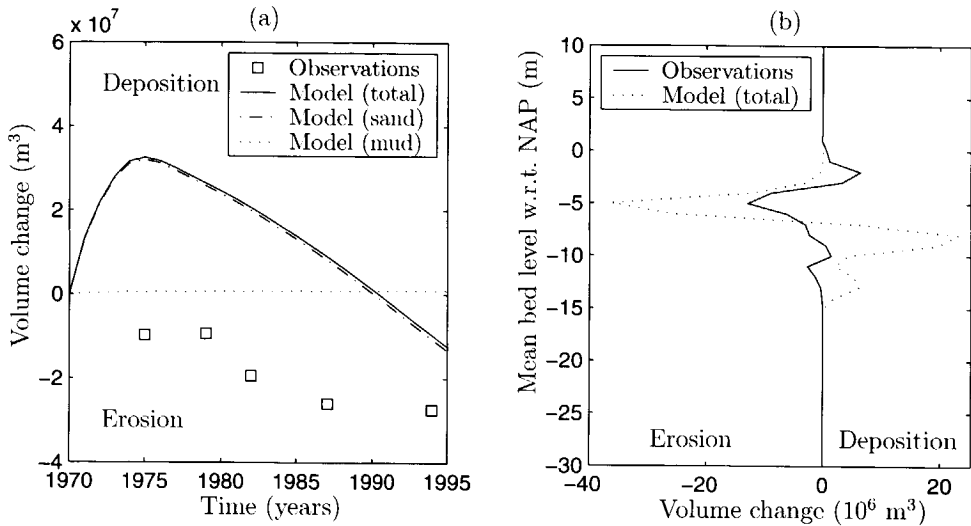


**Figure 6.10:** Observed and computed volume change in the ebb-tidal delta of the Zoutkamperlaag in the period 1970 - 1994: Total volume changes and computed contribution of sand and mud (a), and volume changes as a function of depth at intervals of 1 m (b).

continues during the next 20 years. The observations, however, indicate that the ebb-tidal delta eroded during the entire period, and that the erosion rate probably decreased through time. The volume changes as a function of depth indicate that the initial net deposition in the model results is largely the result of the strong sedimentation in the area below -7.5 m NAP, whereas the observed changes in this depth range are negligible (Figure 6.10b). The observed erosion between -2 and -7.5 m NAP qualitatively follows the observations, but is largely overestimated by the numerical model.

The computed bed composition development in the ebb-tidal delta is not discussed in detail, because the bed level changes in the ebb-tidal delta are purely due to sand exchange (cf. Figure 6.10a). Hence, the bed composition in the ebb-tidal delta remains sandy during the entire period. This agrees with the observation that the fill of the main channel of the ebb-tidal delta is due to sand deposition only (Sha, 1992). Furthermore, the bed surface of the entire ebb-tidal delta in 1994 appears to be sandy with a small mud content, which corresponds with the model results.

### 6.5.3 Tidal basin

The observed and computed bed level changes in the basin show important qualitative similarities and differences (Figure 6.11). Large bed level changes in the observations, as well as in the model results, are mainly limited to the deeper channel of the Zoutkamperlaag. However, the observations indicate strong sedimentation in almost the entire channel, whereas strong

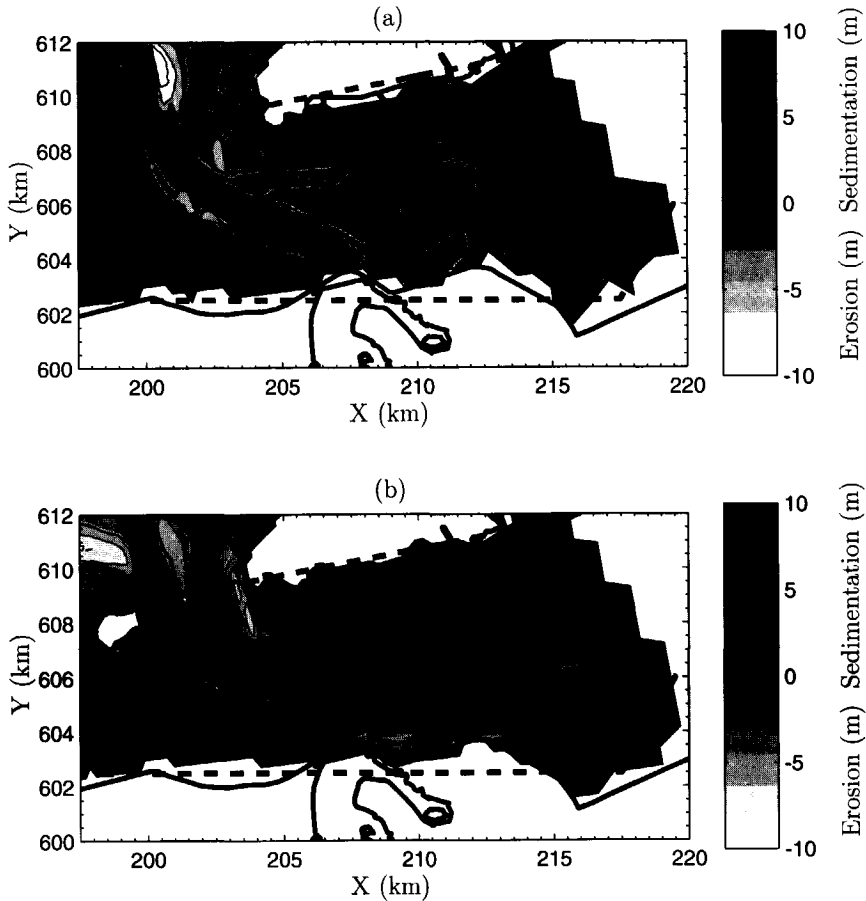


**Figure 6.11:** Observed (a) and computed (b) bed level change in the tidal basin of the Zoutkamperlaag in the period 1970 - 1994. The black dotted line indicates the spatial extent of the basin according to Oost (1995).

sedimentation in the model results is mainly limited to the entrance of the basin and slight erosion is even predicted in the central section of the channel.

The comparison of the volume changes in the basin demonstrates that the net sedimentation in the basin after 25 years is quantitatively well predicted by the model (Figure 6.12a). However, the observed and computed net sedimentation have a different development in time. The observations suggest a decreasing net sedimentation rate in time (see also Table 6.1), whereas the model result has an almost constant sedimentation rate in time. The observed and computed distribution of the volume changes by depth show fair resemblance (Figure 6.12b). Net sedimentation is observed in the deeper parts ( $< -10$  m NAP) and at the intertidal area, whereas



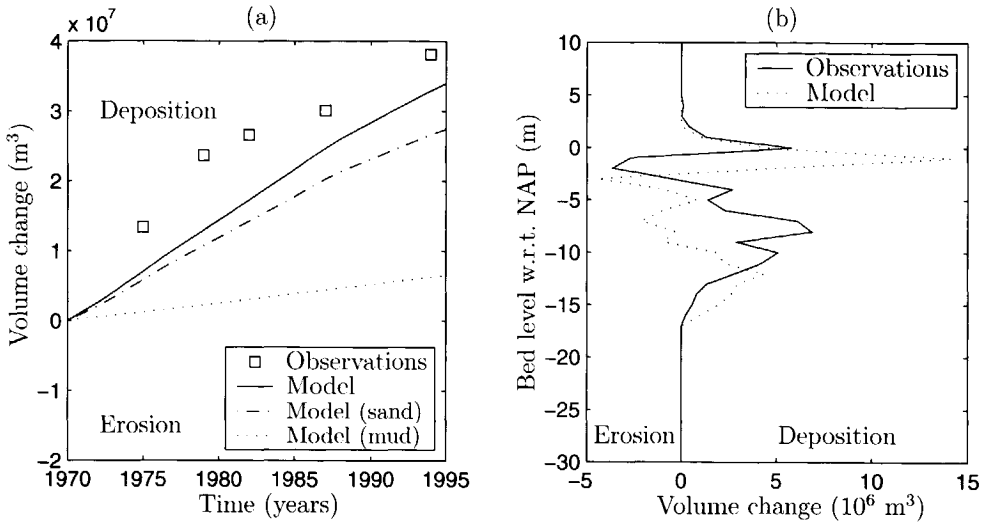


**Figure 6.12:** Observed and computed volume changes in the basin of the Zoutkamperlaag in the period 1970 - 1994: Total volume changes and computed contribution of sand and mud (a), and volume changes as a function of depth at intervals of 1 m (b).

erosion is found between -2 and -5 m NAP. The observed strong net sedimentation between -5 and -10 m NAP, however, is not found in the model results, which show slight erosion in this depth range.

It is also interesting to consider the computed and observed contribution of sand and mud to the total volume changes in the basin (Table 6.10), because both sand and mud contribute significantly to the computed bed level changes in time and space (cf. Figure 6.12a). In this table, the computed ingoing and outgoing fluxes and the resulting net deposition volume in the period 1970 - 1994 are listed. Following the analysis of Oost (1995), a (very) rough estimate is given of the contribution of sand and mud to the net total deposition (see also Section 6.2.3 and Table 6.1). The following assumptions are made: i) the observed eroded sediment volume of the ebb-tidal delta ( $-27.4 \times 10^6 \text{ m}^3$ ) in the period 1970 - 1994 has been deposited completely in the tidal basin, ii) the derived sediments from the ebb-tidal delta consist of sand only, and iii) the difference of  $+14.3 \times 10^6 \text{ m}^3$  between the net erosion in the ebb-tidal delta and the net deposition in the drainage basin consists of mud from the North Sea.

It follows from Table 6.10 that the estimated net deposition of sand in the tidal basin is well predicted with the model in the period 1970 - 1994. However, the model underestimates the net deposition of mud with about a factor two. The computed imported and exported fluxes of sand and mud demonstrate that the computed net deposition is small compared with these gross fluxes: the net deposition of mud differs an order of magnitude with the ingoing and outgoing mud flux.

**Table 6.10:** Sediment balance of the tidal basin in the period 1970 - 1994 for the reference computation.

|       | Model ( $10^6 \text{ m}^3$ ) |               |                | Observations ( $10^6 \text{ m}^3$ ) |
|-------|------------------------------|---------------|----------------|-------------------------------------|
|       | Imported flux                | Exported flux | Net deposition | Net deposition                      |
| Sand  | +73.4                        | -46.8         | +26.6          | +27.4                               |
| Mud   | +96.9                        | -90.6         | +6.3           | +14.3                               |
| Total | +170.3                       | -137.4        | +32.9          | +41.7                               |

Unlike the computed bed composition in the ebb-tidal delta, the composition in the basin changes considerably in time and space, due to the significant deposition of both sand and mud (cf. Figure 6.12a). Figure 6.13 presents the computed mud deposition and the mud content at the bed surface in the basin in the period 1970 - 1994. The locations of the cores in Figure 6.2 are shown in Figure 6.13. In contrast with the bed level development, the observed mud deposition pattern is not known in detail. Hence, a qualitative comparison can only be made between the observations and the model results below.

On the one hand, the observed and computed mud deposition pattern and the accompanying mud content at the bed surface agree well:

- The mud content is predominantly high near the borders of the basin, whereas the intertidal area itself is sandy (Figure 6.13a-c). The bed composition pattern in the period 1950 - 1955 and in 1994 shows a similar pattern, with high mud contents only near the borders of the basin.
- Strong mud deposition is observed near the dike of the Lauwerszee and in the outer bend of the channel near the Engelsmanplaat (Figure 6.13d). This agrees with the lithology of cores s.40 and s.22 near the Lauwerszee and core s.62 in the main channel (cf. Figure 6.3).
- The mud content at the bed surface near the dike of the Lauwerszee remains high during the entire period (Figure 6.13a-c). In particular, core s.40 also indicates that the mud content in this area remained high after closure.
- Mud deposition is absent at the entrance and in the channel towards the watershed between Schiermonnikoog and the mainland (Figure 6.13). This is in agreement with the absence of mud in core s.23 and cores s.6 - s.12.

On the other hand, also several discrepancies can be found between the observed and computed mud deposition pattern. The computed mud deposition is much smaller than observed in the cores. For example, several cores from the period 1980 - 1982 indicate mud deposition with a thickness of several meters (cf. Figure 6.3), whereas the computed mud deposition appears to be at most 1 m after 12 years (cf. Figure 6.13d after 24 years). Moreover, the observed mud deposition in the inner bend of the Zoutkamperlaag is not found in the model results. The cores s.29 - s.31 clearly show strong mud deposition after closure (Figure 6.3), whereas mud

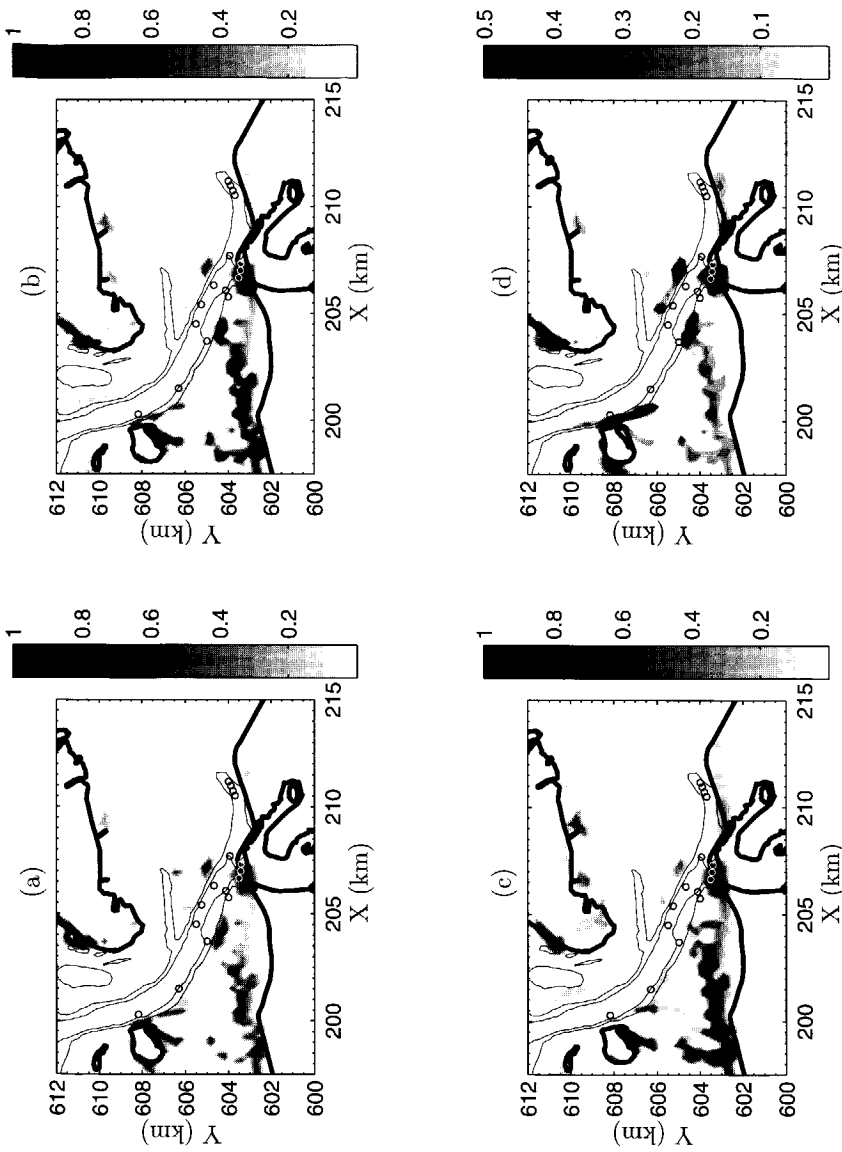


**Figure 6.13:** Computed mud fraction at the bed surface after 8 years (a), after 16 years (b) and after 24 years (c) and mud deposition in meters in the entire period 1970 - 1994 (d) in the basin of the Zoutkammerlaag. The small circles indicate the locations of the cores in Figure 6.2 and 6.3.

deposition is zero in the model results (Figure 6.13d).

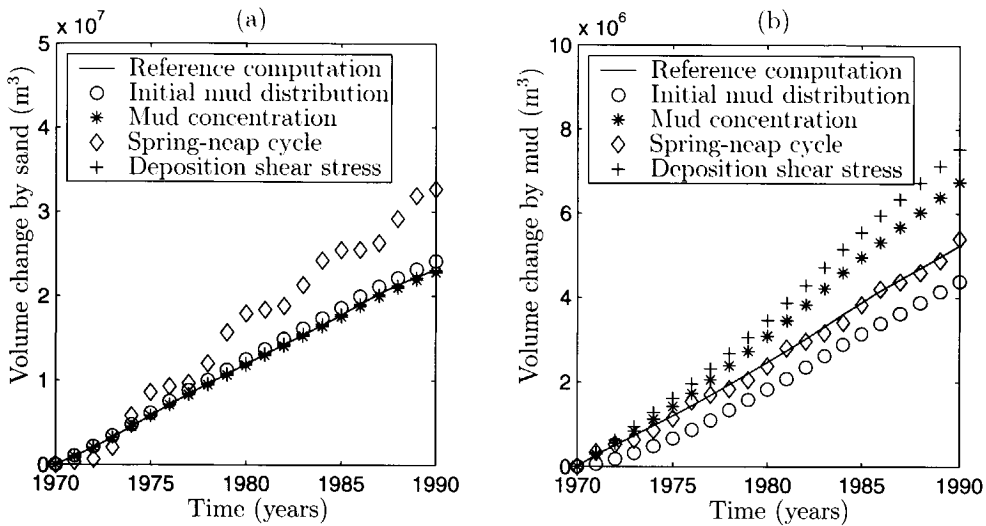
#### 6.5.4 Sensitivity analysis

Several computations are performed to investigate the sensitivity of the computational results to the model settings. These settings can be divided into the initial conditions, the boundary conditions and the parameter settings. Obviously, it is impossible to vary all of them. Therefore, the sensitivity analysis is restricted to the distribution of sand and mud. The observations and computational results in the previous sections have shown that this distribution is particularly important in the basin. The most striking difference is that the computed mud deposition in the main channel is much smaller than observed. Several explanations can be put forward to explain this difference. These are investigated in the sensitivity computations:

- **Initial mud content:** The observed volume changes by depth have demonstrated that the intertidal areas in the basin started eroding immediately after the closure of the Lauwerszee. Hence, these areas have presumably functioned as a source of sand and mud (see e.g. Winkelmolén & Veenstra, 1974; Oost, 1995). This mud source was not taken into account in the reference computation, because the initial bed consisted of sand only. Hence, a sensitivity computation is carried out with a initial variation in bed composition. The initial mud content at the intertidal area of the tidal basin is set at 10%, whereas the channels in the basin and the entire ebb-tidal delta are composed of sand only.
- **Mud concentration at sea boundary:** The imported amount of mud in the basin is partly determined by the magnitude of the mud concentration along the open sea boundaries. In the reference computation, the mud concentration at each boundary was constant in time and space ( $c_{m,0} = 0.05 \text{ kg/m}^3$ ). Obviously, the magnitude of this concentration strongly varies in time and space. In this sensitivity computation, a more realistic long-term mean mud concentration is applied along the open sea boundaries. The mud concentration varies in this computation along the western and eastern boundary between  $0.1 \text{ kg/m}^3$  at the coast and  $0.01 \text{ kg/m}^3$  offshore. Along the northern boundary, the mud concentration is constant and equal to  $0.01 \text{ kg/m}^3$ .
- **Spring-neap cycle:** Mud deposition occurs during periods with low bed shear stress. In the reference computation, the bed shear stress variation is determined by the semi-diurnal ( $M_2$ ) and the quarter-diurnal ( $M_4$ ) tide. Compared with this variation, the spring-neap cycle results in periods with relatively low and high bed shear stress and has probably enhanced the deposition of mud. Therefore, a sensitivity computation is performed in which  $S_2$  and  $MS_4$  tidal components are taken into account (Table 6.11). The characteristics of  $S_2$  and  $MS_4$  in Table 6.11 are derived from the two stations Wierumergronden and Huibertgat in a similar way as in the reference computation (see also Section 6.3.2). Along the northern boundary, these tidal characteristics also vary linearly between the eastern and western boundary.

**Table 6.11:** Boundary conditions water level for a spring-neap cycle.

| Tidal component | Western boundary |                        | Eastern boundary |                        |
|-----------------|------------------|------------------------|------------------|------------------------|
|                 | $\zeta$ (m)      | $\varphi$ ( $^\circ$ ) | $\zeta$ (m)      | $\varphi$ ( $^\circ$ ) |
| $M_0$           | 0.019            | -                      | -0.028           | -                      |
| $S_2$           | 0.251            | 175.50                 | 0.269            | 196.42                 |
| $M_2$           | 0.928            | 254.87                 | 1.014            | 274.21                 |
| $M_4$           | 0.099            | 1.14                   | 0.089            | 25.68                  |
| $MS_1$          | 0.067            | 291.93                 | 0.063            | 317.59                 |

**Figure 6.14:** Computed volume change by sand (a) and mud (b) in the basin of the Friesche Zeegat in the reference computation and the various sensitivity computations.

- Critical shear stress for deposition:** Mud deposition is also determined by the critical shear stress for deposition ( $\tau_d$ ). In the reference computation, an average value for Dutch tidal systems was applied by lack of data ( $\tau_d = 0.15 \text{ N/m}^2$ ). The parameter is set at a higher, but realistic value ( $\tau_d = 0.25 \text{ N/m}^2$ ), in order to investigate the effect on the mud deposition in the basin.

The net deposition of sand in the basin is shown for the reference computations and the sensitivity computations in Figure 6.14a. The results of the ebb-tidal delta are not presented, because the differences with the reference computation are very small. Except for the computation with the spring-neap cycle, the deposition by sand in the basin is not affected much. The computation with the spring-neap cycle clearly results into a much higher sand deposition rate during the simulation period. Furthermore, a variation with a small amplitude is visible. The frequency of this variation is an artifact, due to the application of a morphological factor

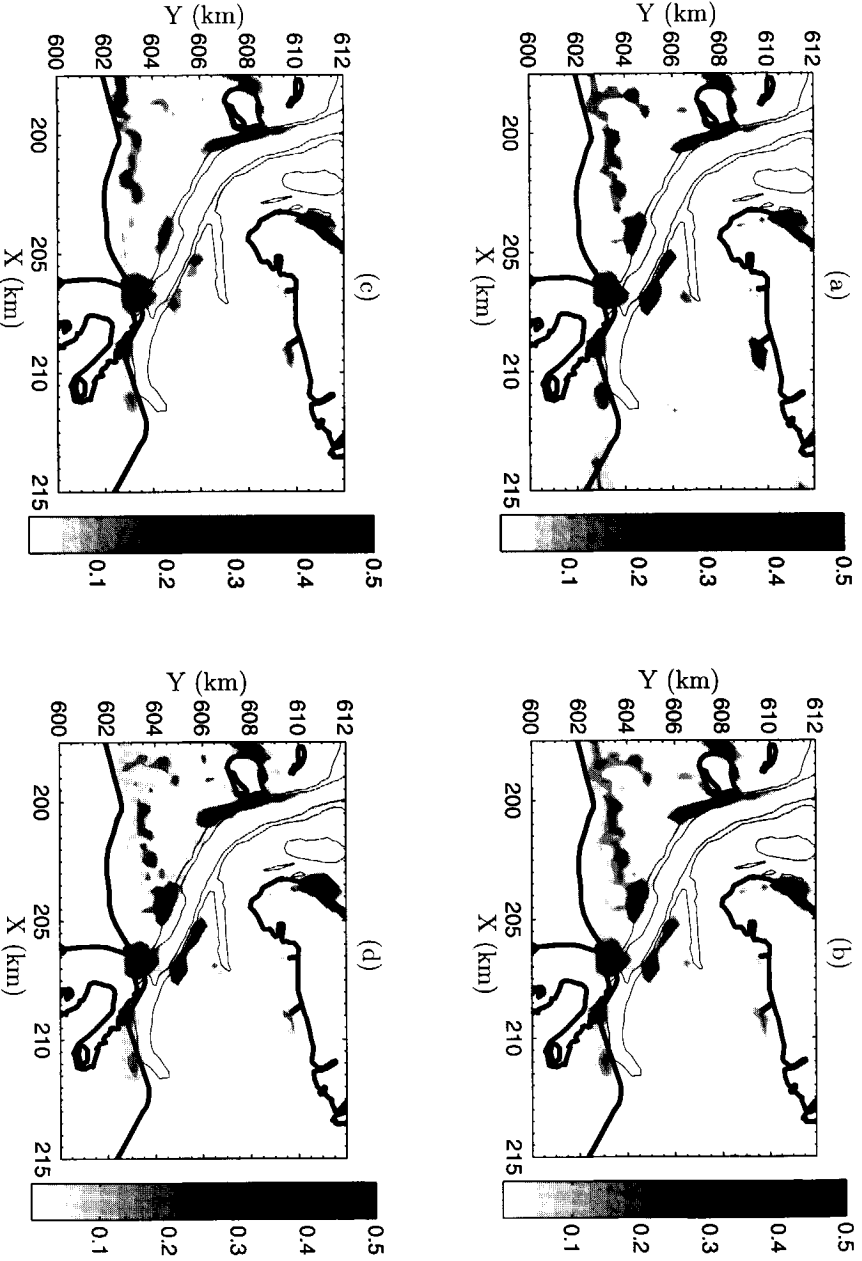


Figure 6.15: Results sensitivity computations with the computed mud deposition in meters after 20 years: Initial mud distribution (a), Mud concentration (b), Spring-neap cycle (c) and Critical deposition shear stress (d).

( $N = 116$ ). This factor stretches the spring-neap period of two weeks with a factor  $N$ , which results in a period of about 4.5 years in the morphological computations. The largest period in all other computations is the tidal period. In combination with the morphological factor, this gives a period of about two months and is therefore too small to be visible in the results.

**Table 6.12:** Mud balance of the tidal basin after 10 and 20 years for the reference computation and the various sensitivity computations.

| Computation                          | After 10 years ( $10^6 \text{ m}^3$ ) |         |      | After 20 years ( $10^6 \text{ m}^3$ ) |         |      |
|--------------------------------------|---------------------------------------|---------|------|---------------------------------------|---------|------|
|                                      | Deposition                            | Erosion | Net  | Deposition                            | Erosion | Net  |
| Reference computation                | +2.2                                  | 0.0     | +2.2 | +5.2                                  | 0.0     | +5.2 |
| Initial mud content                  | +4.1                                  | -2.5    | +1.6 | +7.5                                  | -3.1    | +4.4 |
| Mud concentration at sea boundary    | +2.7                                  | 0.0     | +2.7 | +6.8                                  | 0.0     | +6.8 |
| Spring-neap cycle                    | +2.1                                  | 0.0     | +2.1 | +5.4                                  | 0.0     | +5.4 |
| Critical shear stress for deposition | +3.1                                  | 0.0     | +3.1 | +7.5                                  | 0.0     | +7.5 |

The net deposition of mud in the basin is presented for the reference computations and the sensitivity computations in Figure 6.14b. As expected, the mud deposition in the basin increases with a higher critical deposition shear stress and a higher mud concentration near the entrance of the basin. It also appears that the net mud deposition is not affected by taking into account the spring-neap cycle. Again, a small variation with a period of about 4.5 years is visible in the result with the spring-neap cycle (cf. Figure 6.14a). Finally, the computation with the initial mud distribution does not differ too much from the reference computation. The initial net mud deposition rate in the basin is slightly lower than in the reference computation, but this effect disappears after several years. At the end of the simulation period, the net mud deposition in the basin is a bit lower than in the reference computation.

The mud deposition patterns of the sensitivity computations are shown in Figure 6.15, and the result of the reference computation is found in Figure 6.13d. The scale of mud deposition is equal for all figures to facilitate the comparison between these computations. Qualitatively, the computed mud deposition patterns in the sensitivity computations are similarly distributed in the tidal basin compared to the reference computation. Furthermore, the intensity of mud deposition in the main channel does not differ too much in all computations.

The mud balances of the reference computation and the sensitivity computations are summarised in Table 6.12 in order to compare the results quantitatively. Except for the computation with the initial mud distribution, mud erosion in the basin is of course zero for all other computations, because the initial bed consists of sand only. It follows that the (gross) mud deposition after twenty years in the computation with an initial mud distribution ( $+7.5 \times 10^6 \text{ m}^3$ ) is about 40% higher than the mud deposition in the reference computation ( $+5.2 \times 10^6 \text{ m}^3$ ). The extra supply is due to mud erosion from the nearby intertidal areas in the basin itself ( $-3.1 \times 10^6 \text{ m}^3$ ).

## 6.6 Discussion of the morphological computations

### 6.6.1 Ebb-tidal delta

The hydrodynamic changes in the Zoutkamperlaag due to the closure of the Lauwerszee are of crucial importance to the understanding of the observed and computed morphological response in the previous sections. Therefore, the water level and bed shear stress variation by the tide at four stations in the main channel just before and directly after the closure are further analysed in Figure 6.16. The effect on the bed shear stress variation is large, whereas the water level variation in these locations hardly changes. The bed shear stress in the ebb-tidal delta is strongly reduced, in particular during ebb (Figure 6.16a). Near the Meetpaal and Roode Hoofd, however, the bed shear stress is reduced during flood and ebb (Figure 6.16b-c) and the bed shear stress almost completely vanishes in front of the closure dam near Lauwersoog (Figure 6.16d).

The observed and computed initial sand deposition in the main channel of the ebb-tidal delta is explained by the reduction of the tidal prism after closure of the Lauwerszee (see also Oost, 1995; Biegel & Hoekstra, 1995). Due to this closure, the maximum bed shear stress has decreased more during ebb than during flood (cf. Figure 6.16a). Assuming a zero net transport during the tidal period before closure, this results in a net import of sand after closure, and sand deposition in this area.

The observed and computed absence of mud deposition in the main channel of the ebb-tidal delta directly follows from the bed shear stress magnitude after closure (cf. Figure 6.16a). The bed shear stress after the closure is still much higher than the critical shear stress for deposition and erosion of mud (see Table 6.3). Thus, mud erosion as well as mud deposition occur during the tidal period. Under these conditions, it was shown elsewhere in this thesis that the ratio  $w_m c_{m,0}/M$  determines whether mud erosion ( $w_m c_{m,0}/M \ll 1$ ) or deposition ( $w_m c_{m,0}/M \gg 1$ ) prevails (see also Section 5.4). In the Friesche Zeegat, the ratio  $w_m c_{m,0}/M$  is much smaller than unity (see Table 6.3). So, the mud erosion flux largely exceeds the deposition flux, and the bed surface remains sandy after the closure. Because net mud deposition is mainly limited by the high bed shear stress, this area can be considered as 'flow limited' (cf. Section 5.4).

A discrepancy is found between the computed and observed morphological behaviour of the entire ebb-tidal delta in the first period after closure: net deposition is computed, whereas net erosion is observed (Figure 6.10a). In particular, the pronounced sand deposition at the sea side of the ebb-tidal delta did not match with the observations. The most likely explanation is the difference between the role of short waves in the model and in reality. In the present modelling approach, only the enhancement of the bed shear stress by short waves is taken into account, whereas wave-driven currents and transport are neglected (Figure 6.17a). This approach logically results in a loss of sediment in shallow areas, due to the stirring activity of waves (cf. Figure 6.10b). These sediments are transported by the tidal current and deposited in relatively quiescent channels during flood and the deeper parts offshore during ebb. In reality,



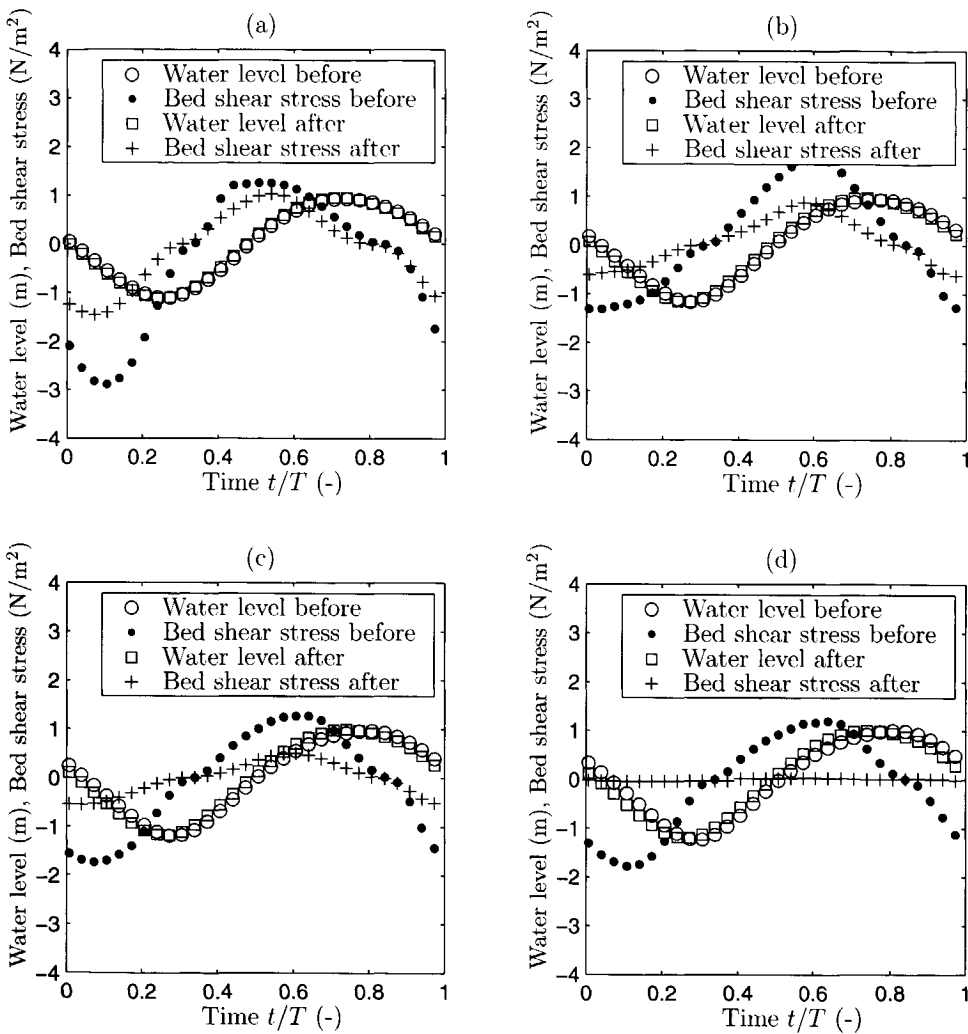


**Figure 6.16:** Computed water level and bed shear stress variation by the tide at four stations in the main channel of the Zoutkamperlaag just before and directly after closure of the Lauwerszce: near Oude Westgat (a), Meetpaal (b), Roodc Hoofd (c) and Lauwersoog (d) (see for locations Figure 6.5).

the sediments are also reworked in the shallow areas due to the stirring activity of short waves (Figure 6.17b). However, these sediments are mainly transported in onshore (!) direction due to short waves (see also Biegel & Hoekstra, 1995). An indication of this transport mechanism is the observed net sedimentation higher up in the profile (cf. Figure 6.10b). Furthermore, wave-driven currents also contribute to the longshore redistribution of sediments along the coast.

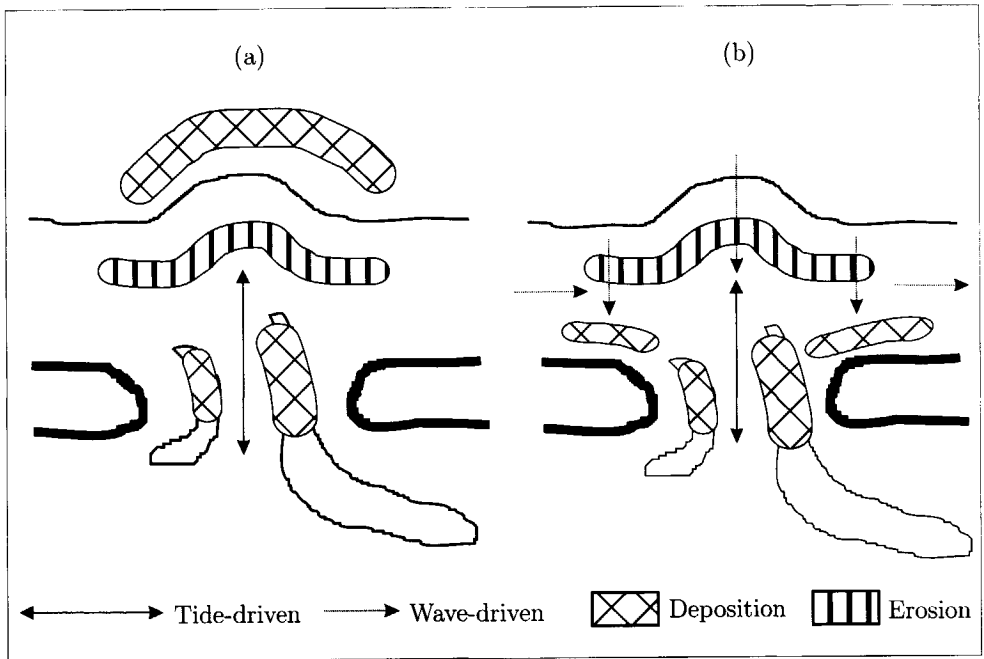


**Figure 6.17:** Conceptual diagram of the morphological behaviour in the Friesche Zeegat: (a) present modelling approach without wave-driven transport, and (b) in reality with wave-driven transport.

### 6.6.2 Tidal basin

The reduction of the backbarrier area explains the observed and computed deposition of sand and mud in the main channel of the basin directly after closure (Figure 6.16). The bed shear stress in the main channel strongly decreases (cf. Figure 6.16b-c), which results in the sand deposition near the entrance. Furthermore, mud deposition is also favoured by the smaller bed shear stress, in particular in the vicinity of the former Lauwerszee (cf. Figure 6.16d). In this area, the bed shear stress is less than the critical erosion shear stress. Therefore, only mud deposition occurs during the tidal period, resulting in strong mud deposition in the main channel near the former Lauwerszee.

Two important differences are found when the observations are compared with the model results. Firstly, the observations suggest a decreasing net sedimentation rate in the period 1970 - 1994, whereas the model predicts an almost constant sedimentation rate through time (Figure 6.12a). Secondly, the thickness of the computed mud layers in the main channel (cf. Figure 6.14) is (much) smaller than the observed mud deposition in the cores (Figure 6.3). These model shortcomings are discussed separately below:

### Long-term net sedimentation rate

The long-term changes in the tidal characteristics are important to understand the observed and computed long-term morphological behaviour in the basin. Therefore, the most important tidal characteristics along the main channel are shown in Figure 6.18 for three different bathymetries: the measured bathymetry of 1970 and 1992 and the bathymetry in 1992 as computed with the morphological model. For convenience, the locations of two stations are indicated in Figure 6.18a. In Section 6.4.1, it was shown that the observed water level and current velocity characteristics in 1992 are reproduced rather well with the flow model (Section 6.4.1). Furthermore, the observed and computed water level characteristics in 1970 agreed reasonably well. Unfortunately, the current velocity characteristics in 1970 could not be verified by lack of data. It is assumed that these characteristics give a good representation at that moment, too.

From the computed results with observed bathymetry of 1970 and 1992, the tidal characteristics along the main channel in the period 1970 - 1992 can be analysed (Figure 6.18). The  $M_2$ -amplitude of the water level only slightly changed near the head of the basin (Figure 6.18a), whereas the  $M_2$ -phase of the water level increased in the entire main channel (Figure 6.18b). The current velocity characteristics indicate that the  $M_2$ -amplitude of the current velocity mainly increased along the main channel in the period 1970 - 1992 (Figure 6.18c). Furthermore, the current velocity in the main channel between 8 - 18 km became more ebb-dominant in that period (Figure 6.18d).

The tidal characteristics with the computed bathymetry in 1992 differ from those with the observed bathymetry in 1992 (Figure 6.18). Firstly, the  $M_2$ -amplitude and the  $M_2$ -phase of the water level are smaller throughout the entire main channel and in particular near the landward end (Figure 6.18a-b). Secondly, the  $M_2$ -amplitude of the current velocity is much smaller in almost the entire channel (Figure 6.18c). Finally, the current velocity is predominantly flood-dominant with the computed bathymetry in 1992, whereas this section is ebb-dominant with the measured bathymetry in 1992 (Figure 6.18d).

The differences in water level characteristics and current velocity amplitude along the main channel between the computed and observed bathymetry in 1992 (Figure 6.18a-c) are consistent with the volume changes by depth (Figure 6.12b). It follows that the model overestimates the sedimentation in the intertidal area between -2 and 0 m NAP and underestimates the sedimentation in the channels between -5 and -10 m NAP. Thus, the channels in the numerical model remain relatively too deep in the numerical model. Because of this, the amplification of the  $M_2$ -amplitude is too small and the tidal propagation is too fast throughout the main channel (cf. Figure 6.18a-b). Furthermore, the lower current velocity amplitude in the computations also follows directly from the relatively deeper channels in the model (Figure 6.18c).

The difference in the relative phase between the computed and observed bathymetry in 1992 is less obvious (Figure 6.18d). A useful analytical model to explain this difference is the proposed 'lumped-parameter model' by Van de Kreeke and Dunsbergen (2000). In their analytical model,

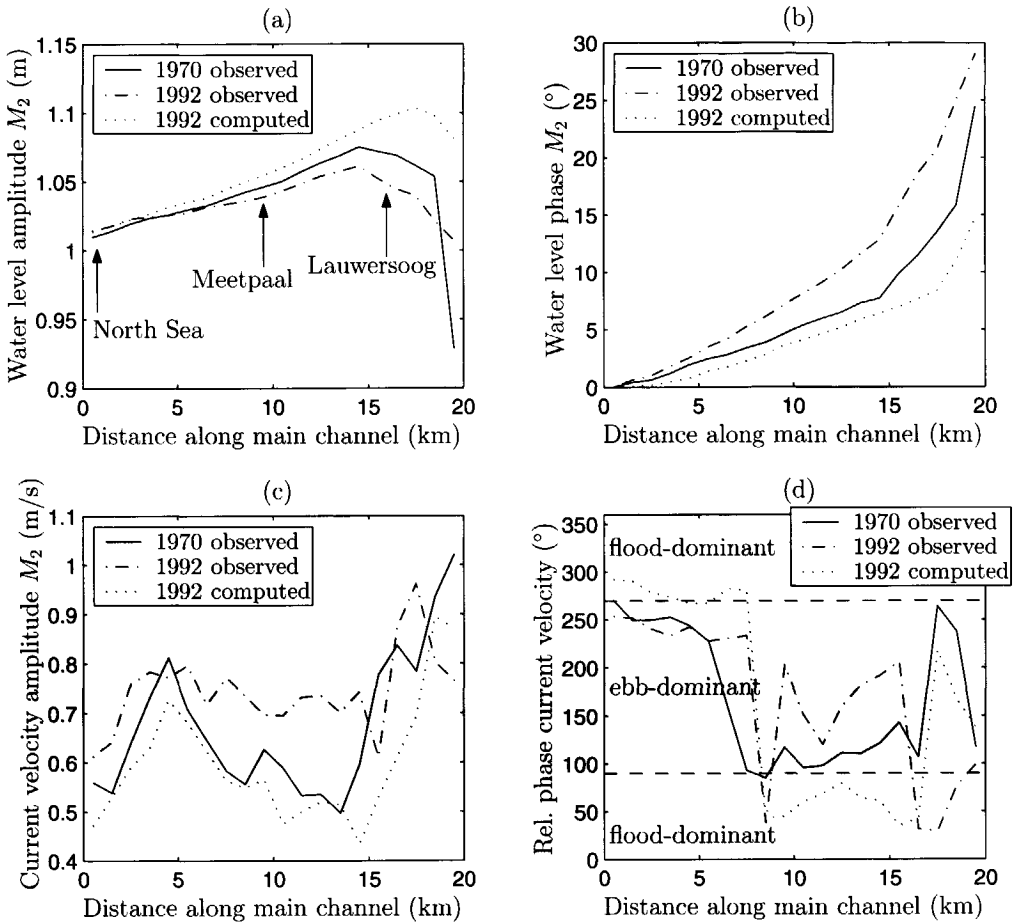


**Figure 6.18:** Tidal characteristics along the main channel of the Zoutkamperlaag with the observed bathymetry of 1970, the observed bathymetry of 1992 and the computed bathymetry of 1992 (see Figure 6.5 for locations).

the Friesche Zeegat is simplified to a single prismatic channel connecting the basin with the North Sea. The water level in the basin ( $\eta_b$ ) itself fluctuates uniformly and the hypsometry, i.e. the surface area ( $A_b$ ) against the water level, is linear:

$$A_b(t) = A_{b0} + C\eta_b \tag{6.3}$$

where  $A_{b0}$  is the surface area at mean water level and  $C$  the rate of change of the surface area  $A_b$  with the water level  $\eta_b$ . Van de Kreeke and Dunsbergen (2000) derive analytical expressions for the water level and current velocity characteristics in the basin. It is shown that the computed relative phase of the current velocity (197 $^\circ$ ) is a reasonable approximation of the observed phase

difference ( $218^\circ$ ) in the main channel of the Friesche Zeegat.

This lumped-parameter model is applied to the three bathymetries as discussed previously in this section. An estimate is made of the relative phase of the current velocity in the main channel (Table 6.13). Three different bathymetries are examined: the observed geometry in 1970 and 1992 and the computed geometry in 1992 (cf. Figure 6.18d). For each bathymetry, the surface area at the mean water level ( $A_{b0}$ ) and the rate of change of the surface area ( $C$ ) in eq. (6.3) are computed and listed in Table 6.13. The other parameters in the lumped parameter model are not changed.

**Table 6.13:** Relative phase of the current velocity ( $\varphi_1 - 2\varphi_2$ ) computed with the lumped-parameter model with three different bathymetries: the observed bathymetry of 1970, the observed bathymetry of 1992 and the computed bathymetry of 1992 (cf. Figure 6.18d).

| Bathymetry    | $A_{b0}$ ( $10^9$ m <sup>2</sup> ) | $C$ ( $10^9$ m) | $\varphi_1 - 2\varphi_2$ ( $^\circ$ ) |
|---------------|------------------------------------|-----------------|---------------------------------------|
| 1970 observed | 96                                 | 40              | 186                                   |
| 1992 observed | 93                                 | 39              | 182                                   |
| 1992 computed | 104                                | 36              | 21                                    |

The relative phase of the current velocity according to the lumped-parameter model (Table 6.13) corresponds quite well with the results in Figure 6.18d: the main channel of the basin (8 - 20 km) is flood-dominant with the computed bathymetry of 1992, whereas the observed bathymetries of 1970 and 1992 resulted in an ebb-dominant main channel. According to the lumped-parameter model, the change in the relative phase directly results from the changes in the hypsometry. Unfortunately, these changes are not correctly predicted with the morphological model (Table 6.13). Compared with the initial geometry in 1970, the computed geometry in 1992 shows an increase in the surface at the mean water level  $A_{b0}$ , whereas it decreases according to the observed geometry in 1992. In addition, the decrease of the rate of change  $C$  is too large in the morphological computations.

The difference between the observed ebb-dominance and computed flood-dominance in the main channel may explain the difference between the observed and computed long-term morphological behaviour (Figure 6.12a). The observations suggest a decreasing sediment import in time, whereas the import of sand and mud appears to be almost constant in the model results. The current velocity in the main channel shifts towards ebb-dominance with the measured geometries, which results in a decreasing import of sediment. The computed geometry in 1992, however, shows the opposite tendency and tends towards a more flood-dominated channel. Consequently, the computed sediment import into the basin is not likely to decrease.

Notice that the assumed relationship between the current velocity dominance and the net sediment transport direction is only valid for relatively coarse sediment, i.e. sediment that (almost) instantaneously adapts to the changing flow conditions (cf. Van de Kreeke & Robaczewska,

1993). In the Friesche Zeegat case, the validity of this assumption can be estimated for sand and mud separately by comparing the settling time ( $h/w_i$ ) of each fraction to the tidal period ( $T$ ). With a water depth  $h$  equal to 10 m, the settling time for sand is about fifteen minutes, whereas the settling time for mud equals three hours (see also Table 6.3). Consequently, the assumption of instantaneous transport is a good approximation for suspended sand, but is not true for mud in suspension. Nevertheless, the computed imported of sand into the basin is the major part ( $\pm 80\%$ ) of the total sediment import (cf. Table 6.10). Therefore, this sediment fraction largely determines the morphological changes in the basin.

### Thickness of the deposited mud layers

Another important difference in the computations is the amount of mud deposited in the main channel: the thickness of the observed mud layers appears to be in the order of meters, whereas the computed mud deposition in the reference computation is at most one meter. Because of this, several sensitivity computations have been carried out with an initial variation in bed composition, a space-varying mud concentration along the open sea boundaries, a spring-neap cycle and a higher critical deposition shear stress for mud. The largest effect on the thickness of the mud layers is found with a higher critical deposition shear stress. The maximum thickness of the mud layers in this computation appears to be 1.5 m. Furthermore, the computation with the initial mud distribution indicates that re-distribution of mud in the basin itself may be an explaining factor for the mud layers in the main channel. The amount of deposited mud in the basin becomes twice as high compared with the reference computation due to net mud erosion from the nearby intertidal areas. The importance of this mechanism is qualitatively in line with the observations of Winkelmolens and Veenstra (1974). Based on a grain size analysis, they conclude that the muddy sediments in the main channel near the Lauwerszee are similar to those at the nearby intertidal area in the basin.

Although the mud layer thickness in the main channel becomes a bit more realistic in the sensitivity computations, it is still much smaller than observed. Various explanations can be put forward to explain these differences like for instance uncertainties in the measurements, the hydrodynamic forcing, the model formulations and the parameter settings. Only the parameter settings are discussed in more detail:

- The sensitivity of four model settings has been investigated separately, whereas a combination is not considered. For instance, let us consider the effect of a higher mud concentration at the boundary and a higher critical deposition shear stress. This combination will surely result in a larger thickness of the mud layers in the main channel compared with the separate sensitivity computations (cf. Figure 6.14). Additionally, the sensitivity of other parameter settings, which have not been investigated, will possibly also increase the amount of deposited mud, like for instance a higher critical shear stress for erosion and a lower erosion rate (cf. Table 6.3).

- An underestimation of the mud availability in the system itself may also explain the relatively small mud deposition in the basin. One computation was carried out with an initial mud content of 10% in the bed of the intertidal area of the basin, whereas the initial bed in all other computations consisted of sand only. As was shown, an initial mud content of 10% on the intertidal area of the basin resulted in a 40% higher (gross) mud deposition compared with an initial sand bed (cf. Table 6.12). The initial variation in mud content, however, is poorly known and a higher initial mud content will definitely lead to an enhancement of (gross) mud deposition in the basin. Another possible mud source, which is not investigated in this study, is the sediment bed of the cbb-tidal delta. Although the mud content in this area is relatively low ( $< 5\%$ ), this area may have functioned as an important source of mud, too

### 6.6.3 Perspectives of model applicability

Despite the presented model shortcomings, the sand-mud model has proven to be a successful tool for increasing the understanding and the predictive capabilities of large-scale sand-mud segregation in estuaries and tidal basins. The application of the model to the idealised systems in Chapter 5 has revealed that sharp transitions exist in tidal systems between areas with high mud content and areas with low mud content when the mud deposition capacity is relatively low (i.e.  $w_m c_m / M \ll 1$ ). Furthermore, the verification of the results with observations in this chapter has demonstrated that the import and distribution of sand and mud in the basin are reasonably well predicted. Although further verification is needed, these results suggest that the model can be applied as a first step to estimate the effects of human interventions and/or natural changes on the large-scale distribution of sand and mud in tidal basins and estuaries.

Three important restrictions of the model applicability are that:

- the effect of the sediment concentration on the turbulent water motion has to be negligible;
- the bed has to consist of a nearly uniform sand fraction and a mud fraction with a constant clay/silt ratio;
- the consolidation process does not have to be taken into account explicitly;

These restrictions have important implications for its applicability in estuaries and tidal basins. The first limitation means that the model is not adequate for modelling turbidity maxima and turbidity currents. The feedback between the water motion and the sediment concentration is generally very important in these phenomena. The restriction of a constant clay/silt ratio in the mud fraction implies that different mud sources in a system (e.g. marine/fluvial mud) should have the same clay/silt ratio. The absence of a consolidation module limits the applicability to systems in which the erosion properties of the bed are more or less the same in time and space. Thus, the model is less suited for systems in which both 'consolidated' mud and 'fresh' mud play an important role.

Finally, it is emphasised that the applicability of the sand-mud model is not limited to estuaries and tidal basins only. In principle, it can be used for other water systems as long as the aforementioned restrictions are fulfilled. Interesting areas in which the distribution of sand and mud is generally encountered, are coastal seas, floodplains in rivers and reservoirs in mountain areas. Based on the presented results, the model can be a powerful tool to investigate the phenomenon of large-scale sand-mud segregation in these areas.

## 6.7 Conclusions

The process-based sand-mud model has been applied to a realistic case, viz. The Friesche Zeegat, a tidal basin in the Dutch Wadden Sea. A substantial amount of sand and mud has been deposited in the basin of the Zoutkamperlaag after a partial closure of that basin in 1969. Firstly, the bed level and bed composition development has been described. Next, the model set-up has been discussed and the flow and short wave results have been calibrated and verified against field measurements. Finally, long-term morphological computations have been performed over the period 1970 - 1994 and the results have been compared with bed level and bed composition measurements. The following conclusions can be drawn:

- Detailed information on the bed level development is available for the period 1970 - 1994. The observations indicate that the ebb-tidal delta eroded in the period 1970 - 1994 ( $-27.4 \times 10^6 \text{ m}^3$ ), whereas net deposition occurred in the basin of the Zoutkamperlaag ( $+41.7 \times 10^6 \text{ m}^3$ ). Apart from the sediments derived from the ebb-tidal delta, the sediment surplus in the basin ( $+14.3 \times 10^6 \text{ m}^3$ ) is explained by import of mud from the North Sea and/or sand import from the adjacent coastal areas.
- Information on the bed composition development is scarce. Nevertheless, a qualitative comparison of two maps with the surface composition indicates that the composition pattern in the intertidal area in 1950 - 1955 is more or less equal to that in 1994. Furthermore, an analysis of the lithology of several cores in the main channel of the basin has revealed three important characteristics. Firstly, an abrupt change in mud content is observed around the bed level of 1967/1970. Secondly, the mud content at the bed surface gradually decreases in time after 1970. Thirdly, mud deposition in the main channel is mainly concentrated near the dike of the Lauwerszee.
- The flow model with the measured bathymetry in 1992 has been calibrated against observed water level characteristics in the main channel of the Friesche Zeegat in 1992. The mean discrepancy between the observed and computed  $M_2$ -amplitude,  $M_2$ -phase and  $M_4$ -amplitude is minimal for a Manning coefficient  $n = 0.021 \text{ s/m}^{1/3}$ . With this calibrated roughness parameter, the current velocity amplitudes and phases of the  $M_2$  and  $M_4$ -constituents appear to be reproduced rather well by the model. According to both observations and the model results, the main channel in 1992 is ebb-dominant.



- Without calibration, the short-wave model has been verified against the observed significant wave height and peak period in the main channel of the Friesche Zeegat in 1995. The observed and computed significant wave height agree well ( $R^2 = 0.95$ ) and the agreement of the peak period is fair ( $R^2 = 0.75$ ), be it that it is consistently underpredicted by the model.
- The long-term results of the morphological computations have shown several similarities and discrepancies between the observed and computed bed level and bed composition development in the period 1970 - 1994. The observed deposition of sand in the main channel of the ebb-tidal delta, the deposition of sand at the entrance of the channel in the basin, the strong deposition of mud in the channel near the Lauwerszee and the overall horizontal mud content pattern are all reproduced by the numerical model. However, the decreasing sedimentation rate in the basin, the net erosion of the entire ebb-tidal delta after closure and a realistic thickness of the mud layers in the main channel of the basin are not found with the model.
- A sensitivity analysis has shown that the thickness of the mud layers in the main channel of the basin increases with an increasing mud concentration near the coast, a higher critical deposition shear stress and an initial mud content of 10% at the intertidal area in the basin. Except for the spring-neap cycle, the thickness of the mud layers becomes a bit more realistic compared with the observations, but it is still much smaller than observed.
- An analysis of the morphological computations has given several explanations for the differences between the observed and computed behaviour. Firstly, the discrepancy in behaviour of the ebb-tidal delta is likely to be the result of neglecting wave-driven currents. Secondly, the absence of a decreasing import rate in the basin is presumably caused by the poor prediction of the changes in the hypsometry of the basin. As a consequence of this, the computed current velocity asymmetry in the main channel tends towards flood dominance, whereas the observations indicate that the system becomes more ebb-dominant. Thirdly, possible reasons for the relatively small thickness of the computed mud layers in the main channel are that i) the sensitivity analysis has been carried out for a limited number of conditions and parameters separately, and ii) the mud sources in the system itself have been underestimated.



## Chapter 7

### Conclusions and recommendations

This thesis concerns the phenomenon of large-scale sand-mud segregation in estuaries and tidal basins. The three research objectives, as introduced at the beginning of this thesis, are addressed as follows:

- A conceptual framework is given to characterise sand-mud segregation and to set up a process-based sand-mud model. This framework includes an overview of large-scale bed composition measurements in Dutch tidal systems. Important characteristics with respect to sand-mud patterns are discussed. Furthermore, relevant sediment transport processes and mechanisms behind sand-mud segregation are summarised. The possibilities and limitations of the currently used models and concepts are reviewed with respect to predicting bed composition variations.
- A prerequisite for a process-based sand-mud model is an erosion formulation for sand-mud mixtures. A scheme is proposed to classify the erosion behaviour of these mixtures and erosion formulations are derived. Both the classification and the formulations are validated against laboratory and field experiments. Next, a process-based morphological sand-mud model is presented in which temporal and spatial mud content variations are included. A numerical prototype of this model is developed by extending the three-dimensional software package Delft3D from WL|Delft Hydraulics.
- Morphological evolution, including the effect of large-scale sand-mud segregation, is investigated by means of numerical experiments with the process-based sand-mud model. Three idealised situations are studied: a local situation, a reservoir and a short tidal basin. Time and length scales are derived that govern the distribution of sand and mud in these situations. Moreover, the results are qualitatively compared with field data. The Friesche Zeegat (the Netherlands) is taken as a real-world case to study the morphological response after closure of the Lauwerszee (1969). The computed long-term bed level and bed composition development of this tidal basin in the period 1970 - 1994 are quantitatively compared with field data.

The conclusions drawn from this research are summarised in Section 7.1. Next, further research steps are discussed in Section 7.2.

## 7.1 Conclusions

### Processes and parameters behind sand-mud segregation

- An analysis of bed composition data in Dutch tidal systems reveals two important characteristics with respect to the phenomenon of sand-mud segregation. The sediment composition in these systems is characterised by a poorly sorted sand fraction ( $\%0.063 - 2$  mm) and a mud fraction ( $\% \leq 0.063$  mm) with a constant ratio between silt ( $\%0.004 - 0.063$  mm) and clay ( $\% < 0.004$  mm). Furthermore, sand-mud patterns are observed at a wide range of (horizontal) spatial scales. These characteristics are not unique, but appear to occur in tidal systems all over the world.
- A literature survey demonstrates that local processes directly affecting the segregation of sand and mud, are erosion and deposition at the bed surface, and mixing in the sediment bed itself, e.g. due to bioturbation. Key parameters in these processes are the exerted bed shear stress, the critical shear stress for erosion and deposition, the sediment concentration, the settling velocity, the erosion coefficient and the mixing coefficient in the sediment bed itself.
- An analysis of these local processes provides an expression for the (tidally-averaged) equilibrium mud content at the bed surface, in which case the mud deposition flux is equal to the mud erosion flux, averaged over one tidal period. The time interval for reaching this equilibrium depends on the ratio between the time scale of bed level changes and mixing. The equilibrium value itself depends on the ratios between the bed shear stress amplitude and the critical shear stress for erosion ( $\hat{\tau}_b/\tau_e$ ) and deposition ( $\hat{\tau}_b/\tau_d$ ), and the ratio between the mud deposition and mud erosion capacity ( $w_m c_m/M$ ).

### Development and validation of a process-based sand-mud model

- A classification is proposed for the erosion behaviour of sand-silt-clay mixtures. A clay content of 5 - 10% governs the transition between non-cohesive and cohesive erosion behaviour of these mixtures. Transitions in the erosion behaviour also have to be expected when the network structure is built by another sediment fraction. This transition depends on the volume content of each sediment fraction. The transition between non-cohesive and cohesive behaviour at 5 - 10% clay content is validated by a re-analysis of several laboratory and field experiments. The use of a 'critical mud content' for this transition is not generic, but practical because of the constant clay/silt ratio in a specific tidal system.
- Based on the aforementioned classification, erosion formulations are derived for non-cohesive and cohesive sand-mud mixtures. For each of these mixtures, equations are presented for the bed load transport rate of sand, and the erosion fluxes of suspended

sand and mud, as a function of the mud content at the bed surface. Comparison with a limited number of erosion experiments shows that these formulations can be used as a first step in a process-based sand-mud model.

- A three-dimensional process-based morphological sand-mud model is developed. This model extends the currently used morphological models in several ways. The erosion characteristics of sand and mud depend on the composition of the bed surface. Moreover, the temporal and spatial variations in bed composition depend on the exchange of sand and mud between the water column and the sediment bed, and on local mixing processes in the sediment bed itself.

The performance of the sand-mud model, with emphasis on the segregation of sand and mud, is tested qualitatively through numerical experiments for three idealised situations: a local situation, a reservoir and a short tidal basin.

- The computed equilibrium mud content in the local situation turns out to enclose observed mud content data at a large number of locations on the Molenplaat, an intertidal flat in the Westerschelde estuary (the Netherlands).
- The occurrence and the shape of the initial sedimentation patterns of sand and mud in the reservoir case are validated qualitatively with the sediment balance in the Noordelijk Deltabekken (the Netherlands) after closure of the Haringvliet Sluices (1970).
- The bed level and bed composition profiles in the equilibrium state of the tidal basin agree qualitatively with those found in the tidal basins of the Dutch and German Wadden Sea.

The predictive capabilities of the sand-mud model are investigated more quantitatively in a real-life application to the Friesche Zeegat (the Netherlands) after the closure of the Lauwerszee (1969).

- The hydrodynamic field data and model results in the 1990's agree reasonably. Two important characteristics of the tidal asymmetry are also found from the model simulations: the asymmetric water level variation offshore shifts towards a symmetric variation in the basin, and the current velocity in the main channel is ebb-dominant. Furthermore, the observed and computed significant wave height agree well ( $R^2 = 0.95$ ). The agreement of the peak periods is reasonable ( $R^2 = 0.75$ ), be it that they are consistently underpredicted by the model.
- The computed volume changes in the basin as a function of depth agree qualitatively with the observations in the period 1970 - 1994. The observed net erosion in the ebb-tidal delta just after the closure and the observed decreasing import rate in the basin in the

period 1970 - 1994 are not predicted correctly. Presumably, the discrepancies between field observations and model results are caused by the omission of wave-driven sediment transport in the ebb-tidal delta and a poor quantitative prediction of the sediment exchange between channels and flats in the basin.

- The computed spatial distribution of sand and mud in the Friesche Zeegat appears to be realistic. The ebb-tidal delta and the entrance of the basin are dominated by sand, whereas mud is found in the main channel near the Lauwerszee and in the shallow areas near the borders of the basin. However, the model underestimates the thickness of the mud layers in the main channel. Explanations for this underestimation appear to be uncertainties in mud parameters (e.g. critical shear stress for deposition) and the role of other mud sources (e.g. erosion of mud from the intertidal areas).

### **Bed level and bed composition behaviour in systems with sand and mud**

- The analysis of the local situation reveals that sharp transitions exist in tidal systems between areas with high mud content and areas with low mud content when the mud deposition capacity is relatively low (i.e.  $w_m c_m / M \ll 1$ ). When the bed shear stress amplitude is lower than the critical erosion shear stress, net mud deposition occurs and the bed is (potentially) muddy. For higher bed shear stress, net mud deposition is almost completely absent and the bed is sandy. The transition between sandy and (potentially) muddy areas is expected to be more gradual for higher values of the mud deposition capacity, e.g. suspended sediment concentration.
- The initial morphological behaviour in the reservoir and in the tidal basin shows two separate deposition waves of sand and mud. This initial separation is directly related to differences in sediment properties (i.e. the settling velocity and the critical shear stress for deposition), whereas the relatively small deposition capacity is important in the tidal basin, too. The shape of the mud deposition wave in the reservoir turns out to be determined by two length scales: a 'settling length scale' and a 'flow length scale'. These length scales are related to the settling process of suspended mud in a unidirectional, decreasing current. Based on these length scales, a clear distinction is found between areas with low mud content due to a relatively high bed shear stress ('flow-limited') and due to a low mud concentration in the water column ('supply-limited').
- When compared to the situation with sand only, the long-term morphological behaviour of the reservoir and tidal basin with sand and mud gives rise to two opposing observations. On the one hand, the presence of mud reduces the morphological adaptation time scale. This reduction is not only caused due to the extra availability of sediment, but

high mud deposition rate near the head of the basin plays a role, too. On the other hand, the bed level profile in the equilibrium state is quite similar to the equilibrium bed level profiles for sand only. The relatively strong hydrodynamic forcing (i.e.  $\tau_b \gg \tau_e$ ) and the relatively small mud deposition capacity (i.e.  $w_m c_m / M \ll 1$ ) result in a predominantly sandy bed surface in the equilibrium state.

- The application to the Friesche Zeegat indicates that sand and mud both contribute significantly to the morphological changes in the tidal basin. The application also shows that morphological changes within the system drastically affect the available amount of mud. These results highlight that both sand and mud, and their interaction, should be considered to understand and predict the long-term morphological behaviour of these systems.

In summary, the present research has resulted in an increased understanding of and greater modelling capabilities for large-scale sand-mud segregation in estuaries and tidal basins. A process-based model for sand and mud has been developed in which temporal and spatial mud content variations are taken into account. A good qualitative agreement has generally been obtained between model results and field data. The analysis of systems with sand and mud has revealed that sharp transitions between sandy and (potentially) muddy areas occur when the mud deposition capacity is relatively low. These results demonstrate that the process-based sand-mud model is a step forward to a better understanding and modelling of sand-mud segregation in estuaries and tidal basins.

## 7.2 Recommendations

- Bed level and bed composition data are necessary to validate the predictive capabilities of the process-based sand-mud model. Such validation is crucial before using this model as a predictive tool for management issues. In the Netherlands, a good possibility in the nearby future may be to track the changes in bed level and bed composition in the Haringvliet - Hollandsch Diep, if and when a new management strategy of the Haringvliet Sluices is effectuated. In addition to the bed level, determination of the mean sand grain size, mud content and clay/silt ratio is sufficient to characterise the sediment bed.
- The validity of the process formulations in the present model partly determines its predictive capabilities. In particular, the erosion formulations for sand-mud mixtures are weakly validated because of a lack of data. Therefore, it is recommended to perform erosion experiments with sand-mud mixtures in the full range between sand and mud, so as to validate and/or improve the proposed erosion formulations in this thesis. During these experiments, attention should be paid to the network structure, the cohesive

properties and the clay/silt ratio of the sediment mixture.

- Analysis of idealised situations with the process-based model appears to be a successful way to increase the understanding of large-scale sand-mud segregation in estuaries and tidal basins. Such an analysis can be further extended by investigating different types of forcing, incorporating other processes and applying different geometries. In the case of a short tidal basin, for instance, including an overtide, adding biological processes and starting with a two-dimensional bathymetry should be considered.
- The first application to the realistic case 'Friesche Zeegat' has shown that the predictive capabilities of the morphological model are promising. However, several discrepancies between modelled and observed behaviour were found in the ebb-tidal delta and within the basin. In the ebb-tidal delta, a significant improvement of the predictive capabilities of the model is expected when wave-induced sediment transport is included. The sediment exchange between channels and flats should be further examined to improve the predicted long-term morphological behaviour in the basin.
- In all cases, the process-based model has been applied with long-term mean conditions at the boundaries. In reality, however, the boundary conditions strongly vary in time and space. Hence, it is recommended to apply the model to other tidal systems with well-documented bed level and bed composition variations in time and space. Special attention should be paid to the role of episodic events (e.g. storms, river discharge variations) in the large-scale distribution of sand and mud.
- Although the focus has been on estuaries and tidal basins, the sand-mud model can be used for other water systems as well. An important restriction is that the sediments can be modelled as two fractions: a uniform sand fraction and a mud fraction with a constant clay/silt ratio. Interesting systems in which the distribution of sand and mud can be investigated with this model, are coastal seas, floodplains along rivers and reservoirs in mountain areas.

The overall perspectives with respect to the understanding and modelling of sand-mud segregation are promising. The understanding of large-scale sand-mud segregation can be further increased by extending the analysis of idealised situations and applying the process-based sand-mud model to new realistic cases with abundant field data. To increase its predictive capabilities, it is recommended to improve the erosion formulations of sand-mud mixtures via laboratory experiments.



## References

- Allersma, E. (1988a). *Morfologisch onderzoek Noordelijk Deltabekken. Morfologische model-  
lering deel IV: Samenstelling en dichtheid van sedimenten (in Dutch)* (Report Z71.03).  
Delft: WL|Delft Hydraulics.
- Allersma, E. (1988b). *Morfologisch onderzoek Noordelijk Deltabekken. Morfologische model-  
lering deel I: Inleiding en Samenvatting (in Dutch)*. (Report Z71.03). Delft: WL|Delft  
Hydraulics.
- Alvarez-Hernandez, E. M. (1990). *The influence of cohesion on sediment movement in channels  
of circular cross-section*. PhD thesis, University of New Castle upon Tyne, New Castle  
upon Tyne.
- Armanini, A. (1995). Non-uniform sediment transport: dynamics of the active layer. *Journal  
of Hydraulic Research*, 33(5), 611-622.
- Aubrey, D. G. (1986). Hydrodynamic Controls on Sediment Transport in Well-Mixed Bays and  
Estuaries. In J. Van de Kreeke (Ed.), *Lecture Notes on Coastal and Estuarine Studies,  
Physics of Shallow Estuaries and Bays* (pp. 245-258). Berlin: Springer-Verlag.
- Bakker, W. T., & Van Kesteren, W. G. M. (1998). Pick-up function for sediment under high  
shear-conditions. In H. Kim, S. H. Lee, & S. J. Lee (Eds.), *Proceedings 3rd International  
Conference On Hydrodynamics, Seoul, Korea* (pp. 535-540). UIAM Publishers.
- Berlamont, J., Ockenden, M., Toorman, E., & Winterwerp, J. (1993). The characterisation of  
cohesive sediment properties. *Coastal Engineering*, 21, 105-128.
- Biegel, E., & Hockstra, P. (1995). Morphological response characteristics of the Zoutkam-  
perlaag, Frisian inlet (The Netherlands), to a sudden reduction in basin area. *Special  
Publications International Association Sedimentology*, 24, 85-99.
- Bisschop, F. (1993). *Erosieproeven op zand met variatie in doorlatendheid (in Dutch)* (Com-  
binatie Speurwerk Baggertechniek BAGT510 No. J714). Delft: WL|Delft Hydraulics.
- Blom, A. (2003). *A vertical sorting model for rivers with non-uniform sediment and dunes*.  
PhD thesis, Twente University, Enschede.
- Blom, A., Parker, G., & Ribberink, J. S. (2001). Vertical exchange of tracers and non-uniform  
sediment in dune situations. In S. Ikeda (Ed.), *IAHR Proceedings of the River, Coastal  
and Estuarine Morphodynamics Conference, Obihiro, Japan* (pp. 207-216).
- Booij, N., Ris, R. C., & Holthuijsen, L. H. (1999). A third-generation wave model for coastal

- regions, 1. Model description and validation. *Journal of Geophysical Research*, 104 (C4), 7649–7666.
- Boudreau, B. P. (1997). *Diagenetic Models and Their Implementation. Modelling Transport and Reactions in Aquatic Sediments*. Berlin: Springer-Verlag.
- Chesher, T. J., & Ockenden, M. C. (1997). Numerical modelling of mud and sand mixtures. In N. Burt, R. Parker, & J. Watts (Eds.), *Cohesive sediments, Proceedings of the 4th Nearshore and Estuarine Cohesive Sediment Transport Conference* (pp. 367–381). John Wiley & Sons Ltd.
- De Bake, D. (2000). *Zand-slibsegregatie in de Westerschelde (in Dutch)*. Msc. thesis, Delft University of Technology, Delft.
- De Boer, D. H. (1992). Hierarchies and spatial scale in process geomorphology: a review. *Geomorphology*, 4, 303–318.
- De Glopper, R. (1967). Over de bodemgesteldheid van het waddengebied (in Dutch). In *Van Zee tot Land (43)*. Zwolle: Tjeenk Willink.
- De Groot, A. J., Zschuppe, K. H., & Salomons, W. (1982). Standardization of methods for analysis heavy metals in sediments. *Hydrobiologia*(92), 689–695.
- Deigaard, R., Drønen, N., Fredsøe, J., Hjelmager Jensen, J., & Jørgensen, M. P. (1999). A morphological stability analysis for a long straight barred coast. *Coastal Engineering*, 36, 171–195.
- De Meijer, R. J., Stapel, C., Jones, D. G., Roberts, P. D., Roozendaal, A., & MacDonald, W. G. (1996). Improved and new uses of natural radioactivity in mineral exploration and processing. *Exploration and Mining Geology*, 6, 105–117.
- De Vriend, H. J. (1991a). Mathematical modelling and large-scale coastal behaviour Part 1: Physical processes. *Journal of Hydraulic Research*, 29(6), 727–740.
- De Vriend, H. J. (1991b). Mathematical modelling and large-scale coastal behaviour Part 2: Predictive models. *Journal of Hydraulic Research*, 29(6), 741–753.
- Dronkers, J. (1986a). Tide-Induced Residual Transport of Fine Sediment. In J. Van de Kreeke (Ed.), *Lecture Notes on Coastal and Estuarine Studies, Physics of Shallow Estuaries and Bays* (pp. 228–244). Berlin: Springer-Verlag.
- Dronkers, J. (1986b). Tidal asymmetry and estuarine morphology. *Netherlands Journal of Sea Research*, 20(2/3), 117–131.
- Dunsbergen, D. (1995). *Verification set Friesche Zeegat. October 1, 1992 - November 17, 1992 (RIKZ-95.035)*. Den Haag: National Institute for Coastal & Marine Management.
- Dyer, K. R. (1986). *Coastal and Estuarine Sediment Dynamics*. Chichester: John Wiley & Sons.
- Dyer, K. R. (1994). Estuarine sediment transport and deposition. In K. Pye (Ed.), *Sediment Transport and Depositional Processes* (pp. 193–218). Edinburgh: Blackwell Scientific Publications.
- Dyer, K. R. (1997). *Estuaries; a physical introduction*. Chichester: John Wiley & Sons.

- Dyer, K. R., Christie, M. C., & Wright, E. W. (2000). The classification of intertidal mud flats. *Continental Shelf Research*, 20, 1039-1060.
- Emery, K. O. (1967). Estuaries and Lagoons in Relation to Continental Shelves. In G. H. Lauff (Ed.), *Estuaries* (pp. 9-11). Washington: American Association for the Advancement of Science.
- Flemming, B. W. (2000). A revised textural classification of gravel-free muddy sediments on the basis of ternary diagrams. *Continental Shelf Research*, 20, 1125-1137.
- Flemming, B. W., & Nyandwi, N. (1994). Land reclamation as a cause of fine-grained sediment depletion in backbarrier tidal flats (Southern North Sea). *Netherlands Journal of Aquatic Ecology*, 28(3-4), 299-307.
- Flemming, B. W., & Ziegler, K. (1995). High-resolution grain size distribution patterns and textural trends in the backbarrier environment of Spiekerroog Island (Southern North Sea). *Senckenberg Maritima*, 26, 1-24.
- Folk, R. L. (1954). The distinction between grain size and mineral composition in sedimentary-rock nomenclature. *Journal of Geology*, 62, 344-359.
- Förstner, U., & Wittmann, G. T. W. (1979). *Metal Pollution in the Aquatic Environment*. Berlin: Springer Verlag.
- Galappatti, R., & Vreugdenhil, C. (1985). A depth-integrated model for suspended sediment transport. *Journal of Hydraulic Research*, 23(4), 359-377.
- Groen, P. (1967). On the residual transport of suspended matter by an alternating tidal current. *Netherlands Journal of Sea Research*, 3/4, 564-574.
- Haring, J. C. (1977). *De geschiedenis van de ontwikkeling van de waterbeweging en het profiel van de rivieren in het Noordelijk Deltabekken over de perioden 1870 - 1970 - 1976, Deel I - De periode 1870 - 1970 (in Dutch)*. (Tech. Rep.). Rijkswaterstaat, Directie Waterhuishouding en Waterbeweging.
- Haring, J. C. (1978). *De geschiedenis van de ontwikkeling van de waterbeweging en het profiel van de rivieren in het Noordelijk Deltabekken over de perioden 1870 - 1970 - 1976, Deel II - De periode 1970 - 1976 (in Dutch)*. (Tech. Rep.). Rijkswaterstaat, Directie Waterhuishouding en Waterbeweging.
- Herman, P. M. J. (2000). *Personal communication*. Yerseke: Netherlands Institute of Ecology, Centre for Estuarine and Coastal Ecology, The Netherlands.
- Herman, P. M. J., Middelburg, J. J., & Heip, C. H. R. (2001). Benthic community structure and sediment processes on an intertidal flat: results from the ECOFLAT project. *Continental Shelf Research*, 21, 2055-2071.
- Hibma, A. (1999). *Process-based modelling of tidal inlet dynamics. Evaluation of Frisian Inlet data*. Prepared for: WL|Delft Hydraulics and Netherlands Institute for Coastal and Marine Management, Delft University of Technology, Delft.
- Hibma, A., De Vriend, H. J., & Stive, M. J. F. (2001). Channel and shoal formation in estuaries.

- In S. Ikeda (Ed.), *IAHR Proceedings of the River, Coastal and Estuarine Morphodynamics Conference, Obihiro, Japan* (pp. 463–472).
- Hirano, M. (1971). River bed degradation with armouring. *Transactions Japan Society of Civil Engineers*, 3, 194–195.
- Hirano, M. (1972). Studies on variation and equilibrium state of a river bed composed of non-uniform material. *Transactions Japan Society of Civil Engineers*, 4, 128–129.
- Houwing, E. J. (2000). *Sediment dynamics in the pioneer zone in the land reclamation area of the Wadden Sea, Groningen, The Netherlands*. PhD thesis, University of Utrecht, Utrecht.
- Hydraulics, W. (1997). *Ecomorfologische module Westerschelde (in Dutch)* (Deelproject A.5.4 No. Z0971). Delft: WL|Delft Hydraulics.
- Jeuken, M. C. J. L. (2000). *On the morphologic behaviour of tidal channels in the Westerschelde estuary*. PhD thesis, University of Utrecht, Utrecht.
- Kennish, M. J. (1986). *Ecology of estuaries Volume 1: Physical and Chemical aspects*. Boca Raton Florida: CRC Press.
- Komarova, N. L., & Hulscher, S. J. M. H. (2000). Linear instability mechanisms for sand wave formation. *Journal of Fluid Mechanics*, 413, 219–246.
- Krumbein, W. C. (1936). Application of logarithmic moments to size frequency distributions of sediments. *Journal of Sedimentary Petrology*, 6, 84–90.
- Kuijper, C. (2001). *Modelling of sand-mud mixtures, Part I: Application of LHEC to Haringvliet - Hollandsch Diep*. (Report Z2840). Delft: WL|Delft Hydraulics.
- Latteux, B. (1995). Techniques for long-term morphological simulation under tidal action. *Marine Geology*, 126, 129–141.
- Le Hir, P., & Karlikow, N. (1992). Sediment Transport Modelling in a Macrotidal Estuary: do we need to account for Consolidation Processes? In B. L. Edge (Ed.), *Proceedings of the 23rd International Coastal Engineering Conference, Venice, Italy* (pp. 3122–3134). New York: American Society of Civil Engineers.
- Lesser, G. (2000). *Computation of Three-dimensional Suspended Sediment Transport within the Delft3D-FLOW Module*. Prepared for: WL|Delft Hydraulics, Institute for Hydraulic Engineering, Delft.
- Lesser, G., Kester, J., & Roelvink, J. (in prep.). Development and validation of a three-dimensional morphological model. *Coastal Engineering, Special issue on morphodynamics (to appear in 2003)*.
- McLaren, P. (1981). An interpretation of trends in grain size measures. *Journal of Sedimentary Petrology*, 51(2), 611–624.
- McLaren, P. (1994). *Sediment transport in the Westerschelde between Baarland and Ruppelmonde* (Prepared for: RIKZ-Rijkswaterstaat). Cambridge: GeoSea Consulting (UK) Ltd.

- McLaren, P., & Bowles, D. (1985). The effects of sediment transport on grain size distributions. *Journal of Sedimentary Petrology*, 55(4), 457–470.
- Merckelbach, L. M. (2000). *Consolidation and strength evolution of soft mud layers*. PhD thesis, Delft University of Technology, Delft.
- Middelburg, J. J., Soetaert, K., & Herman, P. M. J. (1997). Empirical relationships for use in global diagenetic models. *Deep-Sea Research I*, 44(2), 327–344.
- Mitchell, J. K. (1976). *Fundamentals of soil behaviour*. University of California, Berkeley: John Wiley & Sons.
- Mitchener, H., & Torfs, H. (1996). Erosion of mud/sand mixtures. *Coastal Engineering*, 29, 1–25.
- Murray, W. A. (1977). Erosion of coarse sand-clayey silt mixtures. *Journal of Hydraulic Division*, 103(HY10), 1222–1227.
- Nichols, M. M., & Boon, J. D. (1994). Sediment Transport Processes in Coastal Lagoons. In B. Kjerfve (Ed.), *Coastal Lagoon Processes* (pp. 157–219). Amsterdam: Elsevier Science Publishers.
- Oost, A. P. (1995). *Dynamics and sedimentary development of the Dutch Wadden Sea with emphasis on the Frisian Inlet. A study of the barrier islands, ebb-tidal deltas, inlets and drainage basins*. PhD thesis, University of Utrecht, Utrecht.
- Panagiotopoulos, I., Voulgaris, G., & Collins, M. B. (1997). The influence of clay on the threshold of movement on fine sandy beds. *Coastal Engineering*, 32, 19–43.
- Parker, G., Paola, C., & Leclair, S. (2000). Probabilistic Exner Sediment Continuity Equation for Mixtures with No Active Layer. *Journal of Hydraulic Engineering*, 126, 818–826.
- Pejrup, M. (1988). The triangular diagram used for classification of estuarine sediments: a new approach. In P. L. De Boer (Ed.), *Tide-Influenced Sedimentary Environments and Facies* (pp. 289–300). D. Reidel Publishing Company.
- Perillo, G. M. E. (1995). Geomorphology and sedimentology of estuaries: an introduction. In G. M. E. Perillo (Ed.), *Geomorphology and Sedimentology of Estuaries. Developments in Sedimentology* 53 (pp. 1–16). Amsterdam: Elsevier Science B.V.
- Postma, H. (1961). Transport and accumulation of suspended matter in the Dutch Wadden Sea. *Netherlands Journal of Sea Research*, 1/2, 148–190.
- Raudkivi, A. J. (1990). *Loose Boundary Hydraulics* (3rd ed.). Oxford: Pergamon Press.
- Reid, G. K., & Wood, R. D. (1976). *Ecology of inland water and estuaries*. New York: D. Van Nostrand Company.
- Ribberink, J. S. (1987). *Mathematical modelling of one-dimensional morphological changes in rivers with non-uniform sediment*. PhD thesis, Delft University of Technology, Delft.
- RIKZ. (1998). *Sedimentatlas waddenzee* [CD-ROM]. Haren: Rijksinstituut voor Kust en Zee.
- RIKZ. (1999). *De ScheldeAtlas, een beeld van het estuarium (in Dutch)*. Middelburg: Rijksinstituut voor Kust en Zee.

- RIKZ. (2002). *Chlorophyll-a and Bed level data Western Scheldt 1990 - 1999*. Middelburg: Rijksinstituut voor Kust en Zee.
- Ris, R. C., Booij, N., & Holthuijsen, L. H. (1999). A third-generation wave model for coastal regions, 2. Verification. *Journal of Geophysical Research*, 104 (C4), 7667-7681.
- Roelvink, J. A., & Banning, G. K. F. M. (1994). Design and development of Delft3D and application to coastal morphodynamics. In A. Verwey, A. Minns, A. Babovic, & A. Maksimovic (Eds.), *Proceedings of hydroinformatics '94* (pp. 451-456). Rotterdam: Balkema.
- Sanford, L. P., & Halka, J. P. (1993). Assessing the paradigm of mutually exclusive erosion and deposition of mud, with examples of the Chesapeake Bay. *Marine Geology*, 114, 37-57.
- Schuttelaars, H. M., & De Swart, H. E. (1996). An idealized long-term morphodynamic model of a tidal embayment. *European Journal of Mechanics, B/Fluids*, 15, 55-80.
- Schuttelaars, H. M., & De Swart, H. E. (2000). Multiple morphodynamic equilibria in tidal embayments. *Journal of Geophysical Research*, 105 (C10), 24,105-24,118.
- Sha, L. P. (1992). *Geological Research in the Ebb-Tidal Delta of 'Het Friesche Zeegat', The Netherlands*. (R.G.D.-Project 40010). Utrecht.
- Shepard, F. P. (1954). Nomenclature based on sand-silt-clay ratios. *Journal of Sedimentary Petrology*, 24, 151-158.
- Sly, P. G. (1989). Sediment dispersion: part 1, fine sediments and significance of the silt/clay ratio. *Hydrobiologia*, 176/177, 99-110.
- Stelling, G. (1984). *On the construction of computational methods for shallow water flow problems*. PhD thesis, Rijkswaterstaat Communications (no. 35), Delft.
- Struiksma, N., Olesen, K. W., Flokstra, C., & De Vriend, H. J. (1985). Bed deformation in curved alluvial channels. *Journal of Hydraulic Research*, 23(1), 57-79.
- Teisson, C. (1997). A review of cohesive sediment transport models. In N. Burt, R. Parker, & J. Watts (Eds.), *Cohesive sediments, Proceedings of the 4th Nearshore and Estuarine Cohesive Sediment Transport Conference* (pp. 367-381). John Wiley & Sons Ltd.
- Teisson, C., Ockenden, M., Le Hir, P., Kranenburg, C., & Hamm, L. (1993). Cohesive sediment transport processes. *Coastal Engineering*, 21, 129-162.
- Ten Brinke, W. B. M. (1993). *The impact of biological factors on the deposition of fine-grained sediment in the Oosterschelde (The Netherlands)*. PhD thesis, University of Utrecht, Utrecht.
- Thoolen, P., Baptist, M., & Herman, P. (1997). *BEON Habitat Micro Macro* (Beon rapport nr. 98-14 No. IBN 96 H 25). Delft: WL|Delft Hydraulics and NIOO-CEMO.
- Toorman, E. A. (1996). Sedimentation and self-weight consolidation: general unifying theory. *Geotechnique*, 46(1), 103-113.
- Torfs, H. (1995). *Erosion of mud/sand mixtures*. PhD thesis, Katholieke Universiteit Leuven, Leuven.
- Torfs, H., Mitchener, H., Huysentruyt, H., & Toorman, E. (1996). Settling and consolidation of mud/sand mixtures. *Coastal Engineering*, 29, 27-45.

- Van de Kreeke, J., & Dunsbergen, D. W. (2000). Tidal Asymmetry and Sediment Transport in the Frisian Inlet. In T. Yanagi (Ed.), *Interactions between Estuaries, Coastal Seas and Shelf Seas* (pp. 139–159). Terra Scientific Publishing Company.
- Van de Kreeke, J., & Louters, T. (1996). *Water level and current measurements in the Frisian Inlet (including the ebb-tidal delta)* (Prepared for: Rijkswaterstaat-RIKZ No. RKZ-045-045A-045B). HYDREST, INC.
- Van de Kreeke, J., & Robaczewska, K. (1993). Tide-Induced transport of Coarse Sediment: Application to the Ems Estuary. *Netherlands Journal of Sea Research*, 31(3), 209–220.
- Van den Berg, J. H., Jeuken, J. L. J., & Van der Spek, A. J. F. (1996). Hydraulic processes affecting the morphology and evolution of the Westerschelde estuary. In K. F. Nordstrom & C. T. Roman (Eds.), *Estuarine Shores: Evolution, Environments and Human Alterations* (pp. 157–184). John Wiley & Sons Ltd.
- Van den Boogert, J. (2001). *Personal communication*. Leeuwarden: Rijkswaterstaat, Directie Noord-Nederland.
- Van der Spek, A. J. F. (2001). *Personal communication*. Utrecht: TNO-NiTG.
- Van Dongeren, A. R., & De Vriend, H. J. (1994). A model of morphological behaviour of tidal basins. *Coastal Engineering*, 22, 287–310.
- Van Drumel, P. (1995). *Slib- en zandbeweging in het Noordelijk Deltabekken in de periode 1982 - 1992 (in Dutch)*. (Tech. Rep.). Rotterdam: Ministerie van Verkeer en Waterstaat, Directie Zuid-Holland, Afdeling Watersystemkennis.
- Van Kesteren, W. G. M. (2002). *Personal communication*. Delft: WL|Delft Hydraulics.
- Van Kesteren, W. G. M., Cornelisse, J. M., & Kuijper, C. (1997). DYNASTER BED MODEL bed strength, liquefaction and erosion. In *Cohesive Sediments (Rep. 55)*. Delft: WL|Delft Hydraulics and Rijkswaterstaat.
- Van Ledden, M. (2000). *Sediment segregation in estuaries and tidal basins. A literature survey*. (Tech. Rep.). Delft: Delft University of Technology, faculty of Civil Engineering and Geosciences.
- Van Ledden, M. (2001). *Modelling of sand-mud mixtures, Part II: A process-based sand-mud model*. (Report Z2840). Delft: WL|Delft Hydraulics, Technology Foundation STW and Delft University of Technology.
- Van Leussen, W. (1994). *Estuarine macroflocs and their role in fine-grained sediment transport*. PhD thesis, University of Utrecht, Utrecht.
- Van Rijn, L. C. (1984). Sediment Transport, Part I: Bed Load Transport. *Journal of Hydraulic Engineering*, 110(10), 1431–1456.
- Van Rijn, L. C. (1993). *Principles of sediment transport in rivers, estuaries and coastal seas*. Amsterdam: Aqua Publisher.
- Van Straaten, L. M. J. U., & Kuenen, P. H. (1957). Accumulation of fine grained sediments in the Dutch Wadden Sea. *Geologie en Mijnbouw*, 19, 329–354.
- Van Wijngaarden, M., Venema, L. B., & De Meijer, R. J. (2002b). Radiometric sand-mud

- characterisation in the Rhine-Meuse estuary. Part B: In situ mapping. *Geomorphology*, 43, 103–116.
- Van Wijngaarden, M., Venema, L. B., De Meijer, R. J., Zwolsman, J. J. G., Van Os, B., & Gieske, J. M. J. (2002a). Radiometric sand-mud characterisation in the Rhine-Meuse estuary. Part A: Fingerprinting. *Geomorphology*, 43, 87–101.
- Venema, L. B., Groen, P., De Meijer, R. J., Van Os, B., Gieske, J. M. J., & Van Wijngaarden, M. J. (1999). *Radiometric Survey of 'Hollandsch Diep' Part II: Mud-sand mapping*. (Prepared for: National Institute for Inland Water Management and Waste Water Treatment RIZA-30284/WST No. Z-78). Groningen: Nuclear Geophysics Division.
- Venema, L. B., Ten Have, R., De Meijer, R. J., Van Os, B., Gieske, J. M. J., & Zwanenburg-Nederlof, H. P. (1998). *Radiometric Survey of 'Hollandsch Diep' Part I: Feasibility Study and Radiometric and Geochemical Characterisation*. (Prepared for: National Institute for Inland Water Management and Waste Water Treatment RIZA-30283/WST No. Z-70). Groningen: Nuclear Geophysics Division.
- Verlaan, P. A. J. (1998). *Mixing of marine and fluvial particles in the Scheldt estuary*. PhD thesis, Delft University of Technology, Delft.
- Villaret, C., & Latteux, B. (1992). Long-term simulation of cohesive sediment bed erosion and deposition by tidal currents. In P. Partridge (Ed.), *Proceedings International Conference Computer Modelling of Seas and Coastal Regions* (pp. 363–378). Southampton: Computational Mechanics Publications.
- Visser, M. (1993). *On the transport of fine marine sediment in the Netherlands coastal zone*. PhD thesis, University of Utrecht, Utrecht.
- Visser, P. J. (2000). *Bodemontwikkeling Rijnsysteem. Een verkenning van de omvang, oorzaken, toekomstige ontwikkelingen en mogelijke maatregelen (in Dutch)*. (Prepared for: European Commission, MAST3 Programme). Delft: Technische Universiteit Delft, faculteit Civiele Techniek en Geowetenschappen.
- Vreugdenhil, C. B. (1989). *Computational hydraulics: an introduction*. Berlin: Springer.
- Wang, Z. B. (1989). *Mathematical modelling of morphological processes in estuaries*. PhD thesis, Delft University of Technology, Delft.
- Wang, Z. B. (1996). Basic theory for predicting bed composition. In *Cohesive Sediments (Rep. 51)*. Delft: WL|Delft Hydraulics and Rijkswaterstaat.
- Wang, Z. B. (1997). LHEC, A model for predicting mud content in the bed. Pilot application in the Nieuwe Merwede. In *Cohesive Sediments (Rep. 53)*. Delft: WL|Delft Hydraulics and Rijkswaterstaat.
- Wang, Z. B., Louters, T., & De Vriend, H. J. (1995). Morphodynamic modelling for a tidal inlet in the Wadden Sea. *Marine Geology*, 126, 289–300.
- Wartel, S. (1977). Composition, transport and origin of sediments in the Schelde estuary. *Geologie en Mijnbouw*, 56(3), 219–233.
- Wells, J. T. (1995). Tide-dominated estuaries and tidal rivers. In G. M. E. Perillo (Ed.),



- Geomorphology and Sedimentology of Estuaries. Developments in Sedimentology 53* (pp. 179–206). Amsterdam: Elsevier Science B.V.
- Whitehouse, R., Soulsby, R., Roberts, W., & Mitchener, H. (2000). *Dynamics of estuarine muds. A manual for practical applications*. London: Thomas Telford Publishing.
- Williamson, H., & Ockenden, M. (1993). Laboratory and field investigations of mud and sand mixtures. *Advances in Hydro-science and Engineering, 1*, 622–629.
- Winkelmolen, A. J., & Veenstra, H. J. (1974). Size and shape sorting in a Dutch tidal inlet. *Sedimentology, 21*(107), 107–126.
- Winkelmolen, A. J., & Veenstra, H. J. (1980). The effect of a storm surge on near-shore sediments in the Ameland-Schiermonnikoog area N. Netherlands. *Geologie en Mijnbouw, 59*, 97–111.
- Winterwerp, J. C. (1989). Flow induced erosion of cohesive beds. A literature survey. In *Cohesive Sediments (Rep. 25)*. Delft: WL|Delft Hydraulics and Rijkswaterstaat.
- Winterwerp, J. C. (1999). *On the dynamics of high-concentrated mud suspensions*. PhD thesis, Delft University of Technology, Delft.
- Winterwerp, J. C. (2001). Stratification of mud suspensions by cohesive and non-cohesive sediment. *Journal of Geophysical Research, 106* (C10), 22559–22574.
- Winterwerp, J. C. (2002). On the flocculation and settling velocity of estuarine mud. *Continental Shelf Research, 22*, 1339–1360.
- Winterwerp, J. C. (2003). On the deposition flux of cohesive sediment. In J. P. Y. Maa (Ed.), *Book of abstracts 7th International Conference on Nearshore and Estuarine Cohesive Sediment Transport Processes, Virginia, United States*.
- Winterwerp, J. C., & Van Kesteren, W. G. M. (in prep.). *An introduction to the physics of cohesive sediments in the marine environment. Developments in Sedimentology*. Amsterdam: Elsevier.
- WL|Delft Hydraulics. (1998). *A tool for mud flat classification* (Prepared for: European Commission, MAST3 Programme No. Z2037.50). Delft: WL|Delft Hydraulics.
- WL|Delft Hydraulics. (2000). *User manual Delft3D-WAVE* (Tech. Rep.). Delft: WL|Delft Hydraulics.
- WL|Delft Hydraulics. (2001). *User manual Delft3D-FLOW* (Tech. Rep.). Delft: WL|Delft Hydraulics.



## Appendix A

### Erosion formulations for sand-mud mixtures

Van Rijn (1993) presents the following relationships for the bed load transport rate ( $q_b$ ) and the reference concentration ( $c_a$ ) of pure sand beds:

$$q_b = \alpha_{b1} \Delta^{0.5} g^{0.5} d_{50}^{1.5} T^{\alpha_{b2}} D_*^{-0.3} \quad (\text{A.1})$$

$$c_a = 0.015 \frac{d_{50} T^{1.5}}{a D_*^{0.3}} \quad (\text{A.2})$$

where  $\Delta$  is the specific density,  $g$  the gravitational acceleration,  $d_{50}$  the median sand grain size,  $T$  the transport parameter,  $D_*$  the dimensionless diameter,  $a$  the reference height, and  $\alpha_{b1}$  and  $\alpha_{b2}$  coefficients. The coefficients amount to  $\alpha_{b1} = 0.053$  and  $\alpha_{b2} = 2.1$  for  $T < 3$ , whereas for higher  $T$ -values  $\alpha_{b1} = 0.1$  and  $\alpha_{b2} = 1.5$ .

The transport parameter  $T$  and dimensionless grain size  $D_*$  in eq. (A.1) and (A.2) are defined as follows:

$$T = \frac{\tau_b}{\tau_{cr}} - 1 \quad (\text{A.3})$$

$$D_* = d_{50} \sqrt[3]{\frac{\Delta g}{\nu^2}} \quad (\text{A.4})$$

where  $\tau_b$  is the bed shear stress,  $\tau_{cr}$  the critical shear stress for sand only and  $\nu$  the kinematic viscosity. The parameter  $T$  is equal to zero for  $\tau_b < \tau_{cr}$ .

The transport parameter  $T$  in eq. (A.3) is adapted in Section 3.3.2 to include the effects of adding (a small amount of) mud to a non-cohesive sand-mud bed:

$$T_{nc} = \frac{\tau_b}{\tau_{cr} (1 + p_m)^\beta} - 1 \quad p_m < p_{m,cr} \quad (\text{A.5})$$

where  $T_{nc}$  is the transport parameter for non-cohesive sand-mud mixtures,  $p_m$  the mud content at the bed surface,  $p_{m,cr}$  the critical mud content and  $\beta$  an empirical coefficient.

Combining the expressions for pure sand beds (eq. A.1 and A.2) and the transport parameter for non-cohesive sand-mud mixtures (eq. A.5), the bed load transport rate ( $q_b$ ) and the reference concentration ( $c_a$ ) of sand for a non-cohesive sand-mud bed are equal to:

$$q_b = \alpha_{b1} \Delta^{0.5} g^{0.5} d_{50}^{1.5} T_{nc}^{\alpha_{b2}} D_*^{-0.3} \quad p_m < p_{m,cr} \quad (\text{A.6})$$

$$c_a = 0.015 \frac{d_{50}}{a} \frac{T_{nc}^{1.5}}{D_*^{0.3}} \quad p_m < p_{m,cr} \quad (\text{A.7})$$

An erosion formula for the mud fraction is also needed. By definition, the relationship between the erosion rate for mud ( $E_m$ ), the erosion rate for sand ( $E_s$ ) and the total erosion rate ( $E$ ) is given by:

$$E = E_s + E_m = (1 - p_m)E + p_m E \quad (\text{A.8})$$

Thus, the erosion rate for mud ( $E_m$ ) can be expressed in terms of the sand erosion rate ( $E_s$ ) as follows:

$$E_m = \frac{p_m}{1 - p_m} E_s \quad (\text{A.9})$$

The erosion rate for sand ( $E_s$ ) in eq. (A.9) is not known yet, because sand transport is described in terms of a horizontal bed load transport ( $q_b$ ) in eq. (A.6) and the reference concentration ( $c_a$ ) in eq. (A.7). The relationship between the erosion rate and the bed load transport rate of a pure sand bed is defined as follows (see e.g. Van Rijn, 1993):

$$E_s = \frac{q_b}{\lambda} \quad (\text{A.10})$$

where  $\lambda$  is the saltation length of sand particles. Thus, the erosion rate for mud in eq. (A.9) can be written as a function of the bed load transport rate of sand ( $q_b$ ) by using eq. (A.10):

$$E_m = \frac{p_m}{1 - p_m} \frac{q_b}{\lambda} \quad (\text{A.11})$$

Van Rijn (1993) proposes the following relationship for the saltation length of sand particles ( $\lambda$ ) in case of pure sand beds:

$$\frac{\lambda}{d} = 3T^{0.9} D_*^{0.6} \quad (\text{A.12})$$

where  $d$  is the characteristic sand grain size. Herein, we assume that the saltation length for sand particles from a non-cohesive sand-mud bed can be described by applying the transport parameter  $T_{nc}$  for non-cohesive sand-mud mixtures (eq. A.5) instead of  $T$  for sand beds (eq. A.3) in eq. (A.12). Then, an expression for the erosion rate for mud can be derived by combining eq. (A.6), (A.11) and (A.12):

$$E_m = \frac{p_m}{1 - p_m} \frac{\sqrt{\Delta g d_{50}}}{D_*^{0.9}} T_{nc}^{\alpha_{h2} - 0.9} \quad p_m < p_{m.cr} \quad (\text{A.13})$$

where  $E_m$  is the erosion rate of mud from a non-cohesive sand-mud bed.



## Appendix B

### Stability

Consider the following situation:

- The flow is one-dimensional;
- The flow is quasi-steady;
- The bed consists of mud only;
- The water level remains the same as in the initial state;
- The bed shear stress is higher than the critical bed shear stress for erosion;

The bed level equation can then be written as follows:

$$(1 - \varepsilon_p) \frac{z_j^{n+1} - z_j^n}{N\Delta t} = -M \left( \frac{U_j^2}{U_c^2} - 1 \right) + \frac{\alpha}{2N\Delta t} (z_{j+1}^n - z_j^n + z_{j-1}^n) \quad (\text{B.1})$$

The following disturbance in the bed level is examined:

$$Z = \hat{z} e^{ikj\Delta x} \quad (\text{B.2})$$

With help of a linearization, the square of the flow velocity can be written as follows:

$$U_j^2 \simeq \frac{q^2}{h^2} \left( 1 + 2 \frac{\hat{z}}{h} e^{ikj\Delta x} \right) \quad (\text{B.3})$$

From eq. (B.1) - (B.3), it can be derived that:

$$z_j^{n+1} = \rho z_j^n + \frac{M}{1 - \varepsilon_p} \left( 1 - \frac{q^2}{U_c^2 h^2} \right) N\Delta t \quad (\text{B.4})$$

where  $\rho$  is the amplification factor:

$$\rho = 1 - \alpha + \alpha \cos(k\Delta x) - \frac{2}{1 - \varepsilon_p} \frac{Mq^2}{U_c^2 h^3} N\Delta t \quad (\text{B.5})$$

The stability condition is  $|\rho| \leq 1$ . If  $\alpha = 0$ , the stability condition becomes:

$$\frac{1}{1 - \varepsilon_p} \frac{Mq^2}{U_c^2 h^3} N \Delta t \leq 1 \quad (\text{B.6})$$

Notice that this stability condition does not depend on the grid size  $\Delta x$ , but only on the time step  $\Delta t$ . The reason is that the erosion flux only depends on the local velocity and does not depend on horizontal gradients in mud transport.



## Appendix C

### Mud deposition and erosion coefficient

The exchange of mud between the bed and the water column is prescribed by applying Krone's deposition formula and Partheniades' erosion formulae, respectively:

$$D_m = w_m C_m \left(1 - \frac{\tau_d}{\tau_b}\right) H \left(1 - \frac{\tau_d}{\tau_b}\right) \quad (\text{C.1})$$

$$E_m = p_m M \left(\frac{\tau_b}{\tau_e} - 1\right) H \left(\frac{\tau_b}{\tau_e} - 1\right) \quad (\text{C.2})$$

where  $D_m$  is the mud deposition rate,  $w_m$  the settling velocity,  $C_m$  the depth-averaged mud concentration,  $\tau_b$  the bed shear stress,  $\tau_d$  the critical deposition shear stress,  $H$  a Heaviside function,  $E_m$  the mud erosion rate,  $p_m$  the mud content at the bed surface,  $M$  the erosion coefficient and  $\tau_e$  the critical erosion shear stress. The Heaviside function equals 1 when the argument is larger than 0, and equals 0 when the argument is less or equal than 0.

Let us assume a more or less constant concentration  $C_m$  and settling velocity  $w_m$  in eq. (C.1), and mud content  $p_m$  in eq. (C.2) during the tidal period  $T$ . The tidally-averaged deposition rate  $\bar{D}_m$  and erosion rate  $\bar{E}_m$  are equal to:

$$\bar{D}_m = w_m C_m \alpha_D \quad (\text{C.3})$$

$$\bar{E}_m = p_m M \alpha_E \quad (\text{C.4})$$

with

$$\alpha_D = \frac{1}{T} \int_0^T \left(1 - \frac{\tau_d}{\tau_b}\right) H \left(1 - \frac{\tau_d}{\tau_b}\right) dt \quad (\text{C.5})$$

$$\alpha_E = \frac{1}{T} \int_0^T \left(\frac{\tau_b}{\tau_e} - 1\right) H \left(\frac{\tau_b}{\tau_e} - 1\right) dt \quad (\text{C.6})$$

where  $\alpha_D$  is a deposition coefficient and  $\alpha_E$  an erosion coefficient.

In general, the bed shear stress during a tidal period in eq. (C.5) and (C.6) is a complicated function of time. Then, the coefficients  $\alpha_D$  and  $\alpha_E$  cannot be solved analytically. Analytical solutions can only be found for idealised bed shear stress variations in time. The bed shear stress variation during the tide is assumed to be as follows in Section 5.2:

$$\tau_b(t) = \hat{\tau}_b \sin^2(\omega t) \quad (\text{C.7})$$

where  $\tau_b$  is the bed shear stress,  $\hat{\tau}_b$  the bed shear stress amplitude and  $\omega$  the tidal frequency. The following scale parameters are introduced:

$$\tilde{\tau}_d = \frac{\hat{\tau}_b}{\tau_d} \quad (\text{C.8})$$

$$\tilde{\tau}_e = \frac{\hat{\tau}_b}{\tau_e} \quad (\text{C.9})$$

where  $\tilde{\tau}_d$  is the dimensionless critical deposition shear stress and  $\tilde{\tau}_e$  the dimensionless critical erosion shear stress. The analytical derivation of the deposition coefficient  $\alpha_D$  in eq. (C.5) and the erosion coefficient  $\alpha_E$  in eq. (C.6) are discussed separately below.

### Deposition coefficient $\alpha_D$

Applying eq. (C.8) and (C.7) in eq. (C.5), the deposition coefficient  $\alpha_D$  can be written as follows:

$$\alpha_D = \frac{1}{T} \int_0^T (1 - \tilde{\tau}_d \sin^2(\omega t)) H(1 - \tilde{\tau}_d \sin^2(\omega t)) dt \quad (\text{C.10})$$

When the maximum bed shear stress during the tide is lower than the critical shear stress for deposition (i.e.  $\tilde{\tau}_d < 1$ ), mud deposition occurs during the entire tidal period. With help of  $\sin^2(\omega t) = \frac{1}{2} - \frac{1}{2} \cos(2\omega t)$ , the coefficient  $\alpha_D$  follows by integrating eq. (C.10) over the tidal period:

$$\alpha_D = 1 - \frac{1}{2} \tilde{\tau}_d \quad \tilde{\tau}_d < 1 \quad (\text{C.11})$$

When the maximum bed shear stress during the tide is higher than the critical shear stress for deposition (i.e.  $\tilde{\tau}_d > 1$ ), mud deposition only occurs during part of the tidal period. Mud deposition starts/stops at time  $t_d$  at which the bed shear stress is equal to the critical bed shear stress for deposition. The time  $t_d$  is equal to:

$$t_d = n \frac{T}{2} \pm \frac{T}{2\pi} \arcsin \left( \frac{1}{\sqrt{\tilde{\tau}_d}} \right) \quad n = 0, 1, 2, \dots, N \quad (\text{C.12})$$

Combining eq. (C.10) and (C.12), the coefficient  $\alpha_D$  can be written as follows:

$$\alpha_D = 4 \frac{1}{T} \int_0^{t_d} (1 - \tilde{\tau}_d \sin^2(\omega t)) dt \quad (\text{C.13})$$

The solution of eq. (C.13) follows with help of  $\sin^2(\omega t) = \frac{1}{2} - \frac{1}{2} \cos(2\omega t)$ :

$$\alpha_D = 4 \frac{1}{T} \left[ \left(1 - \frac{1}{2} \tilde{\tau}_d\right) t_d - \frac{\tilde{\tau}_d}{4\omega} \sin(2\omega t_d) \right] \quad (\text{C.14})$$

Applying eq. (C.12) in (C.14), the coefficient  $\alpha_D$  becomes:

$$\alpha_D = \left(1 - \frac{1}{2} \tilde{\tau}_d\right) \left(\frac{2}{\pi} \arcsin \frac{1}{\sqrt{\tilde{\tau}_d}}\right) + \frac{1}{2\pi} \sqrt{\tilde{\tau}_d - 1} \quad \tilde{\tau}_d > 1 \quad (\text{C.15})$$

### Erosion coefficient $\alpha_E$

Applying eq. (C.9) and (C.7) in eq. (C.6), the erosion coefficient  $\alpha_E$  equals:

$$\alpha_E = \frac{1}{T} \int_0^T (\tilde{\tau}_e \sin^2(\omega t) - 1) H(\tilde{\tau}_e \sin^2(\omega t) - 1) dt \quad (\text{C.16})$$

Erosion only takes place when the bed shear stress is higher than the critical bed shear stress for erosion (i.e.  $\tilde{\tau}_e > 1$ ). Mud erosion starts/stops at time  $t_e$  at which the bed shear stress is equal to the critical bed shear stress for erosion:

$$t_e = \frac{T}{4} \pm \frac{T}{2\pi} \arcsin \left( \frac{1}{\sqrt{\tilde{\tau}_e}} \right) + n \frac{T}{2} \quad n = 0, 1, 2, \dots, N \quad (\text{C.17})$$

Combining eq. (C.16) and (C.17), the coefficient  $\alpha_E$  equals:

$$\alpha_E = 4 \frac{1}{T} \int_{t_e}^{T/4} (\tilde{\tau}_e \sin^2(\omega t) - 1) dt \quad (\text{C.18})$$

The coefficient  $\alpha_E$  can be solved analytically with help of  $\sin^2(\omega t) = \frac{1}{2} - \frac{1}{2} \cos(2\omega t)$ :

$$\alpha_E = \left(\frac{1}{2} \tilde{\tau}_e - 1\right) \left(1 - \frac{2}{\pi} \arcsin \frac{1}{\sqrt{\tilde{\tau}_e}}\right) + \frac{1}{2\pi} \sqrt{\tilde{\tau}_e - 1} \quad \tilde{\tau}_e > 1 \quad (\text{C.19})$$

By definition, the erosion coefficient  $\alpha_E = 0$  for  $\tilde{\tau}_e < 1$  because no mud erosion occurs during the tidal period.



## Appendix D

### Mud wave characteristics

#### D.1 Onset

The initial bed level of the reservoir is given by (see Section 5.3 and Figure 5.11):

$$z_b(x, t = 0) = i_{be}(L - x) - h_e - (h_1 - h_e)e^{-\frac{L-x}{L_a}} \quad (\text{D.1})$$

where  $z_b$  is the bed level,  $i_{be}$  the equilibrium bed level slope,  $x$  the distance from upstream boundary,  $L$  the length of the reservoir,  $h_e$  the equilibrium water depth,  $h_1$  the initial water depth at the downstream boundary of the reservoir,  $L_a$  the characteristic length of the initial bed level profile. The discharge per unit width is constant in time, and the initial water level slope is assumed to be equal to the equilibrium bed level slope ( $i_{be}$ ) in eq. (D.1). Then, the initial water depth  $h$  and the depth-averaged flow velocity  $U$  along the reservoir are equal to:

$$h(x, t = 0) = h_e + (h_1 - h_e)e^{-\frac{L-x}{L_a}} \quad (\text{D.2})$$

$$U(x, t = 0) = \frac{q}{h_e + (h_1 - h_e)e^{-\frac{L-x}{L_a}}} \quad (\text{D.3})$$

where  $q$  is the discharge per unit width.

The critical bed shear stress for mud deposition can be written in terms of the depth-averaged flow velocity as follows:

$$\tau_d = \mu_c \rho_w \frac{g}{C^2} U_d^2 \quad (\text{D.4})$$

where  $\tau_d$  is the critical shear stress for deposition,  $\mu_c$  a friction coefficient,  $\rho_w$  the water density,  $g$  the gravitational acceleration,  $C$  the Chézy-coefficient and  $U_d$  the critical depth-averaged velocity for mud deposition.

Mud deposition starts when the flow velocity ( $U$ ) in eq. (D.3) is equal to the critical velocity for deposition ( $U_d$ ). The onset of mud deposition ( $x_d$ ) is thus given by:

$$\frac{x_d}{L} = 1 + \frac{L_a}{L} \ln \left( \frac{h_d - h_e}{h_1 - h_e} \right) \quad (\text{D.5})$$

where  $h_d$  is the so-called critical water depth for mud deposition and is defined as  $h_d = q/U_d$ .

## D.2 Mud concentration

If mud erosion is absent, the depth-averaged mud concentration equation can be given by:

$$q \frac{\partial C_m}{\partial x} = -w_m C_m \left( 1 - \frac{U^2}{U_d^2} \right) H \left( 1 - \frac{U^2}{U_d^2} \right) \quad (\text{D.6})$$

where  $C_m$  is the depth-averaged mud concentration and  $w_m$  the settling velocity for mud. At the onset of mud deposition (see Appendix D.1), the flow velocity is equal to the critical velocity for deposition and the water depth is equal to the critical water depth for deposition. Beyond the onset, the water level is assumed to be horizontal. Furthermore, the initial water depth is approximated by a linear initial slope between the onset and the downstream boundary. The depth-averaged flow velocity ( $U$ ) beyond the onset can then be approximated by:

$$U = \frac{q}{h_d + i_{b0} \tilde{x}} \quad (\text{D.7})$$

where  $i_{b0}$  is initial bed slope downstream of the onset for deposition and  $\tilde{x}$  the position relatively to the onset  $x_d$ , i.e.  $\tilde{x} = x - x_d$ . The initial bed slope ( $i_{b0}$ ) is given by:

$$i_{b0} = \frac{h_1 - h_d}{L - x_d} \quad (\text{D.8})$$

The mud concentration along the reservoir ( $C_m$ ) can be written as follows by combining eq. (D.6) and (D.7):

$$\frac{\partial C_m}{C_m} = -\frac{w_m}{q} \partial \tilde{x} + \frac{w_m}{q U_d^2} \frac{q^2}{\left( \frac{q}{u_d} + i_{b0} \tilde{x} \right)^2} \partial \tilde{x} \quad (\text{D.9})$$

Integrating between  $\tilde{x} = 0$  (i.e. onset) and  $\tilde{x} = \tilde{x}$ :

$$\ln C_m = -\frac{w_m}{q} \tilde{x} + \frac{w_m}{q} \frac{1}{i_{b0} U_d^2} \frac{q^2}{\frac{q}{u_d} + i_{b0} \tilde{x}} + c_1 \quad (\text{D.10})$$

Two length scales are introduced:

$$L_m = \frac{q}{w_m} \quad (\text{D.11})$$

$$L_d = \frac{q}{i_{b0}U_d} \quad (\text{D.12})$$

where  $L_m$  is the settling length scale and  $L_d$  the flow length scale. The application of eq. (D.11) and (D.12) in the mud concentration equation (D.10) gives:

$$\ln C_m = -\frac{L_d}{L_m} \left( \frac{\tilde{x}}{L_d} + \frac{1}{1 + \tilde{x}/L_d} \right) + c_1 \quad (\text{D.13})$$

The integral coefficient  $c_1$  can be found by applying the boundary concentration  $C_m = C_{m,0}$  at  $\tilde{x} = 0$  in eq. (D.13):

$$c_1 = \ln C_{m,0} + \frac{L_d}{L_m} \quad (\text{D.14})$$

The application of the integral coefficient  $c_1$  (eq. D.14) in eq. (D.13) gives an expression for the mud concentration ( $C_m$ ) along the reservoir:

$$C_m(\tilde{x}) = C_{m,0} e^{-\frac{1}{L_m} \frac{\tilde{x}^2}{\tilde{x} + L_d}} \quad (\text{D.15})$$

Using the expressions for the flow velocity ( $U$ ) in eq. (D.7) and the mud concentration ( $C_m$ ) in eq. (D.15), the deposition rate at the right-hand side of eq. (D.6) is given by:

$$D_m(\tilde{x}) = w_m C_{m,0} e^{-\frac{1}{L_m} \frac{\tilde{x}^2}{\tilde{x} + L_d}} \left( 1 - \frac{1}{(1 + \tilde{x}/L_d)^2} \right) \quad (\text{D.16})$$

where  $D_m$  is the deposition rate along the reservoir.

### D.3 Maximum mud deposition

The mud deposition along the reservoir (eq. D.16) can be written as follows:

$$D_m(\tilde{x}_d) = w_m C_{m,0} e^{f(\tilde{x}_d)} g(\tilde{x}_d) \quad (\text{D.17})$$

$$f(\tilde{x}_d) = -\frac{L_d}{L_m} \frac{\tilde{x}_d^2}{\tilde{x}_d + 1} \quad (\text{D.18})$$

$$g(\tilde{x}_d) = 1 - \frac{1}{(1 + \tilde{x}_d)^2} \quad (\text{D.19})$$

with

$$\tilde{x}_d = \frac{\tilde{x}}{L_d} \quad (\text{D.20})$$

where  $\tilde{x}_d$  is a dimensionless distance from the onset of mud deposition. The maximum mud deposition occurs when the derivative of the mud deposition rate ( $D_m$ ) to  $\tilde{x}_d$  in eq. (D.17) is equal to zero. The derivative of  $D_m$  to  $\tilde{x}_d$  equals:

$$\frac{dD_m}{d\tilde{x}_d} = w_m C_{m,0} \left( \frac{df}{d\tilde{x}_d} e^{f(\tilde{x}_d)} g(\tilde{x}_d) + e^{f(\tilde{x}_d)} \frac{dg}{d\tilde{x}_d} \right) \quad (\text{D.21})$$

The derivative of function  $f(\tilde{x}_d)$  in eq. (D.18) is given by:

$$\frac{df}{d\tilde{x}_d} = -\frac{1}{L_m} \frac{\tilde{x}_d (\tilde{x}_d + 2)}{(1 + \tilde{x}_d)^2} \quad (\text{D.22})$$

The derivative of function  $g(\tilde{x}_d)$  in eq. (D.19) is given by:

$$\frac{dg}{d\tilde{x}_d} = \frac{2}{L_d} \frac{1}{(1 + \tilde{x}_d)^3} \quad (\text{D.23})$$

Applying eq. (D.22) and (D.23) in eq. (D.21), the derivative of the mud deposition rate reduces to:

$$\frac{1}{w_m C_{m,0} e^{f(\tilde{x}_d)}} \frac{dD_m}{d\tilde{x}_d} = \tilde{x}_d^4 + 4\tilde{x}_d^3 + 4\tilde{x}_d^2 + 2\frac{L_m}{L_d} \tilde{x}_d - 2\frac{L_m}{L_d} \quad (\text{D.24})$$

This is a fourth-order equation in  $\tilde{x}_d$ . The maximum mud deposition occurs when the right-hand side of eq. (D.24) equals zero. Unfortunately, this equation has no analytical solutions. As long as  $\tilde{x}_d \ll 1$ , the first term in eq. (D.24) is small compared to the second and third term. If the first term is neglected in eq. (D.24), the remaining third-order equation has the following analytical (non-dimensionless) solutions:

$$\tilde{x}_m = -L_d \quad (\text{D.25})$$

$$\tilde{x}_m = -\frac{1}{2} \sqrt{2} \sqrt{L_m L_d} \quad (\text{D.26})$$



$$\tilde{x}_m = +\frac{1}{2}\sqrt{2}\sqrt{L_m L_d} \quad (\text{D.27})$$

Only the third solution (eq. D.27) is realistic, because we are only interested in solutions downstream from the onset ( $\tilde{x}_m > 0$ ). According to eq. (D.27), the distance beyond the onset of the maximum deposition rate depends on both length scales  $L_m$  (eq. D.11) and  $L_d$  (eq. D.12).



## List of Figures

|     |                                                                                                                                                                                                                                                                                                                                                                                                                                       |    |
|-----|---------------------------------------------------------------------------------------------------------------------------------------------------------------------------------------------------------------------------------------------------------------------------------------------------------------------------------------------------------------------------------------------------------------------------------------|----|
| 1.1 | Distribution of major estuaries and tidal basins in the world (Perillo, 1995). . . . .                                                                                                                                                                                                                                                                                                                                                | 2  |
| 1.2 | Horizontal sand-mud segregation in the Hollandsch Diep, the Netherlands: a) Location, b) water depth and c) mud content ( $\% \leq 0.063$ mm) in the upper 30 cm of the bed (Venema et al., 1999). . . . .                                                                                                                                                                                                                            | 3  |
| 1.3 | Examples of horizontal bed composition variations: a) Distribution of sediments in the Bristol Channel and Severn estuary (Wells, 1995), b) Mean sand grain size and c) Mud content distribution in the tidal basin south of Spiekeroog Island, German Wadden Sea (Flemming and Ziegler, 1995), d) Percentages of fine-grained matter ( $\% < 0.002$ mm) in the Lauwerszee, Dutch Wadden Sea (Van Straaten and Kuenen, 1957). . . . . | 5  |
| 1.4 | Spatial and temporal scales in estuaries. . . . .                                                                                                                                                                                                                                                                                                                                                                                     | 6  |
| 1.5 | Correlation between the hybrid model LHEC and the observed mud content ( $\% \leq 0.063$ mm) at bed surface of the Nieuwe Merwede, the Netherlands (Wang, 1997). . . . .                                                                                                                                                                                                                                                              | 7  |
| 1.6 | Graphical representation of thesis set-up. . . . .                                                                                                                                                                                                                                                                                                                                                                                    | 9  |
| 2.1 | Locations of large-scale measurements in the Netherlands. . . . .                                                                                                                                                                                                                                                                                                                                                                     | 16 |
| 2.2 | Sand-silt-clay diagrams: a) 1. Jiang Su, China, 2. Wadden Sea, Danmark, 3. Dyfi estuary, Wales b) 4. Minas Basin, Canada and 5. Mugu Lagoon, USA (Flemming, 2000). . . . .                                                                                                                                                                                                                                                            | 18 |
| 2.3 | a) Shoreward fining in a natural natural tidal basin and b) Actual sequence observed in the tidal basin south of Spiekeroog Island (Flemming and Nyandwi, 1994). . . . .                                                                                                                                                                                                                                                              | 20 |
| 2.4 | Types of horizontal bed composition patterns in tidal basins (Nichols and Boon, 1994). . . . .                                                                                                                                                                                                                                                                                                                                        | 21 |
| 2.5 | Mud content in the upper 1 cm of the bed at the Molenplaat (the Netherlands) in March (a), June (b), September (c) and December 1995 (d) (see Figure 2.1 for the location of the Molenplaat). . . . .                                                                                                                                                                                                                                 | 22 |
| 2.6 | Mean mud content (a) and standard deviation of mud content (b) for different sample thickness at Molenplaat in the period June 1996 - June 1997. . . . .                                                                                                                                                                                                                                                                              | 23 |
| 2.7 | Primary scale relationship (After De Vriend, 1993). . . . .                                                                                                                                                                                                                                                                                                                                                                           | 25 |
| 2.8 | Vertical sediment transport processes. . . . .                                                                                                                                                                                                                                                                                                                                                                                        | 27 |

|      |                                                                                                                                                                                                                                                                                               |    |
|------|-----------------------------------------------------------------------------------------------------------------------------------------------------------------------------------------------------------------------------------------------------------------------------------------------|----|
| 2.9  | Effect of mud content on the critical erosion shear stress for two different sand-mud mixtures (After Torfs, 1995). . . . .                                                                                                                                                                   | 28 |
| 2.10 | Important mechanisms for sediment segregation. . . . .                                                                                                                                                                                                                                        | 31 |
| 2.11 | Time variations of the current velocity (a) and the equilibrium suspended load $N_e$ and actual suspended load $N$ (b) during a tidal cycle on an arbitrary scale (After Groen, 1967). . . . .                                                                                                | 32 |
| 2.12 | Correlation between the maximum bed shear stress during the tide and observed mud content at the Molenplaat, the Netherlands (WL Delft Hydraulics, 1997). . . . .                                                                                                                             | 35 |
| 2.13 | Present set-up of process-based & idealised models. . . . .                                                                                                                                                                                                                                   | 37 |
| 2.14 | Hirano's mixing layer concept. . . . .                                                                                                                                                                                                                                                        | 39 |
| 3.1  | Network structure in a sand bed for different volume fractions of sand. . . . .                                                                                                                                                                                                               | 49 |
| 3.2  | Sand-silt-clay triangle with six different bed types depending on the transitions for cohesion (solid line) and network structure (dotted lines). The Roman numbers in the triangle refer to various bed types with the characteristics listed in the table at the top of the figure. . . . . | 50 |
| 3.3  | Classification diagrams for sand-silt-clay mixtures after Shepard (1954) (a) and Folk (1954) (b). . . . .                                                                                                                                                                                     | 52 |
| 3.4  | Transitions in cohesion and network structure for kaolinite and montmorillonite mixtures (After Torfs, 1995). . . . .                                                                                                                                                                         | 54 |
| 3.5  | Estimation of relevant bed types for natural systems. See text for further explanation. . . . .                                                                                                                                                                                               | 56 |
| 3.6  | Comparison between experimental data and proposed equations for relationship between critical shear stress and mud content. . . . .                                                                                                                                                           | 60 |
| 3.7  | Clay content by volume as a function of mud content by dry weight. . . . .                                                                                                                                                                                                                    | 64 |
| 3.8  | Re-analysis of critical erosion shear stress as a function of mud and clay content by dry weight (After Torfs, 1995). . . . .                                                                                                                                                                 | 65 |
| 3.9  | Comparison between Murray's experimental data and the bed load transport formula (eq. 3.10 & 3.12) with a) $\beta = 1.25$ and b) $\beta = 1.75$ . . . . .                                                                                                                                     | 67 |
| 4.1  | Set-up of the proposed sand-mud model. . . . .                                                                                                                                                                                                                                                | 71 |
| 4.2  | Definition coordinate system and flow variables. . . . .                                                                                                                                                                                                                                      | 73 |
| 4.3  | Sand and mud transport. . . . .                                                                                                                                                                                                                                                               | 74 |
| 4.4  | Bed level and bed composition. . . . .                                                                                                                                                                                                                                                        | 79 |
| 4.5  | Model set-up in the vertical direction. . . . .                                                                                                                                                                                                                                               | 83 |
| 5.1  | Model set-up of local approach. . . . .                                                                                                                                                                                                                                                       | 92 |
| 5.2  | Overview of situations. . . . .                                                                                                                                                                                                                                                               | 95 |
| 5.3  | Mud concentration for different values of $k_m/w_m$ with accompanying tidally-averaged equilibrium concentration according to eq. (5.5). . . . .                                                                                                                                              | 96 |

|      |                                                                                                                                                                                                                                       |     |
|------|---------------------------------------------------------------------------------------------------------------------------------------------------------------------------------------------------------------------------------------|-----|
| 5.4  | Mud content top layer for different values of $T_{zb}/T_m$ . . . . .                                                                                                                                                                  | 98  |
| 5.5  | Mud content profile for a) $T_{zb}/T_m = 5.0$ and b) $T_{zb}/T_m = 0.2$ . . . . .                                                                                                                                                     | 98  |
| 5.6  | Mud concentration for different values of $\bar{\tau}_{e.nc}$ . . . . .                                                                                                                                                               | 99  |
| 5.7  | a) Bed level and b) Mud content with accompanying equilibrium mud content according to eq. (5.9) for different values of $\bar{\tau}_{e.nc}$ . . . . .                                                                                | 100 |
| 5.8  | Equilibrium mud content for different values of $w_m C_{m,0}/M$ . . . . .                                                                                                                                                             | 103 |
| 5.9  | Correlation between observed mud content and maximum bed shear stress (De Bake, 2000) and derived equilibrium mud content (eq. 5.9) against maximum bed shear stress for Molcnplaat area (the Netherlands). . . . .                   | 104 |
| 5.10 | Rhine-Meuse estuary (the Netherlands) with the southern axis along the dotted line. . . . .                                                                                                                                           | 105 |
| 5.11 | Model set-up of the reservoir. . . . .                                                                                                                                                                                                | 106 |
| 5.12 | Results reference computation: a) bed level changes by sand deposition, b) bed level changes by mud deposition, c) bed level development and d) mud content at bed surface for time intervals of 30 years. . . . .                    | 110 |
| 5.13 | Results sensitivity computations: a) sand grain size, b) settling velocity of mud, c) critical shear stress for mud deposition and d) upstream mud concentration. . . . .                                                             | 111 |
| 5.14 | Comparison between numerical results after 5 years and analytical expressions for initial situation. . . . .                                                                                                                          | 113 |
| 5.15 | Sediment balances during the periods a) 1971 - 1982 and b) 1982 - 1992 (see Figure 5.10 for locations of branches). . . . .                                                                                                           | 114 |
| 5.16 | Bed level change by sand and mud between a) 0 - 10 years and b) 10 - 20 years after the start of the reference computation. . . . .                                                                                                   | 115 |
| 5.17 | Model set-up of the tidal basin. . . . .                                                                                                                                                                                              | 118 |
| 5.18 | a) Mean bed level change by sand and mud and b) bed level profiles at different moments during reference computation. . . . .                                                                                                         | 120 |
| 5.19 | Results reference computation: a) Bed level changes by sand deposition, b) bed level changes by mud deposition, c) bed level development and d) mud content at bed surface with a morphological time scale $T_m = 115$ years. . . . . | 122 |
| 5.20 | a) Bed level profile and b) mud content at bed surface after morphological time scale $T_m$ for sensitivity computations. . . . .                                                                                                     | 123 |
| 5.21 | a) Bed shear stress variation during tidal period at $x/L = 0.25$ . b) Initial net advective suspended load, bed load, and total transport rate of sand along tidal basin. . . . .                                                    | 124 |
| 5.22 | Bed level change by mud deposition after five years, maximum bed shear stress during the tidal period, critical bed shear stress for erosion and mud deposition and bed level change by mud deposition along the tidal basin. . . . . | 125 |
| 5.23 | Mud distribution ( $\% \leq 0.063$ mm) in Spiekeroog area, Wadden Sea (Flemming and Ziegler, 1995). . . . .                                                                                                                           | 129 |

- 6.1 Friesche Zeegat in the northern part of the Netherlands (Wang et al., 1995). . . 134
- 6.2 Locations and sampling year of the cores in the basin of the Zoutkamperlaag based on data of Van der Spek (2001). . . . . 138
- 6.3 Lithology of the cores with the mud content and the bed level in various years based on data of Van der Spek (2001) (see Figure 6.2 for locations). . . . . 139
- 6.4 Numerical grid with the open boundaries at the North Sea. . . . . 141
- 6.5 Water level and current velocity stations in the Friesche Zeegat. . . . . 145
- 6.6 Mean discrepancy between the observed and modelled water level characteristics for various Manning coefficients. See text for the definition of the mean discrepancy. 146
- 6.7 Wave and wind stations during measurement campaign 1992 (Dunsbergen, 1995). 150
- 6.8 Comparison between observed and predicted significant wave height (a) and peak period (b) in the Friesche Zeegat at October 9, 1992. . . . . 151
- 6.9 Observed (a) and computed (b) bed level change in the ebb-tidal delta of the Zoutkamperlaag in the period 1970 - 1994. The black dotted line indicates the spatial extent of the ebb-tidal delta according to Oost (1995). . . . . 152
- 6.10 Observed and computed volume change in the ebb-tidal delta of the Zoutkamperlaag in the period 1970 - 1994: Total volume changes and computed contribution of sand and mud (a), and volume changes as a function of depth at intervals of 1 m (b). . . . . 153
- 6.11 Observed (a) and computed (b) bed level change in the tidal basin of the Zoutkamperlaag in the period 1970 - 1994. The black dotted line indicates the spatial extent of the basin according to Oost (1995). . . . . 154
- 6.12 Observed and computed volume changes in the basin of the Zoutkamperlaag in the period 1970 - 1994: Total volume changes and computed contribution of sand and mud (a), and volume changes as a function of depth at intervals of 1 m (b). 155
- 6.13 Computed mud fraction at the bed surface after 8 years (a), after 16 years (b) and after 24 years (c) and mud deposition in meters in the entire period 1970 - 1994 (d) in the basin of the Zoutkamperlaag. The small circles indicate the locations of the cores in Figure 6.2 and 6.3. . . . . 157
- 6.14 Computed volume change by sand (a) and mud (b) in the basin of the Friesche Zeegat in the reference computation and the various sensitivity computations. . 159
- 6.15 Results sensitivity computations with the computed mud deposition in meters after 20 years: Initial mud distribution (a), Mud concentration (b), Spring-neap cycle (c) and Critical deposition shear stress (d). . . . . 160
- 6.16 Computed water level and bed shear stress variation by the tide at four stations in the main channel of the Zoutkamperlaag just before and directly after closure of the Lauwerszee: near Oude Westgat (a), Meetpaal (b), Roode Hoofd (c) and Lauwersoog (d) (see for locations Figure 6.5). . . . . 163

- 
- 6.17 Conceptual diagram of the morphological behaviour in the Friesche Zeegat: (a) present modelling approach without wave-driven transport, and (b) in reality with wave-driven transport. . . . . 164
- 6.18 Tidal characteristics along the main channel of the Zoutkamperlaag with the observed bathymetry of 1970, the observed bathymetry of 1992 and the computed bathymetry of 1992 (see Figure 6.5 for locations). . . . . 166





## List of Tables

|     |                                                                                                                                                                                                                                                                                                                                                |     |
|-----|------------------------------------------------------------------------------------------------------------------------------------------------------------------------------------------------------------------------------------------------------------------------------------------------------------------------------------------------|-----|
| 2.1 | Sediment classification. . . . .                                                                                                                                                                                                                                                                                                               | 13  |
| 2.2 | Characteristics of large-scale bed composition measurements in the Netherlands (see Figure 2.1 for the area locations). . . . .                                                                                                                                                                                                                | 15  |
| 2.3 | Bed composition characteristics of Wadden Sea inlets, Ems-Dollard estuary, Western Scheldt and Lower Sea Scheldt: average and standard deviation of the mean sand grain size, the sorting index and the mud content, and the clay/silt ratio with the accompanying correlation coefficient (see Figure 2.1 for area locations). . . . .        | 17  |
| 2.4 | Characteristics of the bed composition concepts for multiple sediment fractions. . . . .                                                                                                                                                                                                                                                       | 41  |
| 3.1 | Definitions and symbols for the fractions in the bed. . . . .                                                                                                                                                                                                                                                                                  | 47  |
| 3.2 | Characteristics of sand-mud mixtures used by Torfs (After Torfs, 1995). . . . .                                                                                                                                                                                                                                                                | 53  |
| 5.1 | Overview of different situations. . . . .                                                                                                                                                                                                                                                                                                      | 94  |
| 5.2 | Overview of equilibria in situation 3. . . . .                                                                                                                                                                                                                                                                                                 | 101 |
| 5.3 | Parameter settings of the reference computation. . . . .                                                                                                                                                                                                                                                                                       | 108 |
| 5.4 | Settings of physical parameters reference computation. . . . .                                                                                                                                                                                                                                                                                 | 119 |
| 5.5 | Results reference computations and various sensitivity computations: Mean bed level changes due to sand and mud in the initial situation and in the end situation, and the morphological time scale $T_m$ . . . . .                                                                                                                            | 121 |
| 5.6 | Equilibrium bed level profiles for short tidal basins (Schuttelaars & De Swart, 1996). . . . .                                                                                                                                                                                                                                                 | 127 |
| 5.7 | Differences between model set-up of Schuttelaars & De Swart (1996) and present model. . . . .                                                                                                                                                                                                                                                  | 128 |
| 6.1 | Net deposited (+)/eroded (-) volume and annual deposition (+)/erosion (-) rate in the ebb-tidal delta and the tidal basin of the Zoutkamperlaag in the period 1927 - 1994 (see also Oost, 1995). The data are corrected for sand extraction by dredging, except for the period 1987 - 1994. The closure of the Lauwerszee was in 1969. . . . . | 136 |
| 6.2 | Water level amplitudes and phases of tidal constituents at Wierumergronden, Huibertgat, Western and Eastern model boundary (see Figure 6.4 for locations). . . . .                                                                                                                                                                             | 142 |
| 6.3 | Settings of physical parameters reference computation. . . . .                                                                                                                                                                                                                                                                                 | 143 |

|      |                                                                                                                                                                                                                                                                                  |     |
|------|----------------------------------------------------------------------------------------------------------------------------------------------------------------------------------------------------------------------------------------------------------------------------------|-----|
| 6.4  | Water level measurements and model results with a Manning coefficient $n = 0.021 \text{ s/m}^{1/3}$ (see Figure 6.5 for locations). . . . .                                                                                                                                      | 146 |
| 6.5  | Current velocity measurements and model results of $M_2$ -constituent with a Manning coefficient $n = 0.021 \text{ s/m}^{1/3}$ (see Figure 6.5 for locations). . . . .                                                                                                           | 147 |
| 6.6  | Current velocity measurements and model results of $M_4$ -constituent with a Manning coefficient $n = 0.021 \text{ s/m}^{1/3}$ (see Figure 6.5 for locations). . . . .                                                                                                           | 147 |
| 6.7  | Measured and modelled relative phase difference $\psi = \varphi_4 - 2\varphi_2$ between $M_2$ and $M_4$ tidal constituents of the water level and current velocity (see Figure 6.5 for locations). . . . .                                                                       | 148 |
| 6.8  | Measured and modelled water level characteristics in 1970/1971 with a Manning coefficient $n = 0.021 \text{ s/m}^{1/3}$ and a bathymetry of 1970 (see Figure 6.5 for locations). . . . .                                                                                         | 148 |
| 6.9  | Boundary conditions short wave computations at different moments during the tidal period (see Figure 6.7 for locations). . . . .                                                                                                                                                 | 149 |
| 6.10 | Sediment balance of the tidal basin in the period 1970 - 1994 for the reference computation. . . . .                                                                                                                                                                             | 156 |
| 6.11 | Boundary conditions water level for a spring-neap cycle. . . . .                                                                                                                                                                                                                 | 159 |
| 6.12 | Mud balance of the tidal basin after 10 and 20 years for the reference computation and the various sensitivity computations. . . . .                                                                                                                                             | 161 |
| 6.13 | Relative phase of the current velocity ( $\varphi_4 - 2\varphi_2$ ) computed with the lumped-parameter model with three different bathymetries: the observed bathymetry of 1970, the observed bathymetry of 1992 and the computed bathymetry of 1992 (cf. Figure 6.18d). . . . . | 167 |

# List of Symbols

## Roman Symbols

|                 |                                                                            |             |
|-----------------|----------------------------------------------------------------------------|-------------|
| $A$             | Activity of clay mineral in eq. (3.2)                                      | -           |
| $A_b$           | Water surface area in eq. (6.3)                                            | $m^2$       |
| $A_{b0}$        | Water surface area at mean water level in eq. (6.3)                        | $m^2$       |
| $a$             | Reference height                                                           | $m$         |
| $a_m$           | Reference height for mud                                                   | $m$         |
| $a_s$           | Reference height for sand                                                  | $m$         |
| $a_1, a_2, a_3$ | Numerical coefficients in eq. (4.28)                                       | -           |
| $B$             | Width                                                                      | $m$         |
| $b_1, b_2, b_3$ | Numerical coefficients in eq. (4.28)                                       | -           |
| $C$             | Chézy-coefficient                                                          | $m^{1/2}/s$ |
| $C$             | Rate of change of the water surface area with the water level in eq. (6.3) | $m$         |
| $C_e$           | Depth-averaged equilibrium sand concentration                              | -           |
| $C_m$           | Depth-averaged mud concentration                                           | -           |
| $C_{m,0}$       | Mud concentration outside the model domain                                 | -           |
| $C_{m,e}$       | Depth-averaged equilibrium mud concentration                               | -           |
| $C_s$           | Depth-averaged sand concentration                                          | -           |
| $c_a$           | Reference concentration for sand                                           | -           |
| $c_m$           | Mud concentration                                                          | -           |
| $c_{m,0}$       | Mud concentration at boundary                                              | -           |
| $c_s$           | Sand concentration                                                         | -           |
| $D_m$           | Mud deposition flux                                                        | $m/s$       |
| $D_s$           | Sand deposition flux                                                       | $m/s$       |
| $D_*$           | Dimensionless grain size, $D_* = d_{50} [(s - 1)g/\nu^2]^{1/3}$            | -           |
| $d$             | Grain size                                                                 | $m$         |
| $d_{16}$        | Sand grain size for which 16% of the sediment by weight is smaller         | $m$         |
| $d_{50}$        | Median sand grain size                                                     | $m$         |
| $d_i$           | Grain size of sediment fraction $i$                                        | $m$         |
| $d_m$           | Mean sand grain size                                                       | $m$         |
| $E$             | Erosion flux in eq. (2.4)                                                  | $kg/(m^2s)$ |
| $E_m$           | Mud erosion flux                                                           | $m/s$       |
| $E_s$           | Sand erosion flux                                                          | $m/s$       |
| $F_m$           | Net mud flux                                                               | $m/s$       |

|             |                                                                  |                    |
|-------------|------------------------------------------------------------------|--------------------|
| $F_s$       | Net sand flux                                                    | m/s                |
| $f_u$       | Remoulded shear strength                                         | kN/m <sup>2</sup>  |
| $g$         | Gravitational acceleration                                       | m/s <sup>2</sup>   |
| $H$         | Heaviside function, $H(a) = 1$ if $a > 0$ , otherwise $H = 0$    | -                  |
| $H_s$       | Significant wave height                                          | m                  |
| $h$         | Water depth                                                      | m                  |
| $h_d$       | Water depth at onset mud deposition, $h_d = q/U_d$               | m                  |
| $h_e$       | Equilibrium water depth, $h_e = (q^2/(C^2 i_{be}))^{1/3}$        | m                  |
| $h_0$       | Initial water depth tidal basin                                  | m                  |
| $h_1$       | Initial water depth at downstream boundary reservoir             | m                  |
| $h_*$       | Water depth at basin entrance in quasi-equilibrium situation     | m                  |
| $i$         | Index sediment fraction ( $s =$ sand, $m =$ mud)                 | -                  |
| $i_{be}$    | Equilibrium bed level slope                                      | -                  |
| $i_{b0}$    | Initial bed level slope reservoir                                | -                  |
| $j$         | Index bed composition layer, $j = 1 \dots j_{max}$               | -                  |
| $K, L$      | Empirical coefficients in eq. (2.3)                              | -                  |
| $k$         | Index water layer, $k = 1 \dots k_{max}$                         | -                  |
| $k_m$       | Transport coefficient in eq. (5.4)                               | m/s                |
| $L$         | System length reservoir and basin                                | m                  |
| $L_a$       | Characteristic length reservoir                                  | m                  |
| $L_b$       | Biological mixing zone                                           | m                  |
| $L_d$       | Flow length scale, $L_d = q/(i_{b0}U_d)$                         | m                  |
| $L_i$       | Adaptation length scale of sediment fraction $i$ , $L_i = q/w_i$ | m                  |
| $L_p$       | Mixing length in eq. (4.14)                                      | m                  |
| $LI$        | Liquidity index                                                  | %                  |
| $LL$        | Liquid limit                                                     | %                  |
| $M$         | Erosion parameter for mud beds                                   | m/s                |
| $M_{nc}$    | Erosion parameter for non-cohesive beds                          | m/s                |
| $M_c$       | Erosion parameter for cohesive beds                              | m/s                |
| $m_e$       | Erosion parameter for mixed beds in eq. (2.4)                    | s/m <sup>3</sup>   |
| $N$         | Morphological factor                                             | -                  |
| $n$         | Offset in eq. (3.2)                                              | -                  |
| $n$         | Manning coefficient                                              | s/m <sup>1/3</sup> |
| $PI$        | Plasticity index                                                 | %                  |
| $PL$        | Plastic limit                                                    | %                  |
| $p_i$       | Content of sediment fraction (by dry weight) $i$                 | -                  |
| $p_m$       | Mud content (by dry weight)                                      | -                  |
| $p_{me}$    | Equilibrium mud content (by dry weight)                          | -                  |
| $p_{me,nc}$ | Non-cohesive equilibrium mud content (by dry weight)             | -                  |
| $p_{m,cr}$  | Critical mud content (by dry weight)                             | -                  |
| $p_{m,sub}$ | Mud content sublayer (by dry weight)                             | -                  |
| $p_s$       | Sand content (by dry weight) in eq. (3.5)                        | -                  |

|               |                                                                                                 |         |
|---------------|-------------------------------------------------------------------------------------------------|---------|
| $p_{sa}$      | Sand content (by dry weight)                                                                    | -       |
| $p_{si}$      | Silt content (by dry weight)                                                                    | -       |
| $p_{cl}$      | Clay content (by dry weight)                                                                    | -       |
| $p_j^n$       | Mud content in layer $j$ at time $n$                                                            | -       |
| $Q$           | Discharge                                                                                       | $m^3/s$ |
| $q$           | Discharge per unit width                                                                        | $m^2/s$ |
| $q_b$         | Bed load transport rate of sand                                                                 | $m^2/s$ |
| $S_i$         | Sorting index, $S_i = \frac{1}{2} \left( \frac{d_{50}}{d_{16}} + \frac{d_{84}}{d_{50}} \right)$ | -       |
| $s_{j+1/2}^n$ | Mud flux through upper boundary of layer $j$ at time $n$                                        | $m/s$   |
| $s_{j-1/2}^n$ | Mud flux through lower boundary of layer $j$ at time $n$                                        | $m/s$   |
| $s_0^n$       | Mud flux at bed surface at time $n$                                                             | $m/s$   |
| $T$           | Tidal period                                                                                    | $s$     |
| $T_c$         | Transport parameter for cohesive sand-mud mixtures                                              | -       |
| $T_i$         | Adaptation time scale of sediment fraction $i$ , $T_i = h/w_i$                                  | $s$     |
| $T_m$         | Time scale of mixing                                                                            | $s$     |
| $T_m$         | Morphological adaptation time scale                                                             | $s$     |
| $T_{nc}$      | Transport parameter for non-cohesive mixtures                                                   | -       |
| $T_p$         | Peak period                                                                                     | $s$     |
| $T_{zb}$      | Time scale of bed level rise                                                                    | $s$     |
| $t$           | Time                                                                                            | $s$     |
| $t_d$         | Starting and stop time of mud deposition                                                        | $s$     |
| $t_e$         | Starting and stop time of mud erosion                                                           | $s$     |
| $U$           | Depth-averaged velocity                                                                         | $m/s$   |
| $\hat{U}$     | Depth-averaged velocity amplitude                                                               | $m/s$   |
| $U_d$         | Depth-averaged critical deposition velocity                                                     | $m/s$   |
| $U_e$         | Depth-averaged critical erosion velocity                                                        | $m/s$   |
| $U_w$         | Wind velocity                                                                                   | $m/s$   |
| $u$           | Current velocity in x-direction                                                                 | $m/s$   |
| $\mathbf{u}$  | Horizontal current velocity                                                                     | $m/s$   |
| $\hat{u}_2$   | Current velocity amplitude $M_2$ -tide                                                          | $m/s$   |
| $\hat{u}_4$   | Current velocity amplitude $M_4$ -tide                                                          | $m/s$   |
| $\hat{u}_2$   | Current velocity amplitude $M_2$ -tide along major/minor axis                                   | $m/s$   |
| $\hat{u}_4$   | Current velocity amplitude $M_4$ -tide along major/minor axis                                   | $m/s$   |
| $u_*$         | Shear velocity                                                                                  | $m/s$   |
| $u_z^n$       | Bed level velocity at time $n$                                                                  | $m/s$   |
| $V_m$         | Annual mud load by dry weight                                                                   | $kg$    |
| $V_s$         | Annual sand load by dry weight                                                                  | $kg$    |
| $w$           | Current velocity in z-direction                                                                 | $m/s$   |
| $w$           | Water content in eq. (3.1)                                                                      | %       |
| $w_{cr}$      | Critical water content in eq. (3.19)                                                            | -       |
| $w_m$         | Settling velocity mud                                                                           | $m/s$   |

|               |                                                                                        |     |
|---------------|----------------------------------------------------------------------------------------|-----|
| $w_s$         | Settling velocity sand                                                                 | m/s |
| $X$           | Paris coordinate (West - East)                                                         | m   |
| $x$           | Horizontal coordinate                                                                  | m   |
| $x_d$         | Position onset mud deposition                                                          | m   |
| $\tilde{x}_d$ | Dimensionless distance from the onset of mud deposition, $\tilde{x}_d = \tilde{x}/L_d$ | -   |
| $\tilde{x}$   | Position relative to onset, $\tilde{x} = x - x_d$                                      | m   |
| $\tilde{x}_m$ | Position maximum mud deposition relative to onset $x_d$                                | m   |
| $Y$           | Paris coordinate (South - North)                                                       | m   |
| $y$           | Horizontal coordinate                                                                  | m   |
| $z$           | Vertical coordinate                                                                    | m   |
| $Z$           | Bed level disturbance in eq. (B.2)                                                     | m   |
| $\hat{z}$     | Amplitude bed level disturbance in eq. (B.2)                                           | m   |
| $z_b$         | Bed level                                                                              | m   |
| $z_c$         | Bed composition coordinate                                                             | m   |

### Greek symbols

|                            |                                                                |                   |
|----------------------------|----------------------------------------------------------------|-------------------|
| $\alpha$                   | Coefficient in eq. (B.1)                                       | -                 |
| $\alpha_{b1}, \alpha_{b2}$ | Coefficients bed load transport rate formula in eq. (3.10)     | -                 |
| $\alpha_c$                 | Consolidation coefficient in eq. (3.5)                         | -                 |
| $\alpha_D$                 | Deposition coefficient, for definition see eq. (5.6)           | -                 |
| $\alpha_E$                 | Erosion coefficient, for definition see eq. (5.10)             | -                 |
| $\alpha_p$                 | Empirical coefficient in eq. (4.14)                            | -                 |
| $\beta$                    | Coefficient in eq. (3.9)                                       | -                 |
| $\beta_i$                  | Efficiency factor of sediment fraction i                       | -                 |
| $\gamma$                   | Coefficient                                                    | -                 |
| $\Delta$                   | Relative sediment density, $\Delta = (\rho_s - \rho_w)/\rho_w$ | -                 |
| $\Delta t$                 | Time step                                                      | s                 |
| $\Delta x$                 | Spatial step in x-direction                                    | m                 |
| $\Delta y$                 | Spatial step in y-direction                                    | m                 |
| $\Delta z$                 | Spatial step in z-direction                                    | m                 |
| $\delta$                   | Layer thickness bed composition                                | m                 |
| $\varepsilon_p$            | Bed porosity                                                   | -                 |
| $\varepsilon_x$            | Sediment diffusivity in x-direction                            | m <sup>2</sup> /s |
| $\varepsilon_y$            | Sediment diffusivity in y-direction                            | m <sup>2</sup> /s |
| $\varepsilon_{z,i}$        | Sediment diffusivity in z-direction for sediment fraction i    | m <sup>2</sup> /s |
| $\zeta$                    | Water level                                                    | m                 |
| $\hat{\zeta}$              | Tidal amplitude                                                | m                 |
| $\hat{\zeta}_2$            | Tidal amplitude $M_2$ -tide                                    | m                 |
| $\hat{\zeta}_4$            | Tidal amplitude $M_4$ -tide                                    | m                 |
| $\eta_b$                   | Water level basin in eq. (6.3)                                 | m                 |

|                      |                                                                                                |                   |
|----------------------|------------------------------------------------------------------------------------------------|-------------------|
| $\theta$             | Numerical coefficient in eq. (4.16)                                                            | -                 |
| $\theta_{wave}$      | Wave direction w.r.t. North, clockwise (+)                                                     | °                 |
| $\theta_{wind}$      | Wind direction w.r.t. North, clockwise (+)                                                     | °                 |
| $\theta_{spreading}$ | Wave spreading                                                                                 | °                 |
| $\kappa$             | Von Karman's constant ( $\approx 0.4$ )                                                        | -                 |
| $\lambda$            | Saltation length sand particles                                                                | m                 |
| $\lambda_c$          | Diffusion number bed composition                                                               | -                 |
| $\mu_c$              | Friction coefficient                                                                           | -                 |
| $\Xi$                | Mixing coefficient, $\Xi = \Xi_p + \Xi_b$                                                      | m <sup>2</sup> /s |
| $\Xi_p$              | Physical mixing coefficient                                                                    | m <sup>2</sup> /s |
| $\Xi_b$              | Biological mixing coefficient                                                                  | m <sup>2</sup> /s |
| $\Xi_{b0}$           | Constant biological mixing coefficient                                                         | m <sup>2</sup> /s |
| $\nu_x$              | Fluid mixing coefficient in x-direction                                                        | m <sup>2</sup> /s |
| $\nu_y$              | Fluid mixing coefficient in y-direction                                                        | m <sup>2</sup> /s |
| $\nu_z$              | Fluid mixing coefficient in z-direction                                                        | m <sup>2</sup> /s |
| $\rho$               | Amplification factor                                                                           | -                 |
| $\rho_b$             | Wet bed density                                                                                | kg/m <sup>3</sup> |
| $\rho_{dry}$         | Dry bed density                                                                                | kg/m <sup>3</sup> |
| $\rho_w$             | Water density                                                                                  | kg/m <sup>3</sup> |
| $\rho_s$             | Sediment density                                                                               | kg/m <sup>3</sup> |
| $\sigma_c$           | Courant number bed composition                                                                 | -                 |
| $\sigma_f$           | Courant number flow                                                                            | -                 |
| $\tau_b$             | Bed shear stress                                                                               | N/m <sup>2</sup>  |
| $\hat{\tau}_b$       | Bed shear stress amplitude                                                                     | N/m <sup>2</sup>  |
| $\tau_{cr}$          | Critical shear stress for sand only                                                            | N/m <sup>2</sup>  |
| $\tau_d$             | Critical deposition shear stress for mud                                                       | N/m <sup>2</sup>  |
| $\tilde{\tau}_d$     | Dimensionless critical deposition shear stress for mud, $\tilde{\tau}_d = \hat{\tau}_b/\tau_d$ | -                 |
| $\tau_e$             | Critical erosion shear stress for mud beds                                                     | N/m <sup>2</sup>  |
| $\tilde{\tau}_e$     | Dimensionless critical erosion shear stress for mud, $\tilde{\tau}_e = \hat{\tau}_b/\tau_e$    | -                 |
| $\tau_{e,nc}$        | Critical erosion shear stress for non-cohesive mixtures                                        | N/m <sup>2</sup>  |
| $\tau_{e,c}$         | Critical erosion shear stress for cohesive mixtures                                            | N/m <sup>2</sup>  |
| $\phi$               | Grain size, $\phi = -2 \log d$                                                                 | -                 |
| $\phi_{cl}$          | Clay content by volume                                                                         | -                 |
| $\phi_{cr}$          | Critical content by volume                                                                     | -                 |
| $\phi_{sa}$          | Sand content by volume                                                                         | -                 |
| $\phi_{si}$          | Silt content by volume                                                                         | -                 |
| $\phi_w$             | Water content by volume                                                                        | -                 |
| $\varphi$            | Phase                                                                                          | °                 |
| $\varphi_2$          | Phase $M_2$ -tide                                                                              | °                 |
| $\varphi_4$          | Phase $M_4$ -tide                                                                              | °                 |
| $\psi$               | Relative phase difference, $\psi = \varphi_4 - 2\varphi_2$                                     | °                 |
| $\omega$             | Tidal frequency, $\omega = 2\pi/T$                                                             | 1/s               |





## Acknowledgements

Promoveren en voetbal hebben één belangrijk ding gemeenschappelijk: het is een teamsport. Bij voetbal ligt dat nogal voor de hand. Uitzonderingen daargelaten is het maken van een doelpunt nauwelijks mogelijk in je eentje. Bij promoveren is dat volgens velen precies omgekeerd. Het produceren van een proefschrift wordt vaak beschouwd als een vierjarige éénmansactie in een klein kamertje op een stoffige universiteit. Hoewel een promovendus na vier jaar zijn of haar eigen punt moet maken, zijn coaches, medespelers, supporters, goede faciliteiten en geld onmisbaar om dit doel te bereiken. De onderstaande opsomming is daarvan het levende bewijs.

Allereerst wil ik mijn promotor Huib de Vriend hartelijk bedanken voor de mogelijkheid om in alle vrijheid vier jaar lang onderzoek te doen. Je enthousiasme voor alles wat met water en sediment te maken heeft, is ongeëvenaard en werkte zeer motiverend. Daarnaast hield je het onderzoek in het goede spoor door telkens te vragen naar de rode draad. Daarnaast wil ik Zheng-Bing Wang bedanken voor de vele goede suggesties en adviezen met betrekking tot de richting van het onderzoek en het opschrijven van de resultaten. Je hebt vaak maar weinig woorden nodig om veel te zeggen. Vaak kwam ik pas later tot de conclusie dat ik beter eerder je raad had kunnen opvolgen. Tenslotte wil ik Han Winterwerp bedanken voor de kennisinbreng over slib. Daarnaast heb ik veel geleerd van je gedetailleerde kritiek op alle geschreven stukken; je suggesties hebben de definitieve teksten sterk verbeterd.

Naast deze begeleiders wil ik Erik-Jan Houwing hartelijk bedanken. De afstudeerplek bij het RIZA in Dordrecht was een mooie opwarmer voor dit onderzoek. De telefonische discussies over uiteenlopende onderwerpen (erosie van zand-slibmengsels, broodjes kroket, lange-termijn morfologie en verre reizen), het bezoek aan de Waddenzee (helaas geen technisch meetweer!) en de uitnodigingen voor de workshops over de morfologische ontwikkeling van het Noordelijk Deltabekken waren een welkome afwisseling tijdens het promotieonderzoek.

Tijdens mijn onderzoek heb ik gedurende twee jaar veel tijd doorgebracht bij WL|Delft Hydraulics op de afdeling MCM. Graag bedank ik Andries Roelfzema voor het beschikbaar stellen van een werkplek. Verder wil ik Dano Roelvink, Giles Lesser, Jan van Kester en Rinze Bruinsma hartelijk bedanken voor de hulp bij het doorgronden van Delft3D. Zonder jullie hulp had het implementeren van de zand-slibformuleringen in Delft3D vele malen langer geduurd. Ook denk ik met heel veel plezier terug aan de samenwerking met Cees Kuijper en Walther van Kesteren tijdens het Doelsubsidieproject "Zand-Slib". Zonder jullie kennis en enthousiasme had ik in dit

onderzoek veel minder kunnen bereiken en samen na denken over hetzelfde probleem was heel motiverend.

Het onderzoek is gesponsord door de Stichting Technische Wetenschappen (STW) onder projectnummer DCT.4895. Ik bedank de leden van de gebruikersgroep: Peter Herman (NIOO), Erik-Jan Houwing (RIZA), Teunis Louters (DHV), Andries Roelfzema (WL|Delft Hydraulics), Ad van der Spek (TNO-NITG) en Harm Verbeek (RIKZ) voor de stimulerende discussies tijdens de vergaderingen. Ook de getoonde interesse en de goede organisatie door Frank van den Berg en Yvonne van Scharenburg (STW) tijdens dit project heb ik zeer gewaardeerd.

Een aantal mensen heeft een bijdrage geleverd in de vorm van het beschikbaar stellen van metingen, het regelen van een veldbezoek of een discussie over een bepaald gebied. Deze mensen bedank ik graag hartelijk voor hun bijdrage: Peter Herman (metingen Molenplaat), Dirk van Maldegem (metingen van de Westerschelde), Albert Oost (Waddenzee discussies), Jaap van den Boogert (metingen Friesche Zeegat), Ad van der Spek (boringen Friesche Zeegat), Harm Verbeek (veldbezoek Westerschelde). Daarnaast heb ik de samenwerking met verschillende afstudeerders zeer op prijs gesteld. Ik bedank Don de Bake, Odelinde Nieuwenhuis, Gertjan Nederbragt en Hariëtte Holzhauser voor de discussies over zand en slib. Christine Lauchlan ben ik dankbaar voor de goede suggesties met betrekking tot de Engelse taal in dit proefschrift. Arjan Schoonhoven maakte met veel toewijding het ontwerp van de omslag. Het was erg leuk om met jou als kunstenaar te praten over zand en slib en het ontwerp te zien groeien.

Naast al deze inhoudelijke bijdragen waren de supporters cruciaal om dit monnikenwerk vol te houden. De promovendi, postdocs en medewerkers van de vakgroep Waterbouwkunde wil ik hartelijk bedanken. De goede sfeer onderling en de discussies tijdens de koffie-, lunch- en theepauzes over belangrijke (politiek, oorlog, ...) en minder belangrijke zaken (voetbal, beurskoersen, ...) heb ik zeer gewaardeerd. Daarnaast bedank ik vrienden voor de organisatie van de broodnodige afdeling: de voetbalwedstrijden in De Kuip, de schaakcompetitie, het discussiëren over 'echte' boeken en de (soms lange) wandeltochten. In het bijzonder bedank ik mijn ouders en verdere familie voor het meeleven tijdens dit onderzoek. De vragen: "Wat doe je nu eigenlijk?", "Lukt het met je onderzoek?" en "Wat kun je daar nu mee?" gaven blijk van interesse en plaatsten het onderzoek telkens weer in het juiste perspectief. Tenslotte bedank ik mijn vader en Karel Terwel in hun rol als paranimf voor de ondersteuning tijdens de promotie.

Vanzelfsprekend sluit ik af met een speciaal woord van dank aan Marjan. Je liefde voor mij en je aandacht voor mijn onderzoek waren continu aanwezig en heb ik heel erg gewaardeerd. Daarnaast werkte je enthousiasme voor de lokatie van de volgende conferentie aanstekelijk om de resultaten van dit onderzoek op te schrijven en te presenteren. Tenslotte zorgde de verhuizing naar Nijmegen ervoor dat ik echt een punt moest zetten achter het onderzoek in Delft. Dat laatste is met deze zin gelukt!

## Curriculum Vitae

Op 25 maart 1975 werd Mathijs van Ledden geboren in Culemborg. Hij volgde het middelbaar onderwijs op het Lambert Franckens College te Elburg en behaalde in 1993 het VWO-diploma. Vervolgens studeerde hij Civiele Techniek aan de Technische Universiteit in Delft. In 1996 liep hij stage bij het ingenieursbureau Sunecon in Paramaribo, Suriname. Met drie medestudenten voerde hij een onderzoek uit naar de haalbaarheid van een stuwdam in de Kabalebo rivier (West-Suriname). Tijdens dit project heeft hij onder meer gekeken naar de hydraulische en morfologische gevolgen van een stuwdam voor de Kabalebo en Corantijn rivier. In 1998 rondde hij zijn studie af met het afstudeerproject "Zand-slibsegregatie in de Nieuwe Merwede" bij het Rijksinstituut voor Zoetwaterbeheer en Afvalwaterbehandeling in Dordrecht. Aansluitend maakte hij bij hetzelfde instituut een vergelijking tussen een empirisch en een proces-gebaseerd model die gebruikt worden om de bodemsamenstellingsvariatie te begrijpen en te voorspellen.

In januari 1999 begon Mathijs met promotieonderzoek onder begeleiding van prof.dr.ir. H.J. de Vriend, dr.ir. Z.B. Wang en dr.ir. J.C. Winterwerp aan de Technische Unversiteit Delft. Hij verrichtte onderzoek naar de segregatie van zand en slib in estuaria en getijdebekkens. Het implementeren en testen van het zand-slibmodel werd voor een belangrijk deel uitgevoerd bij WL|Delft Hydraulics. De Stichting Technische Wetenschappen heeft dit project gefinancierd onder projectnummer DCT.4895 en de resultaten staan beschreven in dit proefschrift. Het onderzoek was tevens ingebed in het Delft Cluster project "Eco-morphology in estuaries and coasts" (DC 03.01.02).

Sinds 1 mei 2003 werkt Mathijs bij de adviesgroep Kust & Rivieren van het advies- en ingenieursbureau Royal Haskoning in Nijmegen.









